AD-A071 394 SYSTEMS TECHNOLOGY INC HAWTHORNE CALIF F/G 14/2
MANNED ENGINEERING FLIGHT SIMULATION VALIDATION. PART I. SIMULA--ETC(U)
FEB 79 L G HOFMANN, S A RIEDEL F33615-77-C-2065
UNCLASSIFIED STI-TR-1110-1 AFFDL-TR-78-192-PT-1 NL

1 OF 3
AD A071394

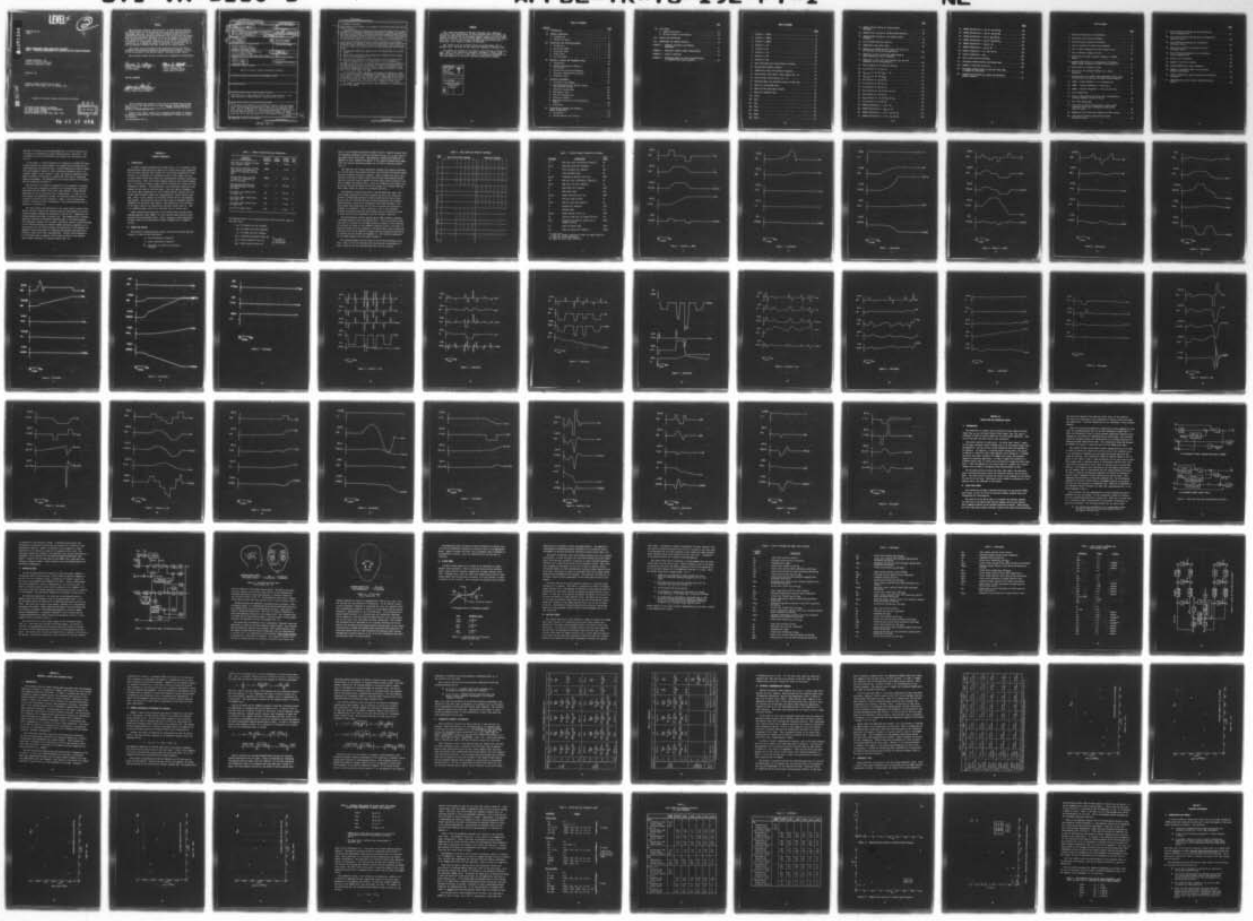

AFFDL-TR-78-192
PART I

MANNED ENGINEERING FLIGHT SIMULATION VALIDATION
PART I: SIMULATION REQUIREMENTS AND SIMULATOR MOTION SYSTEM PERFORMANCE

SYSTEMS TECHNOLOGY, INC.
13766 So. Hawthorne Boulevard
Hawthorne, California 90250

February 1979

TECHNICAL REPORT AFFDL-TR-78-192, PART I
Report for Period August 1977 to November 1978

AIR FORCE FLIGHT DYNAMICS LABORATORY
AIR FORCE WRIGHT AERONAUTICAL LABORATORIES
AIR FORCE SYSTEMS COMMAND
WRIGHT-PATTERSON AIR FORCE BASE, OHIO 45433

NOTICE

When Government drawings, specifications, or other data are used for any purpose other than in connection with a definitely related Government procurement operation, the United States Government thereby incurs no responsibility nor any obligation whatsoever; and the fact that the Government may have formulated, furnished, or in any way supplied the said drawings, specifications, or other data is not to be regarded by implication or otherwise as in any manner licensing the holder or any other person or corporation, or conveying any rights or permission to manufacture, use, or sell any patented invention that may in any way be related thereto.

This report has been reviewed by the Information Office (OI) and is releasable to the National Technical Information Service (NTIS). At NTIS, it will be available to the general public, including foreign nations.

This technical report has been reviewed and is approved for publication.

Marsha B. Tiffany
MARSHA B. TIFFANY, 2LT, USAF
Program Manager

Paul E Blatt
PAUL E. BLATT, Chief
Control Synthesis Branch
Flight Control Division

FOR THE COMMANDER

James R Stanley
JAMES R. STANLEY, Colonel, USAF
Chief, Flight Control Division

"If your address has changed, if you wish to be removed from our mailing list, or if the addressee is not longer employed by your organization please notify _____, W-PAFB, OH 45433 to help us maintain a current mailing list."

Copies of this report should not be returned unless return is required by security considerations, contractual obligations, or notice on a specific document.

AIR FORCE/56780/12 July 1979 — 360

Unclassified

SECURITY CLASSIFICATION OF THIS PAGE (When Data Entered)

REPORT DOCUMENTATION PAGE	READ INSTRUCTIONS BEFORE COMPLETING FORM
1. REPORT NUMBER: AFFDL-TR-78-192, PART I	2. GOVT ACCESSION NO.
3. RECIPIENT'S CATALOG NUMBER	
4. TITLE (and Subtitle): MANNED ENGINEERING FLIGHT SIMULATION VALIDATION; PART I: SIMULATION REQUIREMENTS AND SIMULATOR MOTION SYSTEM PERFORMANCE	5. TYPE OF REPORT & PERIOD COVERED: Final Report, August 1977 — November 1978
	6. PERFORMING ORG. REPORT NUMBER: STI-TR-1110-1
7. AUTHOR(s): L. G. Hofmann, Susan A. Riedel	8. CONTRACT OR GRANT NUMBER(s): F33615-77-C-3065
9. PERFORMING ORGANIZATION NAME AND ADDRESS: Systems Technology, Inc., 13766 So. Hawthorne Boulevard, Hawthorne, California 90250	10. PROGRAM ELEMENT, PROJECT, TASK AREA & WORK UNIT NUMBERS
11. CONTROLLING OFFICE NAME AND ADDRESS: Air Force Flight Dynamics Laboratory, Air Force Systems Command, Wright-Patterson Air Force Base, Ohio 45433	12. REPORT DATE: Feb 1979 13. NUMBER OF PAGES: 198
14. MONITORING AGENCY NAME & ADDRESS (if different from Controlling Office): 210p.	15. SECURITY CLASS. (of this report): Unclassified 15a. DECLASSIFICATION/DOWNGRADING SCHEDULE

16. DISTRIBUTION STATEMENT (of this Report)

Approved for public release; distribution unlimited.

17. DISTRIBUTION STATEMENT (of the abstract entered in Block 20, if different from Report)

18. SUPPLEMENTARY NOTES

19. KEY WORDS (Continue on reverse side if necessary and identify by block number)

Simulation, motion bases, motion fidelity, motion base drive logic, drive logic optimization, LAMARS simulator, nonlinear washout filters

20. ABSTRACT (Continue on reverse side if necessary and identify by block number)

The goal of this research is to establish an orderly, relatively simple method for optimizing the presentation of motion cues in moving base simulations. This is accomplished via choice of the drive logic parameters for a given simulator and flying task. The method developed here is based upon use of motion fidelity criteria. It has been applied to optimize the LAMARS motion base drive logic parameters for an air-to-ground scenario. The methods

(continued) → next page

DD FORM 1 JAN 73 1473 EDITION OF 1 NOV 65 IS OBSOLETE

Unclassified

SECURITY CLASSIFICATION OF THIS PAGE (When Data Entered)

340 425

20. ABSTRACT (concluded)

and procedures of this report can be applied for any given motion base and any desired scenario.

A method for abstracting mission scenarios from strip chart data or verbal descriptions is developed. This method, implemented in FORTRAN, uses approximate time histories for $\dot{p}$, $\dot{q}$, and $\ddot{V}_T$ and linearized kinematic equations to compute body axis angular velocity and specific force time histories which approximate actual flight values for a particular scenario. The latter quantities provide realistic inputs for evaluating and optimizing motion base drive logic.

Criteria for discerning fidelity of motion reproduction are developed. These criteria are composed of various mean-square error measures which reflect differences between simulated and actual in-flight motion. The criteria can be used to answer three questions which arise for every motion base simulation program:

- Is moving base simulation appropriate for the flying tasks to be investigated?
- How can motion base drive logic parameters be optimized for the flying tasks to be investigated?
- Will this set of motion drive logic parameters result in motion within simulator capabilities for the flying tasks to be investigated?

The impact of the three sets of variables which quantify the given elements of the above questions can be investigated individually or simultaneously via these motion fidelity measures and criteria: flying task variables, motion base hardware displacement, velocity and acceleration constraints, and parameters of the motion base drive logic.

A new nonlinear washout technique is developed which exploits the indifference threshold generally acknowledged to be present in the specific force sensory paths. In effect, the nonlinear washout scheme operates to increase the washout rate when the input specific force is subthreshold and the cab is in an off-center position. This is in order to drive the cab to its center position at faster rate than it would be for a comparable linear scheme.

The computer program supporting drive logic optimization is documented in Part II of this report.

PREFACE

This report was prepared by Systems Technology, Inc., Hawthorne, California, under United States Air Force Contract F33615-77-C-2065. The program was administered by the Systems Dynamics Branch, Air Force Flight Dynamics Laboratory, Air Force Systems Command, Wright-Patterson Air Force Base, Ohio. The Air Force project engineers were successively John J. Bankovskis and Lt. Marsha B. Tiffany of AFFDL/FGD.

The contract work was performed during the period August 1977 to November 1978. The draft of this report was submitted in November 1978.

The authors are indebted to test pilot subjects William R. Neeley, Jr., Capt., USAF, of the 4950th Test Wing/DOCA, and Edward L. Daniel, Capt., USAF, and Roger D. Hill, Lt., USN, both of the 3246th Test Wing/TEOF, for their participation in the motion simulation experimental program.

TABLE OF CONTENTS

Page

LIST OF FIGURES

LIST OF TABLES

Page

SECTION I

INTRODUCTION

The principal object of this research is to determine the optimum drive logic configuration for a specific moving base simulator, the Large Amplitude Multi-mode Aerospace Research Simulator (LAMARS), located at WPAFB. The problem of "optimizing" simulator motion reproduction is a general one which need not be application specific. Therefore, any method for determining the optimum LAMARS drive logic configuration is really a general procedure, applicable for any motion base. This provides the motivation to develop a "general" tool which can then be used for LAMARS optimization.

It is important to appreciate the basic concepts of motion simulation from the start. The pilot in any vehicle is able to sense motion as the result of the angular velocity and specific force environment motion provides (visual, aural, thermal, etc., cues aside). The motion simulator is controlled by a computerized drive logic which commands the simulator actuators and, in turn, simulator motion. Put simply, the drive logic need only compute the appropriate commands, based on the particular vehicle's equations of motion, to cause the simulator to reproduce the actual motions. In this way, the pilot will be stimulated by the same angular velocities and specific forces as in actual flight, and motion fidelity of simulation is perfect.

Obviously, the problem is not that simple. This is primarily because the simulator motion base is usually severely constrained to move within some relatively small volume. The challenge of drive logic design is to present high fidelity motion cues within the simulator constraints. Knowledge of the human sensory processes and apparatus is of some help here since it is only necessary to reproduce motions which can be sensed. But the sensory apparatus bandpass is relatively large, so the attenuation obtained on the basis of this consideration alone is insufficient. At this point the central question then concerns the relationship between recovered motion and perceived fidelity (Ref. 1).

The principal components of the drive logic are the washout filters, the limiting scheme and the coordinate transformations. The washout filters are the main object of the optimization process presented here. A washout filter is simply a device for systematically attenuating actual motion. Washout filter properties can be linear, nonlinear, or time-varying. Linear and nonlinear filters are considered in this report. Linear washout filters are characterized by their gain and effective washout break frequency. These are the two parameters which are used for the optimization or "tuning" process.

The first step in evaluating the LAMARS drive logic is to develop a set of typical aircraft maneuver scenarios. These scenarios are the basis for generating representative inputs used when evaluating the washout filters. An approximate method was developed to construct abstracts of the maneuvers from strip chart data. The method uses kinematic equations to compute all required variables. Eight different scenarios were generated. The procedure is described in Section II.

The next step is to design a computer simulation to evaluate the LAMARS drive logic. In addition, this simulation includes models for the human sensory processes and any sensory thresholds which are operative. The inputs to this drive logic/sensory model simulation are the angular velocity and specific force time histories as developed in the scenario generation phase. The outputs include both actual (in flight) and simulated (in simulator) quantities at several points in the model. This modeling process is described in Section III.

Once the various motion quantities are available from the drive logic/sensory model, it is desirable to have a method for comparing the actual and sensed motion in order to evaluate the simulation fidelity. To this end, a set of measures and a resulting criterion were developed to examine and optimize the drive logic. Using these measures, the scenarios were evaluated to choose one which could represent most of the others in the later optimization. Then, using this representative scenario, the gains and break frequencies of the washouts were varied in order to illuminate the sensitivity of the measures to these parameters. This parameter variation exposed the critical axes in terms of optimization, and also

provided a functional relationship between gain and break frequency for the washouts corresponding to given simulator motion constraints. This development and use of the measures and criterion are described in Section IV.

At this point, a piloted simulation is necessary to solidify the relationship between the break frequency of a washout and the resulting criterion value for each critical axis. Piloted simulation is used to expose this relationship in terms of a pilot preference parameter which is an integral element of the criterion. Also, the simulator experiment determines the effect of the g-suit, a sensory aid often used in simulating high-g environments. The experimental plan and the results of the experiment are presented in Section V.

The results of the simulator experiment are then applied to optimize the critical axes, providing a plausible set of optimum gains and break frequencies for the LAMARS linear drive logic washouts. These optimum parameters are for a given drive logic configuration. In order to further examine the optimization scheme, two nonlinear washout filters were included in the drive logic simulation. Again, a set of optimum parameters is obtained for each configuration. This optimization process is reported on in Section VI.

The final results and conclusions on the linear washout scheme optimization, as well as the g-suit evaluation and the investigation of the two nonlinear washout schemes, are presented in Section VII. Suggestions for further research are found in Section VIII. Four appendices are included: Appendix A provides the kinematic equations used in the scenario generation; Appendix B presents the nonlinear "subliminal" washout scheme developed in this research program for possible LAMARS application; Appendix C contains some of the raw fidelity measure data generated in this program; and Appendix D gives a procedure for comparing and extrapolating results for different linear drive logic configurations. Finally, the documentation of the software used in support of this study is found in the Software User's Guide, presented in a separate report (Ref. 2).

SECTION II

SCENARIO GENERATION

A. INTRODUCTION

In order to perform optimization of drive logic, it is necessary to have representative inputs which will expose the critical drive logic parameters. Once the drive logic has been "tuned" for a particular representative input scenario, it is assumed to be optimum not only for that input, but also for any scenario which falls within the representative scenario's particular motion envelope. Thus, the ultimate purpose served by this scenario generation is to provide a range of input scenarios from which to choose one "representative" scenario. The optimization is then performed using the chosen scenario as the input to the drive logic. Note the implicit assumption that drive logic optimization for this "representative" scenario will hold for all other scenarios within the "representative" scenario motion envelope. This, in turn, implies the following restrictions on the optimization process: the process by which the drive logic is optimized should be independent of the drive logic inputs. This restriction is not observed in the strict sense by the optimization procedure stated later on. This is an important point, and will be discussed later in Section IV.B.

Eight scenarios were generated in this effort; these included three handling qualities tasks (HQDT), one air-to-ground weapon delivery task, and four air-to-air gunnery tasks. Table 1 presents a brief description of each scenario, the identification number assigned and its length in seconds.

B. METHOD AND RESULTS

The process of generating each scenario started with abstracting each scenario in terms of three quantities.

$\dot{p}$ – roll acceleration (rad/sec^2)

$\dot{q}$ – pitch acceleration (rad/sec^2)

$\dddot{V}_T$ – derivative of inertial acceleration (ft/sec^3)

TABLE 1. SCENARIO DESCRIPTIONS AND IDENTIFIERS

Scenario Description	Working Notation	Scene Number	Length of Run	Fig. No.
Roll into 4 g constant altitude turn at about 1 g/sec	HQDT1	1	10 sec	1
Roll into 4 g constant altitude turn, unload, and reverse to opposite 4 g constant altitude turn	HQDT2	2	16 sec	2
Wind-up turn from a constant 2 g turn to a constant 6 g turn at 1/3 g/sec	HQDT4	3	20 sec	3
Air-to-ground delivery from lefthand racetrack, 45 deg dive angle	A/G	4	120 sec	4
Air-to-air, low closure rate, low angle off	AA1	5	64 sec	5
Air-to-air, high closure rate, high angle off	AA2	6	17 sec	6
Air-to-air, high closure rate, low angle off	AA3	7	10 sec	7
Air-to-air, head-on pass	AA4	8	15 sec	8

The required results are the quantities which serve as typical inputs to the drive logic:

p_A – in-flight roll rate (rad/sec)

q_A – in-flight pitch rate (rad/sec)

r_A – in-flight yaw rate (rad/sec)

$\dot{u}_{po}$ – longitudinal specific force (g)

$\dot{v}_{po}$ – lateral specific force (g)

$\dot{w}_{po}$ – normal specific force (g)

} At pilot's location in the aircraft

The $\dot{p}$, $\dot{q}$ and $\ddot{V}_T$ input quantities are used to drive a computer program which uses kinematic equations of motion to produce the p_A, q_A, r_A, $\dot{u}_{po}$, $\dot{v}_{po}$ and $\dot{w}_{po}$ inputs to the drive logic. The kinematic equations are presented in Appendix A, and a complete description of the computer program which implements the scenario generation process can be found in the User's Guide (Ref. 2).

The input for the scenario generation consists of an array of discrete $\dot{p}$, $\dot{q}$ and $\ddot{V}_T$ values which specify discrete time intervals and constant values for these variables during the scenario. While it might seem odd to have chosen $\dot{p}$, $\dot{q}$ and $\ddot{V}_T$ as inputs, these variables have been selected because they are relatively easy to specify for most flying tasks of interest, and their integrals are smooth curves. Since the integrals of the inputs (e.g., p_A and q_A) are used as inputs to the drive logic, it is assured that the drive logic inputs are smooth and continuous functions.

Two methods for abstracting the $\dot{p}$, $\dot{q}$ and $\ddot{V}_T$ inputs were used. The first method, employed for the air-to-ground and air-to-air scenarios, consists of developing piecewise constant time histories for $\dot{p}$, $\dot{q}$ and $\ddot{V}_T$ such that the resulting airplane variables produced by the kinematic equations mimic a strip chart recording of those same variables. The strip charts were produced by the Air Force by flying each scenario of interest in a simulator. Table 2 presents a list of the variables recorded on the strip chart for each scenario and an indication of which of those variables were reproduced using the kinematic equations.

The second method, used for generating the HQDT scenarios, employed a strategy similar to the one described above. Since strip chart recordings were not available for the HQDT scenarios, however, it was necessary to construct the inputs to the kinematic equations solely on the basis of verbal descriptions of the scenarios. For these cases, only $\dot{p}$ and $\ddot{V}_T$ were extracted, while $\dot{q}$ was computed to assure that the airplane was maintained in constant altitude flight (see Appendix A). The variables reproduced for the HQDT scenarios are also shown in Table 2.

The following figures provide plots of the resulting airplane variables. Table 3 lists the variables which are plotted, a description of those variables, and the corresponding label used on the plots.

TABLE 2. STRIP CHART AND SCENARIO VARIABLES

VARIABLES	EXIST ON STRIP CHART FOR SCENARIOS:								REPRODUCED FOR SCENARIOS:							
	1	2	3	4	5	6	7	8	1	2	3	4	5	6	7	8
p				×	×	×	×	×	×	×	×	×	×	×	×	×
q				×	×	×	×	×	×	×	×	×	×	×	×	×
r				×	×	×	×	×	×	×	×	×	×	×	×	×
$\dot{p}$					×	×	×	×	×	×	×	×	×	×	×	×
$\dot{q}$					×	×	×	×	×	×	×	×	×	×	×	×
$\dot{r}$					×	×	×	×								
φ				×	×	×	×	×	×	×	×	×	×	×	×	×
θ				×	×	×	×	×	×	×	×	×	×	×	×	×
ψ				×	×	×	×	×	×	×	×	×	×	×	×	×
α				×	×	×	×	×					×	×	×	×
β				×	×	×	×	×								
γ					×	×	×	×								
$\dot{\Phi}$									×	×	×	×	×	×	×	×
$\dot{\theta}$									×	×	×	×	×	×	×	×
$\dot{\psi}$				×					×	×	×	×	×	×	×	×
$\dot{\alpha}$													×	×	×	×
$\dot{u}_{po}$									×	×	×	×	×	×	×	×
$\dot{v}_{po}$									×	×	×	×	×	×	×	×
$\dot{w}_{po}$									×	×	×	×	×	×	×	×
V_T				×					×	×	×	×	×	×	×	×
$\dot{V}_T$												×	×	×	×	×
$\ddot{V}_T$												×	×	×	×	×
H				×	×	×	×	×								
$\dot{H}$				×	×	×	×	×								
M					×	×	×	×								
a_x					×	×	×	×								
a_y				×	×	×	×	×								
a_z					×	×	×	×								
a_{ycg}				×												
V_{Tcal}				×												
δ_a				×	×	×	×	×								
δ_r				×	×	×	×	×								
δ_e				×	×	×	×	×								
δ_F				×												
δ_{SB}				×												
N_z				×												
T				×												
$\dot{V}/U$				×												
Pickle				×												

TABLE 3. PLOTTED SCENARIO GENERATION VARIABLES

VARIABLE	DESCRIPTION	PLOT LABEL
$\dot{q}$*	Body axis pitch acceleration (deg/sec^2)	QD
q_a***	Body axis pitch rate (deg/sec)	QA
$\dot{\theta}$	Pitch attitude rate (deg/sec)	THD
θ	Pitch attitude (deg)	TH
$\dot{u}_{po}$***	Longitudinal specific force (g)	UPOD
$\dot{p}$**	Body axis roll acceleration (deg/sec^2)	PD
p_a***	Body axis roll rate (deg/sec)	PA
$\dot{\phi}$	Bank angle rate (deg/sec)	PHID
φ	Bank angle (deg)	PHI
$\dot{v}_{po}$***	Lateral specific force (g)	VPOD
V_T	Inertial speed (ft/sec)	VT
r_a***	Body axis yaw rate (deg/sec)	RA
$\dot{\psi}$	Heading rate (deg/sec)	PSID
ψ	Heading (deg)	PSI
$\dot{w}_{po}$***	Normal specific force (g)	WPOD
$\dot{V}_T$	Inertial speed rate of change (ft/sec^2)	VTD
$\dddot{V}_T$**	Derivative of inertial speed rate of change (ft/sec^3)	VTDD
$\Delta\alpha$	Angle of attack (deg)	ALFA
$\Delta\dot{\alpha}$	Angle of attack rate (deg/sec)	ALFAD

* input for scenario generation (except for HQDT scenarios)
** input for scenario generation
*** input for drive logic simulation

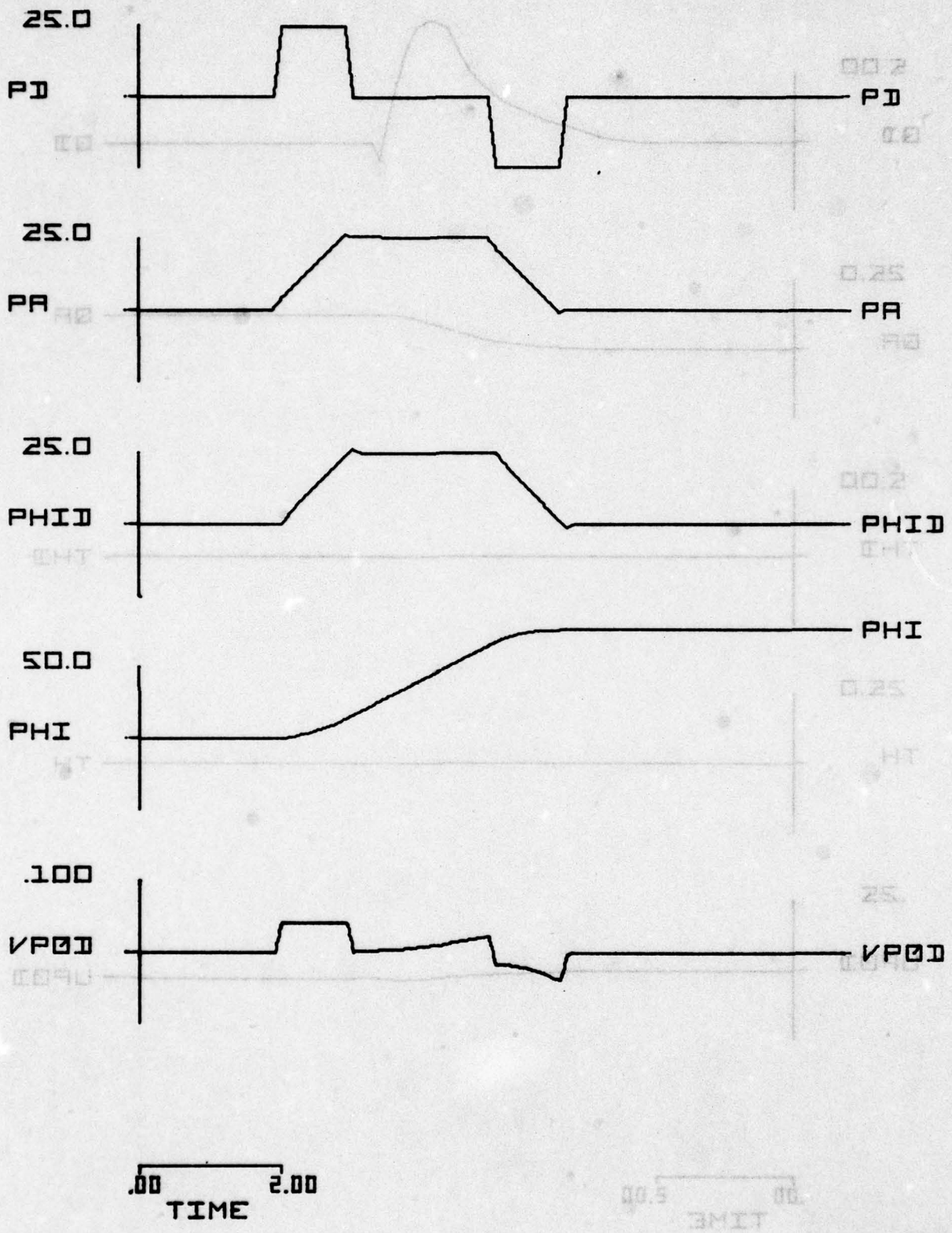

Figure 1. Scenario 1, HQDT1

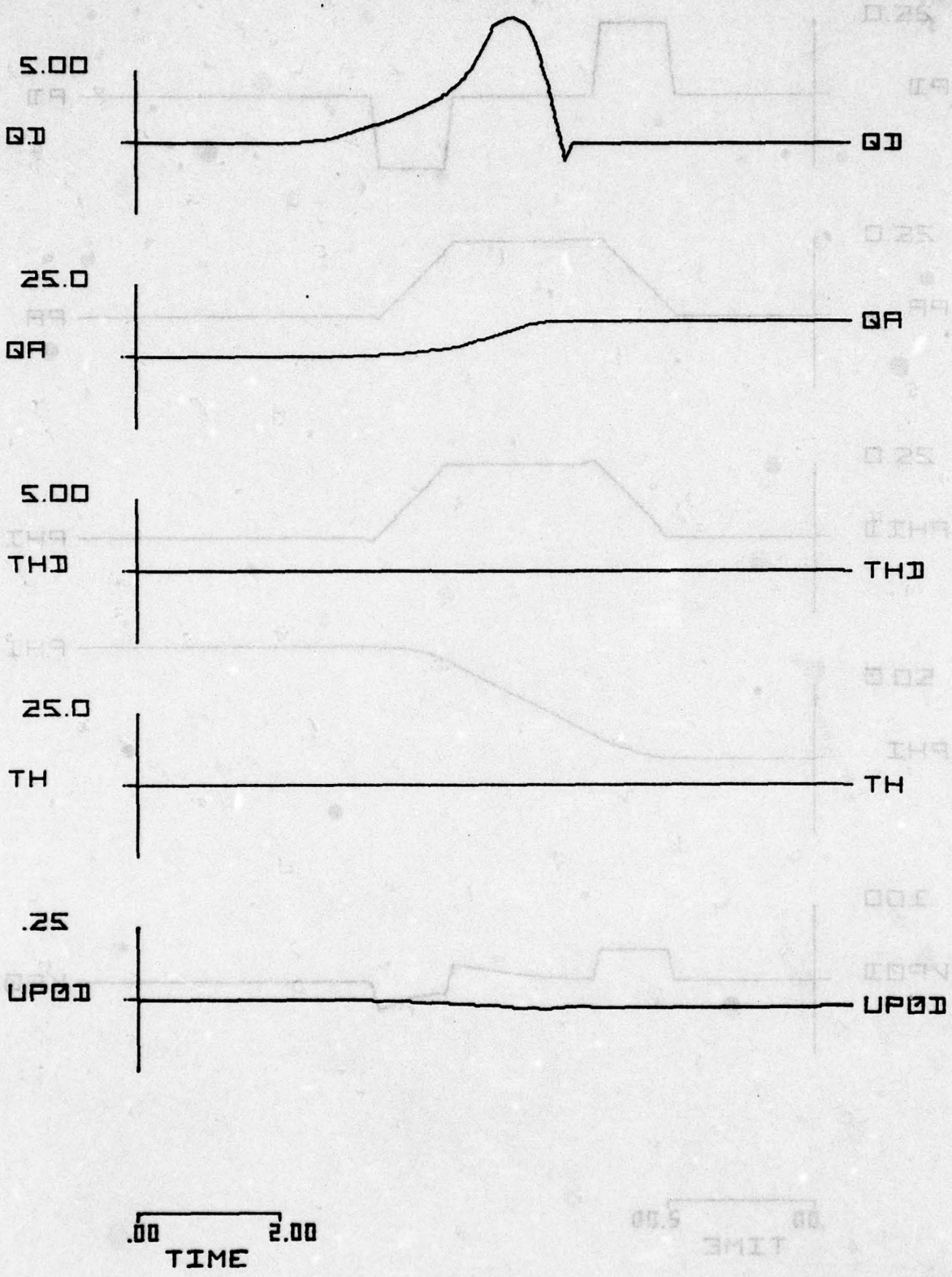

Figure 1. (Continued)

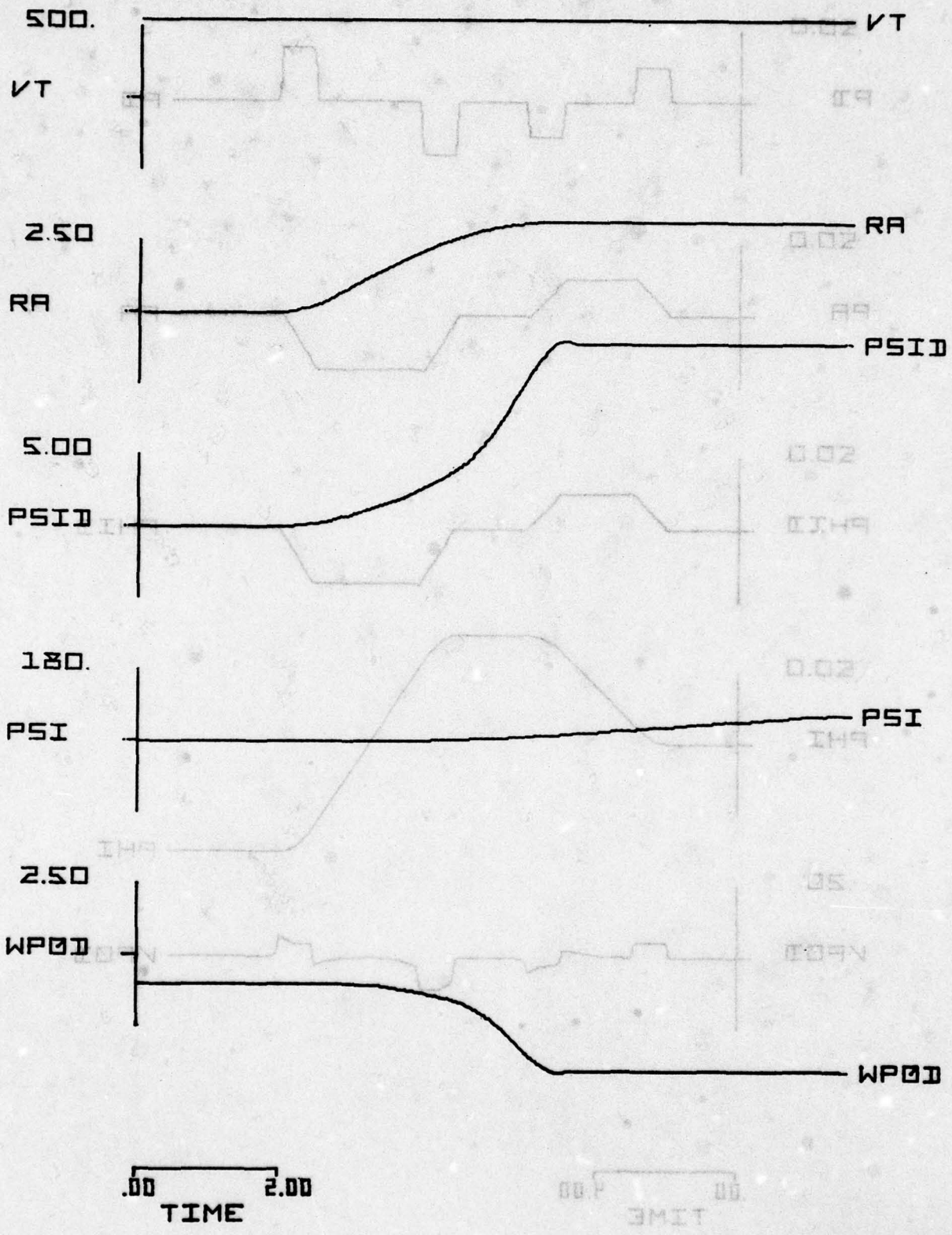

Figure 1. (Concluded)

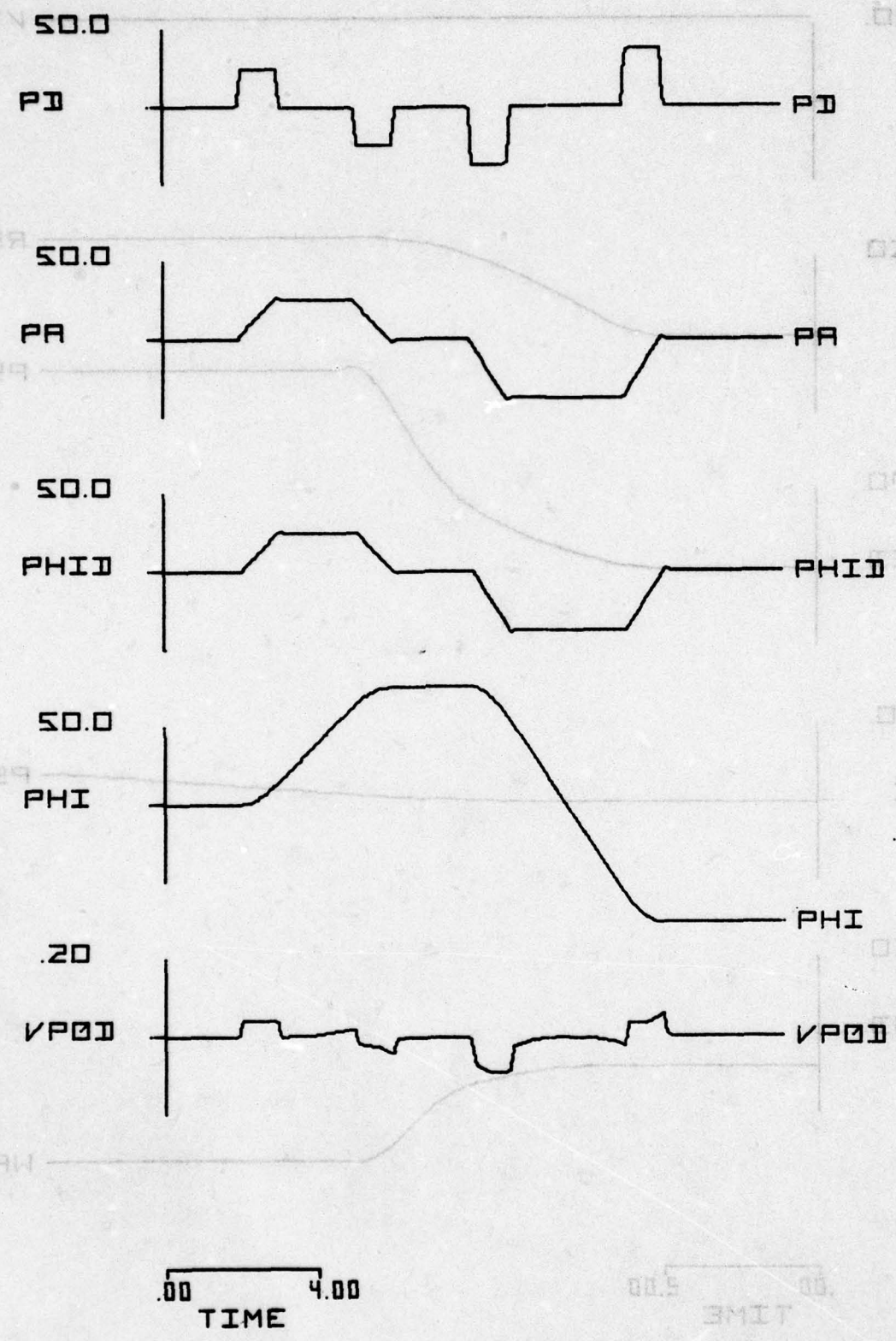

Figure 2. Scenario 2, HQDT2

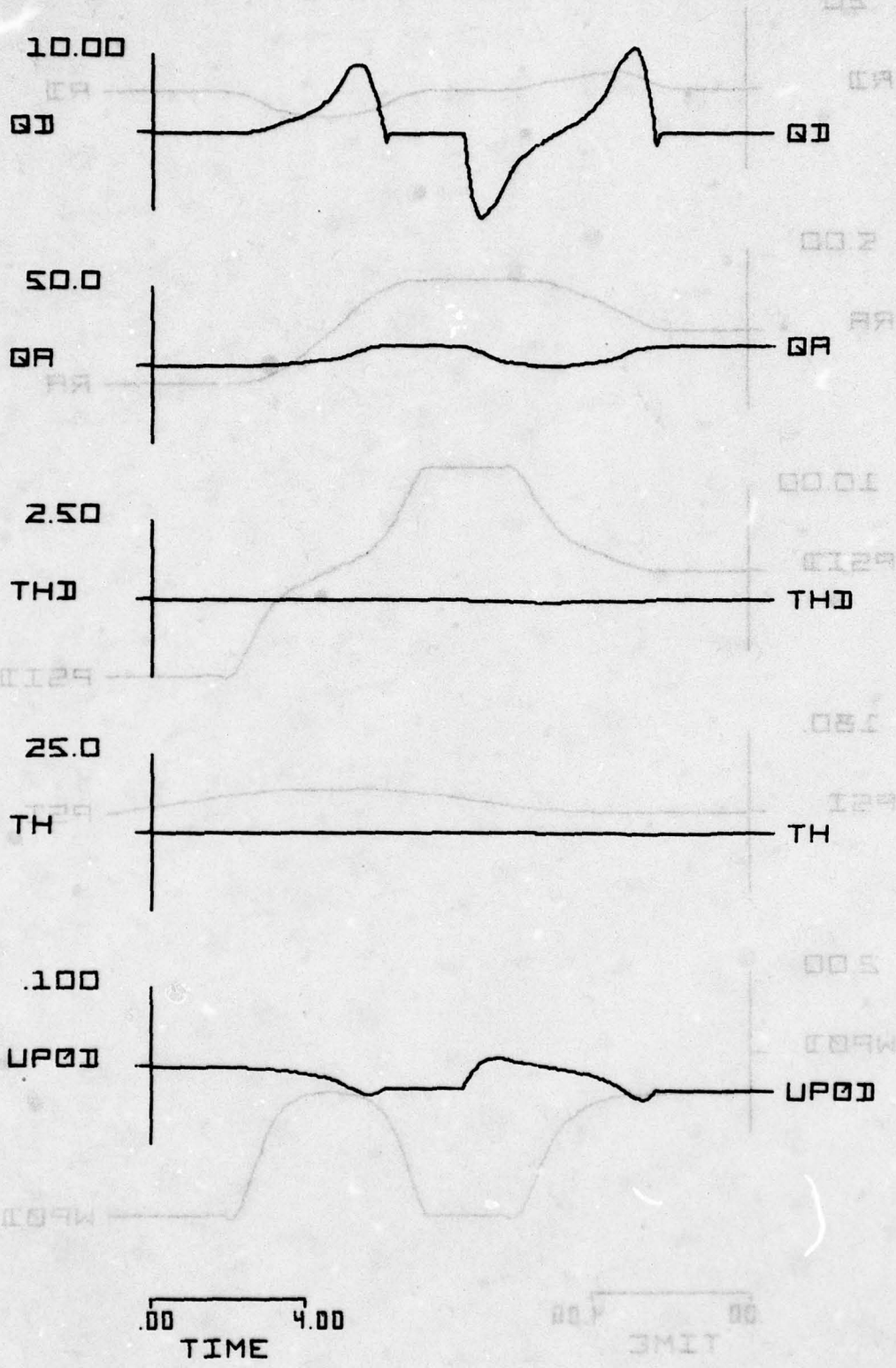

Figure 2. (Continued)

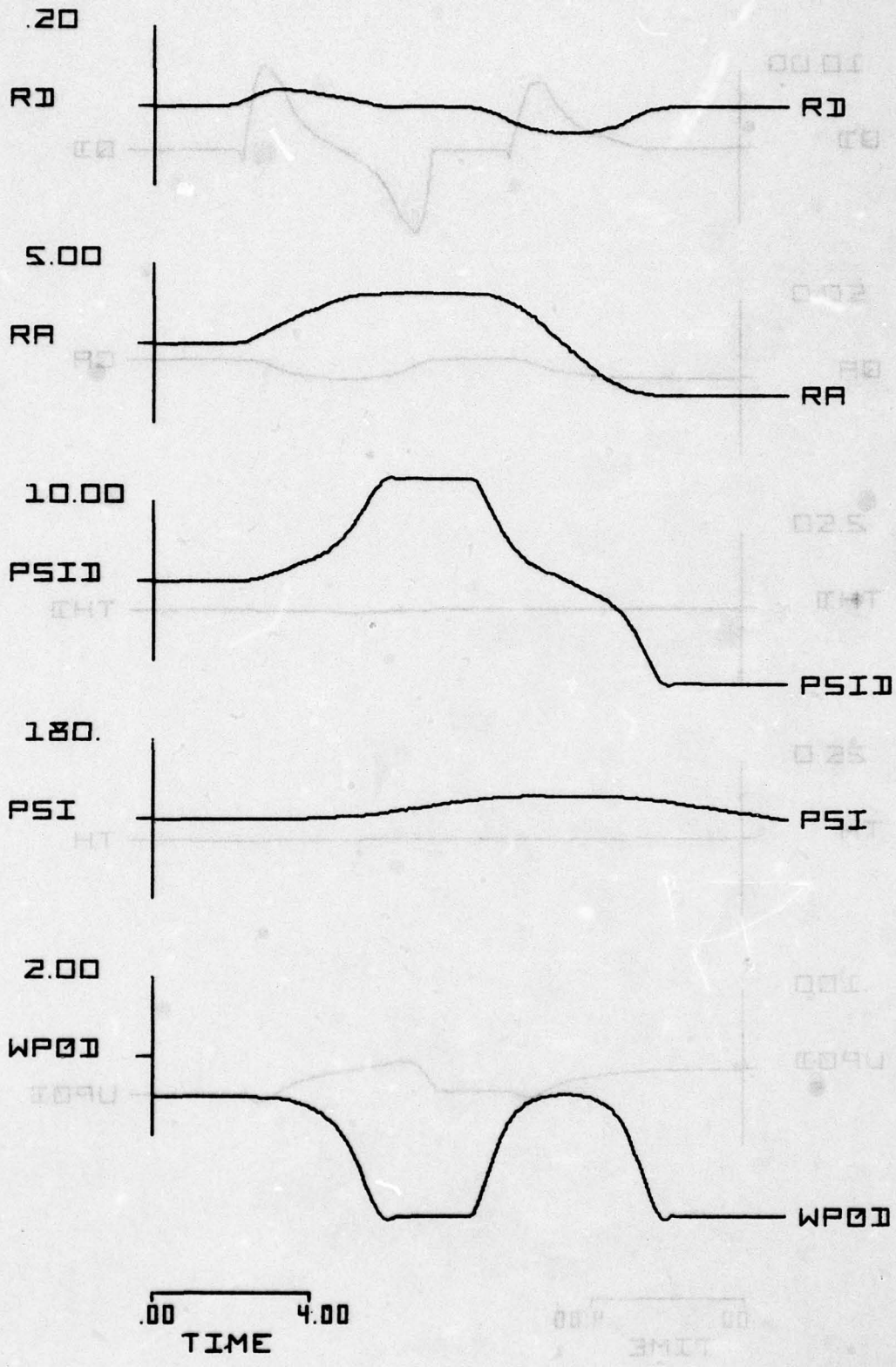

Figure 2. (Continued)

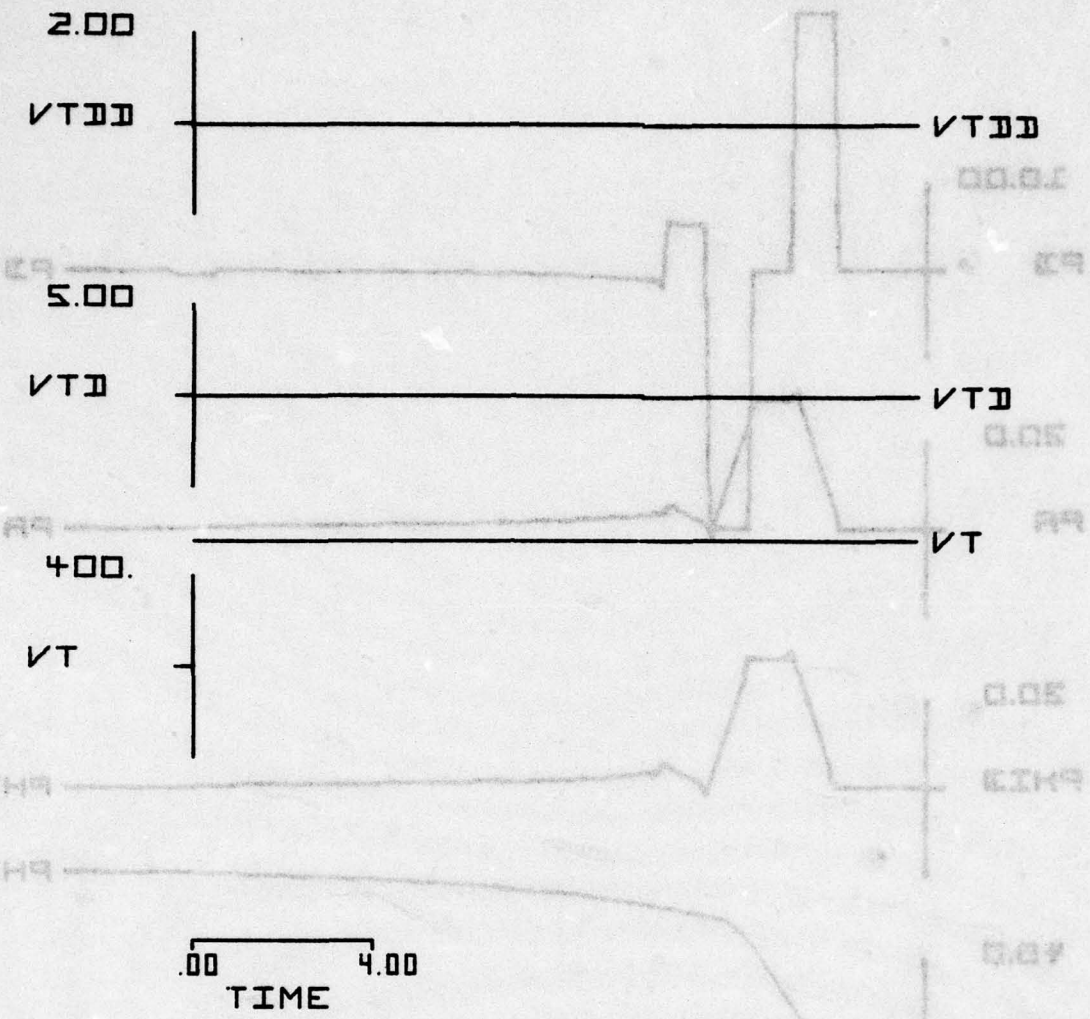

Figure 2. (Concluded)

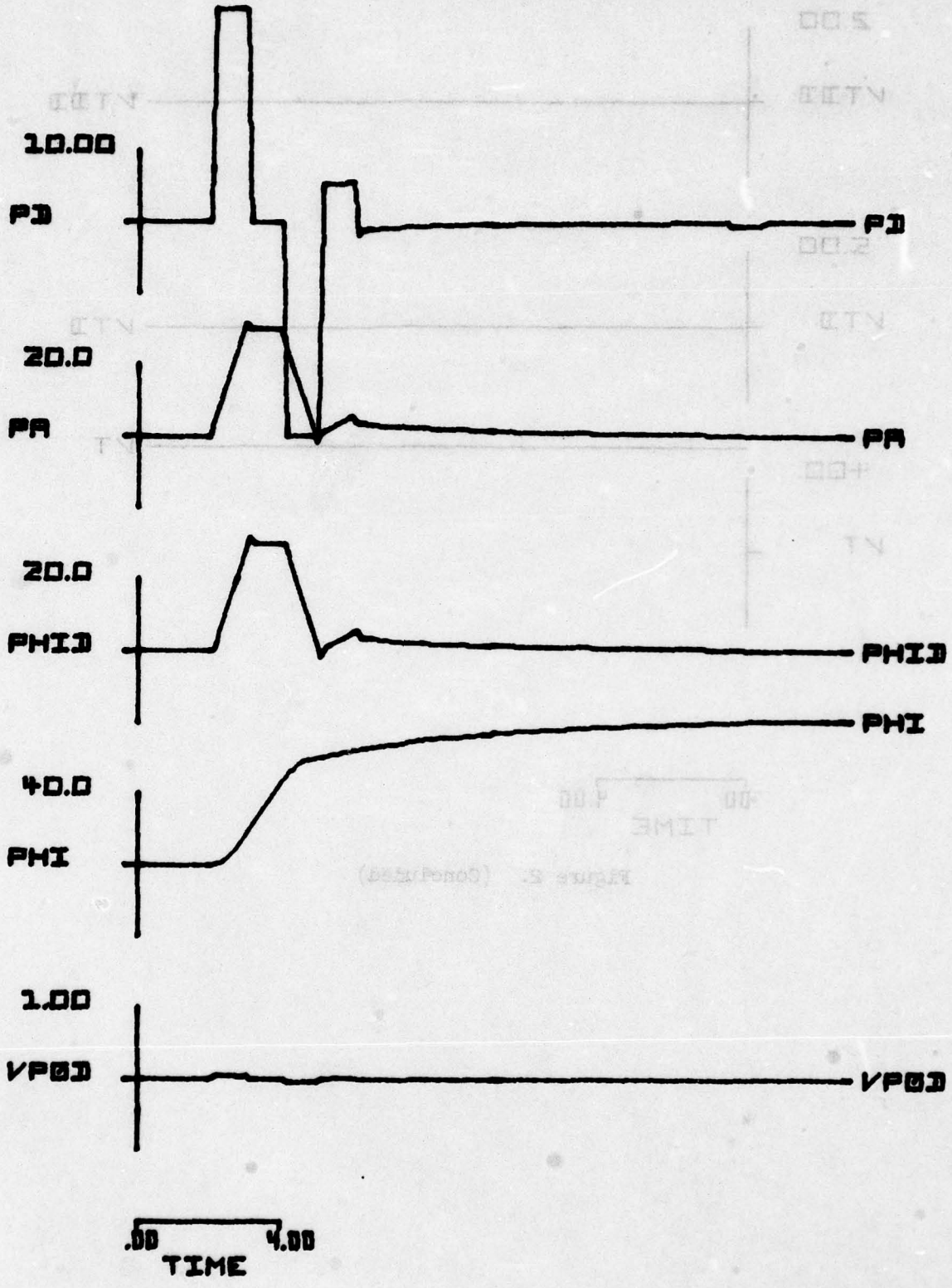

Figure 3. Scenario 3, HQDT[4]

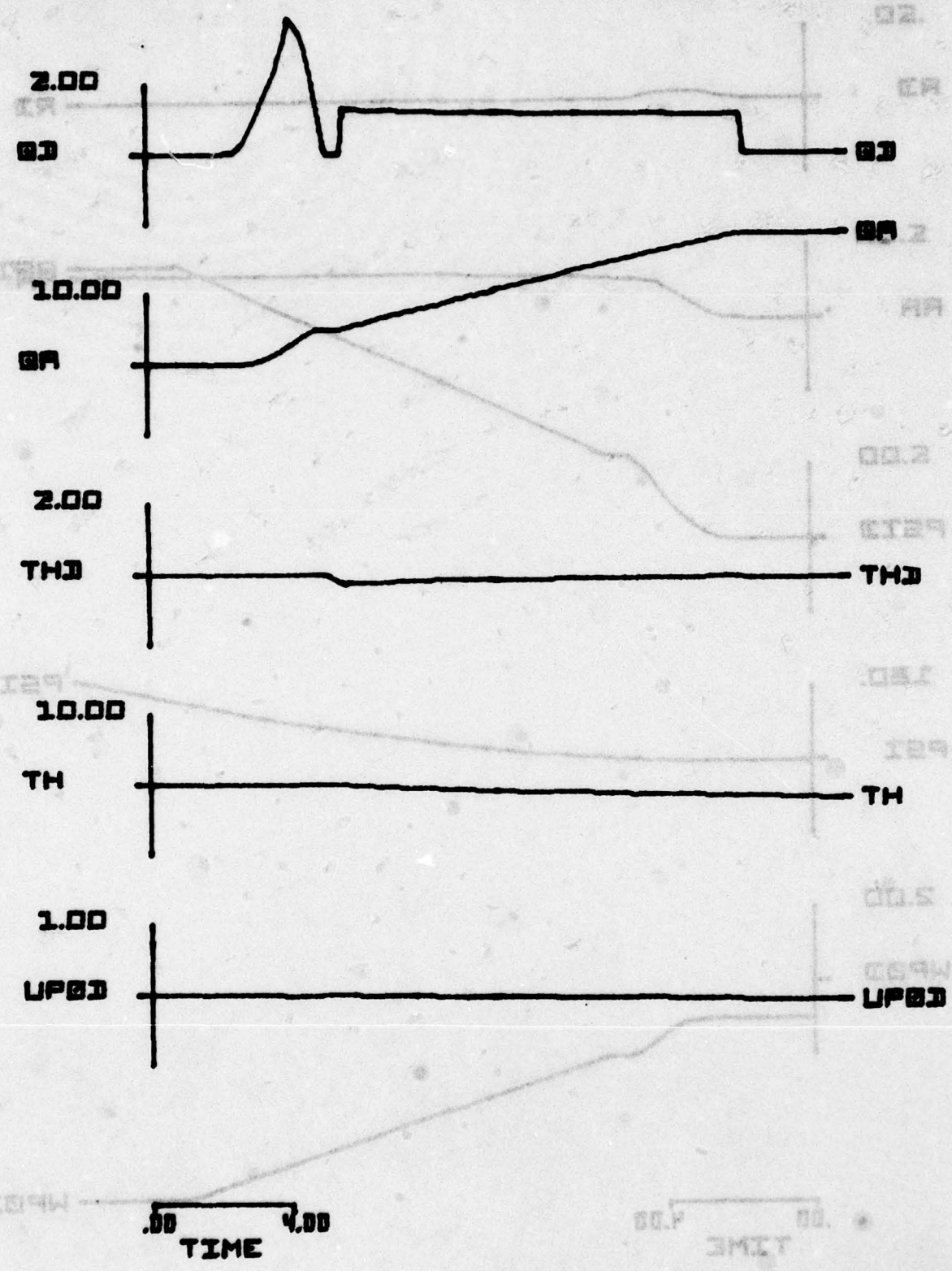

Figure 3. (Continued)

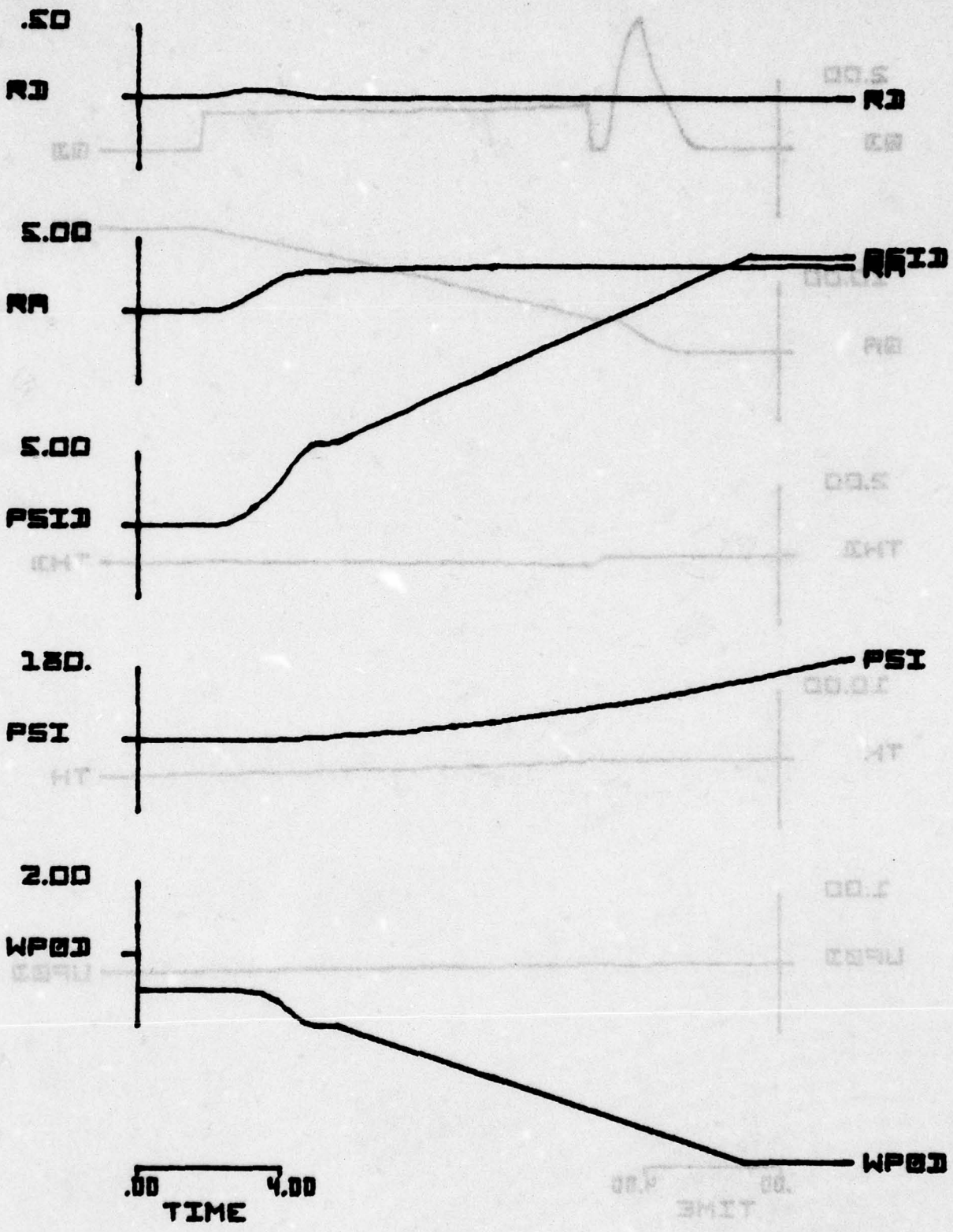

Figure 3. (Continued)

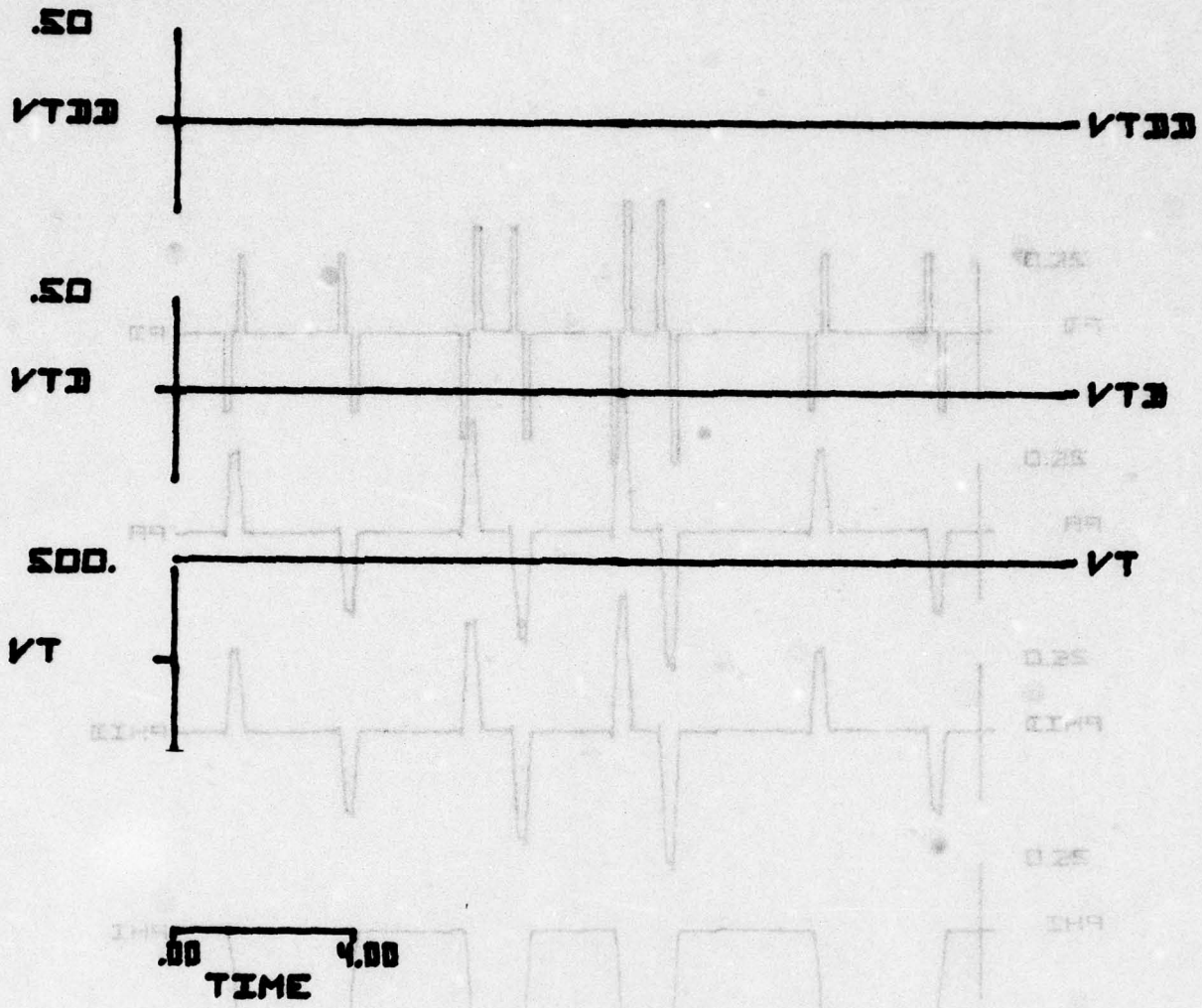

Figure 3. (Concluded)

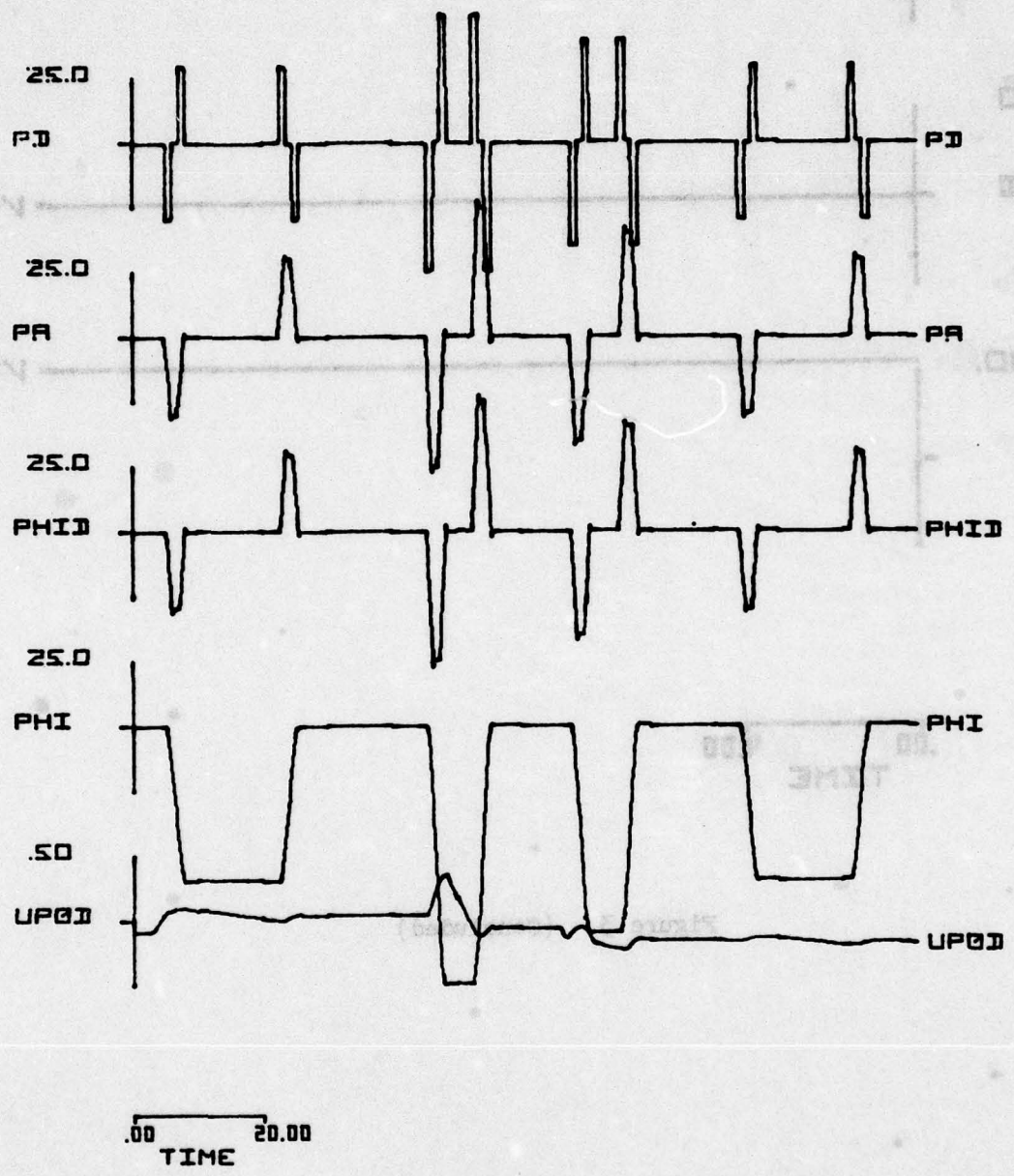

Figure 4. Scenario 4, A/G

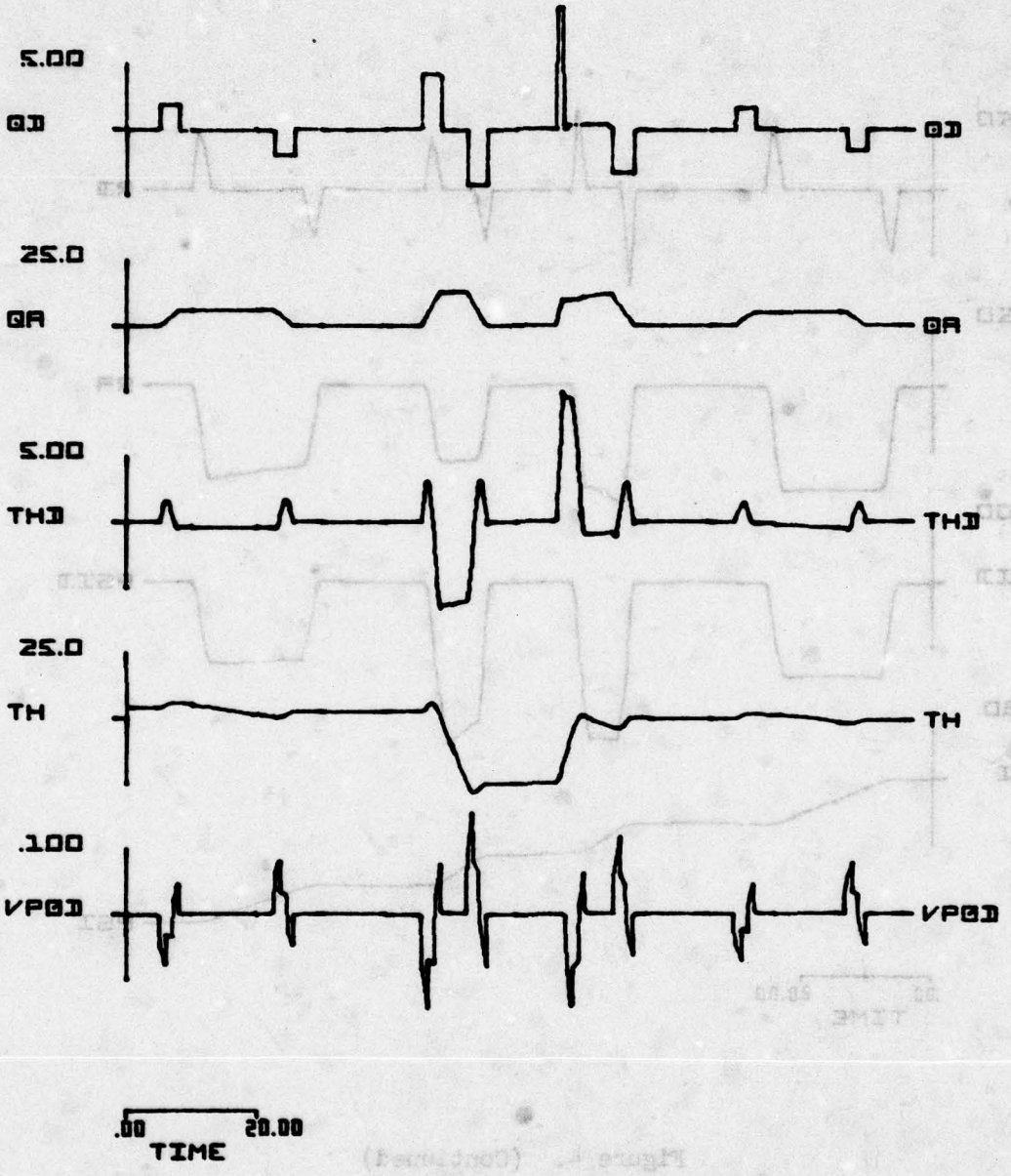

Figure 4. (Continued)

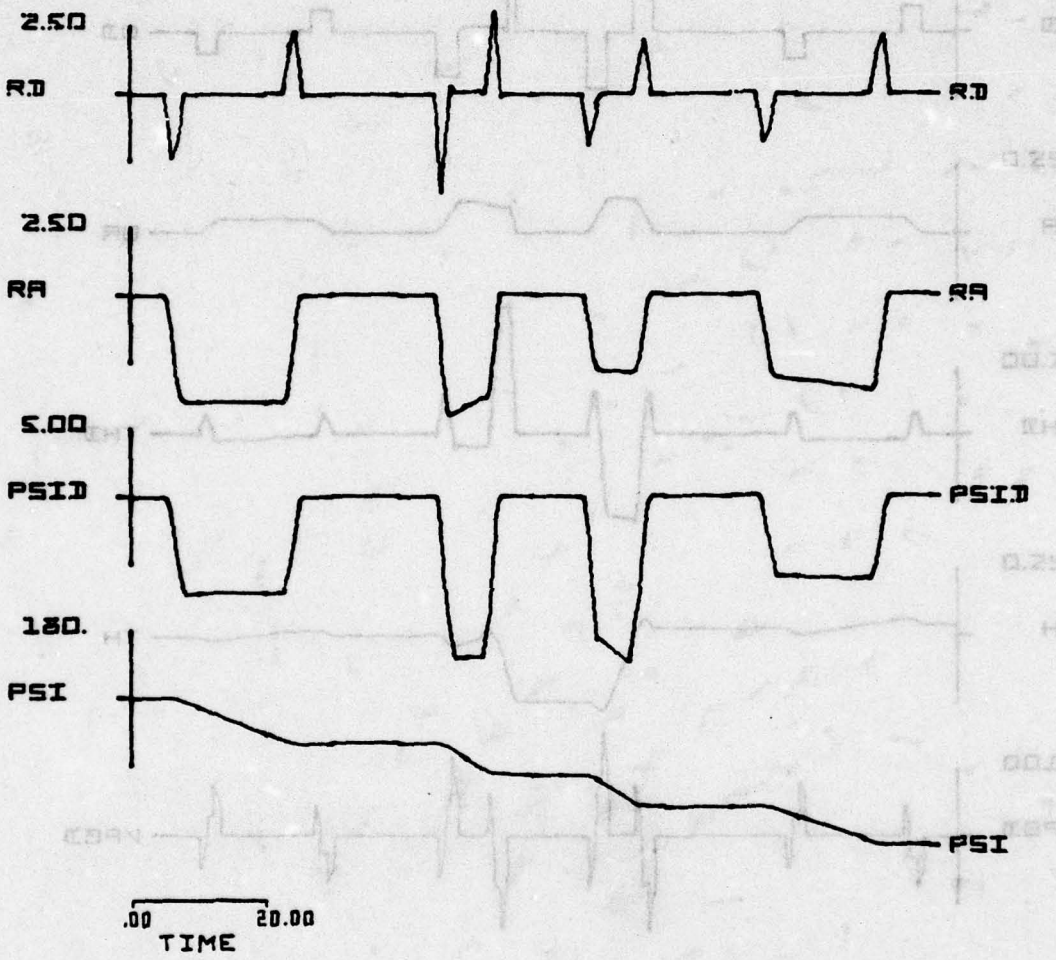

Figure 4. (Continued)

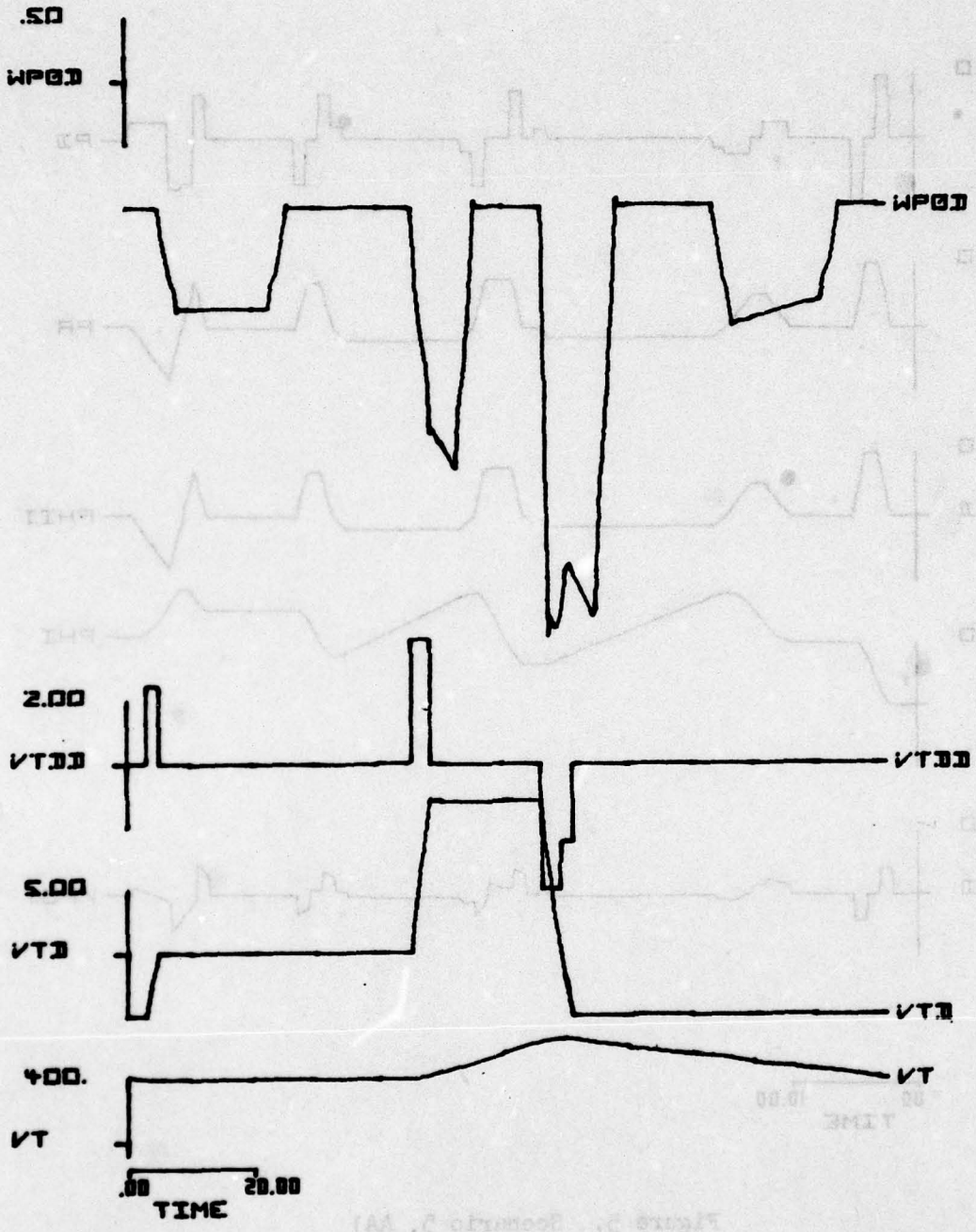

Figure 4. (Concluded)

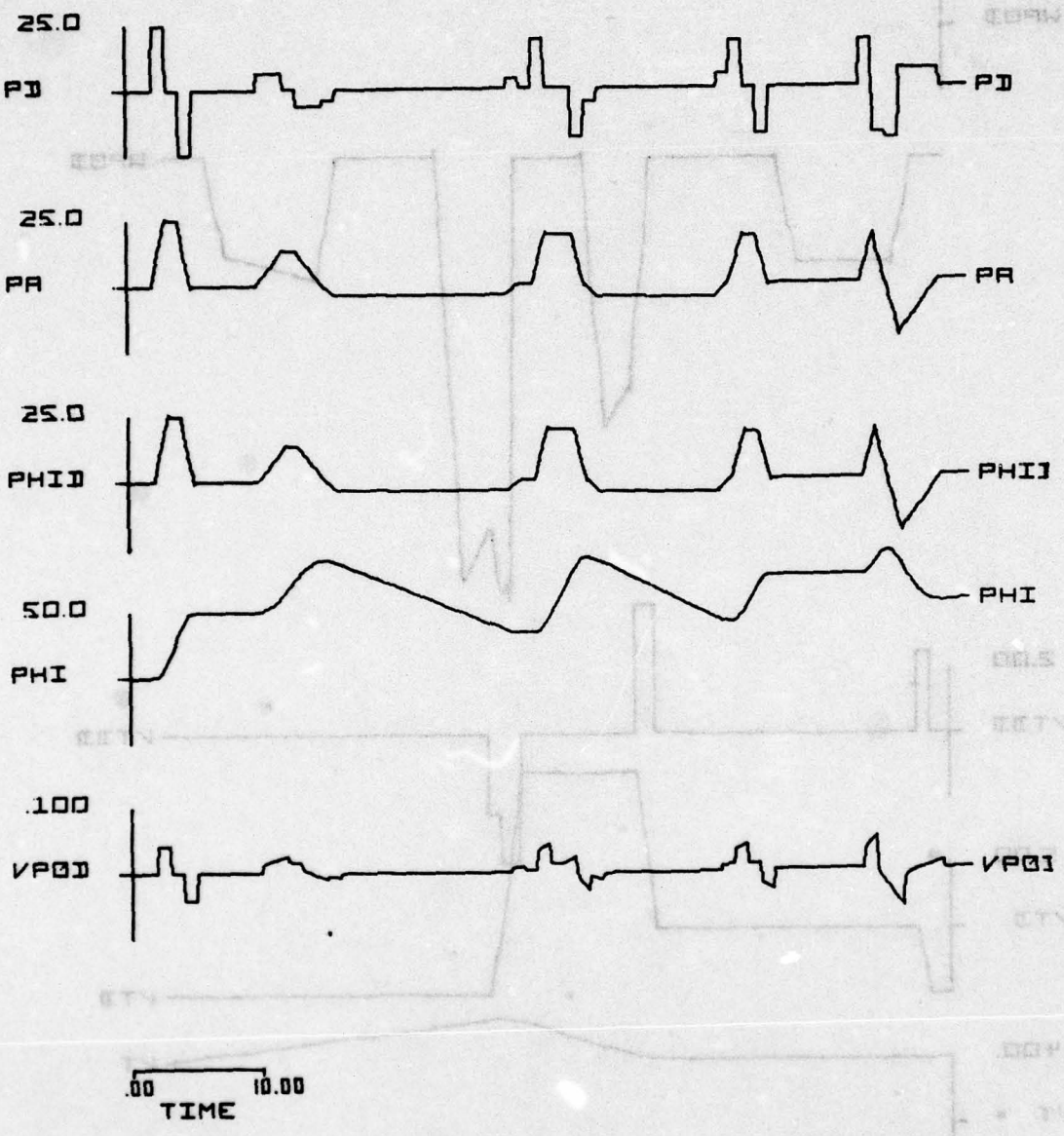

Figure 5. Scenario 5, AA1

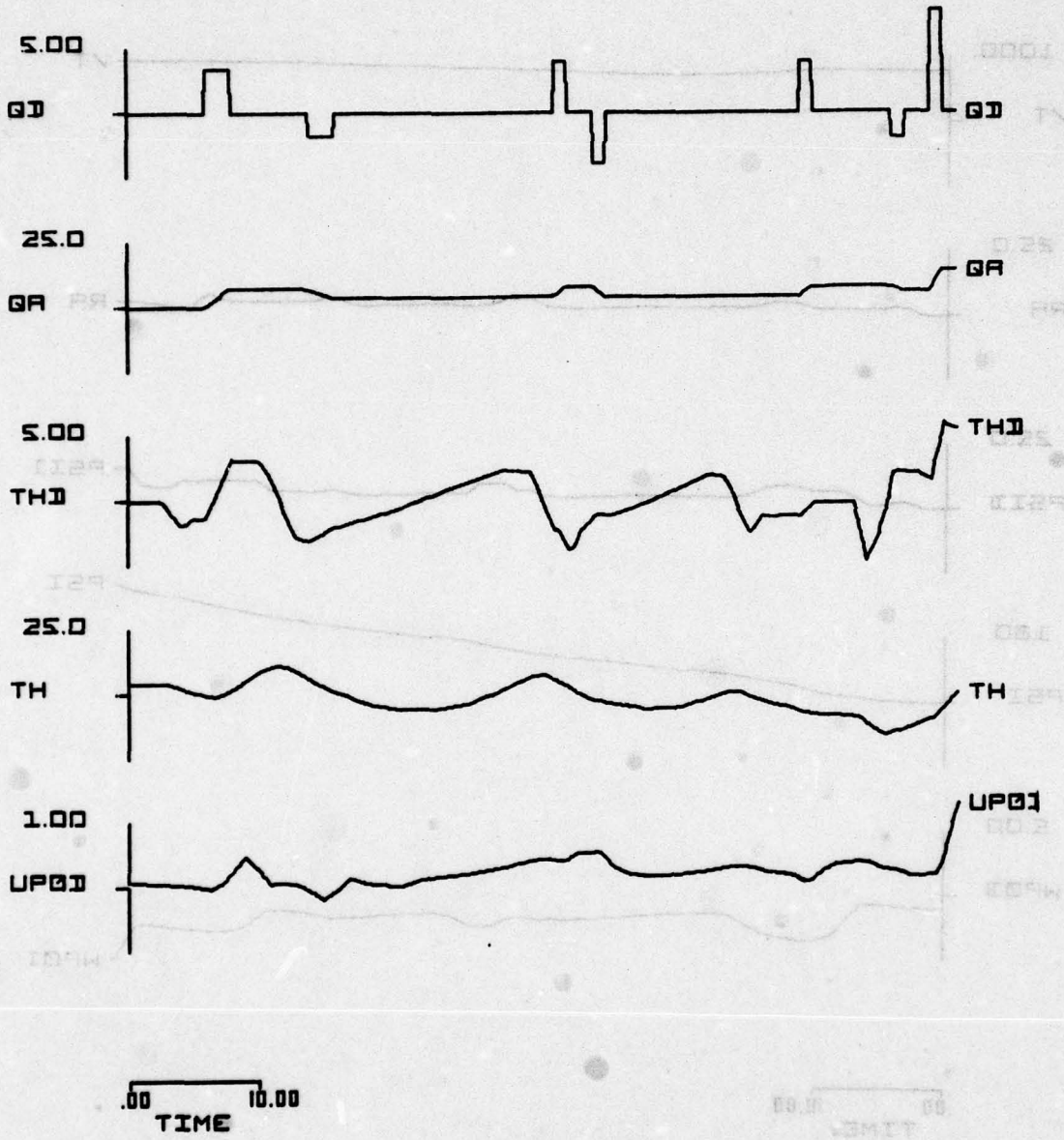

Figure 5. (Continued)

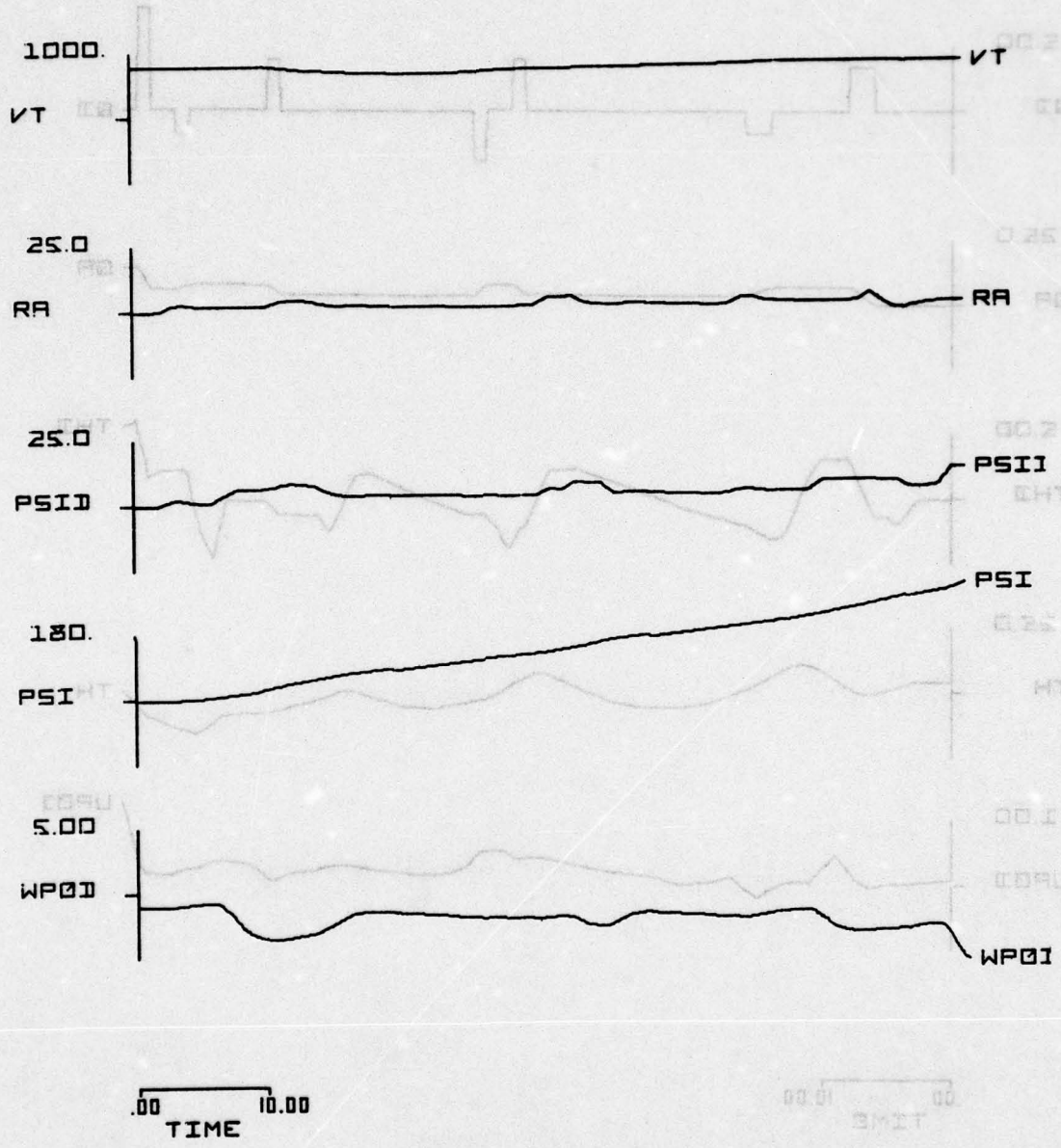

Figure 5. (Continued)

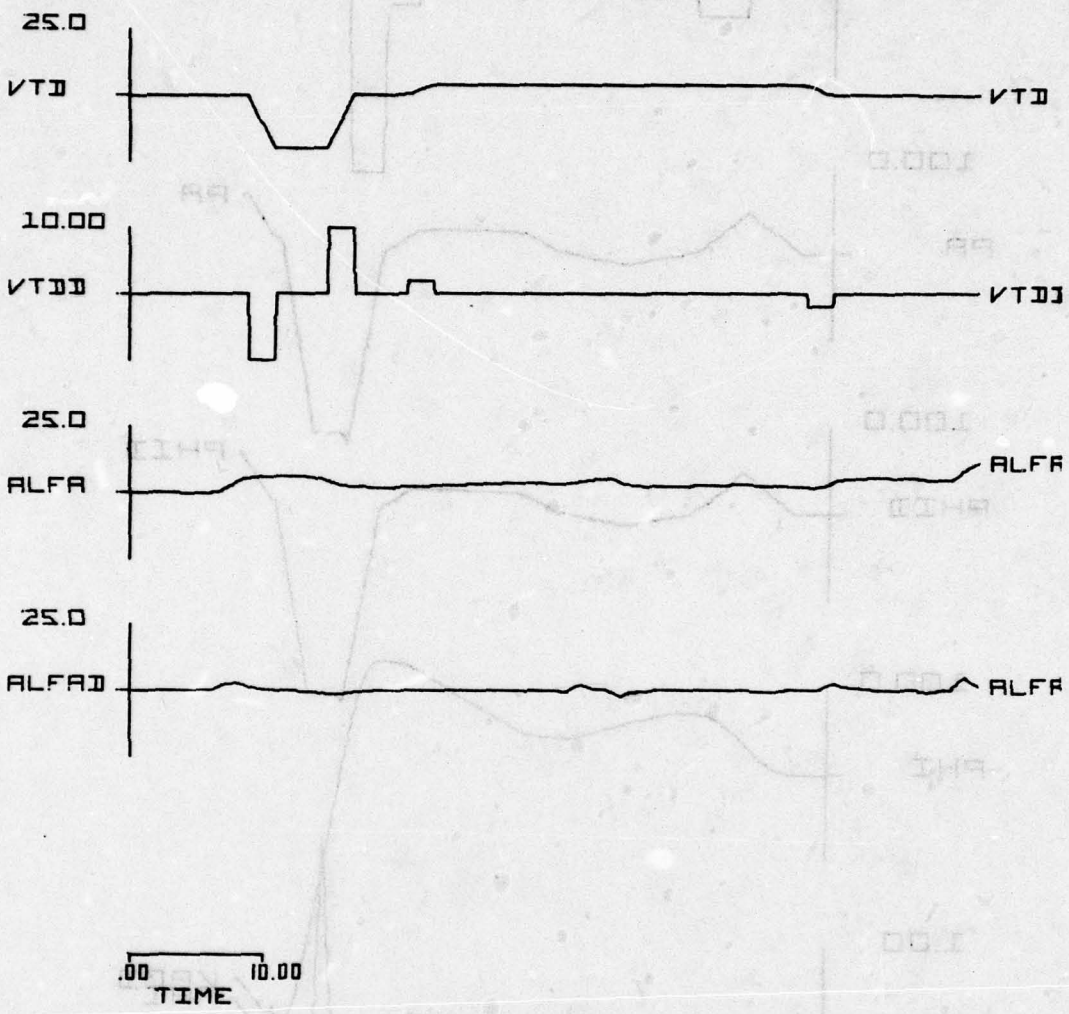

Figure 5. (Concluded)

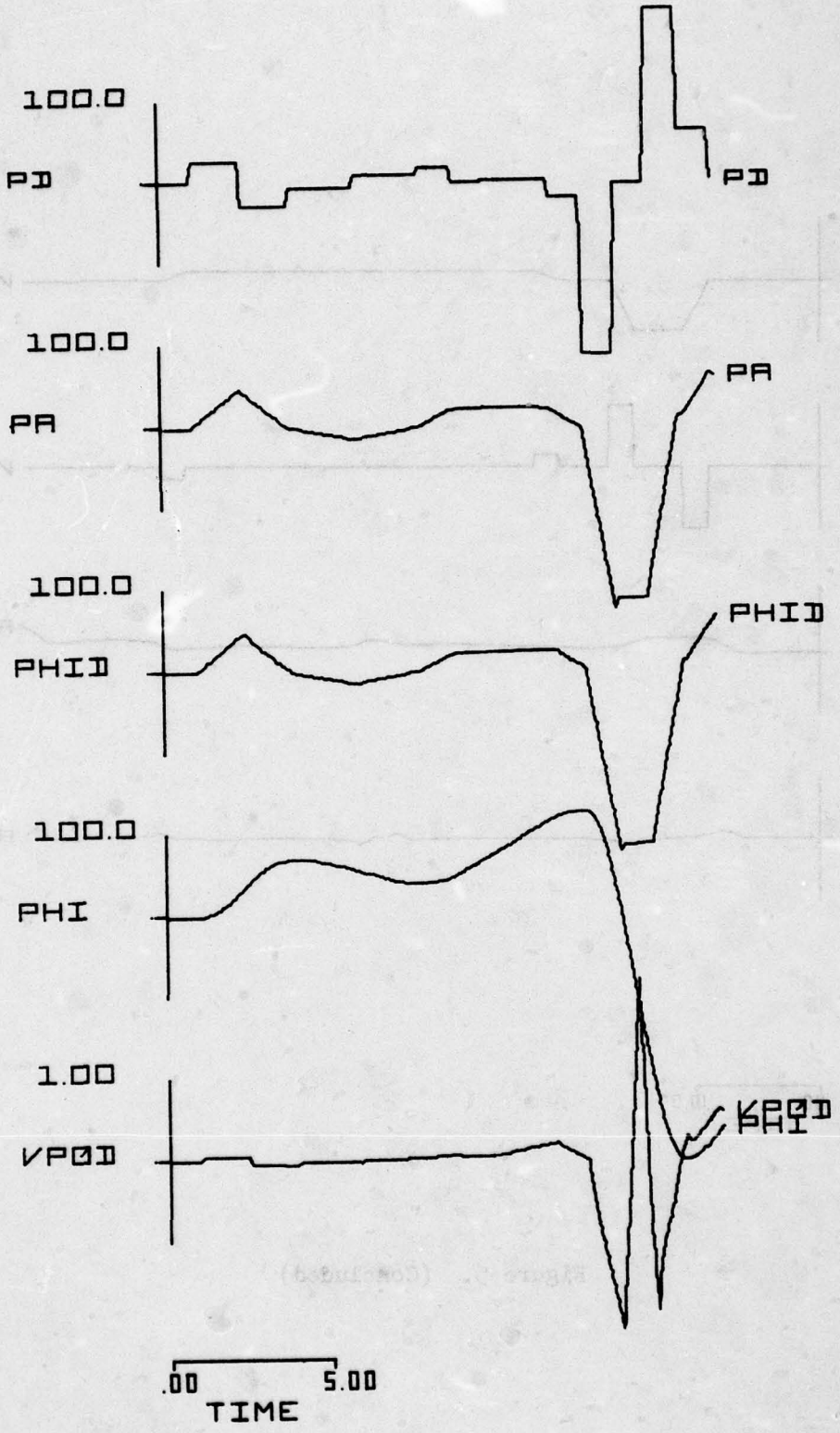

Figure 6. Scenario 6, AA2

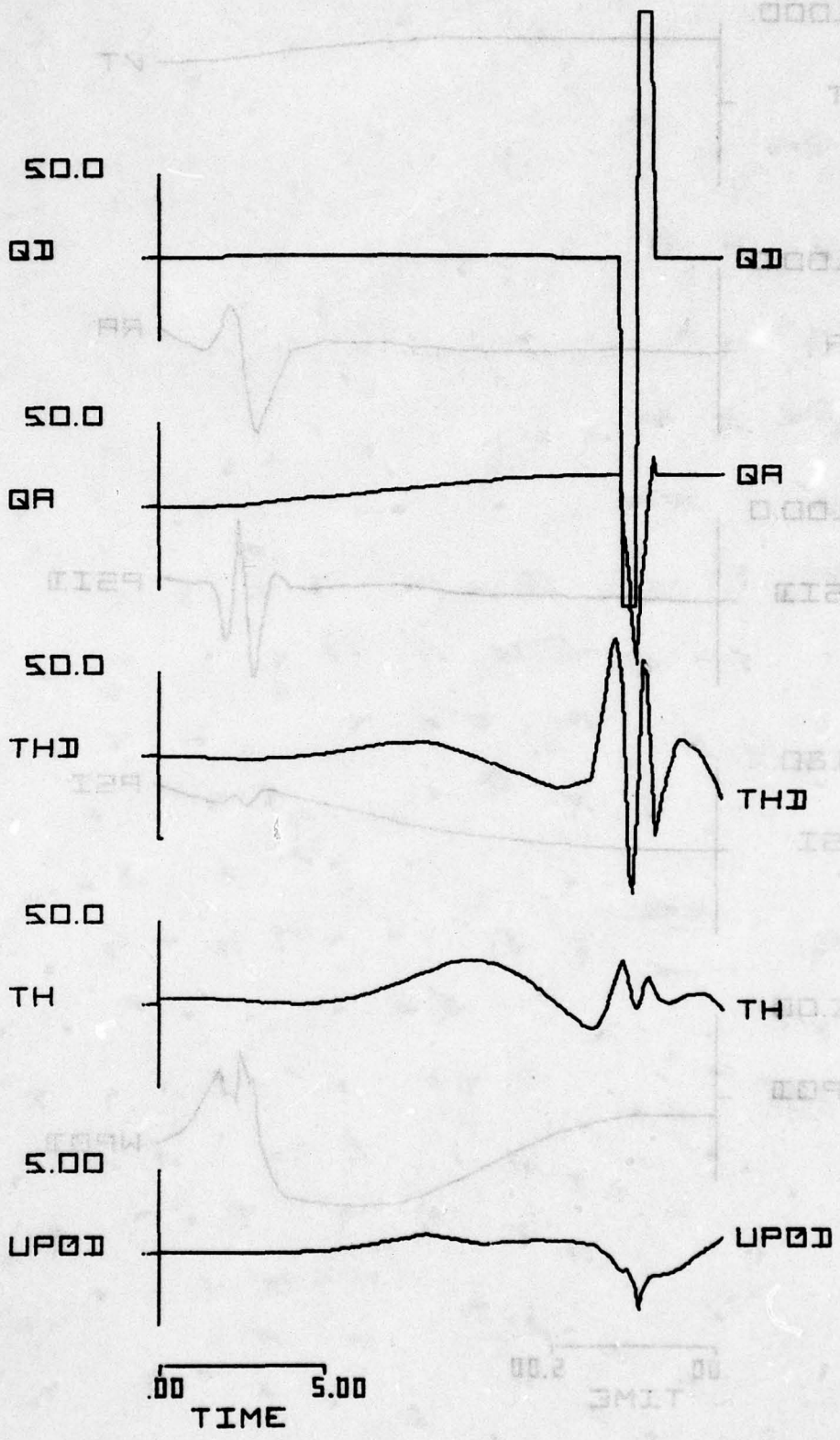

Figure 6. (Continued)

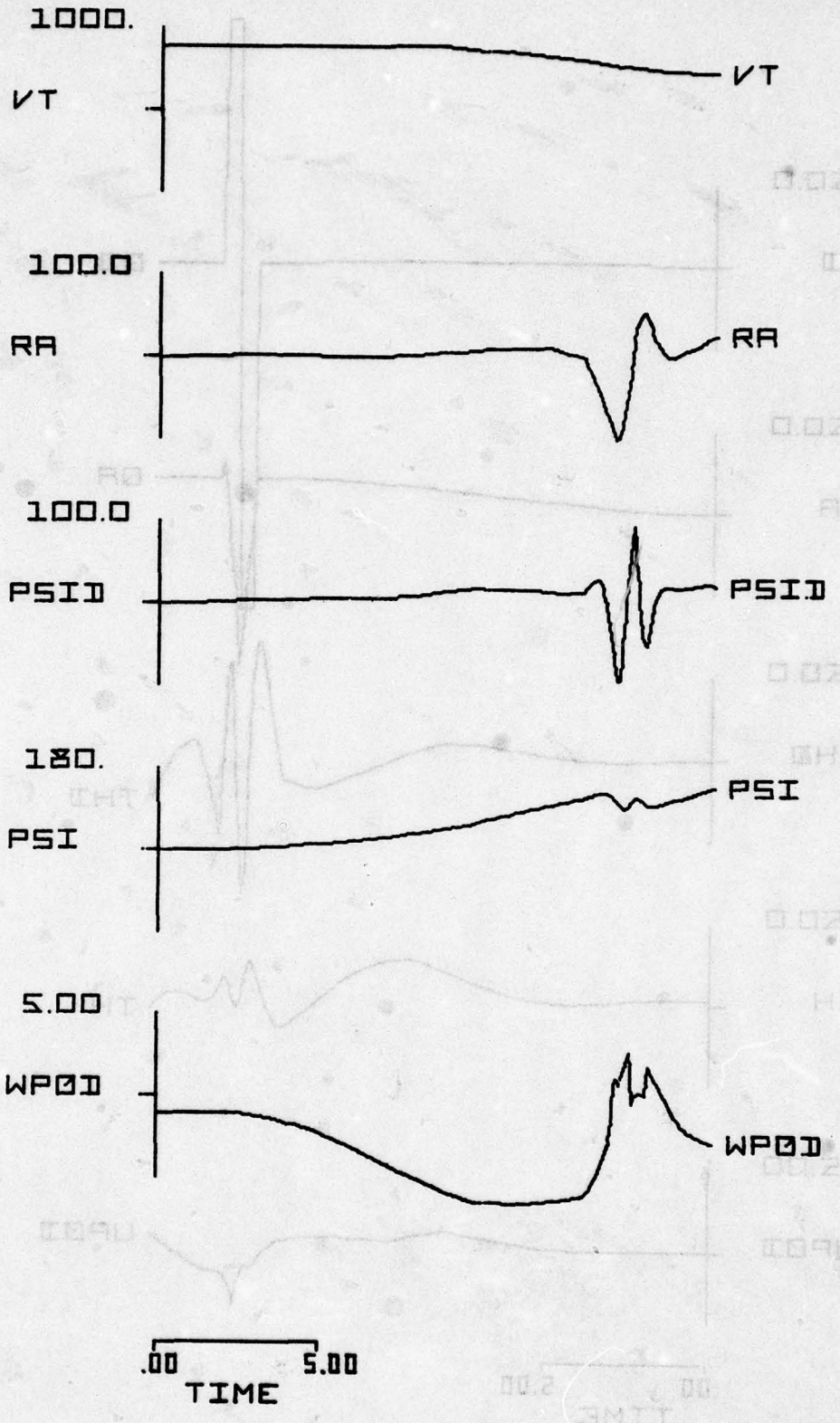

Figure 6. (Continued)

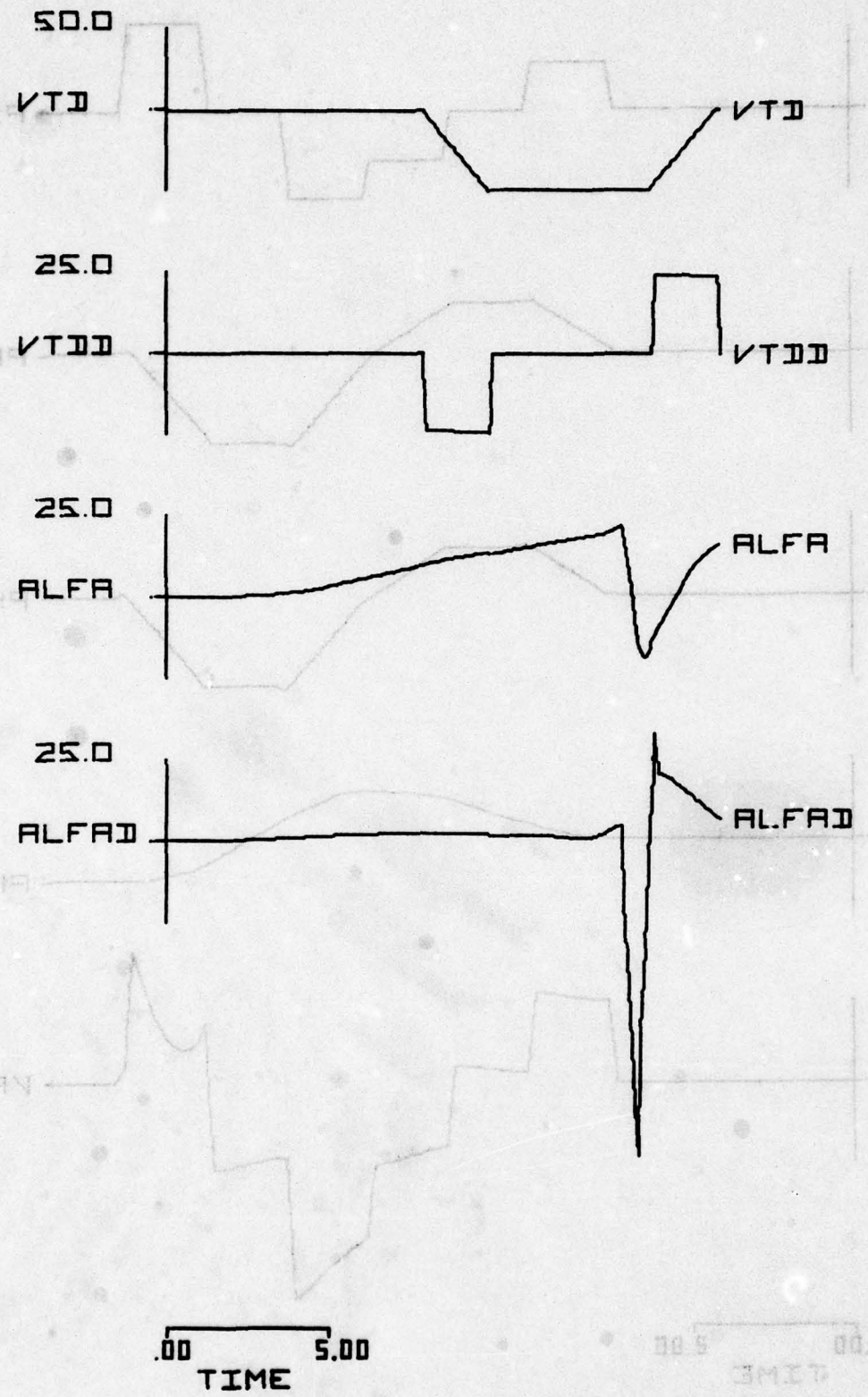

Figure 6. (Concluded)

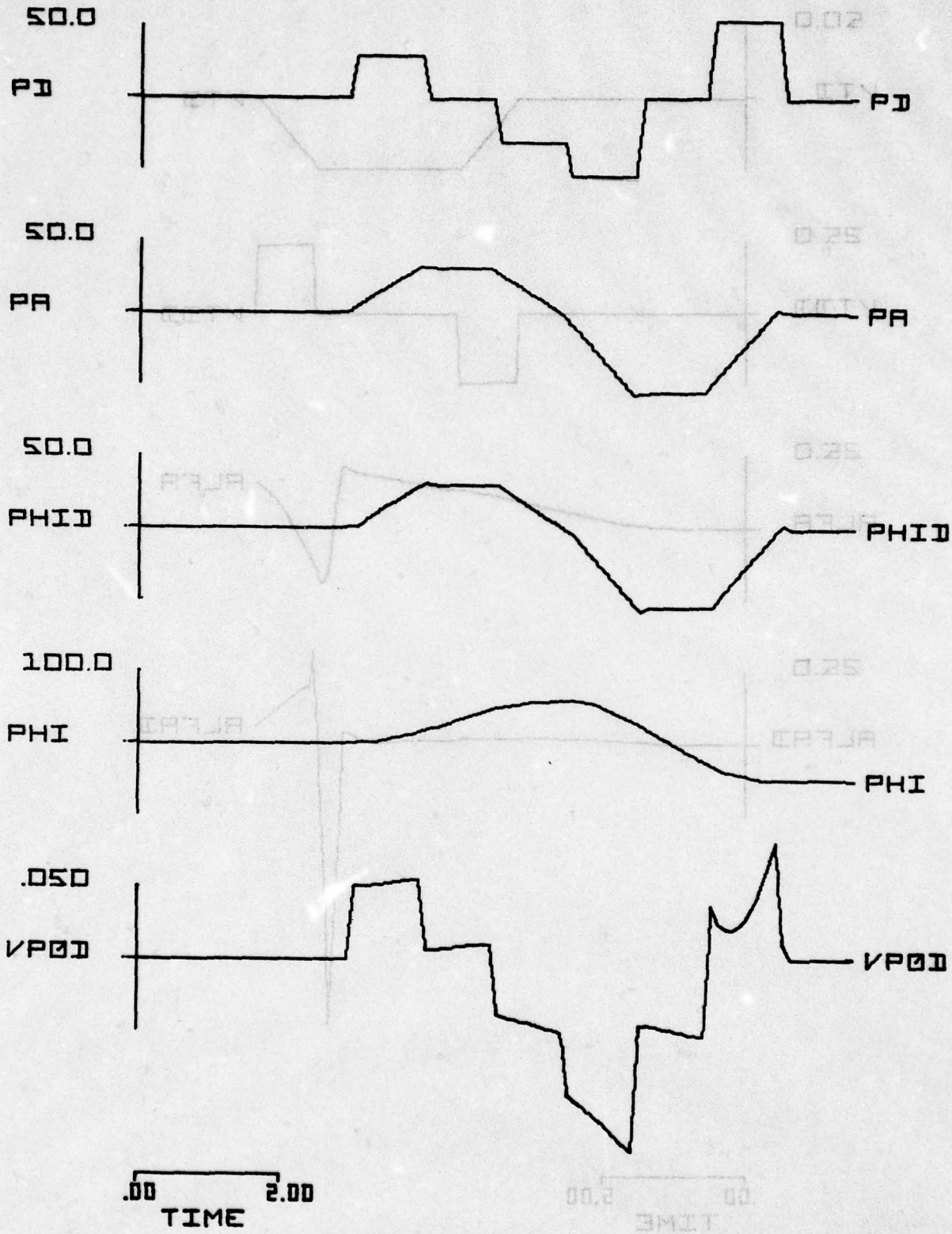

Figure 7. Scenario 7, AA3

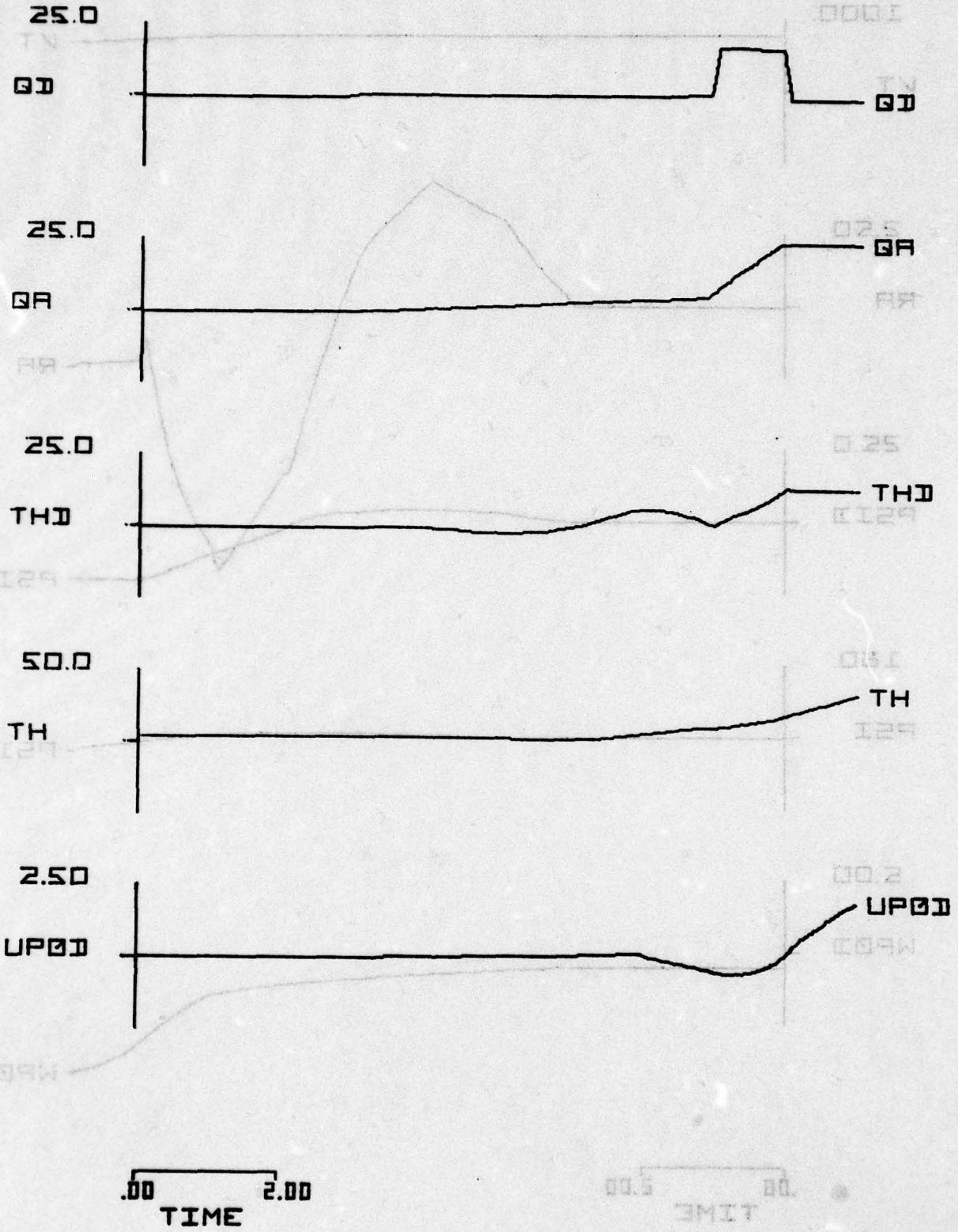

Figure 7. (Continued)

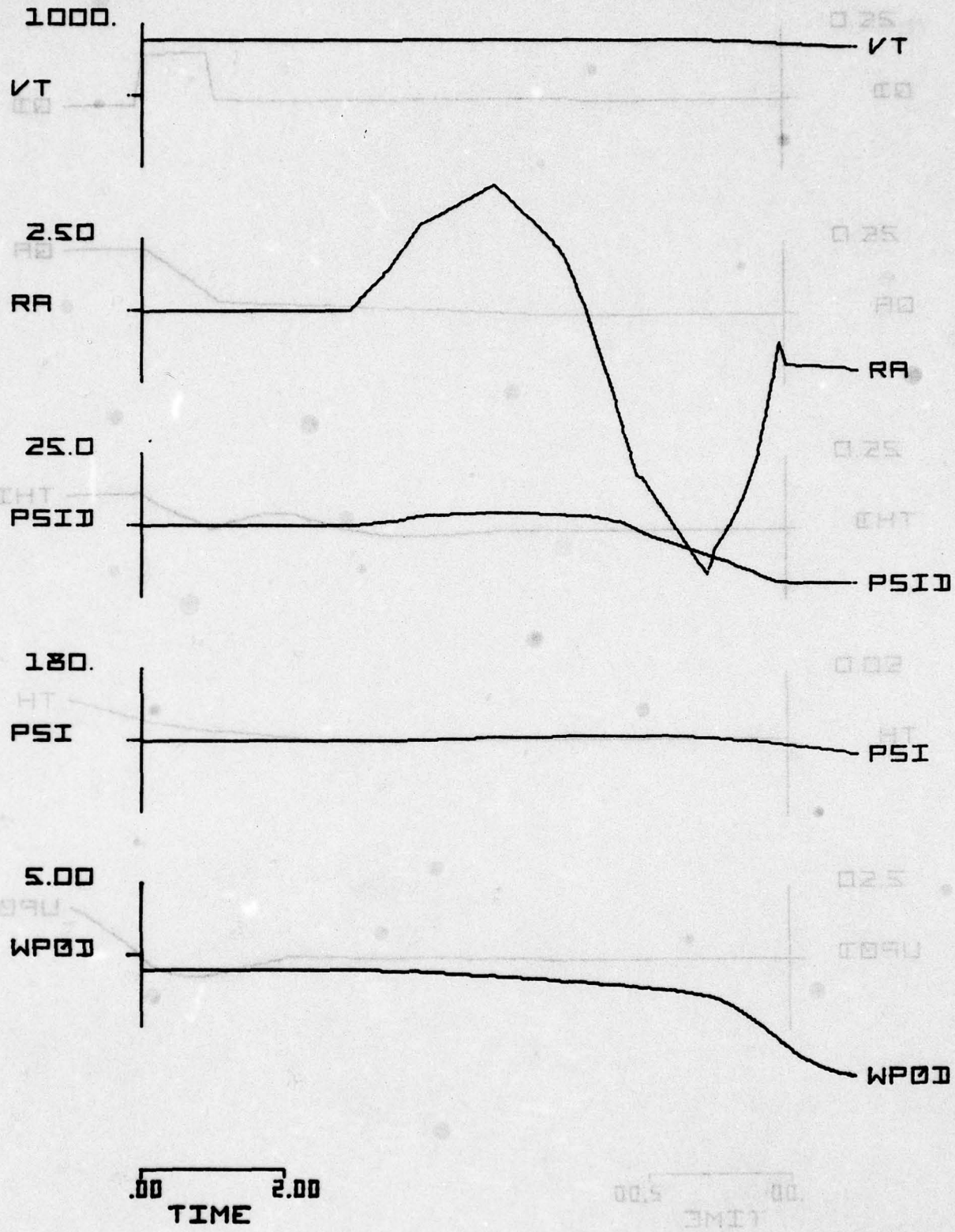

Figure 7. (Continued)

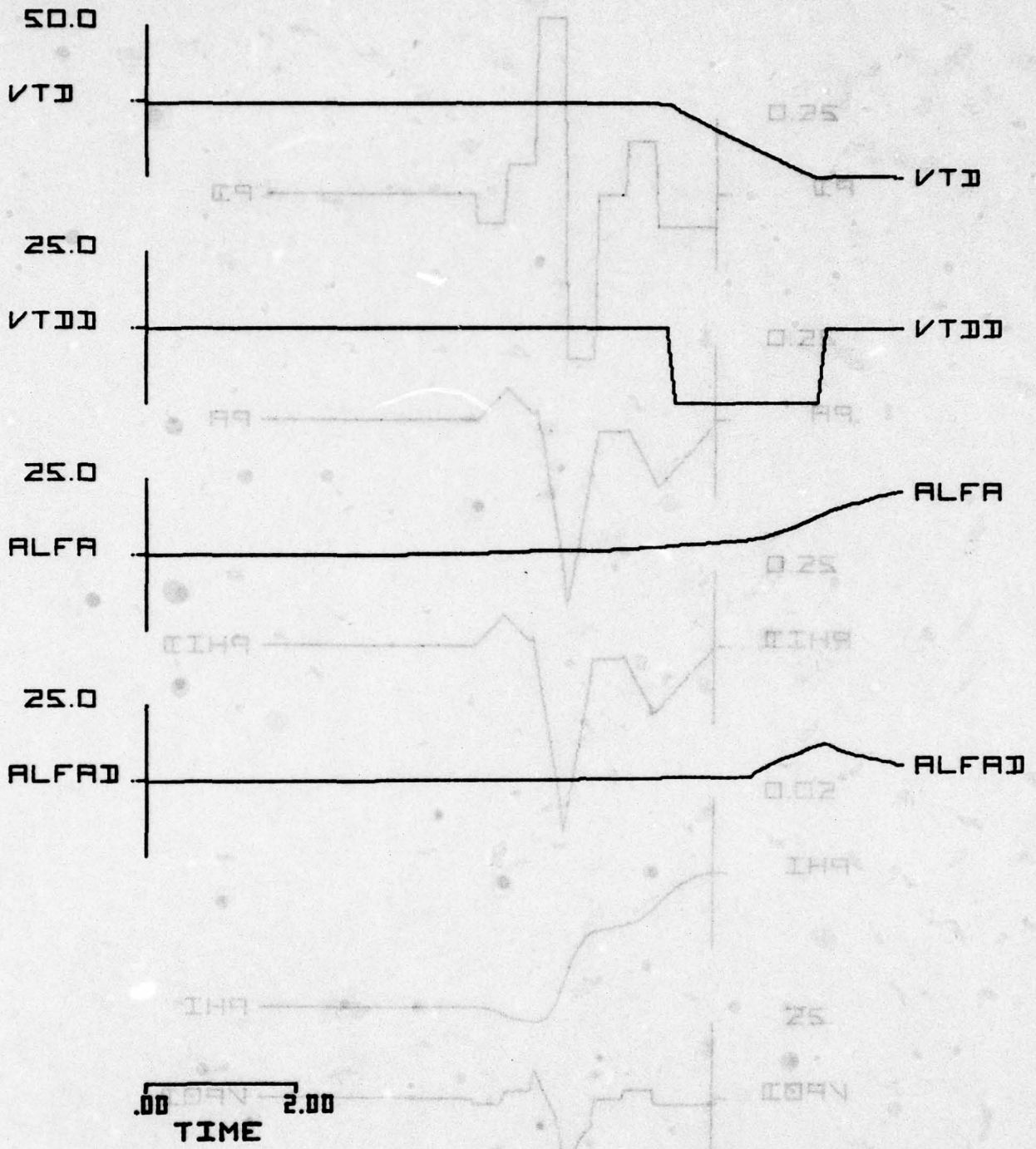

Figure 7. (Concluded)

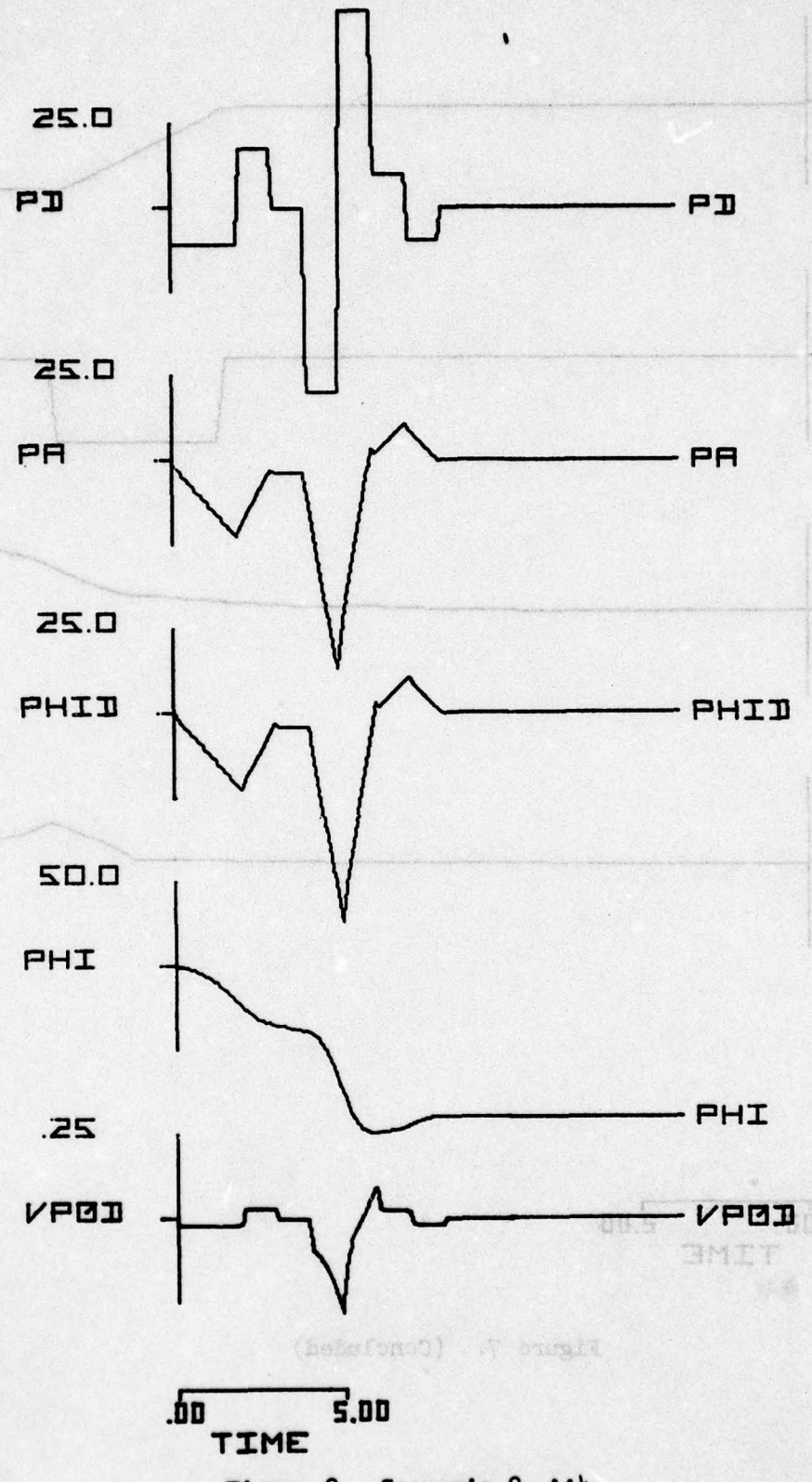

Figure 8. Scenario 8, AA4

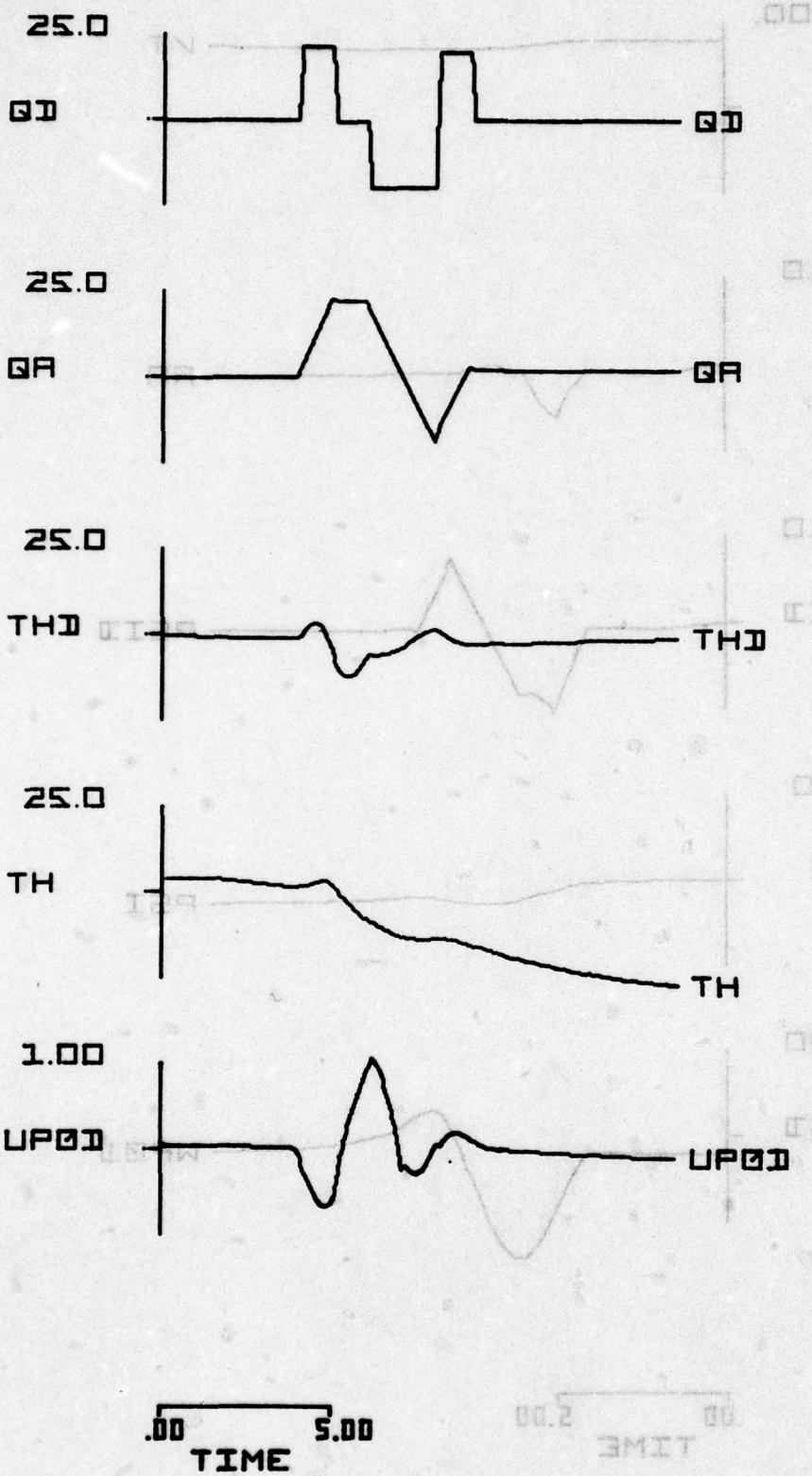

Figure 8. (Continued)

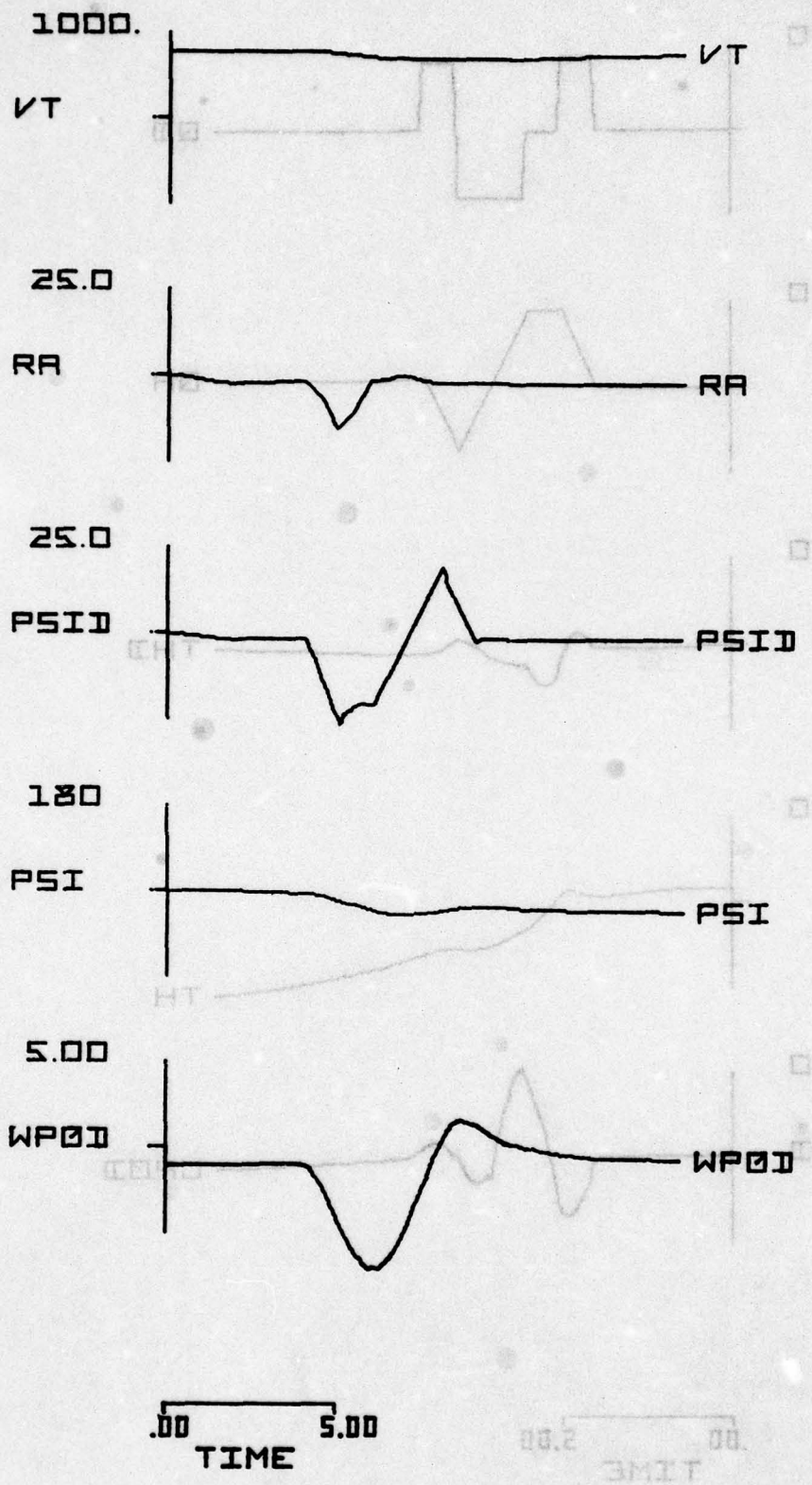

Figure 8. (Continued)

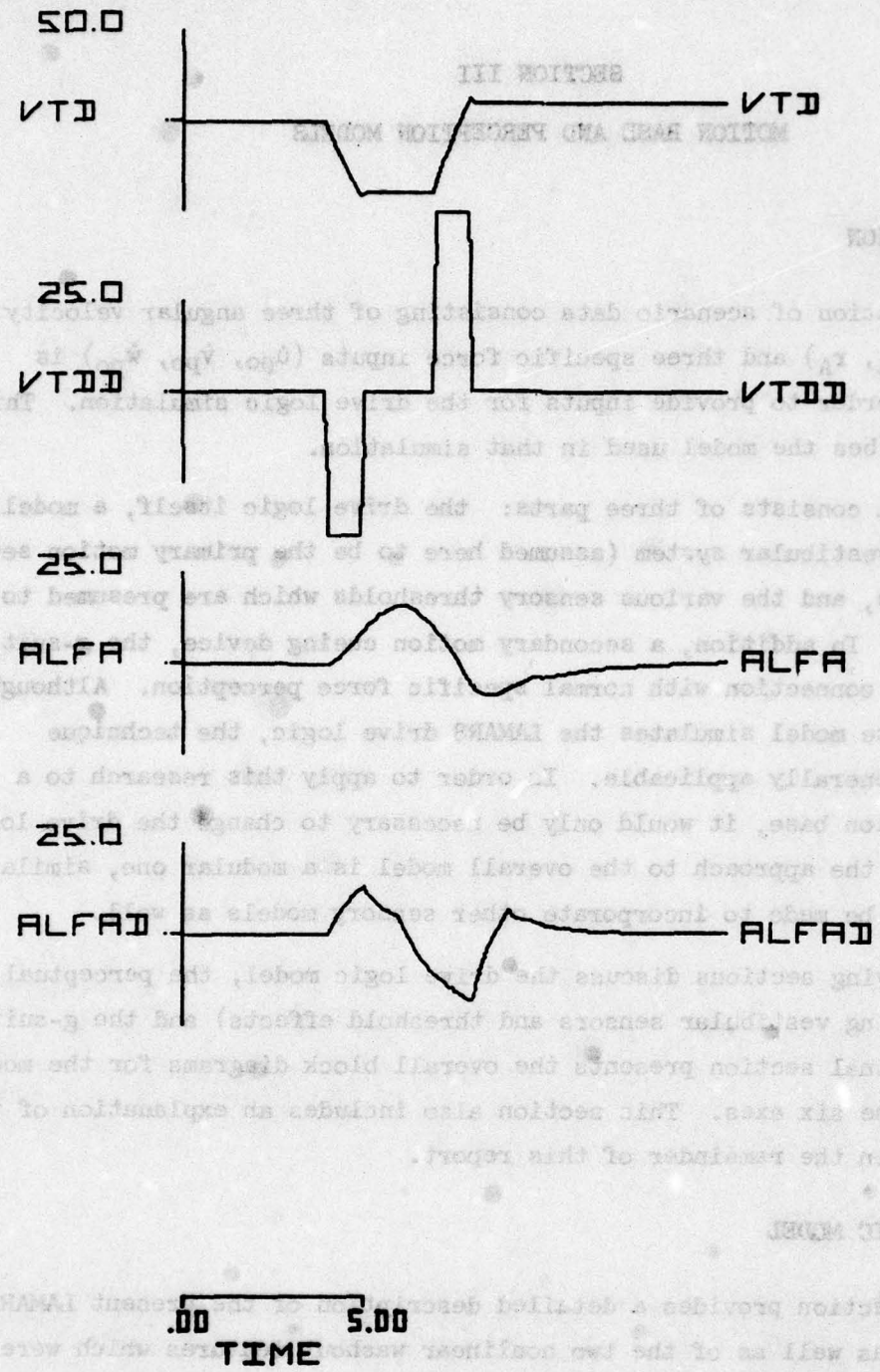

Figure 8. (Concluded)

SECTION III

MOTION BASE AND PERCEPTION MODELS

A. INTRODUCTION

The generation of scenario data consisting of three angular velocity inputs (p_A, q_A, r_A) and three specific force inputs ($\dot{u}_{po}$, $\dot{v}_{po}$, $\dot{w}_{po}$) is necessary in order to provide inputs for the drive logic simulation. This section describes the model used in that simulation.

This model consists of three parts: the drive logic itself, a model of the human vestibular system (assumed here to be the primary motion sensing apparatus), and the various sensory thresholds which are presumed to be operative. In addition, a secondary motion cueing device, the g-suit, is modeled in connection with normal specific force perception. Although the motion base model simulates the LAMARS drive logic, the technique employed is generally applicable. In order to apply this research to a different motion base, it would only be necessary to change the drive logic model. Since the approach to the overall model is a modular one, similar changes could be made to incorporate other sensory models as well.

The following sections discuss the drive logic model, the perceptual model (including vestibular sensors and threshold effects) and the g-suit model. The final section presents the overall block diagrams for the models, for each of the six axes. This section also includes an explanation of the symbols used in the remainder of this report.

B. DRIVE LOGIC MODEL

This subsection provides a detailed description of the present LAMARS drive logic, as well as of the two nonlinear washout features which were incorporated for investigation.

The function of the drive logic is to compute the actuator commands for each axis of the motion base from the angular velocity and specific force commands produced by the aircraft equations of motion. Additionally, the drive logic must provide limiting to prevent the motion base from hitting

the hard stops imposed by the physical travel limits of the simulator. The latter is accomplished by the combination of washout filters and limiting computations. Limiting computations are not considered in this research program.

There are two distinct methods for computing the drive commands for each axis: the crossfeed scheme (Ref. 3) and the crossproduct scheme (Ref. 4). These are illustrated in Fig. 9, which presents simplified linearized block diagrams for roll-sway axis implementation for each scheme. The crossfeed scheme was designed by Bray for implementation on the Flight Simulator for Advanced Aircraft (FSAA) motion base. The crossproduct scheme was designed by Schmidt and Conrad; it forms the basis for the LAMARS drive logic.

The purpose of these two different washout implementations is the same. In order to provide an accurate set of motion cues to the simulator pilot, it is necessary to coordinate roll and sway axis motions and pitch and surge axis motions. The coordination causes an angular command in roll or pitch to also induce a sway or surge acceleration of the motion base as well. This assures that no spurious lateral or longitudinal specific force cues result from the gravitation vector when the simulator cab is tilted from vertical. To accomplish this coordination, the cab angular displacement, φ_m, for example, must be crosscoupled into the lateral specific force path. In order to simulate low frequency components of lateral or longitudinal specific force, components of gravitational force must be used. These components are obtained by tilting the simulator cab. The low frequency components of lateral specific force, for example, must be crosscoupled into the cab tilt (φ_m) path to accomplish this. These are the purposes of the two paths labeled "residual tilt path" and "coordinating path" in the block diagrams of Fig. 9.

Note, however, that the implementation of these coordinating paths is different for the two schemes. In the crossproduct scheme the residual tilt and coordinating paths form a closed loop. There are no closed loops in the crossfeed scheme, which provides the necessary coordination via open-loop crossfeeds. The following observations can thus be made:

- The closed-loop coordination of the crossproduct scheme provides an effective second-order washout filter in the angular velocity axis.

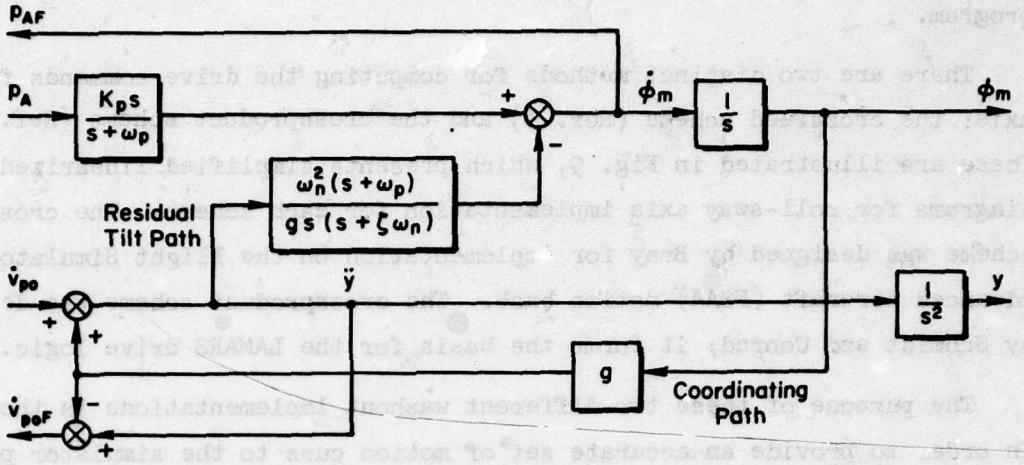

a) Crossproduct Scheme - Schmidt and Conrad - LAMARS

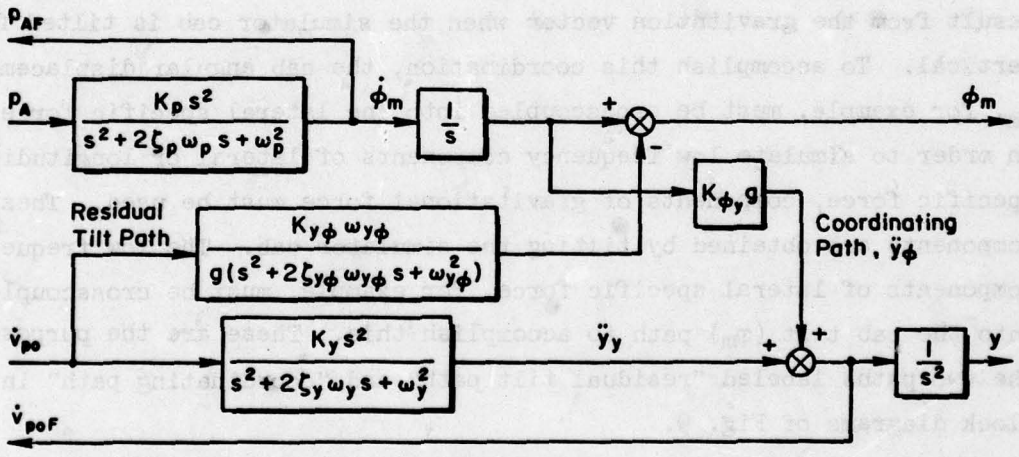

b) Crossfeed Scheme - Bray - FSAA

Figure 9. Basic Roll-Sway Axis Linear Washout Circuits

- The crossproduct scheme is designed to produce perfect recovery of specific force: the transfer function between $\dot{v}_{po}$ and $\dot{v}_{poF}$ is always 1.

- The crossfeed scheme provides a means for introducing deliberate miscoordination. This is accomplished by varying the coordinating path gain, K_{φ_y}.

The crossproduct scheme is the basis for the LAMARS drive logic. The washout filter parameters allow the simulator to be "tuned" to provide the most realistic motion cues available within the displacement, velocity and acceleration constraints of the motion base. The key parameters of the linear, second-order washouts used in the LAMARS scheme are the gain K_p and break frequency ω_n. Variation of the gain of the washout filter provides a method for attenuating the input signal, while variation of the break frequency determines the motion washout rate (Ref. 5).

In the course of this research, two additional nonlinear washout filters were investigated. Each of these adds a nonlinear computation to the underlying linear LAMARS drive logic. The first, the "Parrish" washout filter (Refs. 6, 7), was developed to eliminate the so-called false cue encountered in simulating pulse-type angular motions. This technique uses a cost function to vary the gain of the washout filter automatically. It provides an "optimum" gain for the filter at each point in time, based on a number of time-varying parameters (such as angular velocity and angular displacement). Figure 10a presents a block diagram of the Parrish filter as implemented for an angular velocity axis. The investigation of this technique examined its use in the roll axis only, since results from Parrish's manned simulation (Ref. 8) indicate that it is most effective in that axis. Detailed information on the Parrish washout filter is in Refs. 6-9.

The second scheme, the "subliminal" washout, was developed in this research program (Refs. 10 and 11). It, too, builds on the underlying linear LAMARS drive logic. This scheme employs two nonlinear functions which increase the effective washout rate of the drive logic whenever the input is below a specified "indifference threshold" level. It has been observed by several researchers that a level of angular velocity or specific force cues exist, such that cues which fall below this level are not sensed by a pilot under normal workload conditions. This "indifference" threshold

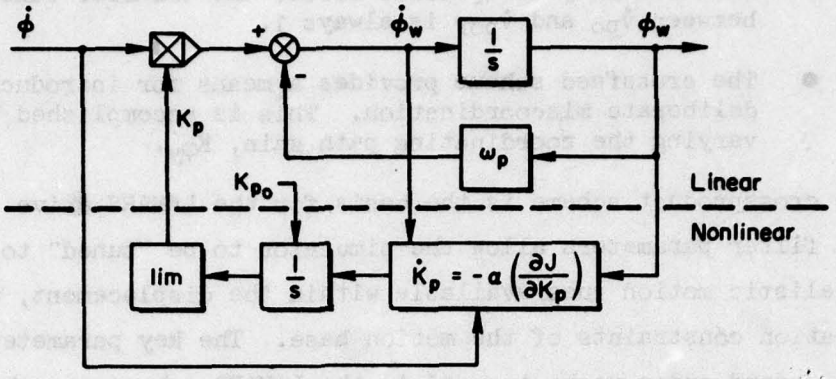

$$\dot{\phi}_\omega = K_p\,\dot{\phi} - \omega_p\,\phi_\omega$$

$$\dot{K}_p = -\alpha\,(\partial J/\partial K_p)$$

$$J = 1/2\left[(\dot{\phi} - \dot{\phi}_\omega)^2 + C_\phi\,\phi_\omega^2 + C_k\,(K_p - K_{p_o})^2\right]$$

a) Parrish Adaptive Gain Scheme

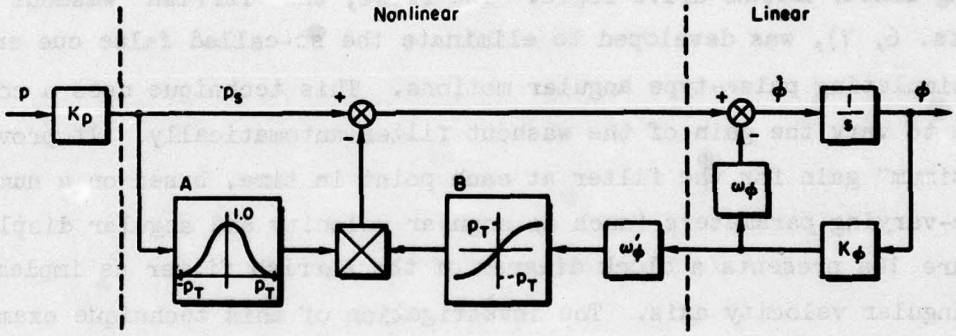

p = Input Angular Velocity

p_s = Scaled Angular Velocity

p_T = Indifference Threshold Level

$\dot{\phi}$ = Commanded Cab Roll Rate

ϕ = Commanded Cab Roll Angle

b) Subliminal Washout Scheme (first order washout)

Figure 10. Two Nonlinear Washout Schemes

is exploited in the subliminal scheme. It provides justification for deliberately introducing translational miscoordination to reduce the sway displacement required. Figure 10b presents a block diagram for implementation of this subliminal scheme for an angular velocity axis. The subliminal scheme was included in the sway axis only, in this investigation, although it can be applied for both sway and surge translational axes. Figure 11 depicts the roll-sway axes for the LAMARS drive logic with both nonlinear schemes included. Further details of the subliminal washout are presented in Appendix B.

C. PERCEPTUAL MODEL

One set of outputs from the simulation is the drive logic commands to the physical motion base actuators. These consist of position commands to any or all of the simulator's axes. A second set of outputs consists of the motion cues presumed to be sensed by the pilot. These include angular velocities and specific forces as appropriate to the six motion axes. In order to include the pilot in the overall simulation of the LAMARS, it is necessary to model the sensory apparatus which enables the pilot to perceive his orientation. This perceptual submodel is the subject of this section.

The vestibular apparatus in the inner ear is the primary sensor of angular velocities and specific forces to be modeled here (Refs. 12-17). The vestibular system is comprised of the semi-circular canals and the otoliths. Each inner ear contains three canals, oriented in an approximately orthogonal axis system. These organs are the angular velocity sensors and are modeled, according to their physical properties, as heavily damped angular accelerometers. A schematic drawing of a set of canals and the accompanying mathematical model relating sensed angular velocity to input angular velocity is given in Fig. 12.

The otoliths are the other sensory organs in the vestibular system (Ref. 18). Each inner ear contains two otolith organs: the saccule is located in an approximately vertical plane, while the utricle is located in a plane inclined approximately 25 deg from the head upright horizontal plane. The otoliths are the principle specific force sensors in the vestibular system. The physical properties of the otoliths are less well defined

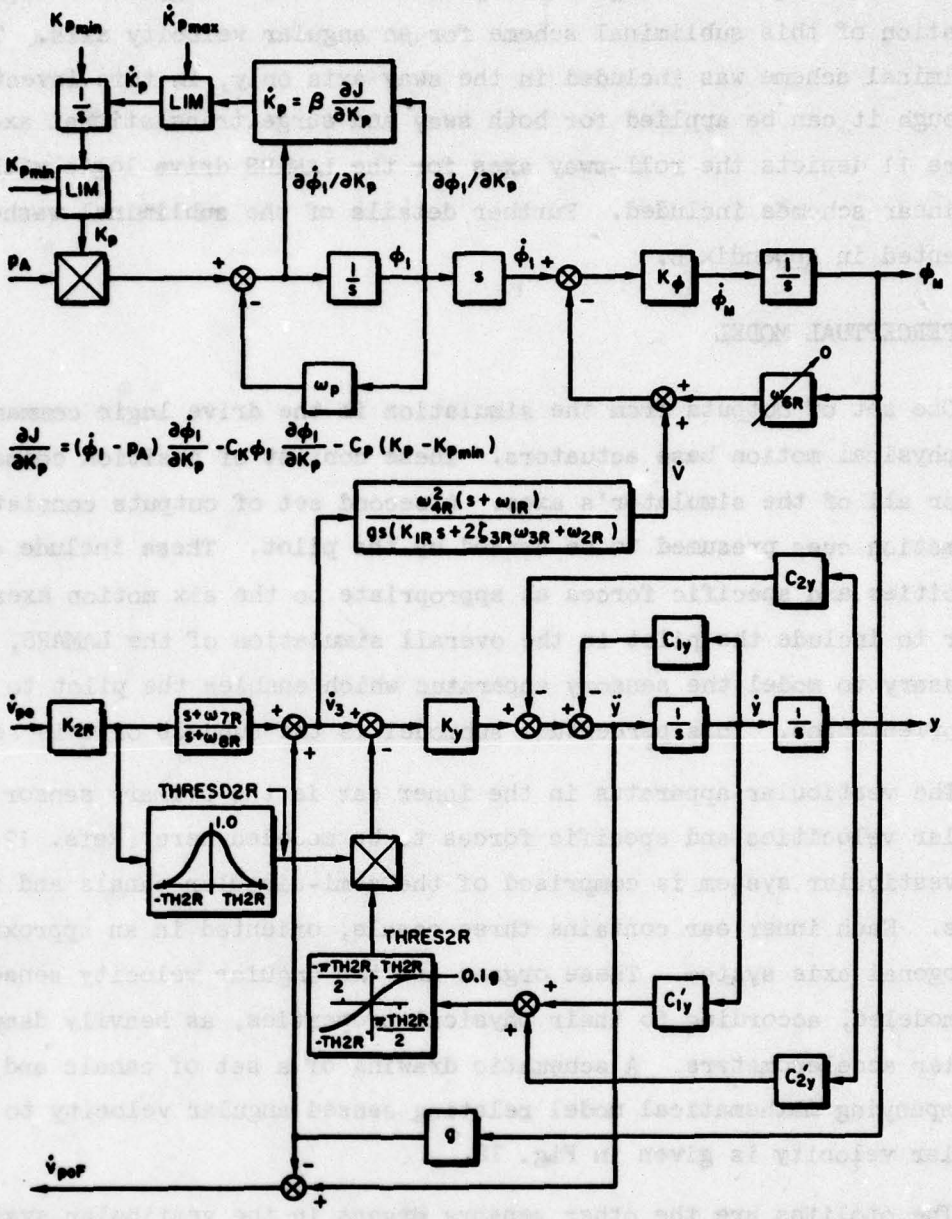

Figure 11. LAMARS Drive Logic with Nonlinear Washouts

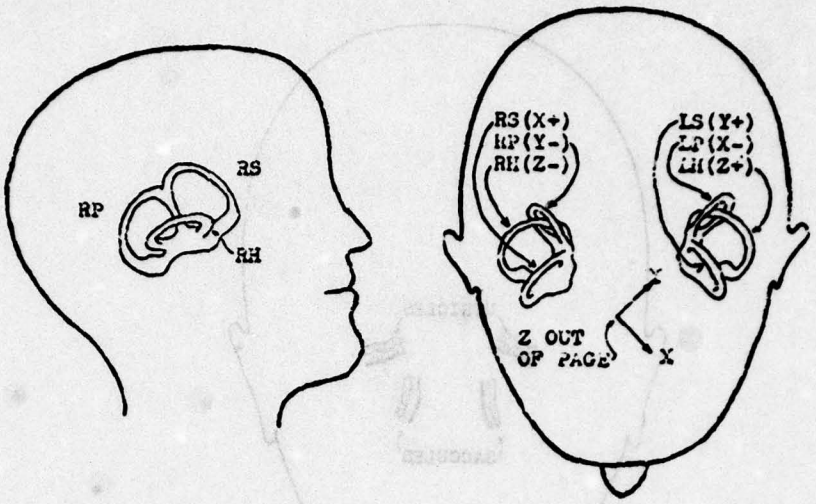

$$\frac{\text{perceived angular velocity}}{\text{input angular velocity}} = \frac{10s}{(s+.2)(s+10)} \text{ , for each axis of sensitivity}$$

Figure 12. Semi-Circular Canal Model
(After Ormsby, Ref. 14)

than the properties of the semi-circular canals. The mathematical model used here, however, accounts for a major portion of the experimentally validated observations of otolithic function. A schematic drawing of the otoliths is shown in Fig. 13. The mathematical model used to compute sensed specific force from input specific force is also included in Fig. 13.

Threshold effects are important in modeling sensory processes. Given a threshold effect, it is assumed that motions whose magnitudes fall below the threshold level will not be perceived by the pilot. There are two types of thresholds modeled here. The first is a sensory threshold; it arises from physical limitations of the organ itself. This threshold type is evident for the semi-circular canals — they are unable to sense angular velocities of magnitude less than .035 rad/sec (Ref. 15).

The second type of threshold is the "indifference" threshold, mentioned previously in connection with the subliminal washout scheme. This threshold type is evident for specific force sensing. Under normal workload, pilots are unable to detect specific forces of magnitude less than approximately 0.1 g (Ref. 20). It is important to note the phrase "under normal workload" in discussions of indifference thresholds. If a subject is asked to concentrate on determining when the sensation of specific force begins, the

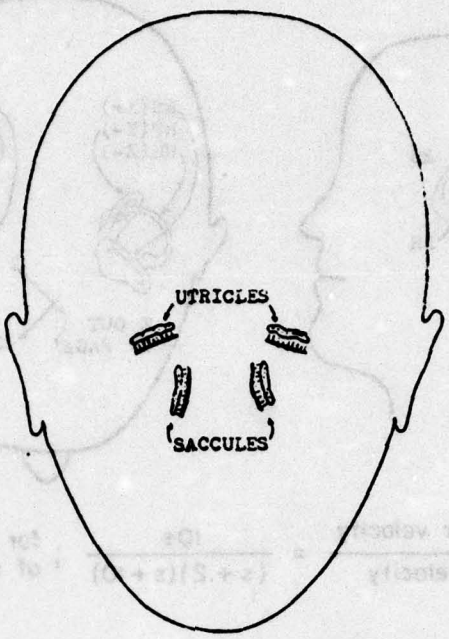

$$\frac{\text{perceived specific force}}{\text{input specific force}} = \frac{10(s+.08)}{(s+.2)(s+10)}$$

Figure 13. Otolith Model
(After Ormsby, Ref. 14)

sensory threshold is found to be approximately 0.005 g (e.g., Ref. 15) — the otoliths are very sensitive to stimulation. If the subject is given a task to perform in addition to indicating the onset of a specific force, this "indifference" threshold is found to be much higher than the sensory threshold — approximately 0.1 g, as stated above. In the simulation of actual flight scenarios, it is assumed that the indifference threshold will be operative, since the pilot's primary task will not be mere detection of the motion cues, but rather an actual flying task. The indifference threshold may be visualized not as a sensory limitation but as the result of an information processing allocation decision made in the central nervous system to weight the primary tasks associated with flying the aircraft more heavily than the task associated with specific force sensing. Although this allocation process is not at all well understood, the resulting threshold effect is easily modeled.

The perceptual model includes the sensory threshold for angular velocity and the indifference threshold for specific force in the appropriate paths. Figure 14 depicts the model used to implement these thresholds as a mathematical function. Also, the threshold level for each axle is indicated.

D. G-SUIT MODEL

A second sensory modality is included in the simulation of normal specific force perception. This is necessary because motion simulator travel limits severely constrain reproduction of normal specific force cues. Although visual scenes are often very compelling in terms of simulating angular and translational velocities, it is not possible to induce a sensation of g's visually. This is because the primary g-force sensory

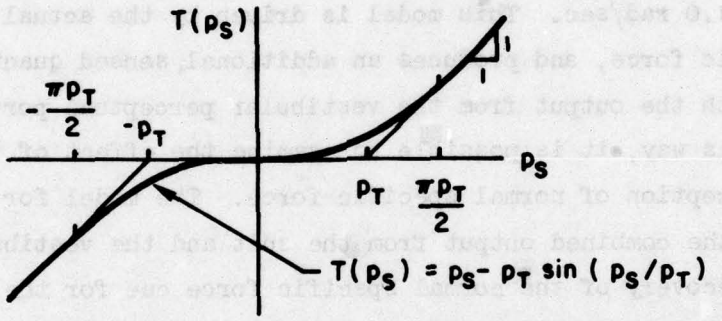

a) Presumed Form of Indifference Threshold

AXIS	THRESHOLD VALUE
Pitch	2 deg/sec
Surge	0.1 g
Roll	2 deg/sec
Sway	0.1 g
Yaw	2 deg/sec
Heave	0.0 g

Figure 14. Threshold Model and Threshold Values for Each Axis

modalities are vestibular, tactile and proprioceptive. One approach to this problem of simulating g-force sensations in an essentially static environment is by means of tactile stimulation using a g-suit (Ref. 19).

The g-suit (or pressure suit) was designed originally for use in high-g environments, in order to reduce the often debilitating head-to-toe hydrostatic blood pressure gradients encountered in high-g aircraft maneuvers. Different use is made of the g-suit in the simulator context. Here, pressure is applied to the pilot via the suit in order to provide tactile stimulation similar to that encountered in flying as normal specific force (g's) vary. The g-suit is driven in accordance with the in-flight normal specific force generated by the aircraft. The objective of g-suit use is to induce a more realistic perception of the normal specific force environment.

The model used for the g-suit pressure response is a lag with break frequency at 1.0 rad/sec. This model is driven by the actual (in-flight) normal specific force, and produces an additional sensed quantity which is integrated with the output from the vestibular perceptual portion of the model. In this way, it is possible to examine the effect of the g-suit on the total perception of normal specific force. The model for the g-suit is such that the combined output from the suit and the vestibular sensors yields full recovery of the normal specific force cue for the in-flight situation. The manner of integrating vestibular and g-suit induced perception of normal specific force is shown in block diagram form in the next subsection.

E. THE TOTAL MODEL

The overall model used in this research in order to evaluate the LAMARS drive logic consists of a simulation of the drive logic itself, and a simulation of the major sensory channels known to be active in the simulator pilot. For each axis, the model combines the drive logic equations for that axis, the appropriate vestibular sensor for that axis (semicircular canal model for angular velocity axes, otolith model for specific force axes) and the particular threshold in effect for that axis (sensory threshold for angular velocity axes, indifference threshold for specific

force axes). In addition, a model for perception of normal specific force via tactile stimulation provided by a g-suit is included in the heave axis. It is presumed that the g-suit provides a more compelling normal specific force simulation than do the visual and motion cues alone. Integration of the g-suit-induced cue is based on this presumption.

The figures which follow illustrate, in block diagram form, the total linear model for each pair of axes. Table 4 presents a list of the major variables for each axis, and Table 5 provides a list of the parameters to be set and their nominal (F-17 configuration from Ref. 1) values. There are several notes which accompany Figs. 15-17:

1) LAMARS has no longitudinal travel capability; therefore, no coefficient values relating to $\ddot{x}$, $\dot{x}$ or x are shown.

2) Roll-sway axes show the linear washout case only; the nonlinear cases are shown in Fig. 11.

3) Yaw and heave axes are uncoupled.

4) No perceptual or indifference thresholds are thought to be applicable in the heave axis, so none are included.

5) An equalization is postulated in the heave axis so that the total in-flight perception computed by summing the g-suit tactile sensation and the vestibular sensation is equal to the in-flight normal specific force.

Further details on the actual software implementation of the model is given in the Software User's Guide.

TABLE 4. LIST OF VARIABLES FOR MODEL BLOCK DIAGRAMS

VARIABLE NAME	DESCRIPTION
q_A	Input pitch velocity (actual)
q_{AF}	Recovered pitch velocity (simulated)
θ_M	Commanded pitch angle
q_e	Scaled error between q_A and q_{AF}
q_{AP}	Actual pitch velocity after perceptual processing
q_{AFP}	Simulated pitch velocity after perceptual processing
q_{Pe}	Scaled error between q_{AP} and q_{AFP}
q_{AI}	Actual pitch velocity with threshold imposed after perceptual processing
q_{AFI}	Simulated pitch velocity with threshold imposed after perceptual processing
q_{Ie}	Scaled error between q_{AI} and q_{AFI}
$\dot{u}_{po}$	Input longitudinal specific force (actual)
$\dot{u}_{poF}$	Recovered longitudinal specific force (simulated)
$\dot{u}_e$	Scaled error between $\dot{u}_{po}$ and $\dot{u}_{poF}$
$\dot{u}_{poP}$	Actual longitudinal specific force after perceptual processing
$\dot{u}_{poFP}$	Simulated longitudinal specific force after perceptual processing
$\dot{u}_{pe}$	Scaled error between $\dot{u}_{poP}$ and $\dot{u}_{poFP}$
$\dot{u}_{poI}$	Actual longitudinal specific force with threshold imposed after perceptual processing
$\dot{u}_{poFI}$	Simulated longitudinal specific force with threshold imposed after perceptual processing
$\dot{u}_{Ie}$	Scaled error between $\dot{u}_{poI}$ and $\dot{u}_{poFI}$
p_A	Input roll velocity (actual)
p_{AF}	Recovered roll velocity (simulated)
Φ_m	Commanded roll angle
p_e	Scaled error between p_A and p_{AF}
p_{AP}	Actual roll velocity after perceptual processing
p_{AFP}	Simulated roll velocity after perceptual processing

TABLE 4. (CONTINUED)

p_{pe}	Scaled error between p_{AP} and p_{AFP}
p_{AI}	Actual roll velocity with threshold imposed after perceptual processing
p_{AFI}	Simulated roll velocity with threshold imposed after perceptual processing
p_{Ie}	Scaled error between p_{AI} and p_{AFI}
$\dot{v}_{po}$	Input lateral specific force (actual)
$\dot{v}_{poF}$	Recovered lateral specific force (simulated)
y_M	Commanded lateral position
$\dot{v}_e$	Scaled error between $\dot{v}_{po}$ and $\dot{v}_{poF}$
$\dot{v}_{poP}$	Actual lateral specific force after perceptual processing
$\dot{v}_{poFP}$	Simulated lateral specific force after perceptual processing
$\dot{v}_{pe}$	Scaled error between $\dot{v}_{poP}$ and $\dot{v}_{poFP}$
$\dot{v}_{poI}$	Actual lateral specific force with thresholds imposed after perceptual processing
$\dot{v}_{poFI}$	Simulated lateral specific force with thresholds imposed after perceptual processing
$\dot{v}_{Ie}$	Scaled error between $\dot{v}_{poI}$ and $\dot{v}_{poFI}$
r_A	Input yaw velocity (actual)
r_{AF}	Recovered yaw velocity (simulated)
ψ_M	Commanded yaw angle
r_e	Scaled error between r_A and r_{AF}
r_{AP}	Actual yaw velocity after perceptual processing
r_{AFP}	Simulated yaw velocity after perceptual processing
r_{pe}	Scaled error between r_{AP} and r_{AFP}
r_{AI}	Actual yaw velocity with thresholds imposed after perceptual processing
r_{AFI}	Simulated yaw velocity with thresholds imposed after perceptual processing
r_{Ie}	Scaled error between r_{AI} and r_{AFI}

TABLE 4. (CONCLUDED)

$\dot{w}_{po}$	Input normal specific force (actual)
$\dot{w}_{poF}$	Recovered normal specific force (simulated)
z_M	Commanded vertical position
$\dot{w}_e$	Scaled error between $\dot{w}_{po}$ and $\dot{w}_{poF}$
$\dot{w}_{poP}$	Actual normal specific force after perceptual processing
$\dot{w}_{poFP}$	Simulated normal specific force after perceptual processing
$\dot{w}_{pe}$	Scaled error between $\dot{w}_{poP}$ and $\dot{w}_{poFP}$
$\dot{w}_{poII}$	Actual normal specific force after equalization
$\dot{w}_{poG}$	Actual normal specific force after g-suit processing
$\dot{w}_{poI}$	Actual total perception of normal specific force
$\dot{w}_{poFI}$	Simulated normal specific force after equalization
$\dot{w}_{Ie}$	Scaled error in total perception of normal specific force without g-suit
$\dot{w}_{se}$	Scaled error in total perception of normal specific force with g-suit
$\dot{w}_{poFS}$	Simulated total perception of normal specific force

TABLE 5. LIST OF MODEL PARAMETERS AND THEIR NOMINAL VALUES

Parameter	Value	Units
K_q	0.5	
K_{2P}	1.0	
ω_q	0.5	rad/sec
ω_{3P}	0.2	rad/sec
ω_{4P}	0.2	rad/sec
ζ_{3P}	0.7	
K_p	0.05	
K_{2R}	0.2	
K_y	1.0	
ω_p	1.57	rad/sec
ω_{1R}	0.266	rad/sec
ω_{2R}	0.65	rad/sec
ω_{3R}	0.65	rad/sec
ω_{4R}	1.0	rad/sec
$C_{1y}/(2\sqrt{C_{2y}})$	0.7	
C_{2y}	0.0025	
ζ_{3R}	0.7	
K_r	0.5	
$K_z \cdot K_{2z}$	0.15	
ω_r	1.0	rad/sec
C_{1Z}	0.05	rad/sec
C_{2Z}	0.0	$(\text{rad/sec})^2$
C_{3Z}	1.4	rad/sec
C_{4Z}	1.0	$(\text{rad/sec})^2$
C_{5Z}	0.3	rad/sec
ω_{6y}	0.0	rad/sec
ω_{6R}	0.0	rad/sec
ω_{6P}	0.0	rad/sec

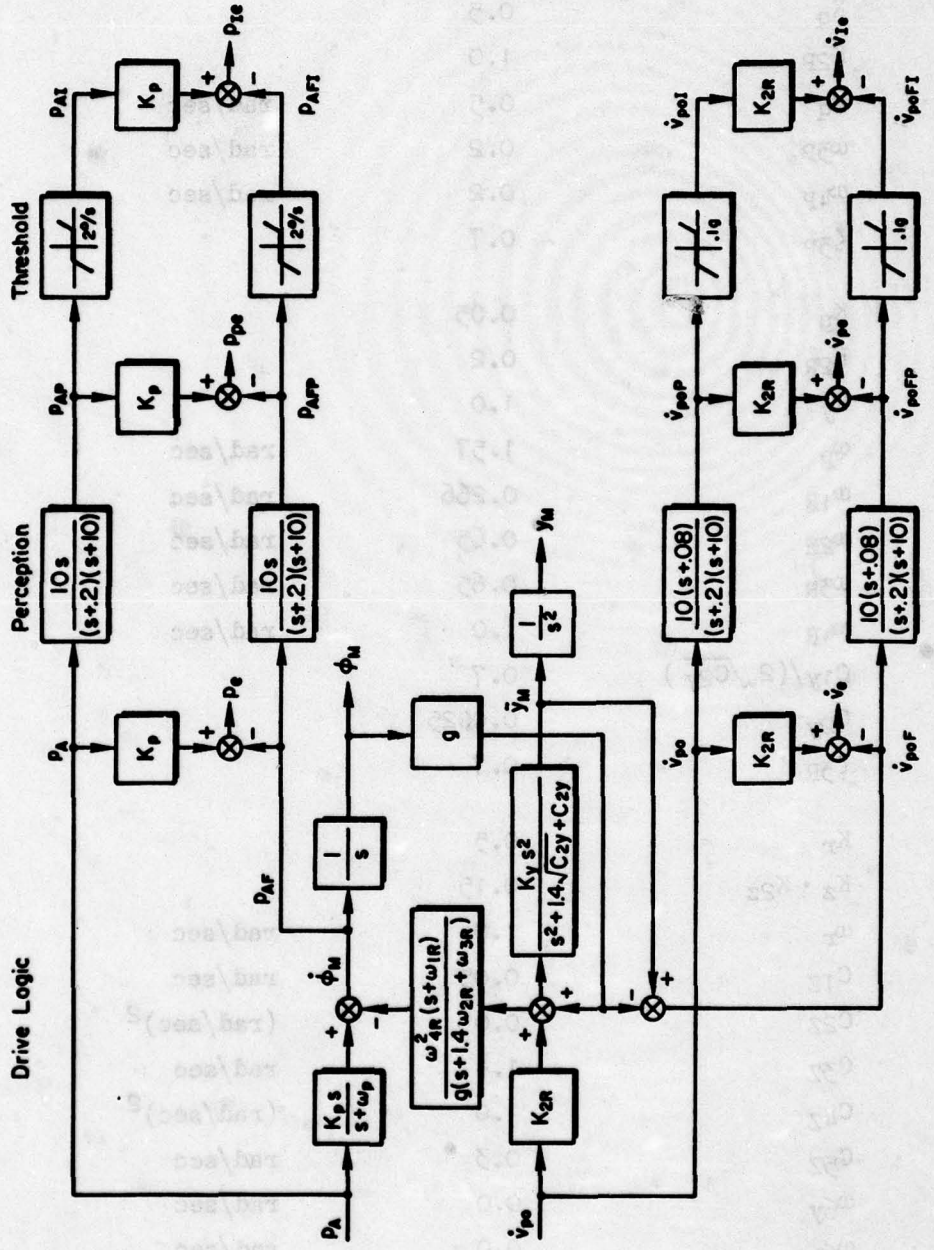

Figure 15. Model for Roll-Sway Axes (Linear)

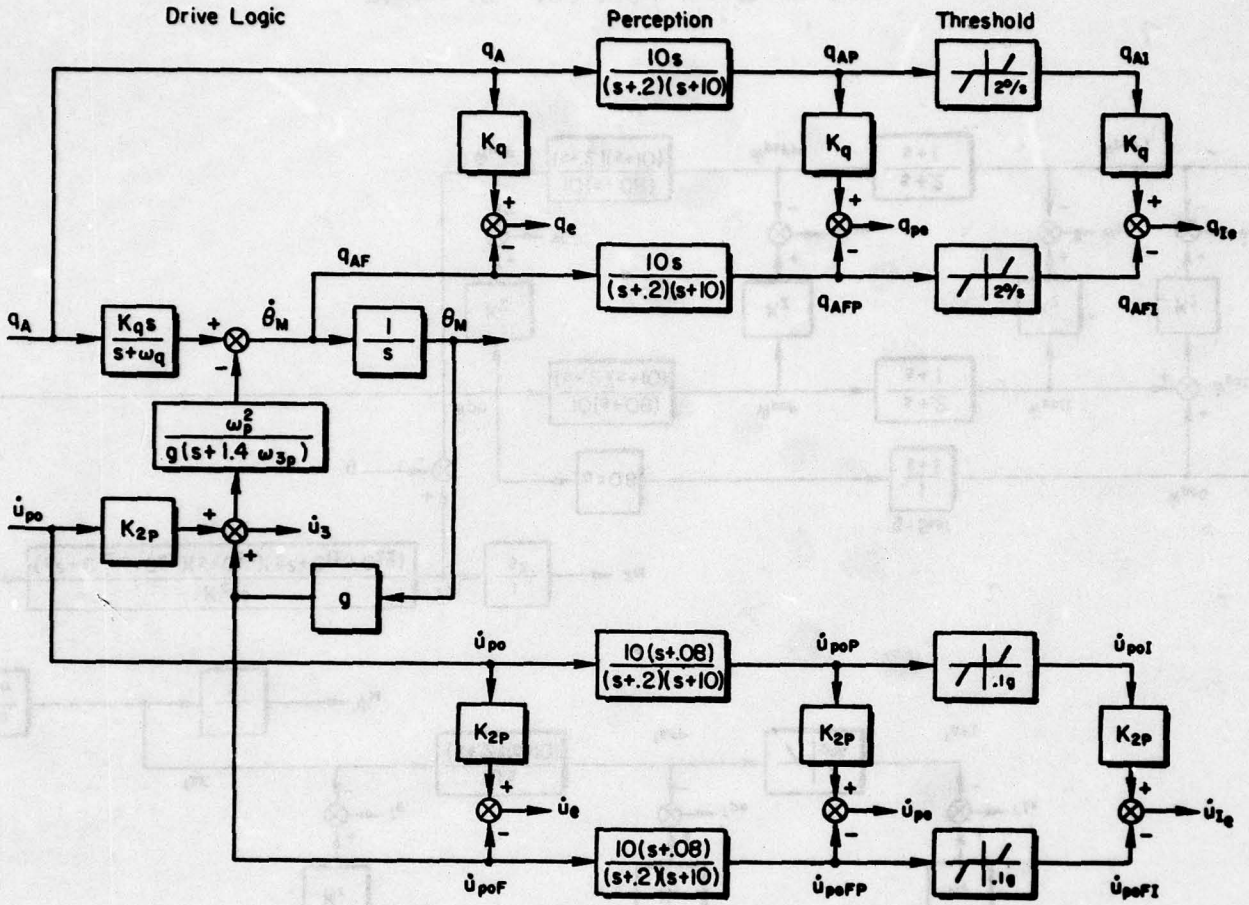

Figure 16. Model for Pitch-Surge Axes

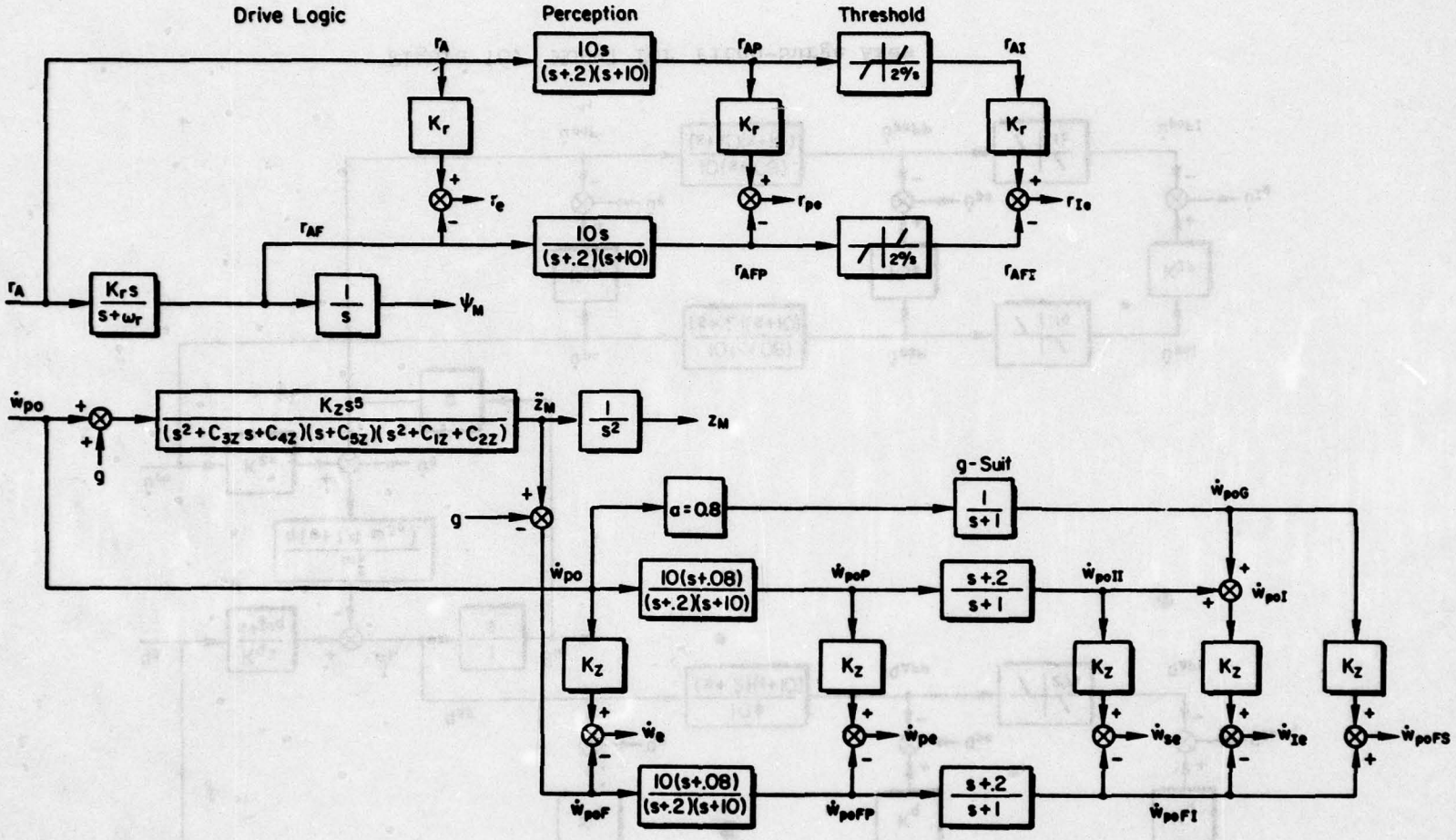

Figure 17. Model for Yaw-Heave Axes

SECTION IV

MEASURES, CRITERIA AND PARAMETRIC STUDY

A. INTRODUCTION

Once scenario data for typical flying tasks and drive logic and perceptual models are in hand, it is possible to compute time histories for all in-flight and simulation variables of interest. In order to interpret this data it is necessary to design a method by which the resulting time histories of the various variables (listed in Table 4) can be evaluated. Evaluation is with respect to effect upon simulator motion fidelity and required acceleration, velocity and displacement as drive logic parameters are varied. The method used in this research employs a set of "measures" computed from the drive logic simulation variables. These measures are of two types. Those of the first type are constituents of a motion fidelity criterion. The constituents are a dissection of a normalized mean square error according to contributory sources believed to be significant. These measures then re-combine to form a criterion for assigning a meaningful "value" to a particular simulator configuration (i.e., given set of drive logic parameters). This value is an index of fidelity for simulator motion reproduction. By using this criterion, it is possible to compare drive logic configurations and thereby choose an "optimum" configuration.

The second type of measure represents peak normalized acceleration, velocity and displacement required of the simulator hardware as a function of key drive logic parameters for a given scenario. These measures are then used to determine those combinations of drive logic parameter values which will not result in exceedence of the physical motion capability of a given simulator (e.g., LAMARS).

The next sub-section begins by motivating the choice of measures and the criterion. A list of the computed measures for each axis is presented. Then, the computed peak measures for the eight scenario inputs to the nominal LAMARS drive logic are compared. This results in the choice of a "representative" scenario for use in the remainder of the study. Using the

representative scenario, a parametric study with respect to the key drive logic parameters is undertaken (see Table 5). Measures for sets of systematic parameter variations are computed. Comparison of the measures exposes the important sensitivities of the motion fidelity criteria to the drive logic parameters, and provides direction for a simulator experiment to determine one remaining key parameter. This key parameter is the marginal utility of dynamic motion reproduction errors with respect to motion scaling errors as implied by pilot subjective choice of optimum motion reproduction. A value for this parameter completes the motion fidelity criterion development. The criterion is thus ready for application as the basis for drive logic optimization.

B. GENERAL EXPLANATION OF MEASURES AND CRITERIA

Suppose a typical motion variable upon which a measure is to be based is x. The actual, in-flight motion variable is x_a, while the simulated motion variable is x_s. Let the scale factor applied to the x_a variable to reduce the level of simulated motion be K, while the scale factor for other motion variables which couple with the x_s response is $\bar{K}$. The purpose of the proposed measure is to provide a meaningful basis for comparing the x_a and x_s variables produced by different drive logic configurations.

Consider one method of comparing the simulated motion with the actual motion: the error variable composed of the difference between actual and simulated motion.

$$\epsilon = x_a - x_s = (1 - K)x_a + (Kx_a - x_s)$$

The algebraic expression on the far right side of the equation separates this error into two distinct parts: the first term $(1 - K)x_a$ is the component of the error arising from scaling, while the second term $(Kx_a - x_s)$ is the component of the error arising from the washout dynamics.

The process of separating the various components of the error can be taken one step further. Consider the mean of the error squared, $\overline{\epsilon^2}$, normalized by the mean of the actual motion variable squared, $\overline{x_a^2}$. The normalization

assures that this measure will be fairly independent of the particular maneuver. This is a desirable feature which was identified earlier in Section II.A. The resulting calculation illustrates this approach to criterion development:

$$J_o = \frac{\overline{\epsilon^2}}{\overline{x_a^2}} = (1 - K)^2 + \frac{\overline{(Kx_a - x_s)^2}}{\overline{x_a^2}} + 2(1 - K)\frac{K\,\overline{x_a^2} - \overline{x_a x_s}}{\overline{x_a^2}}$$

The three terms on the far right of this equation are the constituent measures. The first measure, $(1 - K)^2$, represents the effect of motion scaling error. The second measure represents the effect of dynamic error in reproducing the scaled motion. The third measure corrects for the combined effects of scaling and dynamic error.

This J_o criterion and its component measures constitute a plausible method for application to uncoupled axes such as heave or yaw. In fact, it will be seen that this very criterion is used for those axes, with one important change discussed shortly. A problem exists, however, when attempting to apply this J_o criterion to the coupled roll-sway or pitch-surge axis sets, since it is not possible to distinguish between sources of infidelity arising from dynamics and those arising from coupling between pairs of axes. In order to distinguish between these separate sources, the J_o equation is reformulated in an equivalent, but more elaborated form, as follows:

$$J_1 = (1 - K)^2 + \frac{(Kx_a - x_s)^2_{\overline{K}=0}}{\overline{x_a^2}} + 2(1 - K)\left[\frac{K\overline{x_a^2} - \overline{(x_a x_s)}_{\overline{K}=0}}{\overline{x_a^2}}\right]$$

$$+ \left[\frac{\overline{(Kx_a - x_s)^2} - \overline{(Kx_a - x_s)^2}_{\overline{K}=0}}{\overline{x_a^2}}\right] + 2(1 - K)\frac{\overline{(x_a x_s)}_{\overline{K}=0} - \overline{(x_a x_s)}}{\overline{x_a^2}}$$

This J_1 criterion now includes measures which isolate the coupling effects arising from the two inputs. This is accomplished by evaluating the measures with one input "shut off" (when $\overline{K} = 0$), and then evaluating the incremental effect on the measure with that same input "turned on." Again, the first measure accounts for the effect of motion-scaling error.

The second measure represents the effect of dynamic error in reproducing scaled motion, in the absence of coupling between simulator axes. The third measure corrects for the combined effects of scaling and washout dynamic error in the absence of coupling between the simulator axes. The fourth measure represents the incremental effect of coupling between the simulator axes on the dynamic error in reproducing scaled motion. The fifth measure represents the incremental effect of coupling between simulator axes on the combined effects of scaling and washout dynamic error.

Two criteria forms have been developed for the purpose of comparing various drive logic schemes. The J_o criterion is useful for uncoupled axes, while the J_1 criterion permits the inter-axis coupling effects to be taken into account. One further refinement requires the measures to be normalized by K or K^2 while at the same time allowing for a weighting factor k where $k \triangleq \alpha K$. The following criteria are those used for the remainder of this study:

$$J_o = (1-K)^2 + k^2\left[\frac{\overline{(Kx_a - x_s)^2}}{K^2\,\overline{x_a^2}}\right] + 2k(1-K)\left[\frac{\overline{Kx_a^2} - \overline{(x_a x_s)}}{K\overline{x_a^2}}\right]$$

$$J_1 = (1-K)^2 + k^2\left[\frac{\overline{(Kx_a - x_s)^2}_{\overline{K}=0}}{K^2\,\overline{x_a^2}}\right] + 2k(1-K)\left[\frac{\overline{Kx_a^2} - \overline{(x_a x_s)}_{\overline{K}=0}}{K\overline{x_a^2}}\right]$$

$$+ k^2\left[\frac{\overline{(Kx_a - x_s)^2} - \overline{(Kx_a - x_s)^2}_{\overline{K}=0}}{K^2\,\overline{x_a^2}}\right] + 2k(1-K)\left[\frac{\overline{(x_a x_s)}_{\overline{K}=0} - \overline{(x_a x_s)}}{K\,\overline{x_a^2}}\right]$$

Notice now that α can be treated as a marginal utility parameter which reflects the pilot's subjective perception of the importance of dynamic washout-induced error relative to scaling-induced error. This weighting factor, α, permits the effects of dynamic washout error to be expressed in units which are equivalent, in the pilot's subjective judgment, to the motion scaling error. As will be seen in the next section, it is the purpose of the simulator

experiment to determine this pilot-preference weighting factor, α, in the criterion for each axis.

The J_o and J_1 criteria have been specially constructed to have the following characteristics:

- $J_o = 0$ or $J_1 = 0$ implies ideal motion recovery (i.e., in-flight and simulated motions are identical)
- $J_o \geq 1$ or $J_1 \geq 1$ implies that the simulated motion has ceased to make a positive contribution to the overall simulation fidelity.

Thus, once α has been selected via the piloted simulation experiments, the objective of the drive logic optimization is to minimize J_o or J_1 by selecting the appropriate scaling gain and washout break frequency. The criterion is applied separately for each axis. Optimization with respect to these criteria ultimately results in the determination of drive logic gains and break frequencies for each axis.

C. ALTERNATIVE CRITERIA AND MEASURES

Three alternative criteria for motion fidelity in each axis are considered. These are based upon the normalized mean of the squared errors following drive logic processing (e.g., $\overline{[p_A - p_{AF}]^2}/\overline{p_A^2}$ and $\overline{[\dot{v}_{po} - \dot{v}_{poF}]^2}/\overline{\dot{v}_{po}^2}$ in Fig. 16); following sensory processing (e.g., $\overline{[p_{AP} - p_{AFP}]^2}/\overline{p_{AP}^2}$ and $\overline{[\dot{v}_{poP} - \dot{v}_{poFP}]^2}/\overline{\dot{v}_{poP}^2}$ in Fig. 16); and following threshold processing (e.g., $\overline{[p_{AI} - p_{AFI}]^2}/\overline{p_{AI}^2}$ and $\overline{[\dot{v}_{poI} - \dot{v}_{poFI}]^2}/\overline{\dot{v}_{poI}^2}$ in Fig. 16). Constituent measures must be computed for each of the three alternate criteria for each axis.

Table 6 presents a list of the measures which are computed for each axis and their appropriate units. Basically, there are three sets of measures based on mean square errors for each axis: those computed after the drive logic processing, those computed after sensory processing, and those computed after threshold processing. For the coupled axes (pitch-surge and roll-sway), there are six measures in each set: the mean of the squared actual motion, the four bracketed measures which comprise J_1, and the mean of the squared simulated motion. For the uncoupled (yaw and heave) axes, there are only two bracketed measures which comprise the J_o criterion, so the total number

TABLE 6. LIST OF MEASURES COMPUTED BY AXIS

TABULAR NAME \ AXIS		PITCH	SURGE	ROLL	SWAY	YAW	HEAVE *
POST-DRIVE LOGIC MEASURES	PDLA	$\overline{q_A^2}(deg^2/sec^2)$	$\overline{\dot{u}_{po}^2}(g^2)$	$\overline{p_A^2}(deg^2/sec^2)$	$\overline{\dot{v}_{po}^2}(g^2)$	$\overline{r_A^2}(deg^2/sec^2)$	$\overline{\dot{w}_{po}^2}(g^2)$
	PDL1	$\frac{(\overline{q_e^2})_{K_{2P}=0}}{K_q^2\overline{q_A^2}}$	$\frac{(\overline{\dot{u}_e^2})_{K_q=0}}{K_{2P}^2\overline{\dot{u}_{po}^2}}$	$\frac{(\overline{p_e^2})_{K_{2R}=0}}{K_p^2\overline{p_A^2}}$	$\frac{(\overline{\dot{v}_e^2})_{K_p=0}}{K_{2R}^2\overline{\dot{v}_{po}^2}}$	$\frac{\overline{r_e^2}}{K_r^2\overline{r_A^2}}$	$\frac{\overline{\dot{w}_e^2}}{K_z^2\overline{\dot{w}_{po}^2}}$
	PDL2	$\frac{(\overline{q_e^2})-(\overline{q_e^2})_{K_{2P}=0}}{K_q^2\overline{q_A^2}}$	$\frac{(\overline{\dot{u}_e^2})-(\overline{\dot{u}_e^2})_{K_q=0}}{K_{2P}^2\overline{\dot{u}_{po}^2}}$	$\frac{(\overline{p_e^2})-(\overline{p_e^2})_{K_{2R}=0}}{K_p^2\overline{p_A^2}}$	$\frac{(\overline{\dot{v}_e^2})-(\overline{\dot{v}_e^2})_{K_p=0}}{K_{2R}^2\overline{\dot{v}_{po}^2}}$		
	PDL3	$\frac{K_q\overline{q_A^2}-(\overline{q_Aq_{AF}})_{K_{2P}=0}}{K_q\overline{q_A^2}}$	$\frac{K_{2P}\overline{\dot{u}_{po}^2}-(\overline{\dot{u}_{po}\dot{u}_{poF}})_{K_q=0}}{K_{2P}\overline{\dot{u}_{po}^2}}$	$\frac{K_p\overline{p_A^2}-(\overline{P_AP_{AF}})_{K_{2R}=0}}{K_p\overline{p_A^2}}$	$\frac{K_{2R}\overline{\dot{v}_{po}^2}-(\overline{\dot{v}_{po}\dot{v}_{poF}})_{K_p=0}}{K_{2R}\overline{\dot{v}_{po}^2}}$	$\frac{K_r\overline{r_A^2}-\overline{r_Ar_{AF}}}{K_r\overline{r_A^2}}$	$\frac{K_z\overline{\dot{w}_{po}^2}-\overline{\dot{w}_{po}\dot{w}_{poF}}}{K_z\overline{\dot{w}_{po}^2}}$
	PDL4	$\frac{(\overline{q_Aq_{AF}})_{K_{2P}=0}-(\overline{q_Aq_{AF}})}{K_q\overline{q_A^2}}$	$\frac{(\overline{\dot{u}_{po}\dot{u}_{poF}})_{K_q=0}-(\overline{\dot{u}_{po}\dot{u}_{poF}})}{K_{2P}\overline{\dot{u}_{po}^2}}$	$\frac{(\overline{P_AP_{AF}})_{K_{2R}=0}-(\overline{P_AP_{AF}})}{K_p\overline{p_A^2}}$	$\frac{(\overline{\dot{v}_{po}\dot{v}_{poF}})_{K_p=0}-(\overline{\dot{v}_{po}\dot{v}_{poF}})}{K_{2R}\overline{\dot{v}_{poP}^2}}$		
	PDL5	$\overline{q_{AF}^2}(deg^2/sec^2)$	$\overline{\dot{u}_{poF}^2}(g^2)$	$\overline{P_{AF}^2}(deg^2/sec^2)$	$\overline{\dot{v}_{poF}^2}(g^2)$	$\overline{r_{AF}^2}(deg^2/sec^2)$	$\overline{\dot{w}_{poF}^2}(g^2)$
POST-SENSORY PROCESSING MEASURES	PSEN0	$\overline{q_{AP}^2}(deg^2/sec^2)$	$\overline{\dot{u}_{poP}^2}(g^2)$	$\overline{p_{AP}^2}(deg^2/sec^2)$	$\overline{\dot{v}_{poP}^2}(g^2)$	$\overline{r_{AP}^2}(deg^2/sec^2)$	$\overline{\dot{w}_{poP}^2}(g^2)$
	PSEN1	$\frac{(\overline{q_{pe}^2})_{K_{2P}=0}}{K_q^2\overline{q_{AP}^2}}$	$\frac{(\overline{\dot{u}_{pe}^2})_{K_q=0}}{K_{2P}^2\overline{\dot{u}_{poP}^2}}$	$\frac{(\overline{p_{pe}^2})_{K_{2R}=0}}{K_p^2\overline{p_{AP}^2}}$	$\frac{(\overline{\dot{v}_{pe}^2})_{K_p=0}}{K_{2R}^2\overline{\dot{v}_{poP}^2}}$	$\frac{\overline{r_{pe}^2}}{K_r^2\overline{r_{AP}^2}}$	$\frac{\overline{\dot{w}_{pe}^2}}{K_z^2\overline{\dot{w}_{poP}^2}}$
	PSEN2	$\frac{(\overline{q_{pe}^2})-(\overline{q_{pe}^2})_{K_{2P}=0}}{K_q^2\overline{q_{AP}^2}}$	$\frac{(\overline{\dot{u}_{pe}^2})-(\overline{\dot{u}_{pe}^2})_{K_q=0}}{K_{2P}^2\overline{\dot{u}_{poP}^2}}$	$\frac{(\overline{p_{pe}^2})-(\overline{p_{pe}^2})_{K_{2R}=0}}{K_p^2\overline{p_{AP}^2}}$	$\frac{(\overline{\dot{v}_{pe}^2})-(\overline{\dot{v}_{pe}^2})_{K_p=0}}{K_{2R}^2\overline{\dot{v}_{po}^2}}$		
	PSEN3	$\frac{K_q\overline{q_{AP}^2}-(\overline{q_{AP}q_{AFP}})_{K_{2P}=0}}{K_q\overline{q_{AP}^2}}$	$\frac{K_{2P}\overline{\dot{u}_{poP}^2}-(\overline{\dot{u}_{poP}\dot{u}_{poFP}})_{K_q=0}}{K_{2P}\overline{\dot{u}_{poP}^2}}$	$\frac{K_p\overline{p_{AP}^2}-(\overline{P_{AP}P_{AFP}})_{K_{2R}=0}}{K_p\overline{p_{AP}^2}}$	$\frac{K_{2R}\overline{\dot{v}_{poP}^2}-(\overline{\dot{v}_{poP}\dot{v}_{poFP}})_{K_p=0}}{K_{2R}\overline{\dot{v}_{poP}^2}}$	$\frac{K_r\overline{r_{AP}^2}-\overline{r_{AP}r_{AFP}}}{K_r\overline{r_{AP}^2}}$	$\frac{K_z\overline{\dot{w}_{poP}^2}-\overline{\dot{w}_{poP}\dot{w}_{poFP}}}{K_z\overline{\dot{w}_{poP}^2}}$
	PSEN4	$\frac{(\overline{q_{AP}q_{AFP}})_{K_{2P}=0}-(\overline{q_{AP}q_{AFP}})}{K_q\overline{q_{AP}^2}}$	$\frac{(\overline{\dot{u}_{poP}\dot{u}_{poFP}})_{K_q=0}-(\overline{\dot{u}_{poP}\dot{u}_{poFP}})}{K_{2P}\overline{\dot{u}_{poP}^2}}$	$\frac{(\overline{P_{AP}P_{AFP}})_{K_{2R}=0}-(\overline{P_{AP}P_{AFP}})}{K_p\overline{p_{AP}^2}}$	$\frac{(\overline{\dot{v}_{poP}\dot{v}_{poFP}})_{K_p=0}-(\overline{\dot{v}_{poP}\dot{v}_{poFP}})}{K_{2R}\overline{\dot{v}_{poP}^2}}$		
	PSEN5	$\overline{q_{AFP}^2}(deg^2/sec^2)$	$\overline{\dot{u}_{poFP}^2}(g^2)$	$\overline{P_{AFP}^2}(deg^2/sec^2)$	$\overline{\dot{v}_{poFP}^2}(g^2)$	$\overline{r_{AFP}^2}(deg^2/sec^2)$	$\overline{\dot{w}_{poFP}^2}(g^2)$

* K_z is used to represent K_zK_{2z} for LAWRS.

TABLE 6. (CONCLUDED)

TABULAR NAME \ AXIS		PITCH	SURGE	ROLL	SWAY	YAW	HEAVE*
POST-THRESHOLD PROCESSING MEASURES	PNLA	$\overline{q_{AI}^2}(\text{deg}^2/\text{sec}^2)$	$\overline{\dot{u}_{poI}^2}(g^2)$	$\overline{P_{AI}^2}(\text{deg}^2/\text{sec}^2)$	$\overline{\dot{v}_{poI}^2}(g^2)$	$\overline{r_{AI}^2}(\text{deg}^2/\text{sec}^2)$	$\overline{\dot{w}_{poI}^2}(g^2)$
	PNL1	$\dfrac{(\overline{q_{Ie}^2})_{K_{2P}=0}}{K_q^2\overline{q_{AI}^2}}$	$\dfrac{(\overline{\dot{u}_{Ie}^2})_{K_q=0}}{K_{2P}^2\overline{\dot{u}_{poI}^2}}$	$\dfrac{(\overline{p_{Ie}^2})_{K_{2R}=0}}{K_p^2\overline{p_{AI}^2}}$	$\dfrac{(\overline{\dot{v}_{Ie}^2})_{K_p=0}}{K_{2R}^2\overline{\dot{v}_{poI}^2}}$	$\dfrac{\overline{r_{Ie}^2}}{K_r^2\overline{r_{AI}^2}}$	$\dfrac{\overline{\dot{w}_{Ie}^2}}{K_z^2\overline{\dot{w}_{poI}^2}}$
	PNL2	$\dfrac{(\overline{q_{Ie}^2}) - (\overline{q_{Ie}^2})_{K_{2P}=0}}{K_q^2\overline{q_{AI}^2}}$	$\dfrac{\overline{\dot{u}_{Ie}^2} - (\overline{\dot{u}_{Ie}^2})_{K_q=0}}{K_{2P}^2\overline{\dot{u}_{poI}^2}}$	$\dfrac{(\overline{p_{Ie}^2}) - (\overline{p_{Ie}^2})_{K_{2R}=0}}{K_p^2\overline{p_{AI}^2}}$	$\dfrac{(\overline{\dot{v}_{Ie}^2}) - (\overline{\dot{v}_{Ie}^2})_{K_p=0}}{K_{2R}^2\overline{\dot{v}_{poI}^2}}$		
	PNL3	$\dfrac{K_q\overline{q_{AI}^2} - (\overline{q_{AI}q_{AFI}})_{K_{2P}=0}}{K_q\overline{q_{AI}^2}}$	$\dfrac{K_{2P}\overline{\dot{u}_{Ie}^2} - (\overline{\dot{u}_{poI}\dot{u}_{poFI}})_{K_q=0}}{K_{2P}\overline{\dot{u}_{poI}^2}}$	$\dfrac{K_p\overline{p_{AI}^2} - (\overline{p_{AI}p_{AFI}})_{K_{2R}=0}}{K_p\overline{p_{AI}^2}}$	$\dfrac{K_{2R}\overline{\dot{v}_{Ie}^2} - (\overline{\dot{v}_{poI}\dot{v}_{poFI}})_{K_p=0}}{K_{2R}\overline{\dot{v}_{poI}^2}}$	$\dfrac{K_r\overline{r_{AI}^2} - \overline{r_{AI}r_{AFI}}}{K_r\overline{r_{AI}^2}}$	$\dfrac{K_z\overline{\dot{w}_{poI}^2} - \overline{\dot{w}_{poI}\dot{w}_{poFS}}}{K_z\overline{\dot{w}_{poI}^2}}$
	PNL4	$\dfrac{(\overline{q_{AI}q_{AFI}})_{K_{2P}=0} - (\overline{q_{AI}q_{AFI}})}{K_q\overline{q_{AI}^2}}$	$\dfrac{(\overline{\dot{u}_{poI}\dot{u}_{poFI}})_{K_q=0} - (\overline{\dot{u}_{poI}\dot{u}_{poFI}})}{K_{2P}\overline{\dot{u}_{poI}^2}}$	$\dfrac{(\overline{p_{AI}p_{AFI}})_{K_{2R}=0} - (\overline{p_{AI}p_{AFI}})}{K_p\overline{p_{AI}^2}}$	$\dfrac{(\overline{\dot{v}_{poI}\dot{v}_{poFI}})_{K_p=0} - (\overline{\dot{v}_{poI}\dot{v}_{poFI}})}{K_{2R}\overline{\dot{v}_{poI}^2}}$		
	PNL5	$\overline{q_{AFI}^2}(\text{deg}^2/\text{sec}^2)$	$\overline{\dot{u}_{poFI}^2}(g^2)$	$\overline{P_{AFI}^2}(\text{deg}^2/\text{sec}^2)$	$\overline{\dot{v}_{poFI}^2}(g^2)$	$\overline{r_{AFI}^2}(\text{deg}^2/\text{sec}^2)$	$\overline{\dot{w}_{poFS}^2}(g^2)$
POST-SENSORY PROCESSING MEASURES, WITHOUT G-SUIT	GS1						$\dfrac{\overline{\dot{w}_{Ie}^2}}{K_z^2\overline{\dot{w}_{poI}^2}}$
	GS2						$\dfrac{K_z\overline{\dot{w}_{poI}^2} - (\overline{\dot{w}_{poI}\dot{w}_{poFI}})}{K_z\overline{\dot{w}_{poI}^2}}$
	GS3						$\overline{\dot{w}_{poFI}^2}(g^2)$
NORMALIZED PEAK VALUES	PACC				$\lvert\ddot{y}_K\rvert_{peak}/K_{2R}$ (ft/sec^2)		$\lvert\ddot{z}_K\rvert_{peak}/K_z$ (ft/sec^2)
	PVEL	$\lvert\dot{\theta}_K\rvert_{peak}/K_q$ (deg/sec)		$\lvert\dot{\phi}_M\rvert_{peak}/K_pK_y$ (deg/sec)	$\lvert\dot{y}_M\rvert_{peak}/K_{2R}$ (ft/sec)	$\lvert\dot{\psi}_M\rvert_{peak}/K_r$ (deg/sec)	$\lvert\dot{z}_M\rvert_{peak}/K_z$ (ft/sec)
	PDIS	$\lvert e_M\rvert_{peak}/K_q$ (deg)		$\lvert\phi_M\rvert_{peak}/K_pK_y$ (deg)	$\lvert y_M\rvert_{peak}/K_{2R}$ (ft)	$\lvert\psi_M\rvert_{peak}/K_r$ (deg)	$\lvert z_M\rvert_{peak}/K_z$ (ft)

K_z is used to represent K_zK_{2z} for LAHARS.
No thresholds are operative for the heave axis. Measures for the heave axis in this row are those which model the integrated perception of motion and g-suit effects.

of measures per set is four. For the heave axis, there are additional measures (GS1, GS2, GS5) which are similar to the PNL1, PNL3, and PNL5 computations, but do not include the effect of the g-suit.

D. CHOOSING A REPRESENTATIVE SCENARIO

Besides the measures which comprise the J_o and J_1 criteria, peak value measures are also computed. These measures are the normalized peak values of commanded acceleration, velocity and displacement (refer to Table 6) which are the drive logic outputs. These measures, when compared to the appropriate hardware limits of the particular motion base, provide a basis for choosing the scaling gain and washout break frequency combinations required in order to fit the reproduced motions to the capabilities of a given simulator. These peak value measures are also used to select a representative scenario.

It was stated in the scenario generation discussion that the purpose of generating eight scenarios was to provide a data base from which to choose the scenario which best enveloped the remaining scenarios. This "representative" scenario would then be employed throughout the parametric study/drive logic optimization phases. This is a valid approach, since the criteria and their constituent measures were deliberately developed to be fairly independent of the input. Thus, optimization based on the inputs from a "representative" scenario can be said to be typical for all inputs which fall within those "representative" limits.

In order to choose a representative scenario, each of the eight scenarios was used as the input to the drive logic/sensor simulation. The resulting peak measures for each axis are listed as the PACC, PVEL and PDIS entries in Tables C-1, C-2, and C-3 of Appendix C. Note that the drive logic parameters used in each case are those listed as the "nominal" parameters in Table 5, so the drive logic used to select the representative scenarios is that currently used for LAMARS.

The measures of interest here are the normalized peak values of velocity and displacement for the angular axes, and the peak values of acceleration, velocity and displacement for the translational axes. These peak values are normalized by the scaling gains having primary influence on that peak.

Table 7 presents a summary list of the appropriate LAMARS motion base limits for comparison with the peak values for each scenario. In order to compare the scenarios, some of the peak values are plotted versus scenario. These plots are found in Fig. 18 (refer to Table 1 for interpretation of the scenario numbers). The equation used to compute the normalized LAMARS hardware limit is included on each plot.

As can be seen from Table 7 or the plots, especially the heave and pitch axis plots, Scenarios 6 and 8 clearly do not "fit" on the simulator when the nominal drive logic gains are used. Also, it is evident that, for the most part, Scenario 4 (the air-to-ground weapon delivery task) envelopes the requirements for Scenarios 1 through 5 and 7. On the basis of this observation, Scenario 4 is designated the "representative" scenario (Scenarios 6 and 8 are presumed to be inappropriate for simulation for convenience in presenting subsequent methods and results). It will be used as the drive logic input for the remainder of this research. Once the drive logic is optimized for Scenario 4, it is assumed that the same optimization applies for Scenarios 1 through 5 and 7 as well.

Having chosen the representative scenario, it is now possible to identify the upper bounds on the scaling gain for each axis. This is accomplished by determining that scaling gain value which when multiplied by the normalized peak value for Scenario 4 results in a product which is equal to the LAMARS hardware limit. This determination of the maximum scaling gain assumes the other drive logic parameters are constant. Table 8 presents the results of these computations. These results may be regarded as a first tentative step toward optimizing the drive logic. However, it is usually desirable to optimize with respect to the washout break frequencies as well as the scaling gains. A method for determining those combinations of scaling gain and washout break frequency which satisfy the simulator hardware limits is discussed in the next subsection.

E. PARAMETRIC STUDY

Three goals must be achieved in this drive logic parametric study. First, a range of drive logic parameters must be established for the LAMBS simulator experiments at Vought. In particular, the range of drive logic parameters

TABLE 7. PEAK VALUES FOR RIGHT SCENARIOS COMPARED TO LAMARS LIMITS

	LAMARS LIMITS	SCENARIO 1	SCENARIO 2	SCENARIO 3	SCENARIO 4	SCENARIO 5	SCENARIO 6	SCENARIO 7	SCENARIO 8
Heave									
Displacement	± 10 ft	8.1 ft	8.1 ft	3.75 ft	9.3 ft	6.75 ft	19.5 ft	5.4 ft	15.0 ft
Velocity	13 ft/sec	4.35 ft/sec	6.75 ft/sec	1.5 ft/sec	5.55 ft/sec	3.9 ft/sec	15.0 ft/sec	4.65 ft/sec	15.0 ft/sec
Acceleration	± 96.6 ft/sec^2	3.45 ft/sec^2	5.7 ft/sec^2	1.32 ft/sec^2	5.7 ft/sec^2	3.45 ft/sec^2	22.5 ft/sec^2	5.55 ft/sec^2	15.0 ft/sec^2
Scaling, K_zK_{2z}	0.15								
Sway									
Displacement	± 10 ft	1.48 ft	3.59 ft	1.38 ft	3.52 ft	1.31 ft	2.97 ft	1.86 ft	2.61 ft
Velocity	10 ft/sec	0.55 ft/sec	1.3 ft/sec	0.65 ft/sec	1.7 ft/sec	0.55 ft/sec	6.0 ft/sec	1.55 ft/sec	1.25 ft/sec
Acceleration	± 51.52 ft/sec^2	0.55 ft/sec^2	1.05 ft/sec^2	0.6 ft/sec^2	1.3 ft/sec^2	0.55 ft/sec^2	21.0 ft/sec^2	1.3 ft/sec^2	1.8 ft/sec^2
Scaling, K_pK_y	0.05								
Roll									
Displacement	± 25 deg	0.65 deg	1.25 deg	0.6 deg	1.55 deg	0.6 deg	5.5 deg	1.05 deg	1.5 deg
Velocity	60 deg/sec	0.55 deg/sec	0.6 deg/sec	0.65 deg/sec	1.25 deg/sec	0.5 deg/sec	8.0 deg/sec	1.65 deg/sec	1.55 deg/sec
Acceleration	±460 deg/sec^2								
Scaling, K_p	0.05								
Pitch									
Displacement	± 25 deg								
Derotated*	± 4.76 deg	9.0 deg	8.83 deg	7.15 deg	17.0 deg	20.92 deg	63.3 deg	11.45 deg	12.61 deg
Velocity	60 deg/sec	3.85 deg/sec	3.95 deg/sec	1.6 deg/sec	5 deg/sec	3.35 deg/sec	55.0 deg/sec	7.5 deg/sec	11.0 deg/sec
Acceleration	±400 deg/sec^2								
Scaling, K_q	0.5								
Yaw									
Displacement	± 25 deg								
Derotated*	± 4.76 deg	1.59 deg	1.6 deg	1.62 deg	2.06 deg	2.25 deg	23.9 deg	3.05 deg	4.25 deg
Velocity	50 deg/sec	0.5 deg/sec	0.92 deg/sec	0.57 deg/sec	1.05 deg/sec	1.26 deg/sec	38.36 deg/sec	2.75 deg/sec	4.93 deg/sec
Acceleration	±200 deg/sec								
Scaling, K_r	0.5								

*Derotated numbers assume a beam length of 26 ft and are the result of multiplying the actual cab authority after derotation by a factor of 2 to account for additional authority available because of the correlation between angular and translational motions.

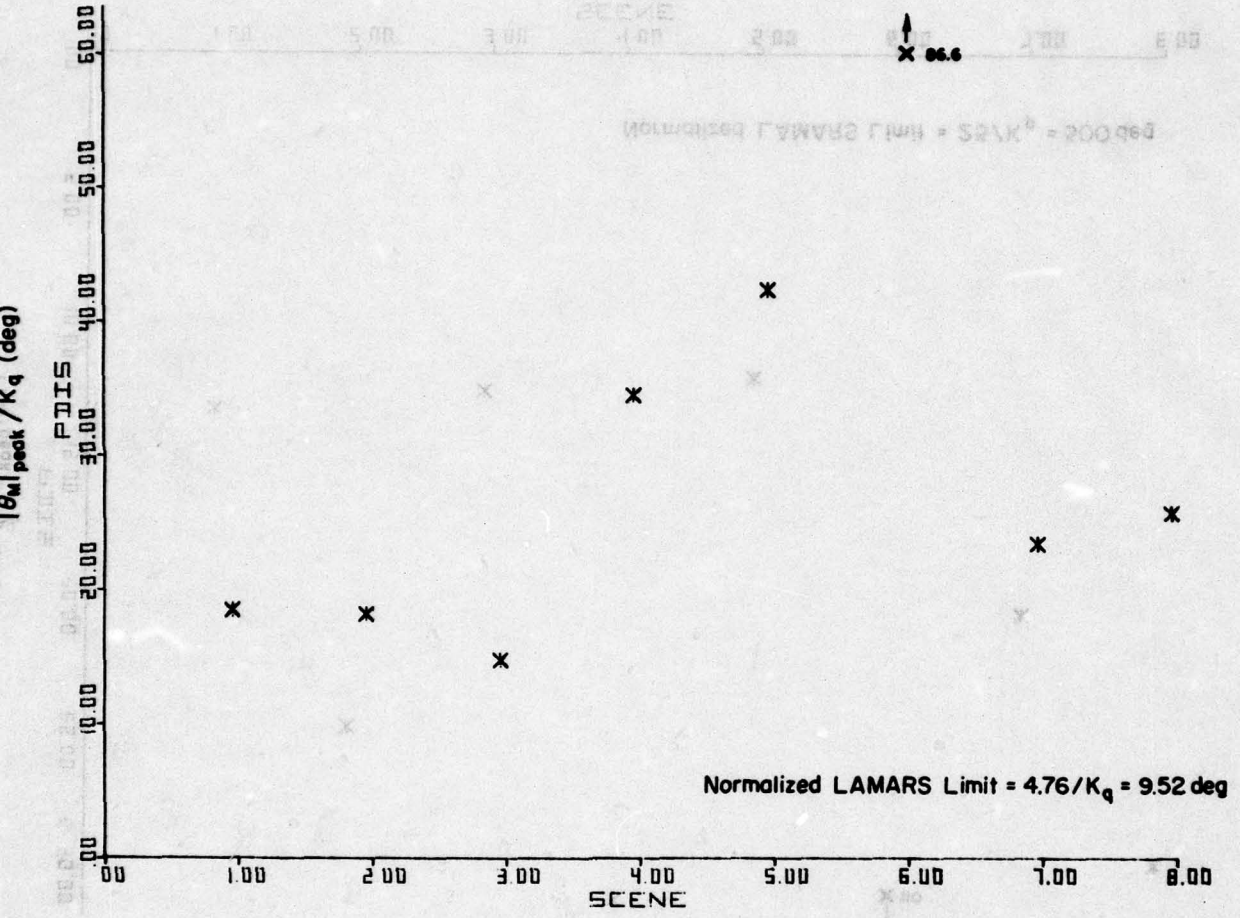

Figure 18a. Pitch

Figure 18b. Roll

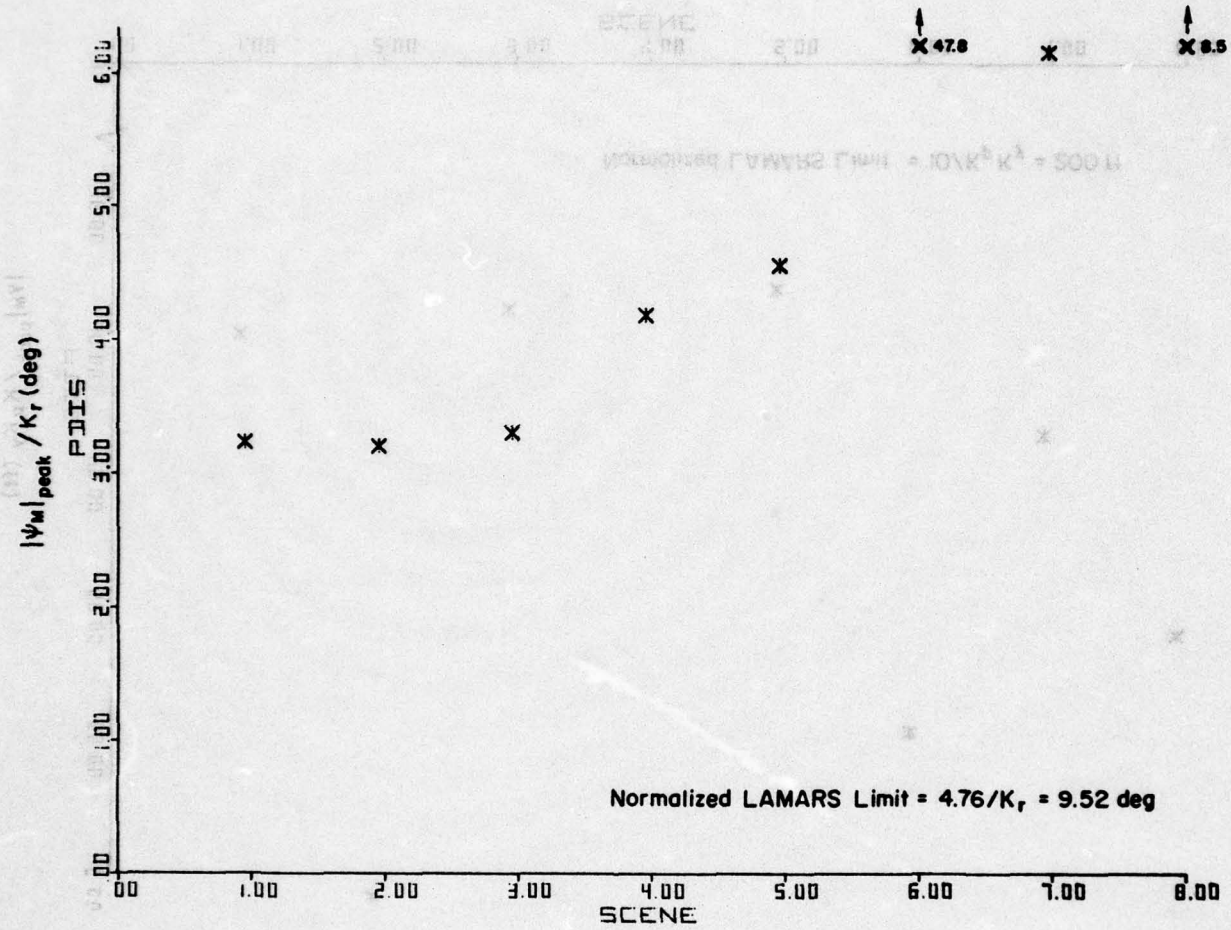

Figure 18c. Yaw

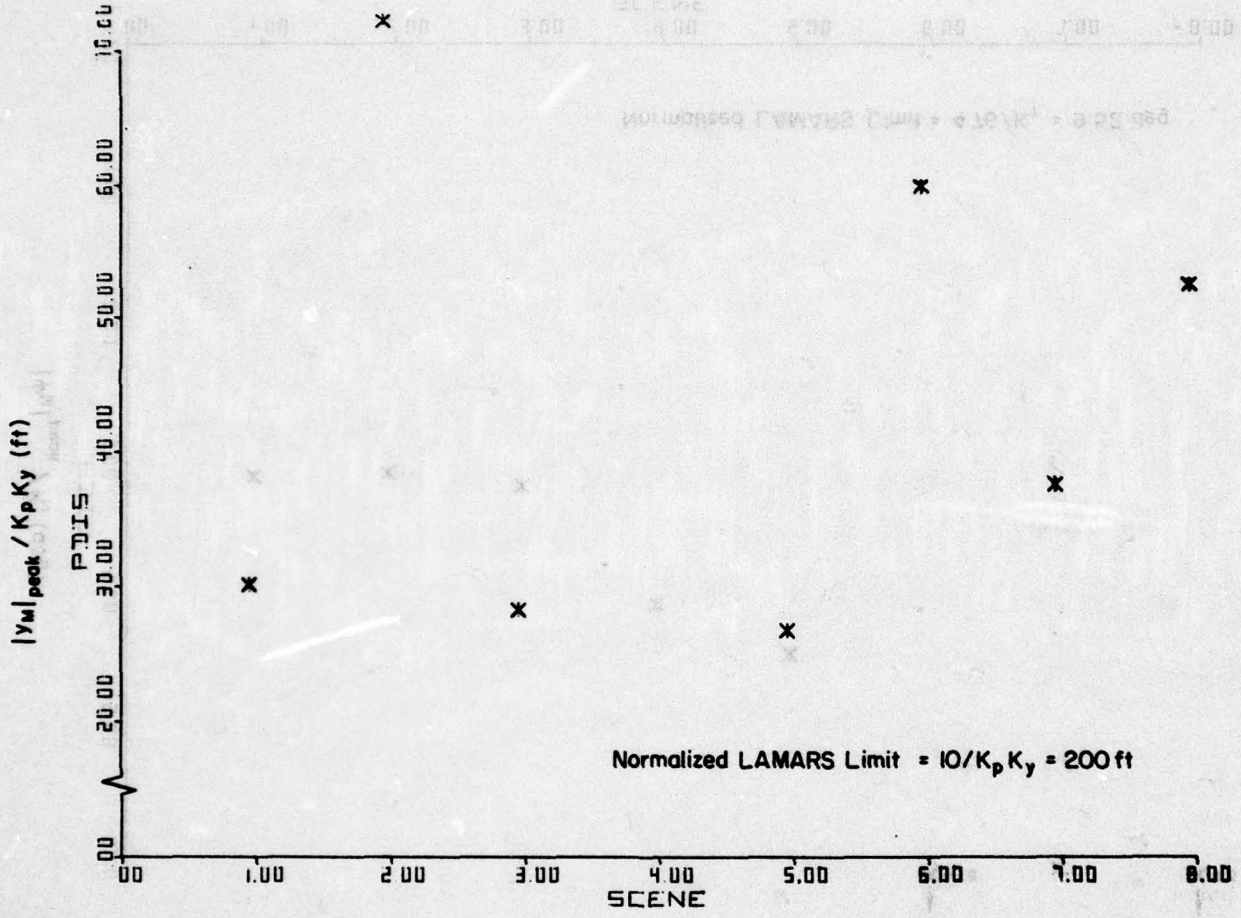

Figure 18d. Sway

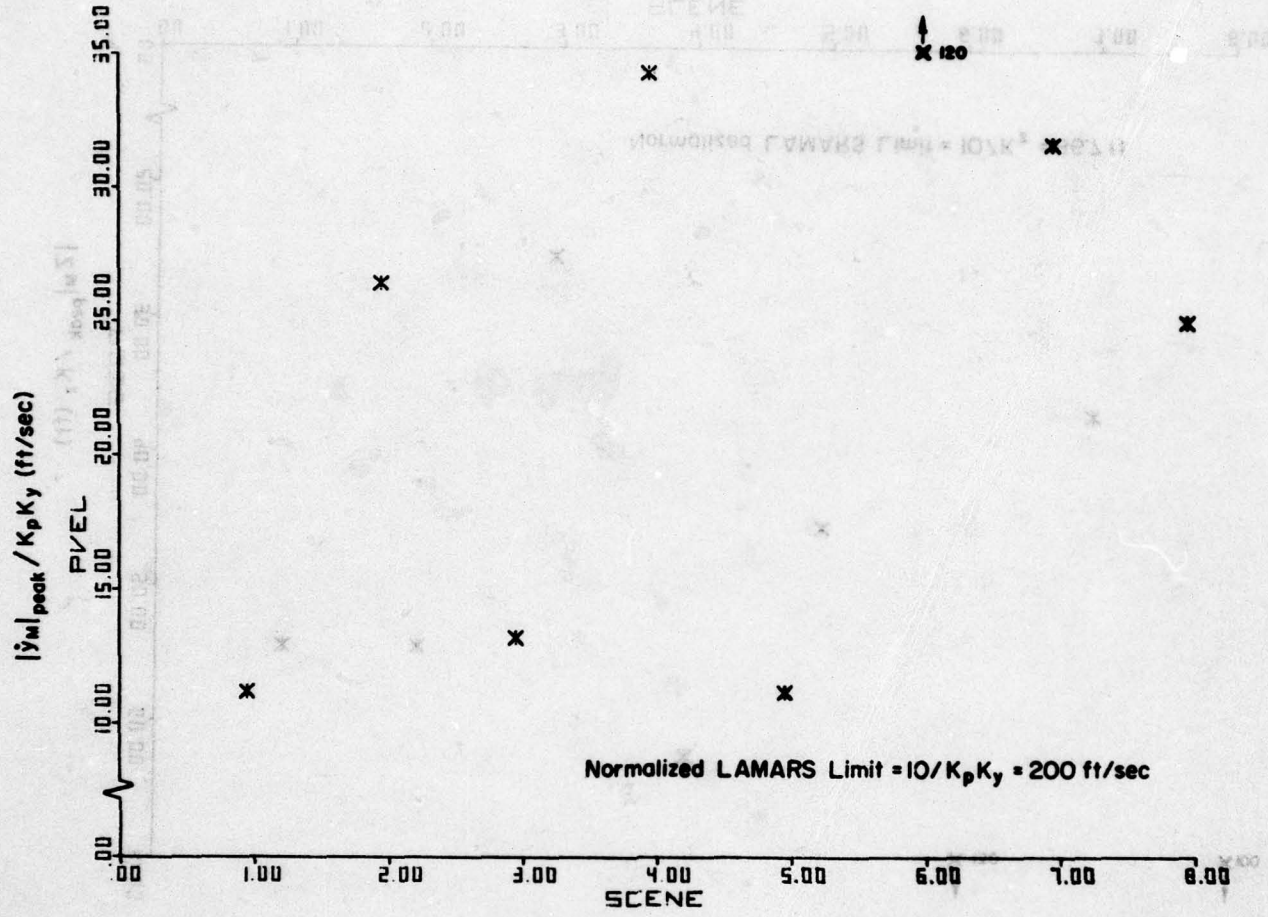

Figure 18e. Sway

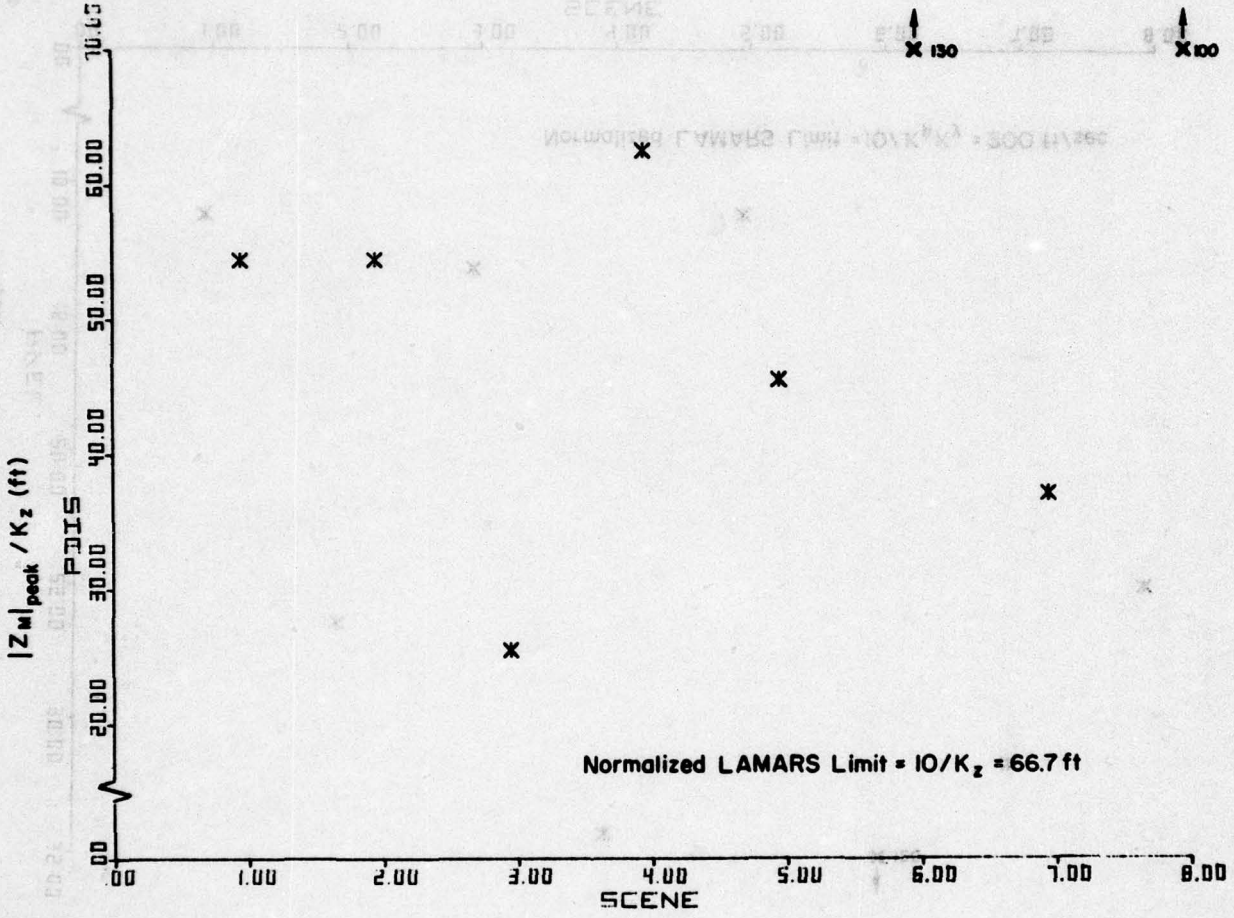

Figure 18f. Heave

Figure 18g. Heave

TABLE 8. COMPUTED UPPER BOUNDS ON SCALING GAINS (FOR NOMINAL WASHOUT BREAK FREQUENCIES OF TABLE 5 AND SCENARIO 4)

Pitch*	$K_q \leq 0.14$
Roll	$K_p \leq 0.81$
Sway	$K_p K_y \leq 0.14$
Yaw†	$K_r \leq 1.0$
Heave	$K_z K_{2z} \leq 0.16$

* LAMARS pitch limits have been reduced to account for the derotation required in connection with heave motion.

† The upper bound of unity on the scaling gains is operative here.

which can be investigated (i.e., which will fit) on that simulator must be defined. ("Fitting" the simulator refers to commanding motions which do not exceed the displacement, velocity and acceleration limits of the motion base). The second goal is to identify the key simulator axes for experimental investigation. The third goal is to obtain the drive logic parametric effects on the measures. This will provide the data base required in the next section for refining the fidelity criteria and for optimizing the LAMARS drive logic. The latter data is also used to define the range of drive logic parameters which result in commanded motions which will fit within the LAMARS limits.

This parametric study is not intended to be exhaustive. Rather it is structured to highlight the most significant effects of the drive logic parameters on the measures and criteria. To this end, certain break frequencies of the LAMARS drive logic are chosen to covary. For example, in the pitch-surge axes the following relationship is used to relate ω_q, ω_{3P} and ω_{4P}:

$$\omega_q = 1.4\,\omega_{3P} = 1.4\,\omega_{4P}$$

Similar relationships are used for the other axes (refer to Table 9). These relationships limit the number of parameters varied to the essential minimum number. Obviously, such relationships are somewhat arbitrary and it is certainly possible to vary each parameter separately. Such a study is outside the bounds of this investigation, however. Furthermore, it is possible to approximate the effects of changes in these secondary parameters from values specified in the given relationships by defining "effective values" of the essential parameters. One procedure for defining values for the effective lead frequency and effective delay parameters is described in Appendix D.

Table 5 lists the parameters available for variation in the existing drive logic. The parametric study uses a linear model of the LAMARS drive logic configuration. Table 9 describes the parameter variation matrix. Comparing the two tables provides a means for understanding which parameters other than scaling gains are thought to be critical for each axis. Scaling gain effects are treated via normalization with respect to the scaling gains since the drive logic model is linear.

The parameter variations result in tables of measures, Tables C-4 through C-14 in Appendix C. Again, it is useful to compare the peak values of acceleration, velocity and displacement for each axis with the hardware constraints of the LAMARS motion base for that same axis. Table 10 makes this comparison.

These data are used to identify drive logic parameter combinations which result in simulated motions which will "fit" on the motion base. As in the previous section, the concept of "fitting" on the simulator is based on the normalized LAMARS limits. And again, the upper bound on the gain necessary to make the motion fit on the motion base can be computed for each value of break frequency, B( ). If we assume that the optimum occurs for the scaling gain at its upper bound a unique relationship between scaling gain and break frequency for motion is defined. Existence of such a relationship greatly simplifies the optimization task. It is then sufficient to optimize with respect to <u>either</u> break frequency <u>or</u> gain, rather than with respect to both.

Scaling gain versus break frequency plots for heave, roll and sway of LAMARS are shown in Figs. 19, 20 and 21, respectively. These plots are

TABLE 9. VALUES USED FOR PARAMETRIC STUDY

PARAMETER	VALUES	
Pitch-Surge		
K_q	0.5	18 cases
K_{2P}	0.0, 0.5, 1.0	
ω_q (1.4 B_q)	.0945, .175, .35, .7, 1.4, 2.8	
ω_{3P} (B_q)	.0675, .125, .25, .5, 1.0, 2.0	
ω_{4P} (B_q)	.0675, .125, .25, .5, 1.0, 2.0	
Roll-Sway		
K_p	0.5	42 cases * This value of K_{2R} is used only with C_{2y} = .0225.
K_{2R}	0.0, 0.5*, 1.0	
K_y	1.0	
ω_p (1.4 B_p)	.0945, .175, .35, .7, 1.4, 2.8	
ω_{1R}	0.0	
ω_{2R}	0.0	
ω_{3R}(B_p)	.0675, .125, .25, .5, 1.0, 2.0	
ω_{4R}(B_p)	.0675, .125, .25, .5, 1.0, 2.0	
C_{2y}	.0025, .0225, .25	
Yaw and Heave		
K_r	0.5	6 cases
$K_z \cdot K_{2z}$	0.15	
ω_r (B_r)	.0675, .125, .25, .5, 1.0, 2.0	
C_{1Z}	.05	
C_{2Z}	0.0	
C_{3Z} (B_z)	.0675, .125, .25, .5, 1.0, 2.0	
C_{4Z} (B_z^2)	.0046, .0156, .0625, .25, 1.0, 4.0	
C_{5Z} (B_z)	.0675, .125, .25, .5, 1.0, 2.0	

TABLE 10

PEAK VALUES FOR PARAMETER VARIATION VS. BREAK FREQUENCY

	LAMARS LIMITS	BF=0.0675 rad/sec	0.125 rad/sec	0.25 rad/sec	0.5 rad/sec	1.0 rad/sec	2.0 rad/sec
Pitch							
Derotated Displ. (deg)	± 4.76						
Velocity (deg/sec)	60.0						
Acceleration (deg/sec^2)	±400.0						
K_{2P} = 0.0							
Derotated Displ. (deg)		20.36	19.41	11.7	5.51	2.12	0.97
Velocity (deg/sec)		5.58	5.43	5.0	3.30	2.16	1.09
K_{2P} = 0.5							
Derotated Displ. (deg)		21.06	22.01	16.0	12.58	10.5	10.42
Velocity (deg/sec)		5.67	5.65	5.73	4.89	3.96	4.51
K_{2P} = 1.0							
Derotated Displ. (deg)		22.79	24.61	20.34	18.26	19.51	20.40
Velocity (deg/sec)		5.75	5.87	6.47	7.07	7.14	8.94
Yaw							
Derotated Displ. (deg)	± 4.76	13.5	7.28	3.97	1.96	0.93	0.35
Velocity (deg/sec)	50.0	1.94	2.18	1.84	1.16	0.72	0.37
Acceleration (deg/sec^2)	±200.0						
Heave							
Displacement (ft)	± 10.0	300.0	210.0	91.5	24.0	6.0	1.41
Velocity (ft/sec)	13.0	42.0	34.5	28.5	8.7	4.5	1.5
Acceleration (ft/sec^2)	± 96.6	14.4	15.0	13.05	8.4	4.8	3.9
Roll (K_p = 0.5)							
Displacement (deg)	± 25.0						
Velocity (deg/sec)	60.0						
Acceleration (deg/sec)^2	± 460						
K_{2R} = 0.0							
Displacement (deg)		42.88	43.6	41.63	26.05	11.05	5.33
Velocity (deg/sec)		27.9	28.33	24.01	21.03	16.31	7.88
K_{2R} = 0.5							
Displacement (deg)		42.8	43.8	41.5	24.9	9.37	4.6
Velocity (deg/sec)		27.9	28.3	23.7	20.7	14.7	5.1
K_{2R} = 1.0							
Displacement (deg)		42.9	43.7	41.3	24.0	9.0	4.6
Velocity (deg/sec)		27.9	28.3	23.5	20.5	13.4	4.3

TABLE 10. (CONCLUDED)

	LAMARS LIMITS	BF=0.0675 rad/sec	0.125 rad/sec	0.25 rad/sec	0.5 rad/sec	1.0 rad/sec	2.0 rad/sec
Sway							
Displacement (ft)	± 10.0						
Velocity (ft/sec)	10.0						
Acceleration (ft/sec^2)	± 51.52						
K_{2R} = 0.0, C_{2y} = 0.0025							
Displacement (ft)		900.0	460.0	195.0	75.0	21.5	5.5
Velocity (ft/sec)		85.0	90.0	48.5	27.5	11.0	3.6
Acceleration (ft/sec^2)		26.9	23.6	24.16	13.7	5.84	3.14
K_{2R} = 0.0, C_{2y} = 0.0225							
Displacement (ft)		365.0	340.0	180.0	65.0	20.0	5.5
Velocity (ft/sec)		80.0	65.0	55.0	30.0	10.5	3.4
Acceleration (ft/sec^2)		26.4	28.0	21.7	10.7	6.33	3.4
K_{2R} = 0.0, C_{2y} = 0.25							
Displacement (ft)		80.0	70.0	60.0	35.0	12.0	3.45
Velocity (ft/sec)		28.4	30.2	29.8	12.9	6.36	2.33
Acceleration (ft/sec^2)		13.3	11.5	10.8	9.9	6.35	3.12
K_{2R} = 0.5, C_{2y} = 0.0225							
Displacement (ft)		365.0	345.0	180.0	65.0	22.0	6.5
Velocity (ft/sec)		80.0	65.0	55.0	30.5	11.5	4.0
Acceleration (ft/sec^2)		25.0	26.5	22.0	10.7	6.4	4.0
K_{2R} = 1.0, C_{2y} = 0.0025							
Displacement (ft)		900.0	470.0	200.0	85.0	26.0	8.0
Velocity (ft/sec)		85.0	90.0	50.0	29.0	12.5	5.0
Acceleration (ft/sec^2)		25.6	22.6	24.1	14.2	7.4	5.2
K_{2R} = 1.0, C_{2y} = 0.0225							
Displacement (ft)		365.0	345.0	185.0	70.0	24.0	8.0
Velocity (ft/sec)		80.0	65.0	55.0	31.0	12.5	4.9
Acceleration (ft/sec^2)		24.4	26.9	21.8	11.6	7.1	5.2
K_{2R} = 1.0, C_{2y} = 0.25							
Displacement (ft)		80.0	70.0	60.0	37.5	14.0	5.0
Velocity (ft/sec)		27.1	29.0	24.3	13.7	7.2	3.4
Acceleration (ft/sec^2)		12.2	10.8	10.7	9.7	7.9	4.7

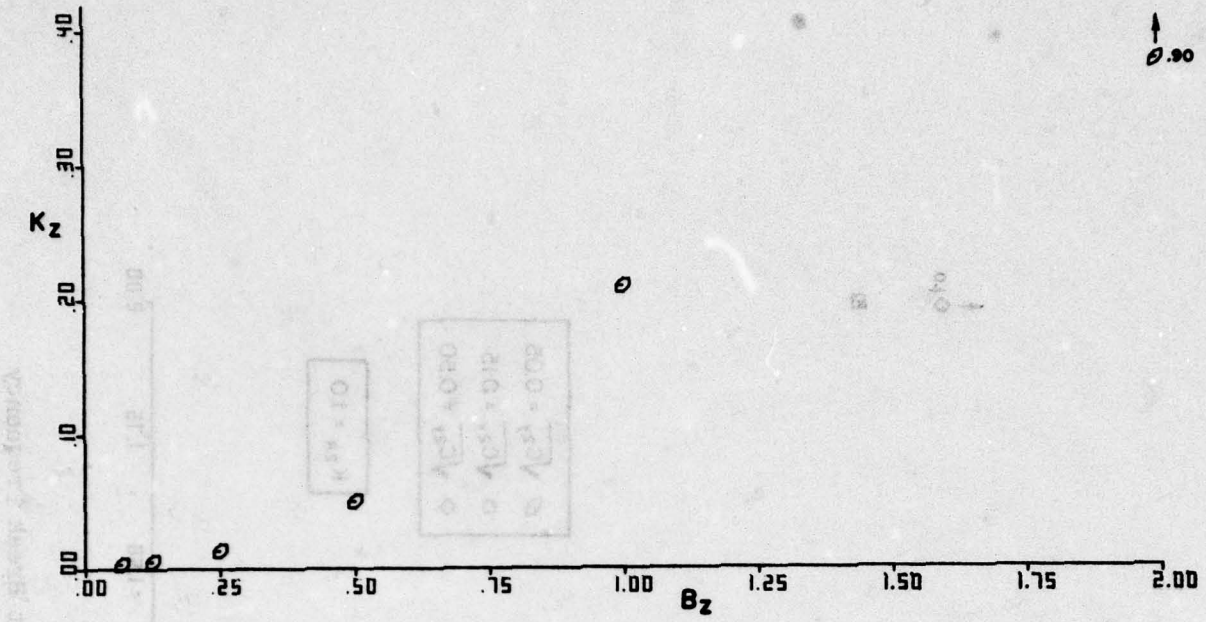

Figure 19. Computed Heave Scaling vs. Washout Break Frequency

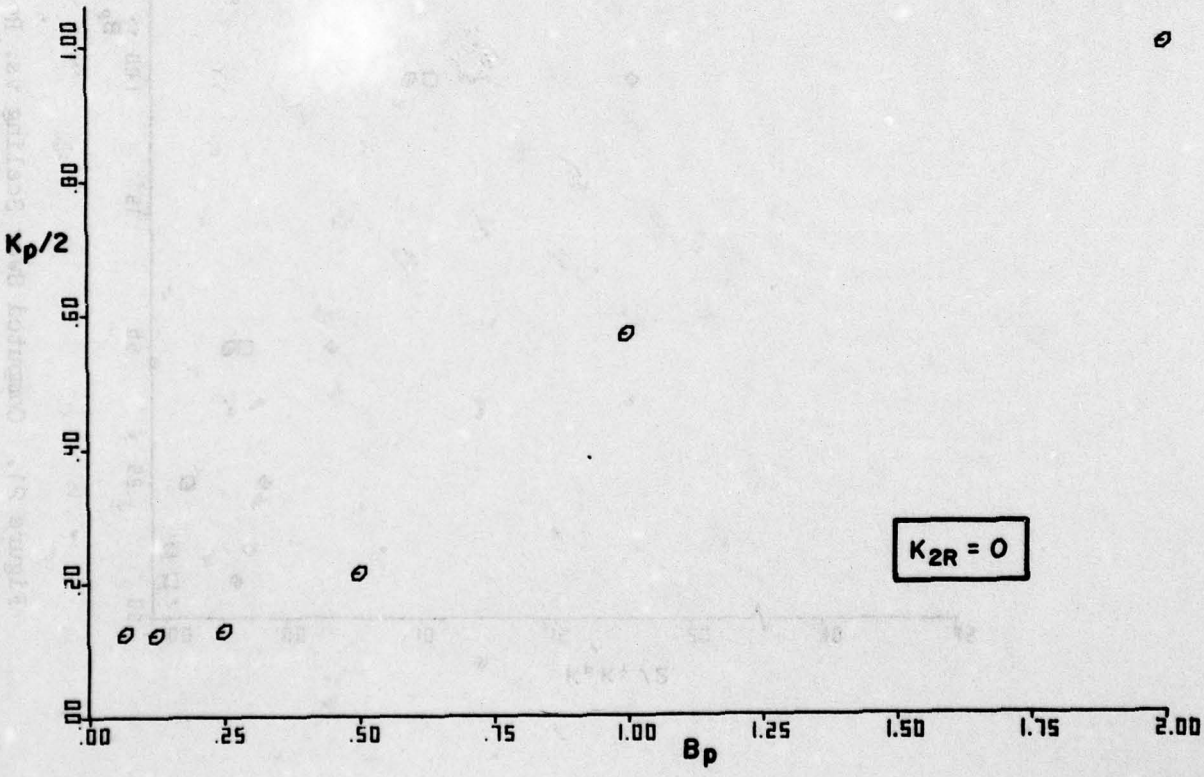

Figure 20. Computed Roll Scaling vs. Washout Break Frequency

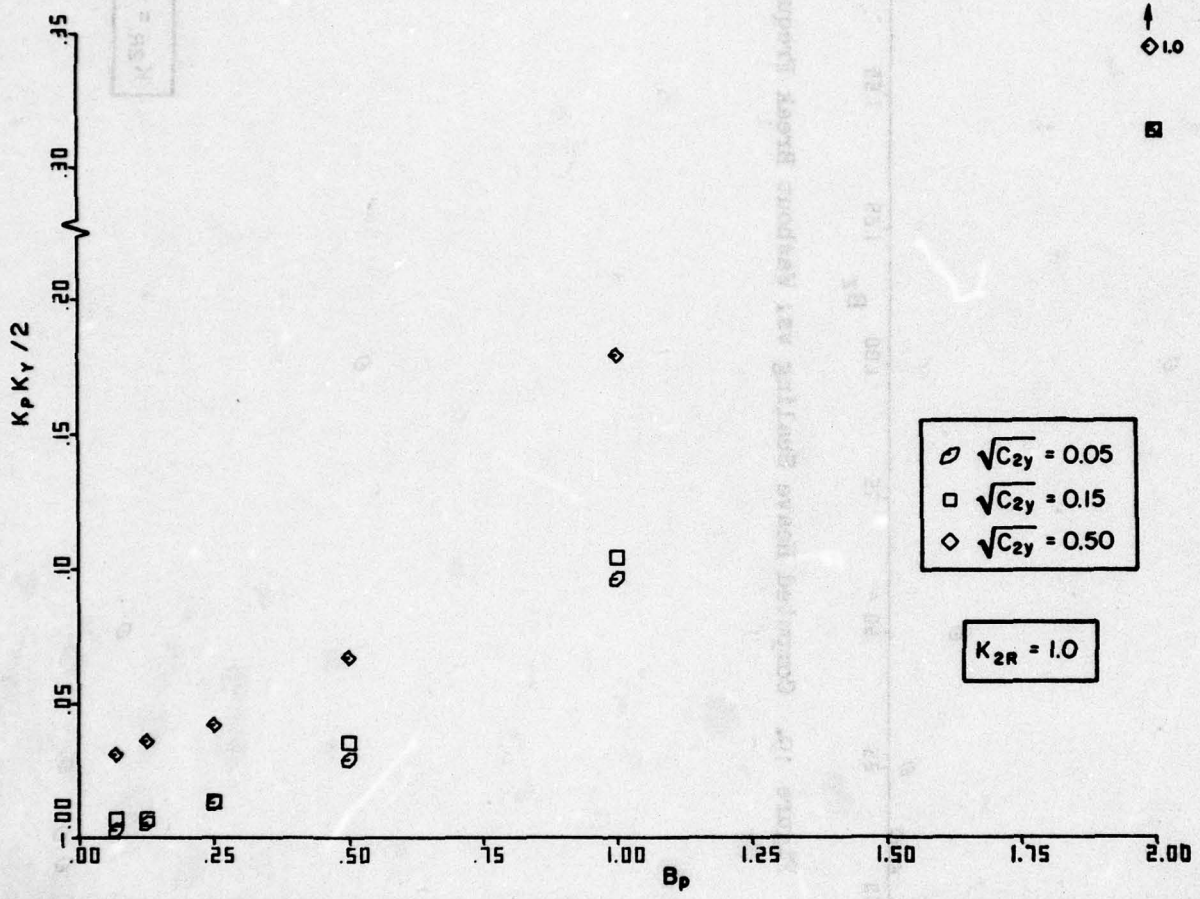

Figure 21. Computed Sway Scaling vs. Roll Washout Break Frequency

derived from the PACC, PVEL and PDIS entries in Tables C-9, and Tables 11-14 and the LAMARS motion limits listed in Table 7. Notice that the sway axis is also sensitive to variations in C_{2y} (as expected), so Fig. 21 is actually a family of curves. Table 11 provides a set of relationships which define the scaling gains for each axis. These relationships define the gains for the subsequent simulator experiment.

There is one important unknown left in the optimization process — the pilot marginal utility parameter, α. The marginal utility can be determined by a series of piloted simulation experiments. These are run for each axis using several combinations of gain and break frequency satisfying the relationships given in Table 11. Pilot opinion ratings and commentary can be used to establish the best among the several combinations and a relative ranking of the combinations. An estimate of the marginal utility parameter α, for the critical axis may then be inferred by means of the following process. The criterion (J_o or J_1) is evaluated as a function of α for each gain and break frequency combination used in the simulation experiment. The value of α which results in the minimum criterion value for the pilot-identified "best" combination and also results in the correct relative ranking according to criterion value, is accepted as the "true" marginal utility parameter value. The results of such an experiment will be presented in the next section.

Once the criterion and associated marginal utility parameter value, α, for each axis are available, this motion fidelity criterion is ready for application.

The next section presents the simulator experiments and results, which are used in the manner indicated above to discover appropriate values for the marginal utility parameter, α, for each axis.

TABLE 11. RELATIONSHIPS WHICH DEFINE LAMBS EXPERIMENT SCALING GAINS FOR EACH AXIS AS A FUNCTION OF WASHOUT BREAK FREQUENCY

Heave	$K_z = B_z^2/4$
Sway	$K_y = 2\sqrt{C_{2y}}$
Roll	$K_p = 0.286\ B_p$
Pitch	$K_q = 0.286\ B_q$
Yaw	$K_r = 0.286\ B_r$

SECTION V

SIMULATOR EXPERIMENTS

A. INTRODUCTION AND SUMMARY

A piloted simulation experimental series run on the Vought Corporation LAMBS moving base simulator was necessary to guide development of the drive logic optimization procedure. This provides:

- A data base including pilot ratings and rankings with systematic variations in drive logic parameters.
- A basis for selecting key parameters in motion fidelity criteria.
- A systematic survey of critical issues in moving base simulation for moderate maneuver amplitude flying tasks, particularly: g-suit effectiveness and roll sway coordination.

The first point is particularly important because there is no extant data base for moderate (or large) maneuver amplitude flying tasks wherein systematic variations of drive logic parameters have been explored. Such a data base is required in order to formulate an orderly drive logic optimization procedure.

Key experimental results obtained for three subject pilots and three air-to-ground delivery scenarios are:

- G-suit use is essential to perception of load factor for positive g maneuvering.
- Load factor representation via simulator heave motion is so distorted by washout effects that maximum subjective fidelity results for zero scaling gain (i.e., no motion) for this axis.
- Full simulator sway coordination for cab roll angle is required at high frequencies.
- Small roll axis scaling gains and associated small values of roll washout break frequencies result in maximum subjective fidelity. Furthermore, some small amount of roll axis motion is required to ameliorate vertigo when using limited field-of-view visual displays.

AD-A071 394 SYSTEMS TECHNOLOGY INC HAWTHORNE CALIF F/G 14/2
MANNED ENGINEERING FLIGHT SIMULATION VALIDATION. PART I. SIMULA--ETC(U)
FEB 79 L G HOFMANN, S A RIEDEL F33615-77-C-2065
UNCLASSIFIED STI-TR-1110-1 AFFDL-TR-78-192-PT-1 NL

2 OF 3
AD
A071394

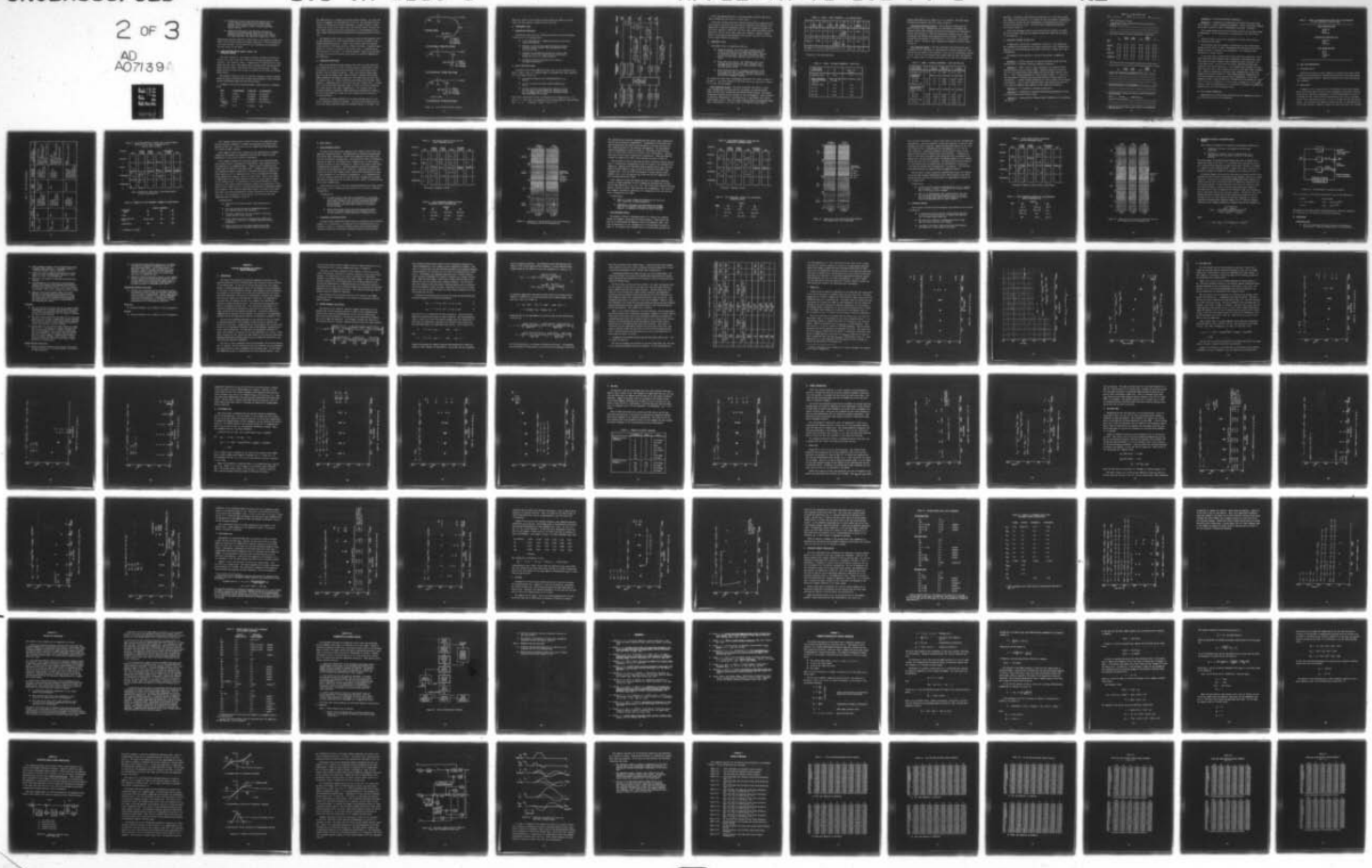

- Combinations of sway translation and residual cab tilt in roll should be such that lateral specific force response increases monotonically for a step lateral specific force command in order to maximize perceived motion fidelity.

- Subjective evaluations of yaw and pitch rate motion fidelity are not particularly sensitive to drive logic parameter variations over the range of practical interest for large amplitude, five degree-of-freedom motion bases.

Additionally, the data required to infer values of the marginal utility parameters (α's) relating scaling and dynamic components of motion reproduction error were obtained. Actual values for these parameters are developed in the next section of the report.

B. LARGE AMPLITUDE MOTION SYSTEM, COCKPIT, AND SIMULATED AIRCRAFT

The motion system is a five degree-of-freedom configuration (vertical, lateral, roll, yaw, pitch) that is driven by hydraulically powered linear actuators. The simulator cockpit is supported at the forward end of a rigid twenty-four foot beam. Beam angular motion through an aft mounted two-axis gimbal provides cockpit linear heave and lateral accelerations. Cockpit angular motion in pitch, roll and yaw is provided by the three-axis forward gimbal system.

The hydraulic system is a 500 to 3,200 psi, 360 gpm continuous, 560 gpm transient supply containing three 120 gpm electro-hydraulic servo controlled variable displacement pumps and three 250 hp motors.

A summary of the motion system performance characteristics is presented below:

Axis	± Displacement	± Velocity	± Acceleration
Roll	15 deg	34 deg/sec	59 rad/sec^2
Yaw	22.5 deg	48 deg/sec	29 rad/sec^2
Pitch	35 deg	77 deg/sec	68 rad/sec^2
Vertical (Heave)	10 ft	25 ft/sec	3.4g (from 1g)
Lateral	10 ft	13 ft/sec	1.5g

The LAMBS cockpit is a single place general purpose design. Its layout and general arrangement are representative of the A-7. The instrument display consists of conventional aircraft instruments. Cockpit controls include a conventional center stick, rudder pedals and throttle lever. Variable primary flight control feel forces are provided by an electrohydraulic force servo system longitudinally and laterally and a mechanical system directionally.

The external visual scene is a 36 deg by 48 deg (60 deg diagonal) field-of-view presentation on a 1000 line monochrome television display in the forward windscreen position. A 4000:1 scale terrain board with limited relief provides a VFR visual scene up to 8000 ft altitude. A gunnery range feature (in relief) is included on the terrain board. A computer-driven g-suit feature is available. A-7 aircraft dynamics, valid at all attitudes and angle of attack and including speed brakes and stability augmentation, are simulated.

C. SIMULATION FLYING TASKS

Three air-to-ground delivery scenarios were used; one curvilinear and two conventional with 15, 30 and 45 deg dive angles, respectively (it was not possible to use pop-up deliveries because the visual display cannot provide a horizon during the pop-up). These air-to-ground flying tasks were set up by Bill Neely, Capt. USAF to provide a maximum face validity within simulation environment constraints. The three scenario plan views are shown in Fig. 22. Initial conditions and g levels are indicated. Each scenario is terminated with a 4 g pull-off and left climbing turn. In formal runs, each scenario was flown three times in order to obtain an evaluation of a single motion drive logic configuration. (All scenarios were not necessarily flown to evaluate a single drive logic configuration, however.) The fixed sight depression angle for these flying tasks was appropriate to rocket delivery.

Differences in flying technique for Air Force and Navy pilots is evident in conventional delivery scenarios. Air Force pilots tend to roll-in in the dive plane, and then execute an unloaded roll-out on to final. The

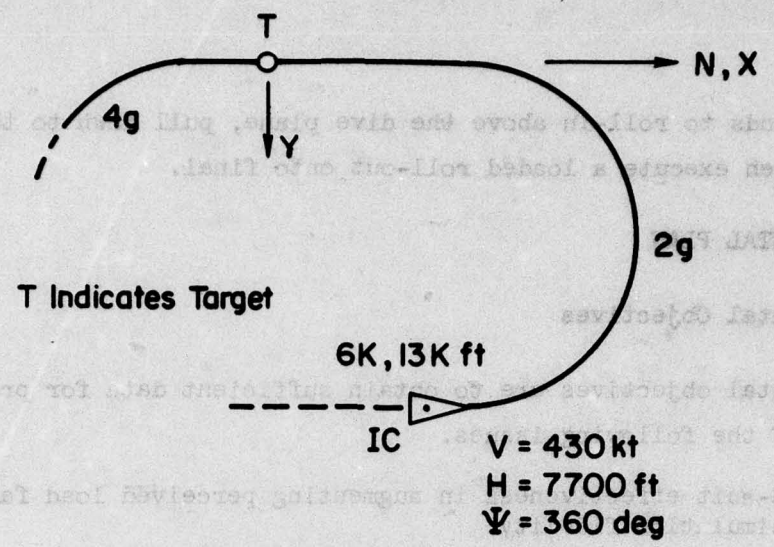

a) Curvilinear, 15 deg Dive Angle

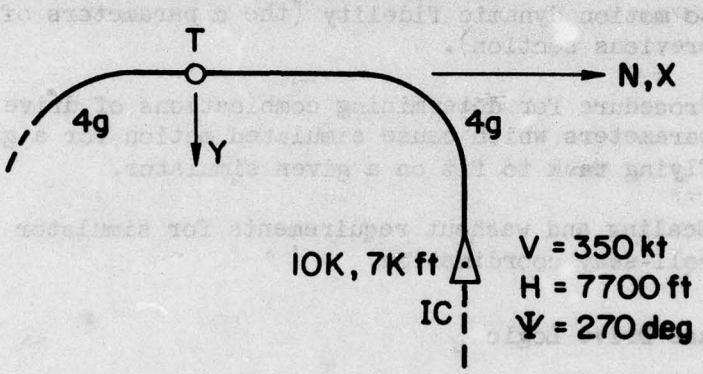

b) Conventional, 30 deg Dive Angle

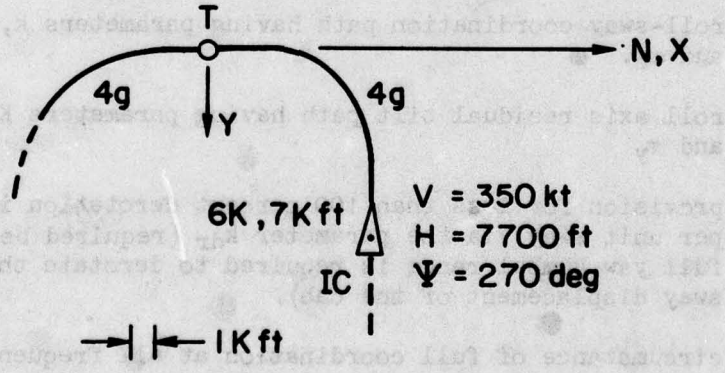

c) Conventional, 45 deg Dive Angle

Figure 22. Air-to-Ground Delivery Scenarios

Navy pilot tends to roll-in above the dive plane, pull down to the dive plane, and then execute a loaded roll-out onto final.

D. EXPERIMENTAL PLAN

1. Experimental Objectives

Experimental objectives are to obtain sufficient data for preliminary resolution of the following issues.

- G-suit effectiveness in augmenting perceived load factor simulation fidelity.
- Marginal utility of motion amplitude fidelity relative to motion dynamic fidelity (the α parameters of the previous section).
- Procedure for determining combinations of drive logic parameters which cause simulated motion for a given flying task to fit on a given simulator.
- Scaling and washout requirements for simulator roll-sway coordination.

2. Motion Base Drive Logic

The general form of the LAMBS drive logic used in this experimental program is shown in Fig. 23. Features added to the LAMBS drive logic expressly for this program include the

- roll-sway coordination path having parameters k, ζ_c, and ω_c.
- roll axis residual tilt path having parameters K_{YT} and τ_y
- provision for less than 100 percent derotation in yaw per unit sway via the parameter k_{dr} (required because full yaw gimbal range is required to derotate the full sway displacement of the cab).

Under ideal circumstance of full coordination at all frequencies, $k_c = 1.0$ and $\omega_c = 0$. Under ideal circumstances of full lateral specific force recovery, $K_{YT} = 1.0$, $\tau_y \doteq [2\zeta_{BR_Y}\omega_{BR_Y} + 2\zeta_Y\omega_Y]^{-1}$ and $K_Y = 1.0$.

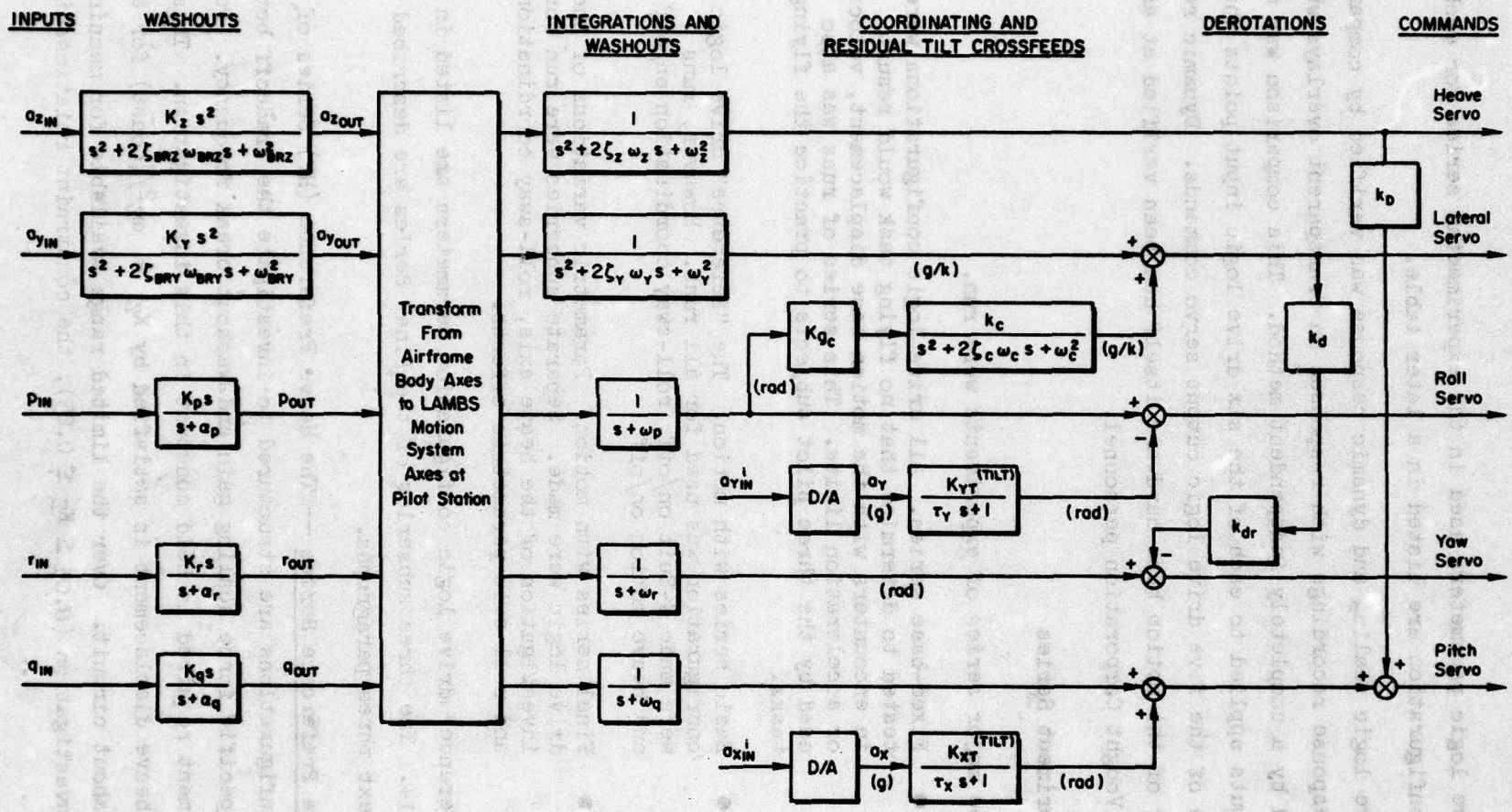

Figure 23. LAMBS Motion Base Drive Logic

Drive logic parameters used in the experimental series for each drive logic configuration are listed in a later table.

Drive logic scaling and dynamic response was verified by comparing strip chart response recordings with responses on transparent overlays which were computed by a completely independent method. This comparison was made for step inputs applied to each of the six drive logic input points while recording each of the five drive logic output servo commands. Dynamic response fidelity of the motion base hardware itself had been verified at an earlier time by Vought Corporation personnel.

3. Experiment Series

Three major series of experiments were run.

- Fixed-base series. All drive logic configurations were tested to determine that no flying task would result in encounters with the motion base displacement, velocity or acceleration limits. This series of runs was also used by the three pilot subjects to practice the flying tasks.

- Basic series with motion. The "Reference" drive logic configuration was used for all runs. However, runs were made G-Suit on/off, roll-sway coordination on/off and heave motion on/off.

- Final series with motion. Parametric variations of the drive logic were made. Separate subseries were run for investigation of the heave axis, roll-sway coordination and roll axis parametric effects.

The "Reference" drive logic configuration parameters are listed in Tables 12 through 14. The three subseries of the Final Series are described in detail by the next three paragraphs.

Heave Preference Series — The Heave Preference (HP) Series of drive logic configurations are structured to investigate the tradeoff between normal specific force scaling gain and washout break frequency. Peak heave displacement required is held constant in this investigation. This constraint on peak heave displacement is satisfied by $K_Z \doteq \omega_Z^2/(\text{const})$ for a fourth order washout circuit. Over the limited range available for meaningful experimental investigation ($0.05 \leq K_Z \leq 0.25$), the constraint relationship is

TABLE 12. LAMBS — FIXED PARAMETERS — ALL CONFIGURATIONS

K_r —	$\alpha_r = \omega_r$ rad/sec	ω_r rad/sec	K_q —	$\alpha_q = \omega_q$ rad/sec	ω_q rad/sec	K_{XT} deg/ft/sec^2	τ_x sec	K_{YT} deg/ft/sec^2	τ_y sec
0.2	0.7	0.7	0.2	0.7	0.7	0.890 (deg/g 28.65)	2.0	0.890	2.0

ζ_{BR_Z} —	ζ_Z —	ζ_{BR_Y} —	ζ_Y —	ζ_c —	K_{g_c} ft/sec^2/deg	k_d deg/ft	K_Y —	k_{dr}* —	
0.707	0.5	0.707	0.5	0.707	0.562	0.0	0.5	0.9	

* Fraction of full yaw derotation

TABLE 13. LAMBS — VARIABLE PARAMETERS — HEAVE AXIS

DRIVE LOGIC CONFIGURATION	K_Z —	$\omega_{BR_Z} = \omega_Z$ rad/sec
Reference Case	0.10	1.0
Heave Preference (with and without g-Suit)	(Roll and Sway axes at Reference Case settings)	
Reference Case	0.10	1.00
HP 0.15	0.15	1.15
HP 0.20	0.20	1.30
HP 0.25	0.25	1.45

further approximated as $\omega_Z \doteq 3(K_Z - 0.1) + 1.0$ rad/sec. The drive logic configuration parameters used are listed in Table 13.

Coordination Preference Series — The Coordination Preference (CP) Series of drive logic configurations are structured to investigate the tradeoff between high frequency coordination scaling gain and coordination washout break frequency. Peak sway displacement required and roll rate scaling gain and washout break frequency are held constant. The constraint on peak sway displacement is satisfied by $k_c \doteq 2.0\ \omega_c$ for a second order washout circuit. The drive logic configuration parameters used are listed in Table 14.

Roll Preference Series — The Roll Preference (RP) Series drive logic configurations are structured to investigate the tradeoff between roll rate scaling gain and washout break frequency. Peak cab roll displacement required is held constant at that constant value which allows the sway axis displacement to remain within the motion base limit for all roll axis configurations

TABLE 14. LAMBS — VARIABLE PARAMETERS — ROLL AND SWAY AXES

DRIVE LOGIC CONFIGURATION	K_p —	$\alpha_p = \omega_p$ rad/sec	$\omega_{BR_Y} = \omega_Y$ rad/sec	k_c —	ω_c rad/sec
Reference Case	0.2	0.7	0.625	1.0	0.5
Coordination Preference		(Heave axis at Reference Case settings)			
CP 0.25	0.2	0.7	0.625	0.25	0.125
CP 0.50	0.2	0.7	0.625	0.50	0.25
Reference Case	0.2	0.7	0.625	1.00	0.5
Roll Preference (Washed Out, Full Coordination)		(Heave axis at Reference Case settings)			
RP 0.05	0.05	0.175	0.625	1.00	0.5
RP 0.15	0.15	0.525	0.625	1.00	0.5
Reference Case	0.20	0.70	0.625	1.00	0.5
RP 0.30	0.30	1.05	0.625	1.00	0.5

specified. Coordination high frequency scaling gain is 1.0 and the coordination washout break frequency is 0.5 rad/sec for all roll washout configurations. The constraint on peak cab roll displacement is satisfied by $Kp \triangleq \omega_p/3.5$ for a second order washout circuit. The drive logic configuration parameters are listed in Table 14.

Drive logic parameter values for the pitch and roll residual tilt paths and for the second order yaw rate washout circuit were fixed and not subject to investigation.

4. Subjective Ratings and Protocols

A sample pilot rating form is reproduced in Table 15. One rating form was completed for each group of runs using a single drive logic configuration. Typically all three flying tasks were flown to evaluate a single drive logic configuration.

The purpose of each question on the pilot rating form is summarized below.

Question 1. — Obtain indication of special simulator flying technique. Requires pilot to identify limitations imposed by simulator.

Question 2. — Basic source of pilot rating data for simulated motion quality/fidelity vis-a-vis actual flight. Separate ratings are solicited for the pilot body-oriented three angular velocity and three specific force axes. A "one" rating corresponds to "same as actual flight". A "five" rating corresponds to "aborting the flying task because of nausea and/or disorientation". A "three" rating corresponds to a "net no value" for the motion cue presented. "Net no value" indicates either that the positive value factors offset the negative value factors or zero value of all factors.

Question 3. — A crosscheck on ratings of Question 2.

Question 4. — Separation of combined visual/motion presentation factors from motion presentation factors alone.

Question 5. — Opportunity to interpret motion infidelity as a disturbance-like effect.

TABLE 15. PILOT RATING FORM

RUN _____ SUBJECT _____ DATE _____

Read run number, name, day to tape.

1. Is your real-world flying technique modified because you are piloting a simulator? Yes ___, No ___.
   If Yes, how _____

2. Rate the motion quality for each axis by placing one X in each column.

MOTION IS:	ROLL	LATERAL G FORCE	NORMAL G FORCE	PITCH	LONGITUDINAL G FORCE	YAW	
1 REALISTIC							1
2 USEFUL							2
3 DISTRACTING							3
4 DISORIENTING							4
5							5

☐ Check if you have recorded comments supporting above ratings on tape.

3. Circle the axes for which "no motion" would be preferred to the motion provided.

ROLL LATERAL G FORCE NORMAL G FORCE PITCH LONGITUDINAL G FORCE YAW

4. Are the visual scene and motion sensations consistent? Yes ___, No ___, Possibly ___. Describe any inconsistencies _____

5. Do you detect turbulence or other disturbances? Yes ___, No ___ If Yes, describe characteristics of the disturbances. _____

6. If the G-Suit drive is active, does it add to, or detract from realism of G-force sensations?

   ADDS TO ___, NO EFFECT ___, DETRACTS FROM ___

   Comments on G-force sensations _____

7. Please tape record other comments on task, fidelity of A-7 representation, visual fidelity, etc.

Question 6. — G-suit effectiveness evaluation.

Question 7. — Separation of simulated motion factors from other simulation factors. Collect serendipitous comments. Attract nonrelevant comments which might otherwise be made in responding to Questions 1 through 6.

Pilot rating forms were filled out in their entirety for the Basic Series of experiments. In the Final Series, only Questions 2 and 3 were filled out.

During all Series, pilots were instructed to restrict their flying to the three prescribed tasks.

No particular order was observed in performing the three flying tasks during the Basic Series of runs. Replications were performed as the pilots deemed necessary to formulate their evaluations. All evaluations were delivered in a single session.

In the Final Series, flying tasks A and C were flown alternately. Three replications for each task-drive logic configuration combination were flown. Strip chart and digital magnetic tape recorded data were collected on the second replication. If that trial was "blown", additional records were collected on the third replication. Pilot comments were recorded on rating forms and voice tape at the conclusion of runs for each drive logic configuration. Orders of presentation for drive logic configurations in the Final Subseries are listed in Table 16. After completing each configuration the pilot was reminded of the motion axis under investigation. He was then prompted to make a forced declaration of preference for the motion (in that axis) of the last configuration or next-to-last configuration. He was also asked to order the configurations in the Subseries according to his subjective preference for the motion provided by each.

5. Pilot Subject Background

Backgrounds for the three participating pilots are summarized in Table 17. All three are test pilot school graduates.

TABLE 16. ORDERS OF PRESENTATION FOR DRIVE LOGIC CONFIGURATIONS IN FINAL SUBSERIES (G-SUIT-ON ONLY)

Heave Preference (HP)
Reference
HP.25
Reference
Coordination Preference (CP)
Reference
CP.50
Reference
Roll Preference (RP)
RP.05
RP.15
Reference
RP.30

E. DATA AND INTERPRETATION

1. Fixed-Base Series

Monitoring of the drive logic commands to the motion base servos showed validity of the procedure for constraining peak values of selected commands to be approximately constant. High face validity of the three flying tasks was confirmed.

2. Basic Series

A summary of pilot rating data for the "Reference" drive logic configuration and various special cases of that configuration are given in Table 18. No motion was identified as preferable to the motion provided for 12 out of 15 ratings for the "lateral g-force" presentation; for 2 out of 15 ratings for the "roll" presentation and for 1 out of 14 ratings for the "yaw" presentation. This indicates that numerical ratings for the roll axis motion tend to be biased downward. Numerical ratings for other axes tend to be confirmed.

TABLE 17. TEST PILOT BACKGROUNDS

SUBJECT	TOTAL TIME (HRS)	TYPE AIRCRAFT/ TIME	COMBAT HOURS	OPERATIONAL EXPERIENCE	EDUCATION (SPECIAL SCHOOLS)
ED (Capt., USAF)	2500	F-4/1370 F-100/500 Various Mil/200 Training/230 Light A/C/200	376 (F-100) (Air-to-Ground)	10 years Operational Fighters Air-to-Ground and Air-to-Air	BS-AFA 1967 Science [Physics] MBA – University of Utah (USAF Fighter Weapons School) (USAF Test Pilot School)
RH (LT., USN)	2000	F-4/150 A-4/400 A-7/1200 Other jet/200 Other prop/100	*None*	8 years Operational Attack/ Fighters	BS-USNA 1970 (USNTPS-71) (Top Gun School) (Have Gun Fleet Adversary School) (LTV Advanced Weapons School)
BN (Capt., USAF)	3100	O-2/850 C-141/1400 T-38/800 Other/100	850 (O-2)	Forward Air Controller, Transport Pilot, Air Training Command Instructor	BSME (USAF Test Pilot School)

TABLE 18. PILOT MOTION FIDELITY RATING DATA FOR BASIC SERIES
(Reference drive logic configuration and
special cases as noted)

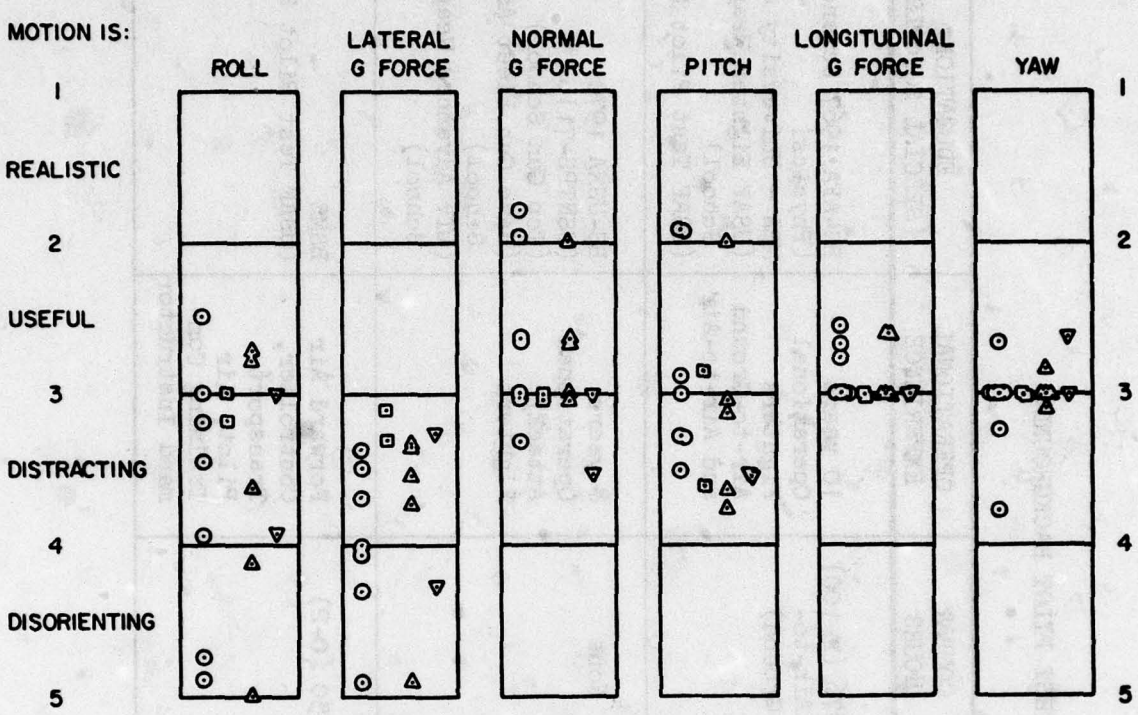

Legend: ⊙ Reference Case; Special Cases: ⊡ Normal Specific Force Off, ▽ G-Suit Off, △ Coordination Off

TABLE 19. SUMMARY OF PILOT PREFERENCE COMMENTS FOR BASIC SERIES

PREFERENCE ISSUE	SUBJECT PREFERENCE ED	RH	BN
G-Suit	ON	ON	ON
Normal Specific Force	OK ON or OFF	OFF	OFF
Coordination	ON*	ON*	ON*

* Preference is slight

Pilot comments indicate g-suit induced cues have very significant value. This was especially apparent in comments delivered when the subjects were deprived of this cue. G-suit cues have only slight value when maneuvering in a nearly unloaded condition.

Pilot comments indicate that "lateral g force" presentation is slightly improved by the presence of coordination, but that the "lateral g force" presentation is poor with or without coordination.

Pilot comments indicate that the g-suit induced cues considerably dominate "normal g force" in perception of load factor. These separate cues are not perceived in an integrated manner. "Normal g force" presentation has a small positive effect at load factor onset. "Normal g force" presentation has a moderately negative effect when a sustained load factor is pulled on as for rapid roll-in to a moderate g turn, or as in pulling off the target. Pilots describe this negative effect as a "pitch hop". (This is the result of rapid washout of the normal specific force cue.) Pilots tend to comment on the "normal g force" cue presentation in the "pitch" evaluation in distinction to the "normal g force" evaluation column of the rating form. Elimination of the "normal g force" cue presentation resulted in generally favorable pilot comments. Most reflected improvement because of absence of the "pitch hop" while some reflected degradation because of absence of the load factor onset cue. Pilot preferences for the special case conditions have been summarized from the comments in Table 19.

Interpretations:

- Fidelity of the lateral specific force presentation is poor.
- Roll axis fidelity ratings are downgraded because of poor lateral specific force fidelity.
- Roll-sway coordination has some influence on perceived lateral specific force fidelity.
- G-suit induced cues have a strong positive effect upon perception of load factor in moderate amplitude positive g maneuvers.
- Normal specific force cues may actually detract from simulation fidelity for moderate amplitude maneuvers.

3. Final Series

a. Heave Preference Series

The Basic Series experiments suggested that "normal g force" onset cues might have significant value. This hypothesis was tested by comparing data for a drive logic configuration (HP.25) which emphasized onset cues, with that for the Reference configuration. The experimental order of presentation is given in Table 16. The subjects were informed only as to which motion axis was the focus of this investigation. Subjects were asked to rank three configurations by preference. Resulting numerical ratings are summarized in Table 20 and rankings are given in Table 21. Numerical rating and ranking for the "pitch" and "normal g force" presentation evaluations both show a clear preference for the Reference configuration. It is remarkable that 2 of the 3 subjects identified the first and third configurations as being the same even though there was no reason for them to expect two presentations of the same configurations.

Time histories in Fig. 24 show the increased emphasis given normal specific force (a_{z_M}) onset by configuration HP.25 relative to that for the Reference configuration.

Interpretation:

- No normal specific force motion is preferable to that which could be provided within the constraints of these experiments. This result is based on both the Heave Preference and Basic Series findings. The rapid washout which must be used in normal specific force drive logic channels is responsible for this finding.

- Normal specific force onset cues have some positive value, but this is largely overshadowed by the negative effects of rapid washouts for abrupt maneuvers of moderate g level.

b. Coordination Preference Series

The Basic Series experiments showed washed out coordination was preferred slightly to no coordination. The purpose of the Coordination Series is to determine if there is a favorable tradeoff between reduced high frequency coordination path gain and reduced coordination washout break frequency.

TABLE 20. PILOT MOTION FIDELITY RATING DATA FOR HEAVE PREFERENCE SERIES

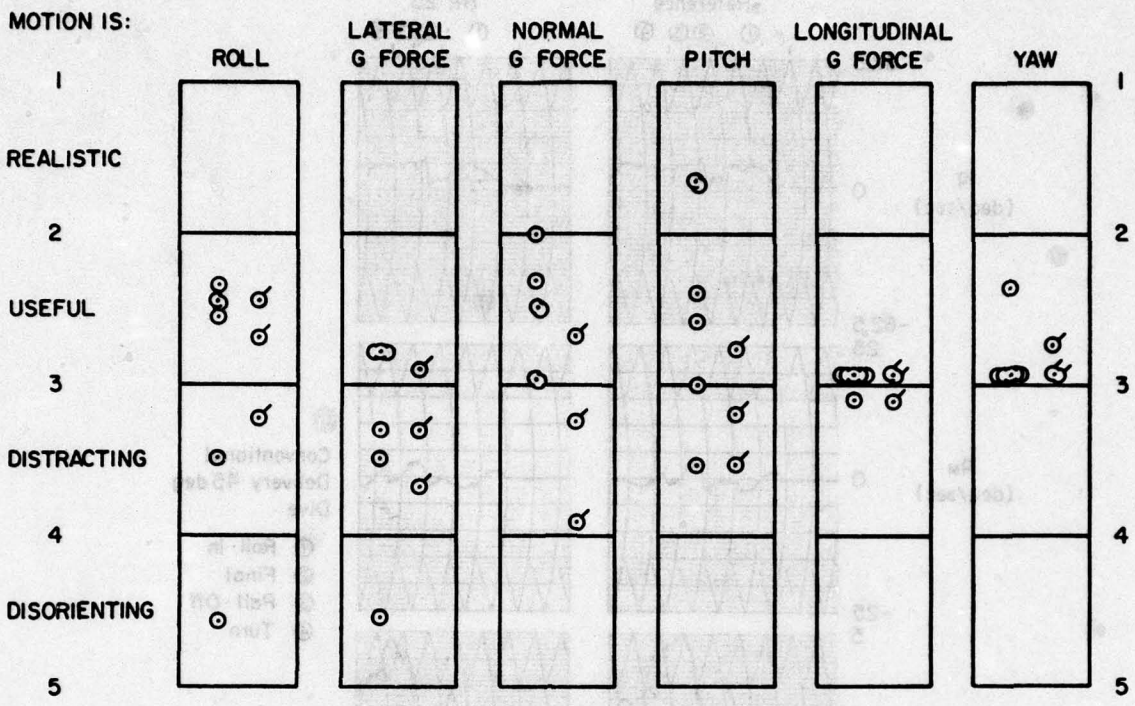

TABLE 21. PILOT PREFERENCE RANKINGS FOR HEAVE PREFERENCE SERIES CONFIGURATIONS

RANK	SUBJECT ED	RH	BN
1	1st Ref.	Last Ref.	Last Ref.
2	Last Ref.	1st Ref.	1st Ref.
3	HP.25	HP.25	HP.25

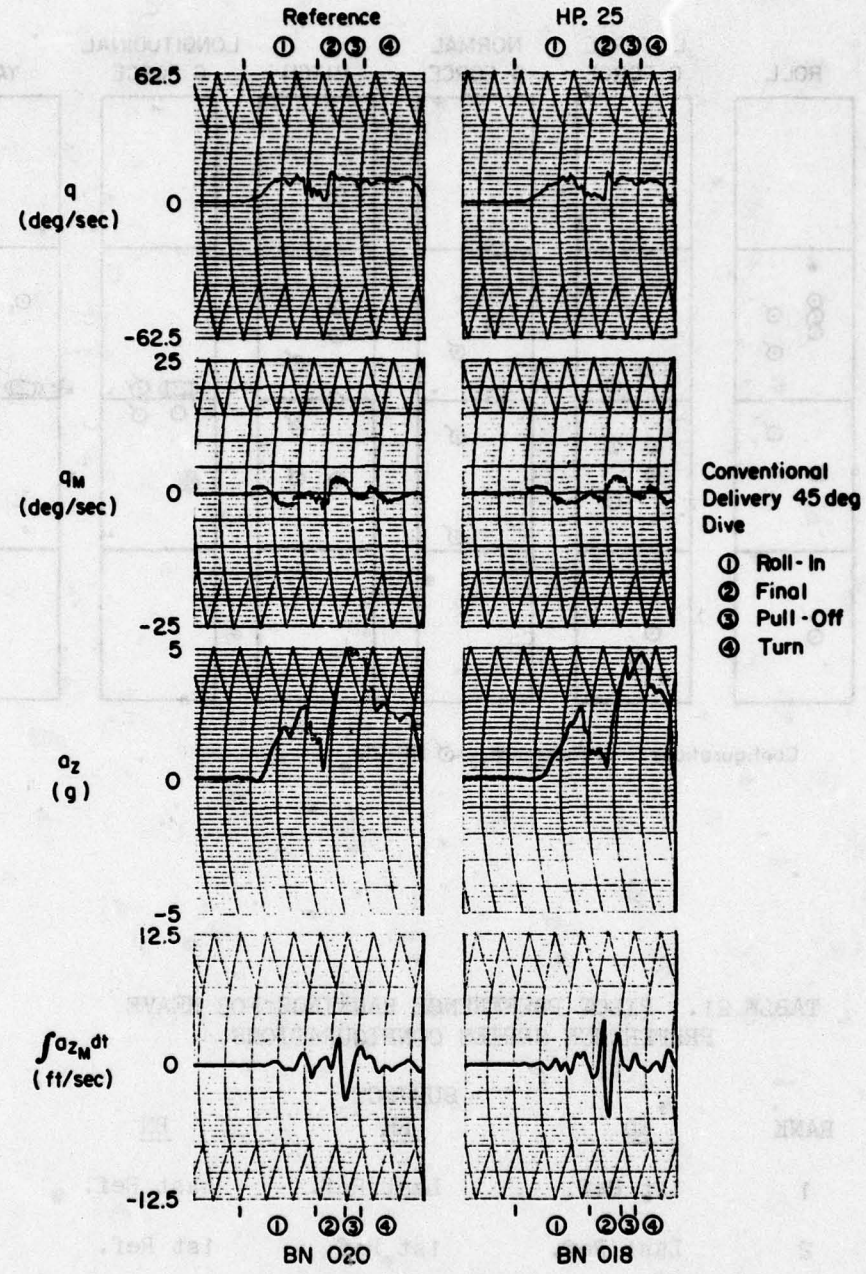

Figure 24. Comparison of Normal Specific Force Time Histories for Reference and HP.25 Configurations

This hypothesis was tested by comparing data for a drive logic configuration (CP.50) and the Reference configuration. Configuration CP.50 reduces both high frequency gain and washout break frequency to one-half the values in the coordination path for the Reference configuration. The experimental order of presentation is given in Table 16. The subjects were informed only as to which motion axis was the focus of this investigation. Subjects were asked to rank three configurations by preference. Resulting numerical ratings are summarized in Table 22 and rankings are given in Table 23.

Time histories in Fig. 25 show that the level of spurious lateral specific force is increased for configuration CP.50 with respect to the Reference configuration. Phasing of the presented lateral specific force, a_{y_M}, with the actual in-flight quantity, $a_{y_{IN}}$, is seen to be good for both drive logic configurations. Since the input scaling gain on lateral specific force commands is $K_Y = 0.5$, the $a_{y_{IN}}$ and a_{y_M} traces are directly comparable for the recording sensitivities used.

Pilot numerical rating and ranking data and pilot comments generally indicate a slight preference for the configuration providing full coordination at high frequencies (i.e., $k_c = 1.0$). Two of the three subjects indicated spurious "lateral g forces" were least for this configuration. The third subject comments indicated his preference for configuration CP.50 over the Reference configuration was slight.

Interpretation:

- There is at least slight pilot preference for full roll-sway coordination at high frequencies.
- Experimental conclusions are weak because the maximum level of low frequency coordination available provided marginal or inadequate roll-sway axis motion fidelity.

c. Roll Preference Series

The purpose of the Roll Preference Series is to explore the tradeoff between roll washout scaling gain and break frequency. These results are also key in establishing the marginal utility (α_p) parameter value. The order of presentation of the configurations in the experiment is given in Table 16. The subjects were informed only as to which motion axis was the

TABLE 22. PILOT MOTION FIDELITY RATING DATA FOR COORDINATION PREFERENCE SERIES

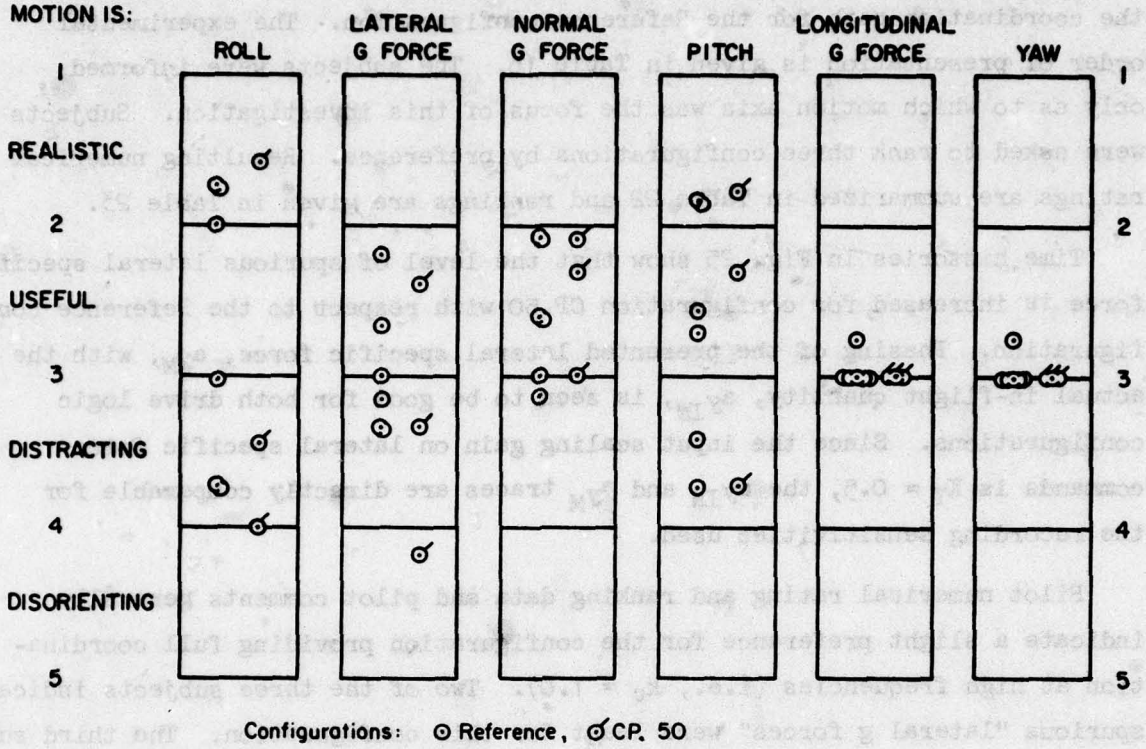

TABLE 23. PILOT PREFERENCE RANKINGS FOR COORDINATION PREFERENCE SERIES

	SUBJECT		
RANK	ED	RH	BN
1	1st Ref.	CP.50	1st Ref.
2	Last Ref.	1st Ref.	Last Ref.
3	CP.50	Last Ref.	CP.50

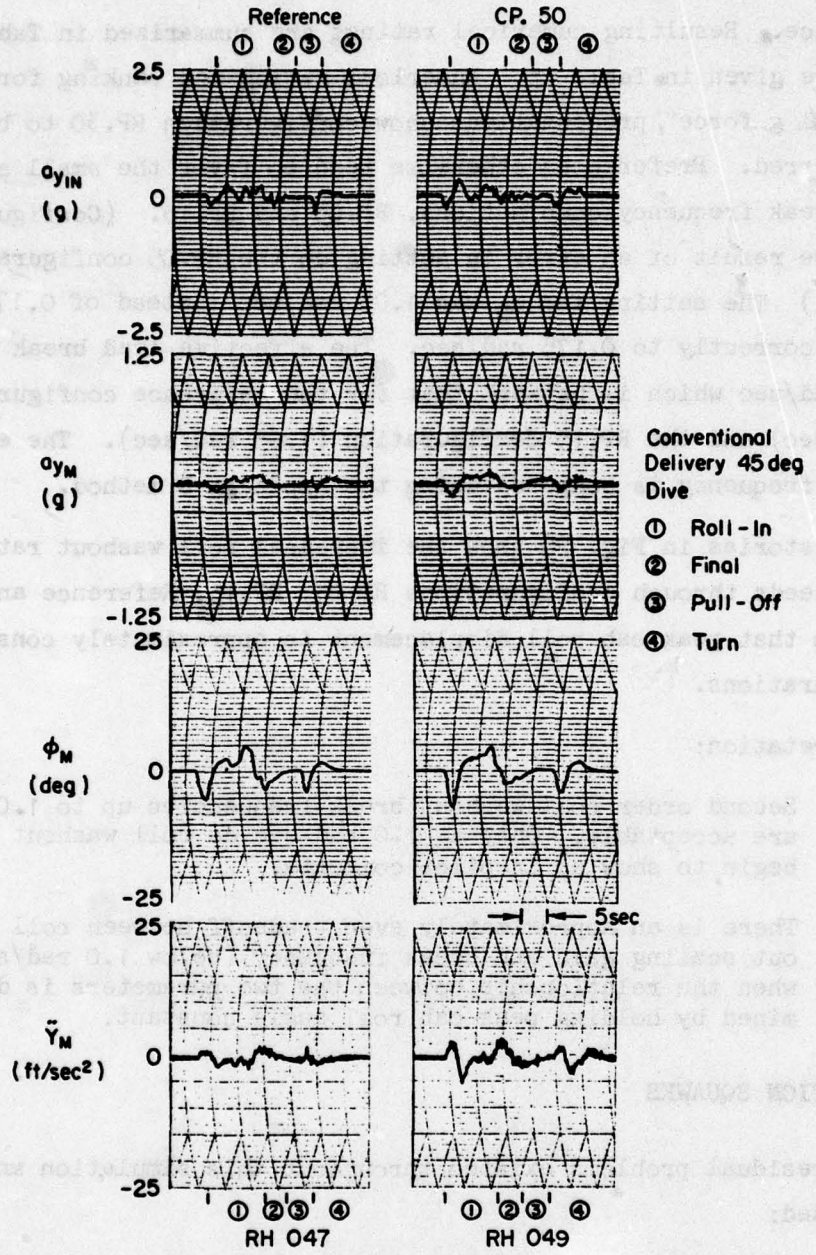

Figure 25. Comparison of Full and Partial High Frequency Gain Coordination Circuit Responses

focus of this investigation. Subjects were asked to rank four configurations by preference. Resulting numerical ratings are summarized in Table 24, and rankings are given in Table 25. Numerical rating and ranking for the "roll" and "lateral g force" presentations show configuration RP.30 to be the least preferred. Preferences otherwise tend to favor the small scaling gain/low break frequency combinations, RP.05 and RP.15. (Configuration RP.18 is the result of an error in setting up the RP.05 configuration for subject RH.) The setting for α_p was 1.05 rad/sec instead of 0.175 rad/sec. ω_p was set correctly to 0.175 rad/sec. The effective lead break frequency is 1.225 rad/sec which is between that for the Reference configuration (1.40 rad/sec) and the RP.15 configuration (1.05 rad/sec). The effective lead break frequency is computed using the Appendix D method.

Time histories in Fig. 26 show the increased roll washout rate effects as one proceeds through configurations RP.05, RP.15, Reference and RP.30. Notice also that peak cab roll displacement is approximately constant for all configurations.

Interpretation:

- Second order roll washout break frequencies up to 1.0 rad/sec are acceptable. Only at 1.0 rad/sec do roll washout effects begin to show up in pilot comments.
- There is an approximately even tradeoff between roll washout scaling gain and break frequency (below 1.0 rad/sec) when the relationship between the two parameters is determined by holding peak cab roll angle constant.

F. SIMULATION SQUAWKS

Three residual problems existed throughout this simulation and could not be eliminated:

- A-7 equations of motion produce strong proverse yaw while in fact the actual aircraft has an adverse yaw characteristic at these flight conditions.
- The motion base produces a "shuddering" motion in sway when the sign of cab roll rate changes.
- Occasional, very small, sway axis glitches give subjects the impression of small rudder kick inputs.

TABLE 24. PILOT MOTION FIDELITY RATING DATA
FOR ROLL PREFERENCE SERIES

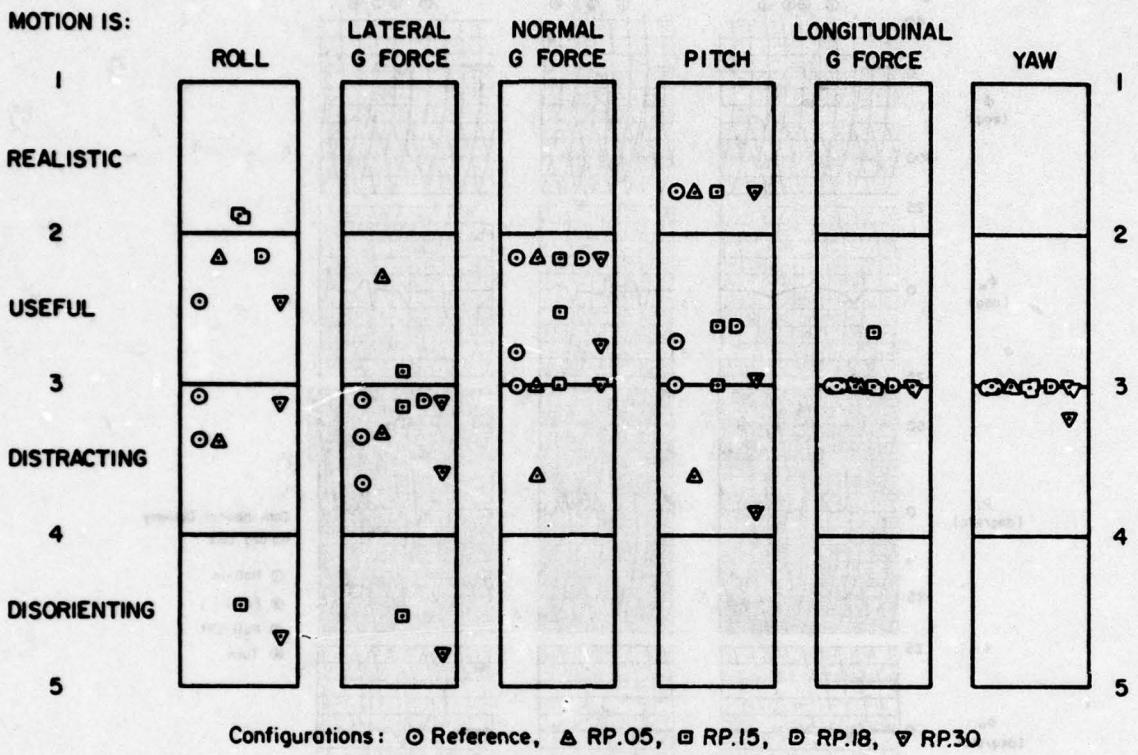

TABLE 25. PILOT PREFERENCE RANKINGS FOR ROLL PREFERENCE SERIES CONFIGURATIONS

	SUBJECT		
RANK	ED	RH	BN
1	RP.15	RP.15, RP.18	RP.05
2	RP.05, RP.30		REF.
3		REF.	RP.15
4	REF.	RP.30	RP.30

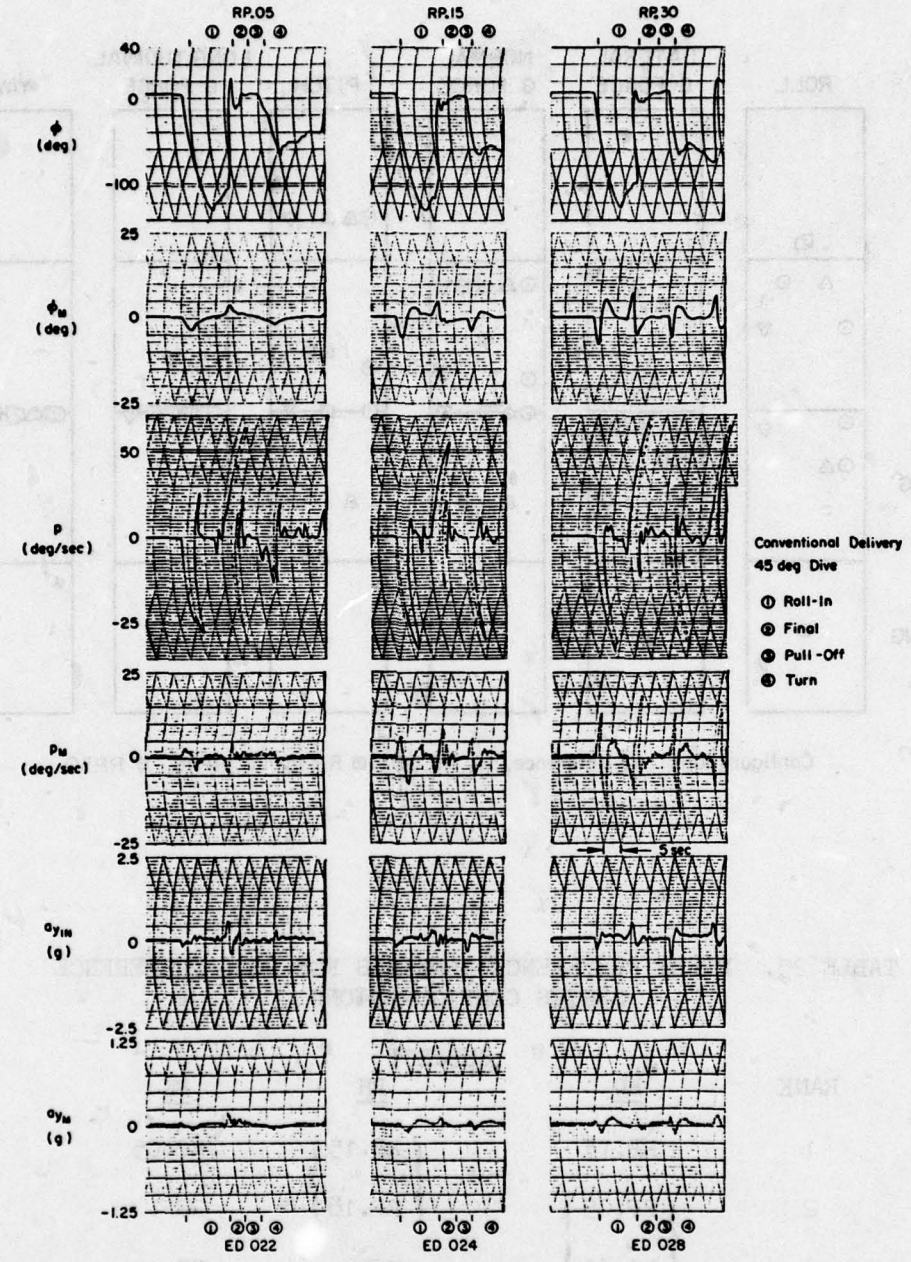

Figure 26. Comparison of Roll Axis Time Histories for the Roll Preference Series Configurations

G. QUALITATIVE ANALYSIS OF MISCOORDINATION EFFECTS

Pilot subjective impressions relating to miscoordination effects are:

- Sensation of falling to the inside of the turn upon initiation.
- Sensation of sitting on top of a rotating drum, i.e., significantly above the pilot's location in the actual aircraft.

The first comment is easily explained because the pilot is indeed tilted toward the inside of the "turn". To the extent that simulator cab tilt is not coordinated with simulator cab sway acceleration, the pilot is exposed to a spurious lateral specific force, $(-[g\varphi_M - \ddot{Y}_M])$ which is exactly that required to produce the sensation of falling to the inside of the turn.

The second comment arises from the same aspect of lateral specific force reproduction, but requires interpretation from a dynamic rather than a static viewpoint. Consider the following block diagram which shows components of lateral specific force arising from cab tilt, ideal sway coordination and the missing component of sway coordination which must be endured as a practical matter because of limited simulator sway displacement capability. The dashed path in Fig. 27 represents the kinematic effect of locating the pilot's seat above the cab roll axis when $(-\ell_z)>0$. Consider the $(-\ell_z)$ value giving equivalence between the "missing coordination component" and the "sitting on top of a drum" paths at an arbitrary frequency, ω. This is obtained by evaluating the frequency response for s^{-2} times the transfer function for the "missing coordination component" path at the frequency, ω.

$$(-\ell_z) = \frac{g\sqrt{1 + (2\zeta\omega/\omega_c)^2}}{\omega^2\sqrt{[1 - (\omega/\omega_c)^2]^2 + [2\zeta\omega/\omega_c]^2}}\, e^{j\theta}$$

where

$$\theta = \tan^{-1} 2\zeta\omega/\omega_c - \tan^{-1}[2\zeta\omega/\omega_c]/[1 - (\omega/\omega_c)^2]$$

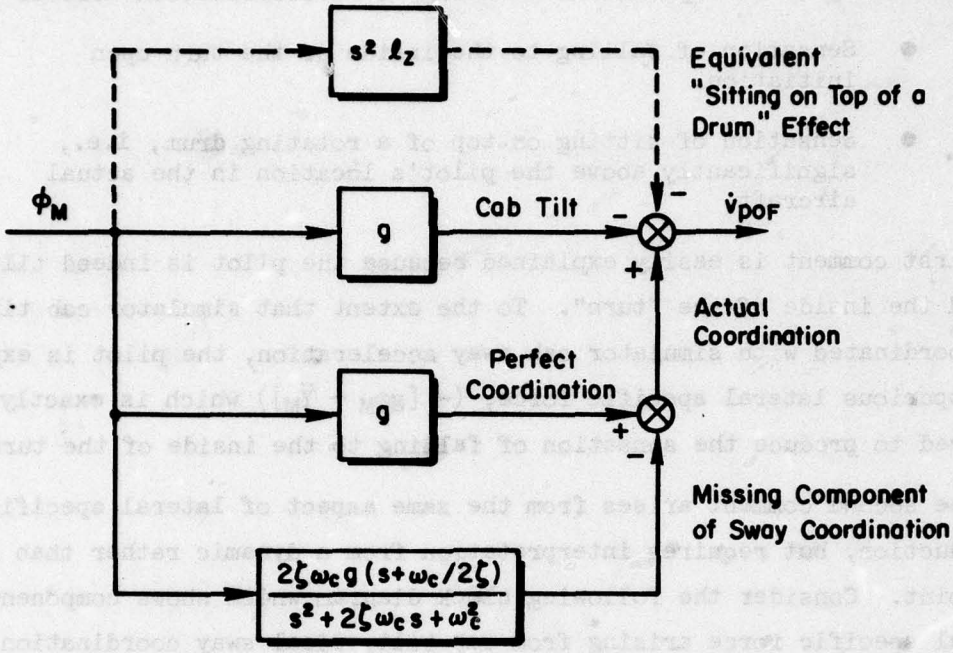

Figure 27. Block Diagram for Coordination Effects

Let $\zeta = 0.5$ and $\omega_c = 0.5$ rad/sec and evaluate $(-\ell_z)$ at key frequencies.

$$\omega \to 0 \qquad (-\ell_z) \to g/\omega^2$$

$$\omega = 0.5 \text{ rad/sec} \qquad (-\ell_z) = 4\sqrt{2}\, g\, e^{-j\pi/4}$$

$$\omega \to \infty \qquad (-\ell_z) = g/\omega^3\, e^{-j\pi/2}$$

The values of $(-\ell_z)$ which result clearly justify the subjective impression of "sitting on top of a drum" at low and mid frequencies.

H. CONCLUSIONS

Load Factor Axis

- G-suit cue dominates any motion which can be provided by the simulator. Subjects strongly prefer to use the g-suit.

- G-suit pressure schedule could be improved for better unloaded flight sensation. 1 g pressure could be increased, gradient could be increased.
- G-suit cue is not integrated with motion cue in perception. G-suit cue essentially "replaces" z axis motion cue roles in the flying task.
- Near-zero g and negative g simulation sensations are missing.
- Pilot preference in a z axis motion scaling versus washout rate tradeoff (with simulator heave axis displacement held constant) tends to favor zero scaling gain and zero washout rate. That is, no z-axis motion is preferred. This result presumes the g-suit is used.
- Spurious z-axis motion washout effects are quite apparent for moderate amplitude maneuvers such as are used in air-to-ground flying tasks (e.g., tight turn entry, pull-off). Subjectively these effects are identified as a "pitch hop," a rapid washout of the normal specific force.

Roll Axis

- Roll rate scaling and washout rate do not appear to have a direct sensitive influence upon angular motion perception. Effects are secondary because of the influence of these two characteristics upon the degree of coordination which can be achieved.
- Roll rate scaling gains over the range 0.05 to 0.30 (with washout rate set to give constant peak cab roll displacement, and with constant coordinating crossfeed characteristics) did not result in pilot comments indicating perceptual sensitivity to roll rate scaling.
- Second-order roll rate washout break frequencies ranged from 0.175 to 1.05 rad/sec in a manner consistent with the roll rate scaling gains to achieve constant peak cab roll displacement. Only at the most rapid washout rate (1.05 rad/sec) did roll washout effects begin to show up in pilot comments. Washout break frequencies up to 1.0 rad/sec therefore seem acceptable. Break frequencies should be limited to this value by appropriate use of scaling gain.

Lateral Specific Force Axis

- Moderate amplitude maneuvers having rapid onset characteristics require full roll-sway simulator coordination at high frequencies.

- A second-order washout break frequency of 0.5 rad/sec was found to be marginally acceptable for the roll-sway coordination path. A still lower value is desirable. Lack of roll-sway coordination at lower frequencies tends to give the pilot the impression that he is sitting further above the aircraft roll axis than is actually the case.
- Simulator lateral g response to lateral g step commands should be monotonically increasing with time in order to avoid dynamic cue infidelity for rudder inputs. A residual tilt wash-in first-order break frequency of 0.5 rad/sec results in acceptable tilt rates.

Longitudinal Specific Force Axis

- Residual tilt representation of longitudinal g forces was adequate as long as there was no rapid, large application of thrust or speed brakes. Rapid, large applications resulted in excessive tilt rates and inadequate sensation of acceleration. A residual tilt wash-in first-order break frequency of 0.5 rad/sec is a good compromise for the air-to-ground flying task.

Pitch Axis

- Generally adequate, not a subject of this investigation.

Yaw Axis

- Generally adequate, not a subject of this investigation.

SECTION VI

UTILIZING THE MEASURES AND CRITERIA — LAMARS OPTIMIZATION

A. INTRODUCTION

The results obtained from the simulator experiment described in the previous section are used to further refine the criteria for motion fidelity in the various axes. In the case of the yaw and heave axes, this simply amounts to inferring appropriate values for the marginal utility parameters on the basis of the experimental results. These marginal utility parameters are selected to cause trends in the criterion values consistent with pilot subjective evaluations elicited as the experimental variables were changed. For the pitch, surge, roll and sway axes it turns out, the experimental data show that the original criteria are inadequate for defining the subjective optimum reproduced motion. The roll-sway and pitch-surge axes must be considered as coupled sets. This necessitates development of a method for combining the criteria for, say, the roll and sway axes into a single criterion for the coupled roll-sway set. A plausible combination, suggested by the variation of the measures as a function of the experimental variables and by the experimental results, is developed in parametric form.

Once the final parameterized forms for the revised criteria are chosen, the measures generated in the parametric study are used to evaluate the criteria for each axis. Assumed values for the parameters and the particular values for the experimental variables used in the simulator experiments are used in these evaluations. For each axis, the appropriate criterion (J) values were computed as functions of the free parameters (α, β and λ). These three constants are then chosen such that trends in the criterion values with changing experimental variables match the pilot subjective evaluations elicited during the simulator experiment.

Once the α, β and λ parameter values are determined, the criteria development is complete, and the resulting criteria are ready for use for optimizing any particular motion base configuration for any given task. In this study, the LAMARS motion base is optimized for the air-to-ground scenario. Also,

two nonlinear washout features added to the basic LAMARS framework are considered briefly once the basic LAMARS drive logic is optimized.

Obviously, the method described in this chapter is based upon a relatively few simulator experimental conditions explored in this limited scope program. The significance of the results transcends the limitations imposed by this modest experimental data base, however. This is so because the main contribution is the demonstration of an orderly method for predicting the effectiveness of simulating motion for a particular task on a particular motion base, and an orderly procedure for optimizing the available parameters of the simulation drive logic. This method and procedure may be applied readily by simulation engineers.

The following sections discuss revision of the criteria, the LAMARS optimization and the investigation of the Parrish and subliminal nonlinear washout features.

B. REVISED MEASURES AND CRITERIA

The results of the simulator experiment suggest reexamination of the measures and criteria developed earlier in order to more comprehensively reflect motion fidelity requirements for the two sets of coupled axes. This necessity arises mainly in connection with the translational washouts used in the surge and sway axes. As an example, consider the equation for the original sway axis criterion computed using the post-drive logic measures:

$$J_1 = (1-K_{2R})^2 + k^2\left\{\left[\frac{\overline{(K_{2R}\dot{v}_{po} - \dot{v}_{poF})^2_{K_p=0}}}{K_{2R}^2\overline{\dot{v}_{po}^2}}\right] + \left[\frac{\overline{(K_{2R}\dot{v}_{po} - \dot{v}_{poF})^2} - \overline{(K_{2R}\dot{v}_{po} - \dot{v}_{poF})^2_{K_p=0}}}{K_{2R}^2\overline{\dot{v}_{po}^2}}\right]\right\}$$

$$+ 2k(1-K_{2R})\left\{\left[\frac{\overline{K_{2R}\dot{v}_{po}^2 - (\dot{v}_{po}\dot{v}_{poF})_{K_p=0}}}{K_{2R}\overline{\dot{v}_{po}^2}}\right] + \left[\frac{\overline{(\dot{v}_{po}\dot{v}_{poF})_{K_p=0}} - \overline{(\dot{v}_{po}\dot{v}_{poF})}}{K_{2R}\overline{\dot{v}_{po}^2}}\right]\right\}$$

This criterion treats lateral specific force reproduction fidelity virtually independently of roll angular velocity reproduction fidelity. However, it is clear that roll axis scaling and washout rate strongly influence lateral specific force fidelity and vice versa via requirements for coordination. Furthermore, low frequency representations of lateral specific force achieved via residual tilt results in spurious roll angular velocity cues. These two facts make it clear that a single criterion must be formulated for the roll and sway axes considered together. This criterion must also combine all key and usually competing demands upon the simulator for motion fidelity in these two axes. Similarity of the pitch and surge axes to the roll and sway axes makes the above remarks appropriate for the pitch-surge axes as well.

Consider the following criteria for the roll-sway and pitch-surge axes which are responsive to the above requirements.

$$J_{YP} = [1 - \beta]\, J_Y + \beta([1 - \lambda]\, J_P + \lambda\, J_{YT}) \qquad (1)$$

$$J_{XQ} = [1 - \beta]\, J_X + \beta([1 - \lambda]\, J_Q + \lambda\, J_{XT}) \qquad (2)$$

Each criterion is a combination of three subcriteria. Each subcriterion emphasizes one particular aspect of motion fidelity. The free parameters, β and λ, allow us to tailor the relative weights given the subcriteria in order that the combination correspond with subjective pilot evaluations. The particular form of the right hand sides for Eq. 1 and 2 assures that:

If $J_Y = J_P = J_{YT} = 1$ then $J_{YP} = 1$

and

If $J_Y = J_P = J_{YT} = 0$ then $J_{YP} = 0$

thereby maintaining the original limiting case properties for these new criteria. Next consider the subcriteria. J_{YT} is new, and J_Y is modified

from its original definition. J_{YT} represents motion reproduction error effects of the lateral specific force response to lateral specific force command inputs in the absence of roll rate commands (i.e., with $K_p = 0$).

$$J_{YT} = (1 - K_{2R})^2 + k^2 \left[\frac{\overline{(K_{2R}\,\dot{v}_{po} - \dot{v}_{poF})^2_{K_p=0}}}{K_{2R}^2\,\overline{\dot{v}_{po}^2}} \right] + 2k(1 - K_{2R}) \left[\frac{K_{2R}\,\overline{\dot{v}_{po}^2} - \overline{(\dot{v}_{po}\,\dot{v}_{poF})_{K_p=0}}}{K_{2R}\,\overline{\dot{v}_{po}^2}} \right] \tag{3}$$

J_Y represents <u>sway</u> motion reproduction error effects for the sway axis in response to coordination and lateral specific force command inputs. The error upon which J_Y is based is:

$$\epsilon_s = \dot{v}_{po} - \dot{v}_{poF} = \dot{v}_{po} - (\ddot{y} - g\varphi_m) = (g\varphi_m + \dot{v}_{po}) - \ddot{y}$$

$$= (1 - K_y)(g\varphi_m + \dot{v}_{po}) + K_y(g\varphi_m + \dot{v}_{po}) - \ddot{y}$$

Remaining steps in the development of J_Y are the same as those used earlier in Section IV.

$$J_Y = (1 - K_y)^2 + k^2 \left\{ \left[\frac{\overline{[K_y(g\varphi_m + \dot{v}_{po}] - \ddot{y})^2_{K_p=0}}}{K_y^2\,\overline{(g\varphi_m + \dot{v}_{po})^2}} \right] + \left[\frac{\overline{(K_y[g\varphi_m + \dot{v}_{po}] - \ddot{y})^2} - \overline{(K_y[g\varphi_m + \dot{v}_{po}] - \ddot{y})^2_{K_p=0}}}{K_y^2\,\overline{(g\varphi_m + \dot{v}_{po})^2}} \right] \right\}$$

$$+ 2K(1 - K_y) \left\{ \left[\frac{K_y\,\overline{(g\varphi_m + \dot{v}_{po})^2} - \overline{[(g\varphi_m + \dot{v}_{po})\ddot{y}]_{K_p=0}}}{K_y\,\overline{(g\varphi_m + \dot{v}_{po})^2}} \right] + \left[\frac{\overline{[(g\varphi_m + \dot{v}_{po})\ddot{y}]_{K_p=0}} - \overline{[(g\varphi_m + \dot{v}_{po})\ddot{y}]}}{K_y^2\,\overline{(g\varphi_m + \dot{v}_{po})^2}} \right] \right\}$$

The third subcriterion, J_p, retains its original definition. J_p represents motion reproduction error effects for the roll axis in response to roll rate

and lateral specific force command inputs. (Lateral specific force command inputs produce a false roll rate cue response because residual tilt is used to provide low-frequency lateral specific force reproduction.)

Corresponding definitions apply for J_{XT}, J_X, and J_Q respectively. The resulting criteria, J_{YP} and J_{XQ}, now embody terms representing all effects which potentially may compromise motion fidelity in the roll-sway and pitch-surge axis respectively.

The final step in revision of the criteria is to limit the measures used for all criteria (other than for the heave axis with the g-suit active) to those computed from post-drive logic variables. The main reason for this decision is the finding that, almost without exception, post-perceptual processing and post-threshold processing measures are little different and are frequently larger than corresponding post-drive logic quantities. This disappointing finding is contrary to a key initial premise. Namely, it had been presumed at the outset that post-perceptual processing and post-threshold processing measures would be significantly smaller than corresponding post-drive logic measures. This turned out to be false.

There is one notable exception to the above finding. The post-perceptual processing measures which incorporate perceptual integration of normal specific force motion and g-suit tactile cues show marked reduction with respect to corresponding post-drive logic measures (which do not include g-suit effects). However, the post-perceptual processing measures without g-suit effects approximate the corresponding post-drive logic measures. This result is consistent with the experimental subjective opinion that g-suit cues, when present, dominate normal specific force cues for the air-to-ground flying task. Post-perceptual processing measures are used in the heave axis criterion when the g-suit is active.

A summary of the revised criteria and the subcriteria used in Eqs. 1 and 2 is given in Table 26.

Now that the measures and criteria are in their final form, the last step in the criteria development process can proceed. In this step values for

TABLE 26. REVISED LIST OF MEASURES

	PDL1	PDL2	PDL3	PDL4	PEAK ACCELERATION	PEAK VELOCITY	PEAK DISPLACEMENT
J_P	$\frac{(\overline{p_e^2})_{K_{2R}=0}}{K_p^2\overline{p_A^2}}$	$\frac{(\overline{p_e^2}) - (\overline{p_e^2})_{K_{2R}=0}}{K_p^2\overline{p_A^2}}$	$\frac{K_p\overline{p_A^2} - (\overline{p_A p_{AF}})_{K_{2R}=0}}{K_p\overline{p_A^2}}$	$\frac{(\overline{p_A p_{AF}})_{K_{2R}=0} - (\overline{p_A p_{AF}})}{K_p\overline{p_A^2}}$		$\frac{\lvert\dot{\phi}_M\rvert_{peak}}{K_pK_y}$	$\frac{\lvert\phi_M\rvert_{peak}}{K_pK_y}$
J_Y	$\frac{\overline{[K_y(\varepsilon\omega_m + \dot{v}_{po}) - y]^2}_{K_p=0}}{K_y^2\overline{(\varepsilon\omega_m + \dot{v}_{po})^2}}$	$\frac{\overline{[K_y(\varepsilon\omega_m + \dot{v}_{po}) - y]^2}}{K_y^2\overline{(\varepsilon\omega_m + \dot{v}_{po})^2}}$ - PDL1	$\frac{K_y\overline{(\varepsilon\omega_m + \dot{v}_{po})^2} - \overline{(\varepsilon\omega_m + \dot{v}_{po})y}_{K_p=0}}{K_y\overline{(\varepsilon\omega_m + \dot{v}_{po})^2}}$	$\frac{\overline{(\varepsilon\omega_m + \dot{v}_{po})y}_{K_p=0} - \overline{(\varepsilon\omega_m + \dot{v}_{po})y}}{K_y\overline{(\varepsilon\omega_m + \dot{v}_{po})^2}}$	$\frac{\lvert\ddot{y}_M\rvert_{peak}}{K_pK_y}$	$\frac{\lvert\dot{y}_M\rvert_{peak}}{K_pK_y}$	$\frac{\lvert y_M\rvert_{peak}}{K_pK_y}$
J_{YT}	$\frac{(\overline{v_e^2})_{K_p=0}}{K_{2R}^2\overline{\dot{v}_{po}^2}}$		$\frac{K_{2R}\overline{\dot{v}_{po}^2} - (\overline{\dot{v}_{po}\dot{v}_{poF}})_{K_p=0}}{K_{2R}\overline{\dot{v}_{po}^2}}$				
J_Q	$\frac{(\overline{q_e^2})_{K_{2p}=0}}{K_q^2\overline{q_A^2}}$	$\frac{(\overline{q_e^2}) - (\overline{q_e^2})_{K_{2p}=0}}{K_q^2\overline{q_A^2}}$	$\frac{K_q\overline{q_A^2} - (\overline{q_A q_{AF}})_{K_{2p}=0}}{K_q\overline{q_A^2}}$	$\frac{(\overline{q_A q_{AF}})_{K_{2p}=0} - (\overline{q_A q_{AF}})}{K_q\overline{q_A^2}}$		$\frac{\lvert\dot{\theta}_M\rvert_{peak}}{K_q}$	$\frac{\lvert\theta_M\rvert_{peak}}{K_q}$
J_X	$\frac{\overline{[K_x(\varepsilon\theta_m + \dot{u}_{po}) - \ddot{x}]^2}_{K_q=0}}{K_x^2\overline{(\varepsilon\theta_m + \dot{u}_{po})^2}}$	$\frac{\overline{[K_x(\varepsilon\theta_m + \dot{u}_{po}) - \ddot{x}]^2}}{K_x^2\overline{(\varepsilon\theta_m + \dot{u}_{po})^2}}$ - PDL1	$\frac{K_x\overline{(\varepsilon\theta_m + \dot{u}_{po})^2} - \overline{(\varepsilon\theta_m + \dot{u}_{po})\ddot{x}}_{K_q=0}}{K_x\overline{(\varepsilon\theta_m + \dot{u}_{po})^2}}$	$\frac{\overline{(\varepsilon\theta_m + \dot{u}_{po})\ddot{x}}_{K_q=0} - \overline{(\varepsilon\theta_m + \dot{u}_{po})\ddot{x}}}{K_x\overline{(\varepsilon\theta_m + u_{po})^2}}$			
J_{XT}	$\frac{(\overline{u_e^2})_{K_q=0}}{K_{2R}^2\overline{\dot{u}_{po}^2}}$		$\frac{K_{2p}\overline{\dot{u}_{po}} - (\overline{\dot{u}_{po}\dot{u}_{poF}})_{K_q=0}}{K_{2R}\overline{\dot{u}_{po}}}$				
J_R	$\frac{\overline{r_e^2}}{K_r^2\overline{r_A^2}}$		$\frac{K_r\overline{r_A^2} - (\overline{r_A r_{AF}})}{K_r\overline{r_A^2}}$			$\frac{\lvert\dot{\psi}_M\rvert_{peak}}{K_r}$	$\frac{\lvert\psi_M\rvert_{peak}}{K_r}$
J_Z	$\frac{(\overline{\dot{v}_e^2})}{K_z^2\overline{\dot{v}_{po}^2}}$		$\frac{K_z\overline{\dot{v}_{po}^2} - (\overline{\dot{v}_{po}\dot{v}_{poF}})}{K_z\overline{\dot{v}_{po}^2}}$		$\frac{\lvert\ddot{z}_M\rvert_{peak}}{K_z}$	$\frac{\lvert\dot{z}_M\rvert_{peak}}{K_z}$	$\frac{\lvert z_M\rvert_{peak}}{K_z}$
$J_{Z_{gs}}$	$\frac{(\overline{\dot{v}_{Ie}^2})}{K_z^2\overline{\dot{v}_{poI}^2}}$		$\frac{K_z\overline{\dot{v}_{poI}^2} - (\overline{\dot{v}_{poI}\dot{v}_{poFS}})}{K_z\overline{\dot{v}_{poI}^2}}$				
$J_{Z_{ngs}}$	$\frac{(\overline{\dot{v}_{Ie}^2})}{K_z^2\overline{\dot{v}_{poI}^2}}$		$\frac{K_z\overline{\dot{v}_{poI}^2} - (\overline{\dot{v}_{poI}\dot{v}_{poFI}})}{K_z\overline{\dot{v}_{poI}^2}}$				

the free parameters α, β, and λ are found for each axis (or set of axes) such that the criterion values for a given set of experimental variables reflect the trends in subjective pilot rankings obtained when the same values for the experimental variables were used in the simulator experiment. This step is carried out by constructing plots of the various criteria and subcriteria as a function of the principal experimental variable, washout break frequency, and with α, β and λ as parameters. α, β and λ values are then selected to cause the respective criterion values to display the same optimum and trends as the subjective pilot evaluations.

1. Heave Axis

Results from the simulator experiment for the heave axis are complicated by the use of the g-suit to simulate normal specific force cues. To begin, compare the J_Z criterion computed with the post-drive logic measures for four different values of α, using Fig. 28 . The object here is to match the relative values of J_Z across the range of break frequencies with the subjective rankings of the pilots during the simulator experiment. In the simulator, the ratings showed a preference for the low break frequencies and a dislike for the higher break frequencies — particularly those greater than 1.0. The J_Z values for $\alpha_Z = 1.2$ present the best match to the pilot preferences.

Since the heave axis is uncoupled from the others, α_Z is the only constant which needs to be determined in this first optimization step. It is interesting, however, to examine the effect of the g-suit on the criteria values. Figure 29 presents a plot of $J_{Z_{g\text{-suit}}}$ vs. break frequency. Note here that $K_z = 1.0$ for all values of the break frequency. This is because the gain of the g-suit perception is presumed to be unity. The values computed for $J_{Z_{g\text{-suit}}}$ indicate that the g-suit is essential for realistic simulation of normal specific force cues; the $J_{Z_{g\text{-suit}}}$ values are at least an order of magnitude less than the $J_{Z_{no\ g\text{-suit}}}$ values shown in Fig. 30. This observation is in total agreement with the subjective pilot ratings concerning the usefulness of the g-suit cues.

---

*Tables of measures used to compute the J values throughout this chapter can be found in Appendix C.

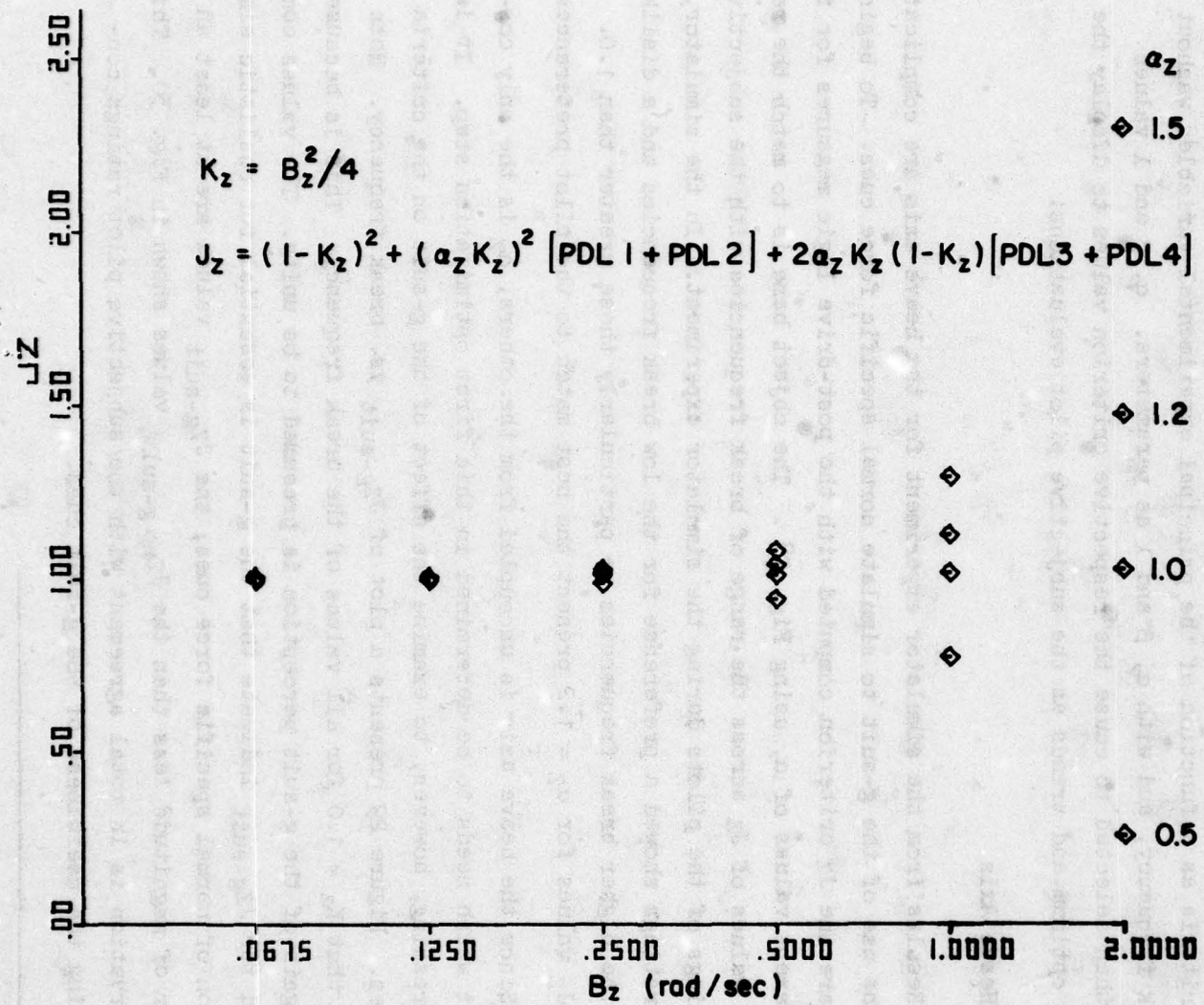

Figure 28. J_Z Criterion vs. B_z and α_Z

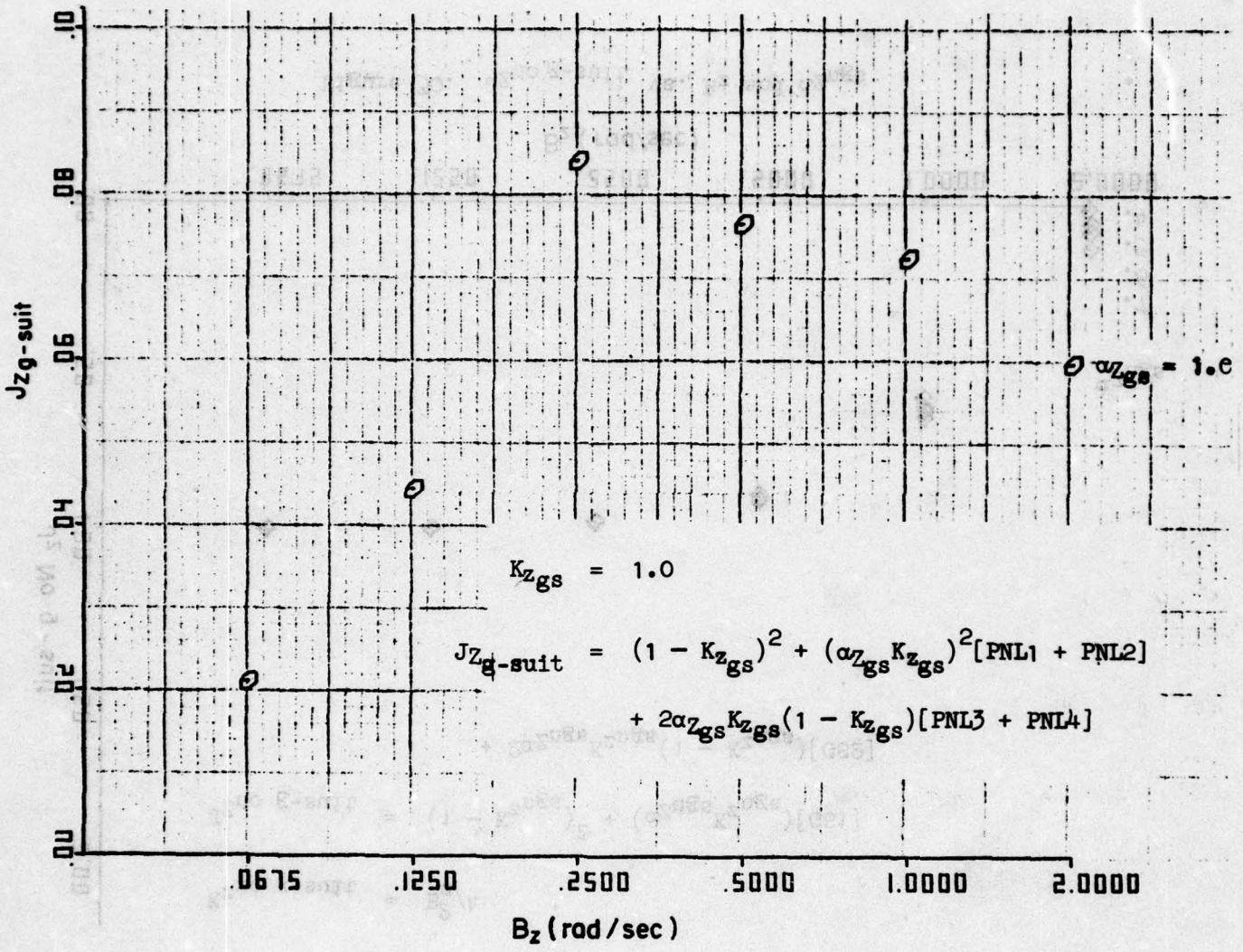

Figure 29. $J_{Zg\text{-suit}}$ vs. B_z with $\alpha_{Z_{gs}} = 1.0$

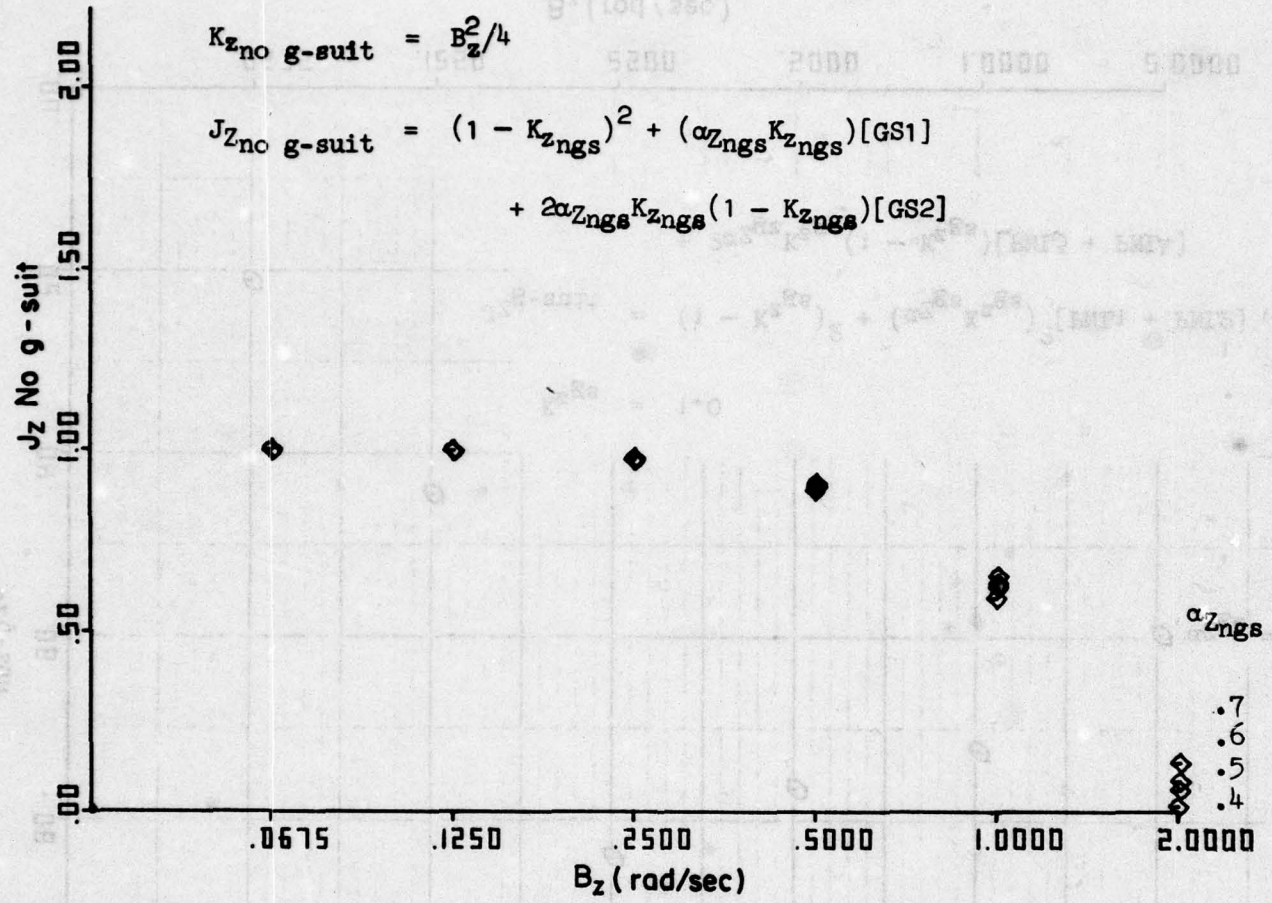

Figure 30. $J_{Z_{no\ g\text{-}suit}}$ vs. B_z and $\alpha_{Z_{ngs}}$

2. Roll-Sway Axes

For this coupled axis set the procedure is two-fold — first, the α values for each axis must be determined separately. Once this is accomplished, the J values must be combined to determine the β and λ values. At each stage it is necessary to match the shape of the criterion curve with the subjective pilot ranking trends.

Figure 31 is a plot of J_P vs. break frequency for several values of α_P. The pilot rankings presented in the previous chapter ordered the break frequency settings in the following way: 0.525 (best), 0.175, 0.70, 1.05 (worst). $\alpha_P = 1.2$ value best approximates the relative ordering of the K_p, B_p combinations as determined by the simulator pilots.

The J_Y criterion must be evaluated as a function of α_Y and C_{2y}, since B_p was held constant in the experiments while C_{2y} was varied. The values used for the other parameters are indicated in Fig. 32 — note that the gain K_y is here a function of C_{2y}. The pilot rankings of the C_{2y} values were as follows: 0.25 (best), 0.0625, 0.0 (worst). Any value for α_Y less than 0.6 orders the C_{2y} values properly so $\alpha_Y = 0.5$ was chosen somewhat arbitrarily. Figure 33 presents a plot of the J_Y criterion versus B_p and α_Y for a value of $C_{2y} = 0.25$; this plot merely serves as a check of the behavior of J_Y vs. B_p for the values of α_Y used in Fig. 32. These values of α_Y will also be used in the J_{YP} computation.

Only a single value of J_{YT} was computed, since there was no simulator data upon which to base a selection of α_{YT}. The best guess at this value is $\alpha_{YT} = 1.0$. Then, assuming $B_p = 0.5$, $K_{2R} = 0.5$ and $C_{2y} = 0.25$,

$$J_{YT} = (1 - K_{2R})^2 + (\alpha_{YT}K_{2R})^2[PDL1] + \alpha_{YT}K_{2R}(1 - K_{2R})[PDL3]$$

$$= 0.628$$

Now that the α's have been selected for the three subcriteria, the appropriate J's can be combined to form the J_{YP} criterion.

Figure 34 is the plot of J_{YP} versus B_p for three values of β_{YP} and λ_{YP}. According to the pilot rankings of the roll-sway axis set fidelity, the

$$K_p = .286\ B_p$$

$$J_P = (1 - K_p)^2 + (\alpha_p K_p)^2[PDL1 + PDL2] + 2\alpha_p K_p(1 - K_p)[PDL3 + PDL4]$$

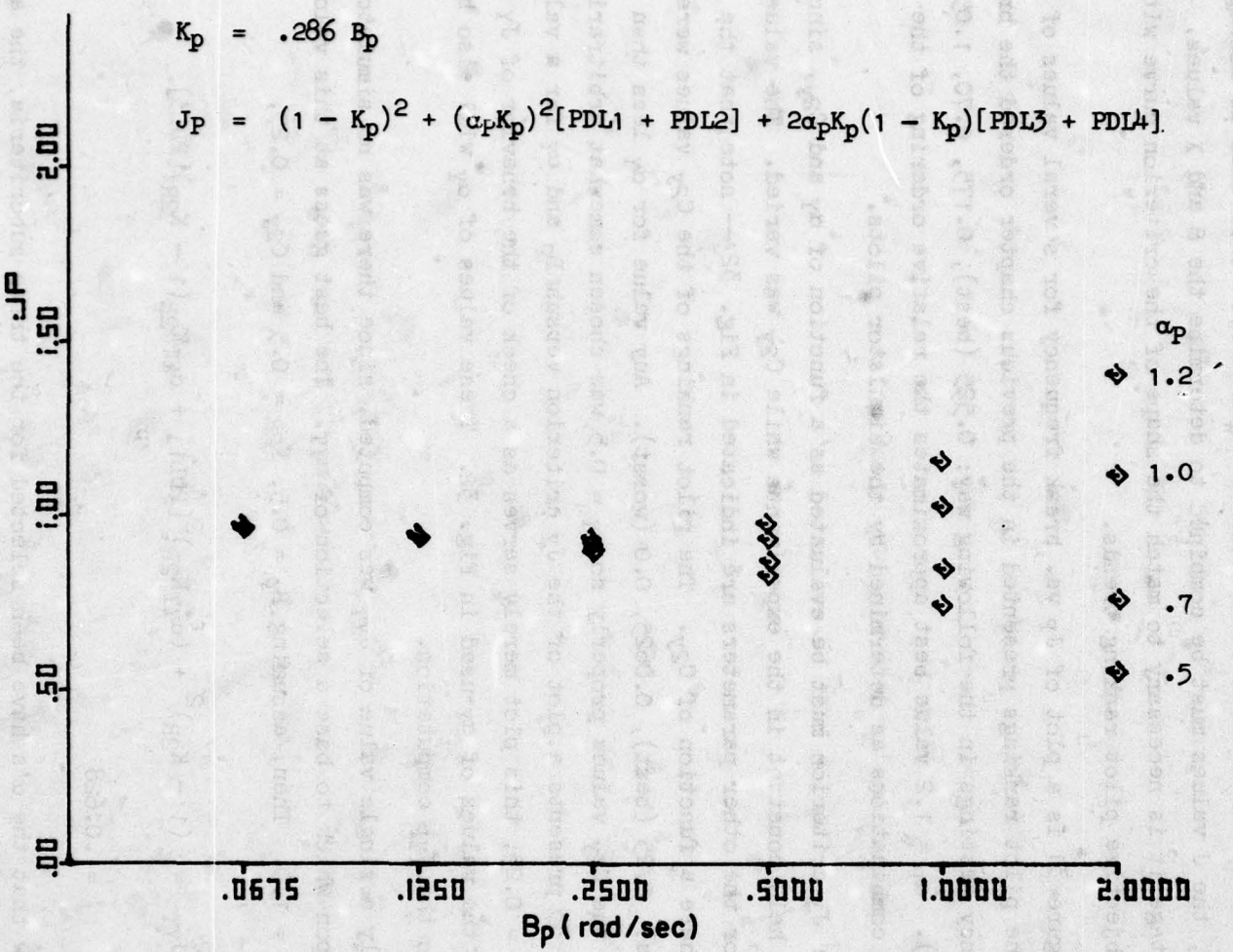

Figure 31. J_P Criterion vs. B_p and α_p

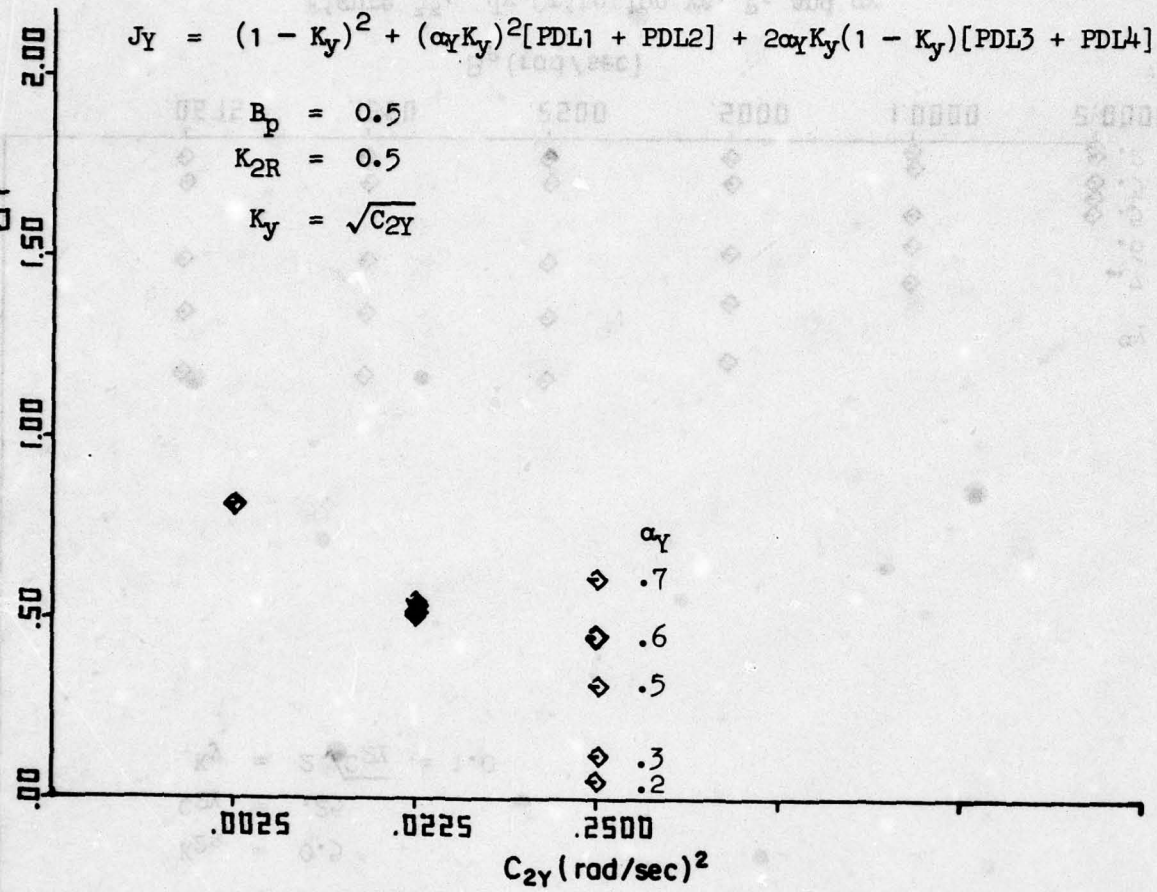

Figure 32. J_Y Criterion vs. C_{2Y} and α_Y

$$J_Y = (1 - K_y)^2 + (\alpha_Y K_y)^2[PDL1 + PDL2] + \alpha_Y K_y(1 - K_y)[PDL3 + PDL4]$$

$K_{2_R} = 0.5$

$C_{2Y} = .25$

$K_y = 2\sqrt{C_{2Y}} = 1.0$

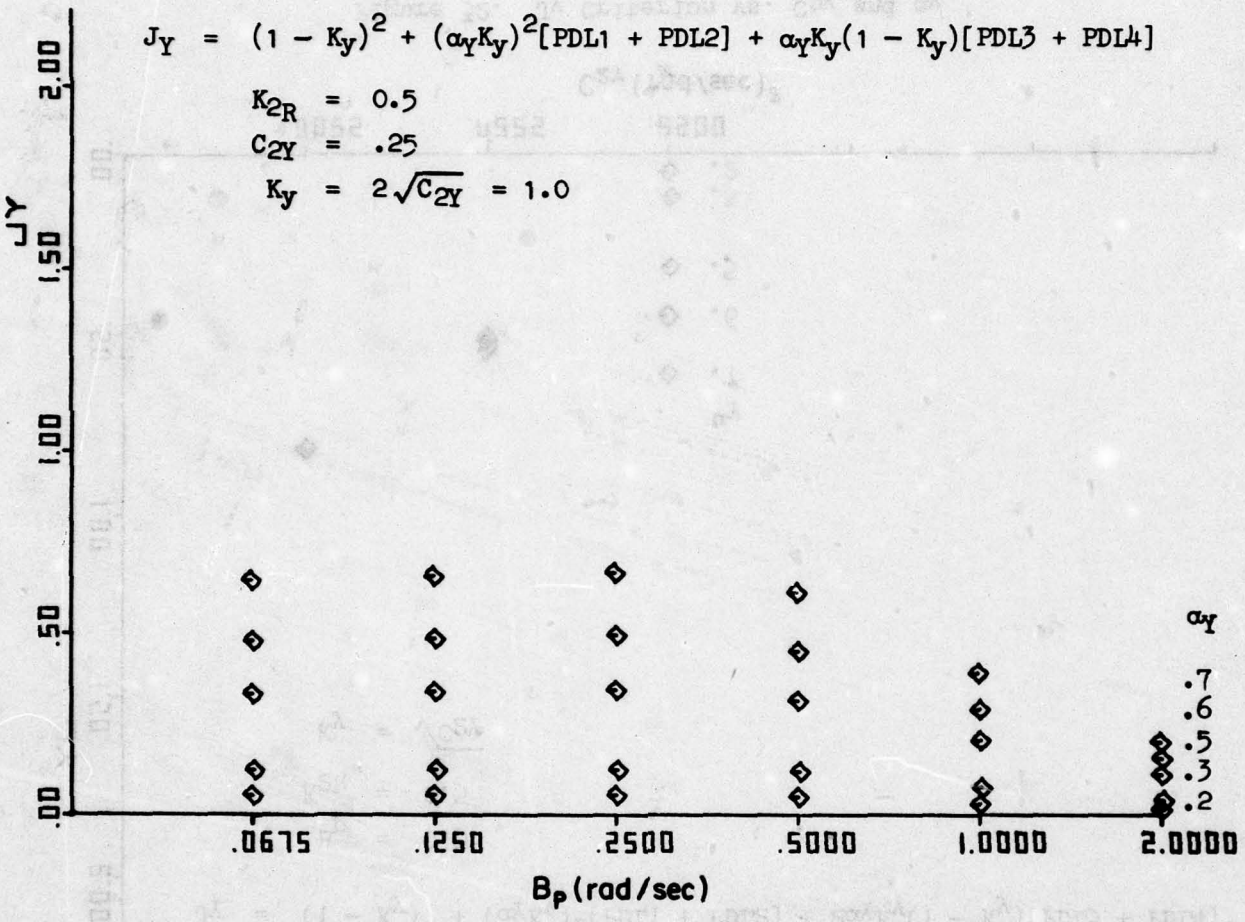

Figure 33. J_Y Criterion vs. B_p and α_Y

appropriate combination of β_{YP} and λ_{YP} would be one which places a "minima" in the J_{YP} curve at a B_p of approximately 0.5 rad/sec. From Fig. 34, the curve which best fits the relative rankings of the simulator pilots and contains a minima of J_{YP} at $B_p = 0.5$ rad/sec has $\beta_{YP} = 0.45$ and $\lambda_{YP} = 0.1$. Note that many other combinations of β_{YP} and λ_{YP} were tried before selecting these values. For the sake of clarity, only three values are plotted in Fig. 34. These three values came closest to matching the subjectively optimum experimental conditions.

3. Pitch-Surge Axes

Very little data is available from the piloted simulation experiments for the pitch-surge axes. For this reason, it was assumed that the α values for J_X, J_P and J_{XT} would be the same as those for J_Y, J_Q and J_{YT}, respectively. To examine the appropriateness of this assumption, the J_Q criterion was plotted versus $B_$, for several values of α_Q, as shown in Fig. 35. In comparing this plot to the J_P plot in Fig. 31, no significant difference is found. Thus, the assumption that $\alpha_P = \alpha_Q$ seems reasonable.

As was the case for J_{YT}, only a single value of J_{XT} is computed:

For $\alpha_{XT} = 1.0$, $B_q = 0.5$, $K_{2p} = 0.5$

$$J_{XT} = (1 - K_{2P})^2 + (\alpha_{XT}K_{2P})^2[PDL1] + \alpha_{XT}K_{2P}(1 - K_{2P})[PDL3]$$

$$= 0.392$$

Also, a single value is computed for J_X, since in this special case (LAMARS does not have a surge motion degree of freedom), $K_x = 0$. Thus, $J_X = 1.0$. The assumption that $\alpha_X = \alpha_Y = 0.5$ is still asserted but cannot be validated in this study.

Again, in the absence of simulator data, it is assumed that $\beta_{XQ} = \beta_{YP}$ and $\lambda_{XQ} = \lambda_{YP}$. Figure 36 is a plot of J_{XQ} vs. B_q for three values of β_{XQ} and λ_{XQ} — the assumed values of $\beta_{XQ} = 0.45$ and $\lambda_{XQ} = 0.1$ provide a J_{XQ} curve with a shallow minimum between B_q values of 0.25 and 0.5 rad/sec.

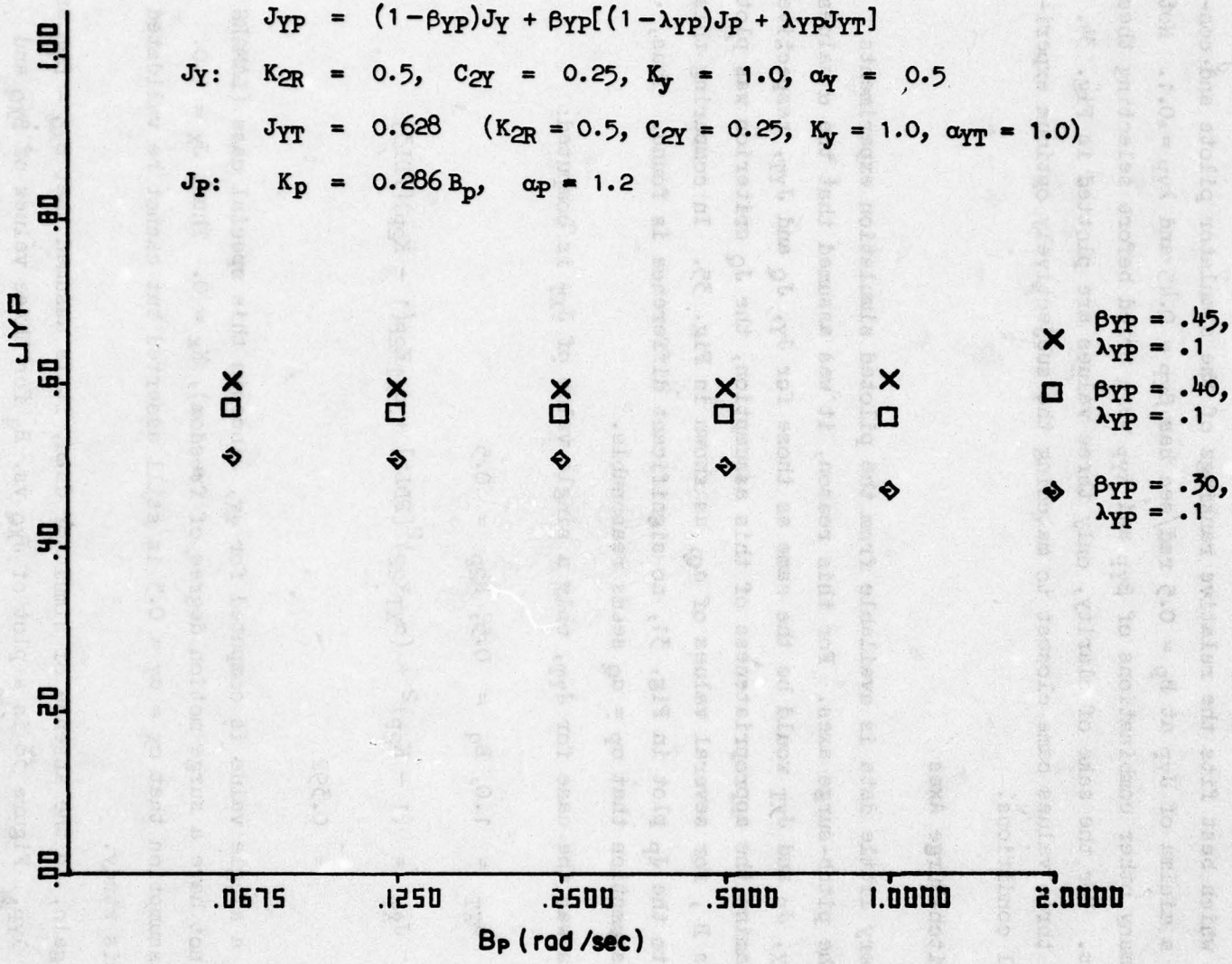

Figure 34. J_{YP} Criterion vs. B_p and β_{YP} and λ_{YP}

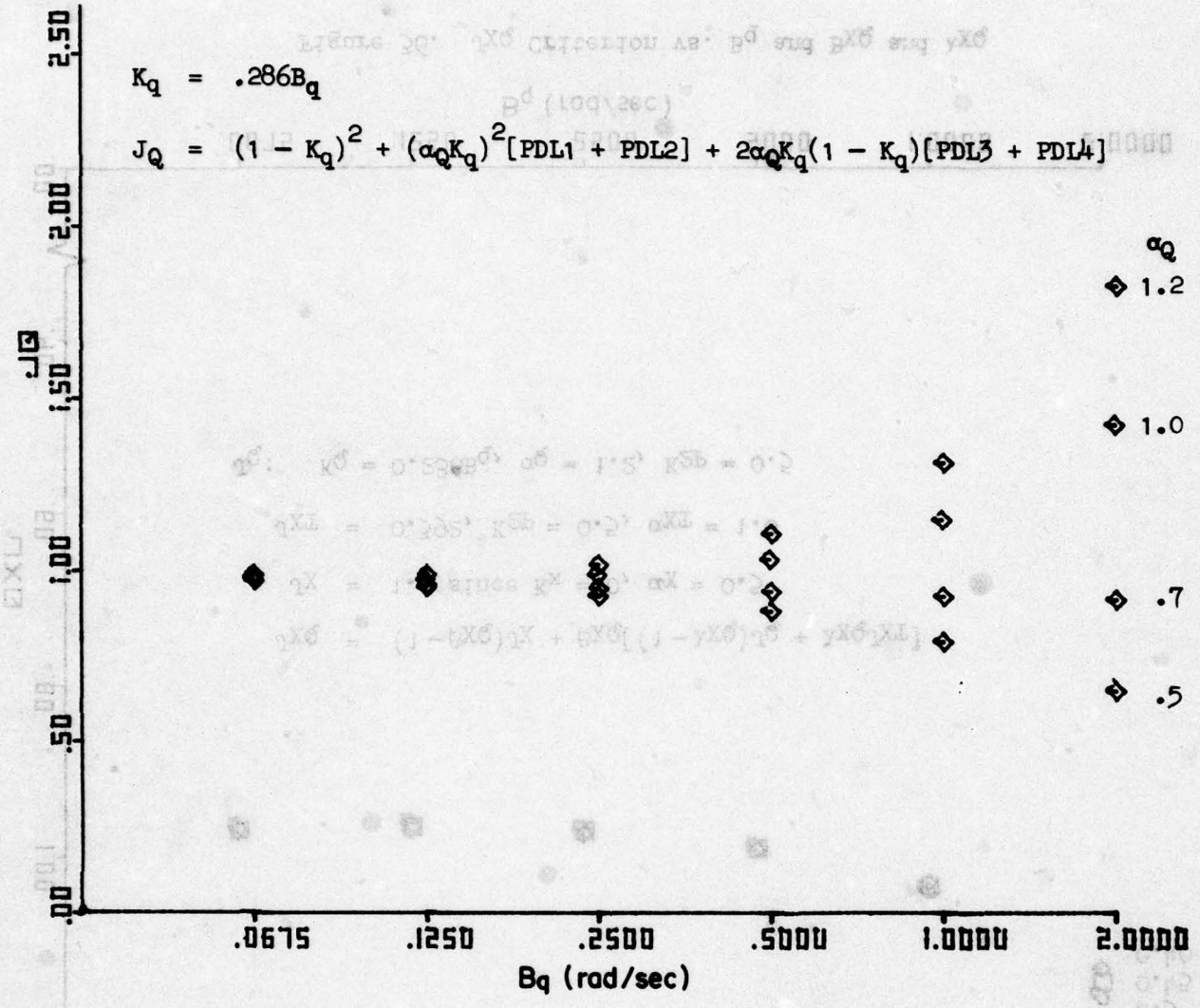

Figure 35. J_Q Criterion vs. B_q and α_Q

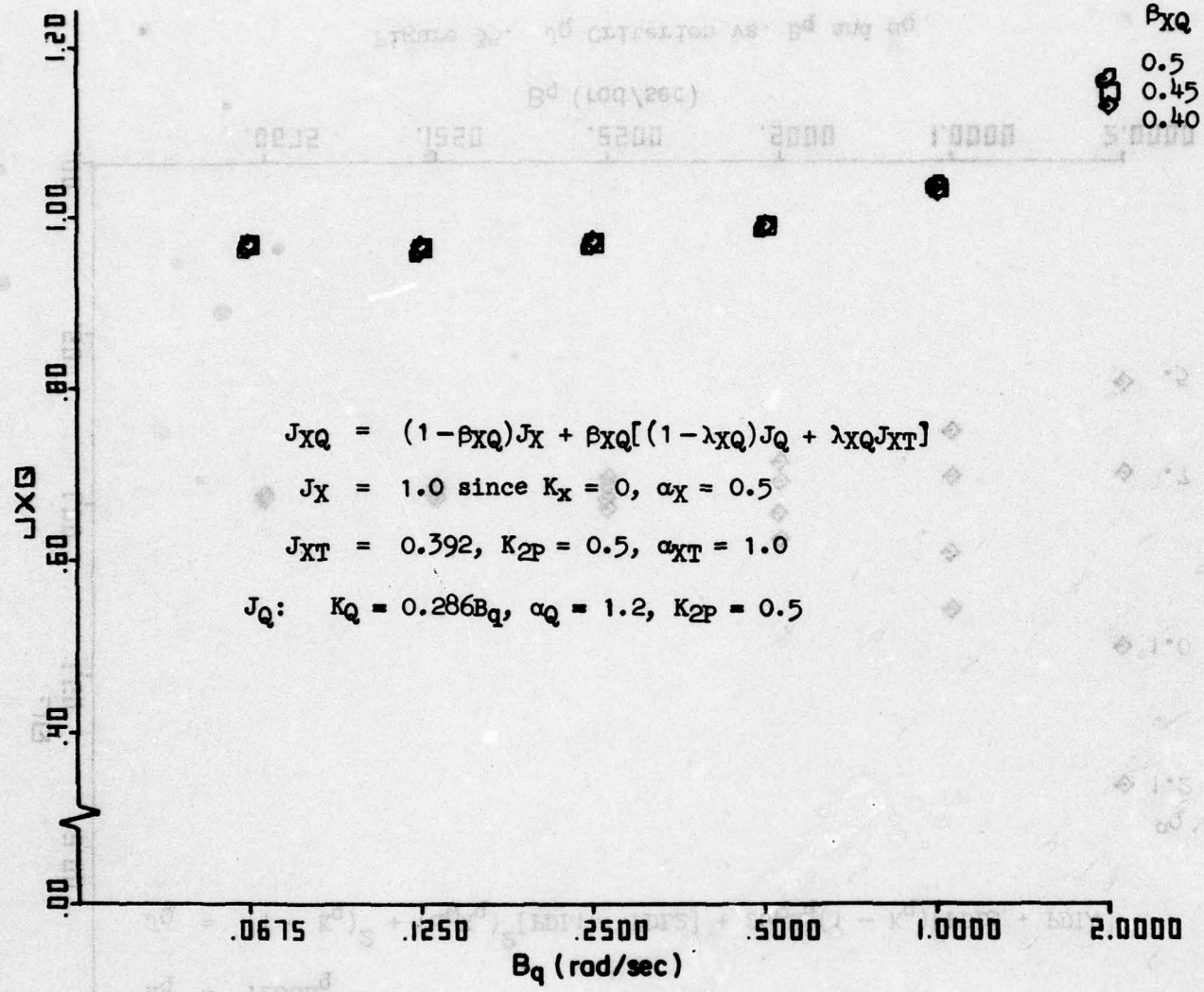

$$J_{XQ} = (1-\beta_{XQ})J_X + \beta_{XQ}[(1-\lambda_{XQ})J_Q + \lambda_{XQ}J_{XT}]$$

J_X = 1.0 since $K_X = 0$, $\alpha_X = 0.5$

J_{XT} = 0.392, $K_{2P} = 0.5$, $\alpha_{XT} = 1.0$

J_Q: $K_Q = 0.286B_q$, $\alpha_Q = 1.2$, $K_{2P} = 0.5$

Figure 36. J_{XQ} Criterion vs. B_q and β_{XQ} and λ_{XQ}

4. Yaw Axis

The yaw axis, like the pitch-surge axes, has little simulator data upon which to base a choice of α_R. The assumption is again made that $\alpha_R = \alpha_P = \alpha_Q$ with the notion that the angular velocity axes can in some sense be treated similarly. Figure 37 presents a plot of J_R versus B_r for several values of α_R, which compares favorably with the plots of J_Q vs. B_q and J_P vs. B_p, shown in Figs. 35 and 31, respectively. Since the yaw axis, like the heave axis, is uncoupled, α_R is the only parameter to be determined. $\alpha_R = 1.2$ is chosen.

Table 27 lists the values of α, β and λ for each axis or set of axes which have been selected in the process of matching the subjective optimum and relative rankings of the simulator experiments. The values of the criteria produced when these parameter values are used suggest the same optimum and relative ranking of the configurations as did the experiments.

TABLE 27. SUMMARY OF CRITERIA CONSTANTS

	PARAMETER	VALUE	AXIS
Marginal Utility Parameters	α_X	0.5	Pitch-Surge
	α_Y	0.5	Roll-Sway
	α_Z	1.2	Heave
	α_P	1.2	Roll-Sway
	α_Q	1.2	Pitch-Surge
	α_R	1.2	Yaw
	α_{XT}	1.0	Pitch-Surge
	α_{YT}	1.0	Roll-Sway
Coupled Criteria Parameter	β_{XQ}	0.45	Pitch-Surge
	β_{YP}	0.45	Roll-Sway
	λ_{XQ}	0.1	Pitch-Surge
	λ_{YP}	0.1	Roll-Sway

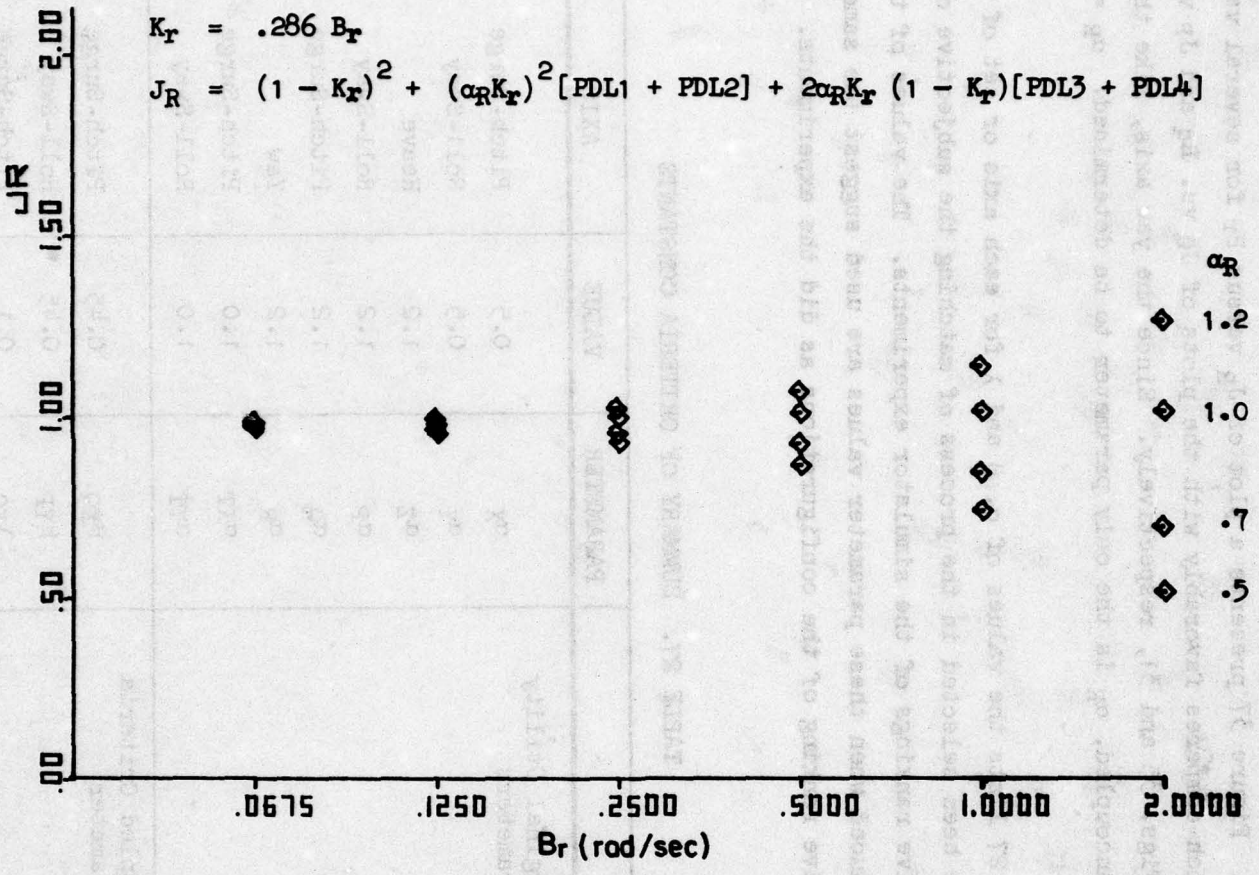

Figure 37. J_R Criterion vs. B_r and α_R

C. LAMARS OPTIMIZATION

Given the criteria forms and α, β and λ values of the preceding subsection, a flying task and a set of motion simulator hardware constraints, it is now possible to optimize the drive logic for that motion base. Consider the air-to-ground flying task and the LAMARS motion base and drive logic as a specific example.

The motion base hardware constraints are satisfied via scaling selection. Scaling gains are chosen by comparing the peak displacement values obtained at each value of washout break frequency of interest with the hardware constraint for each axis. Gains are then computed for each break frequency so that the peak displacement will not exceed the hardware constraints. This identifies those scaling gain-break frequency parameter combinations which may be considered further.

For each parameter combination, then, the appropriate J value can be calculated and compared with the J values for all other parameter combinations for each axis or coupled axes. The optimum parameter combination for each axis corresponds to the minimum J value. If all of the J values for a given axis are greater than or equal to 1.0, this indicates that simulated motion in that axis does not contribute to the simulation fidelity.

The following subsections discuss the LAMARS optimization for each axis or coupled axis set: heave, roll-sway, pitch-surge and yaw.

1. Heave Axis

Figure 38 is a plot of J_Z vs. break frequency. This washout break frequency and scaling gain are the only parameters varied for this axis. The g-suit is presumed not used for Fig. 38. K_Z values are computed such that the peak displacement never exceeds 10 ft. These values are also given in the figure. Since all of the J_Z values are greater than 1.0, it is apparent that the perceived normal motion fidelity is not improved with the use of simulator motion. Therefore, the optimum drive logic parameters for the heave axis are both 0.0, as indicated in the figure.

Figure 39 is again the heave axis criterion, but here the effects of the g-suit upon perceived motion fidelity are included. The $J_{Z_{gs}}$ and $\alpha_{Z_{gs}}$ values

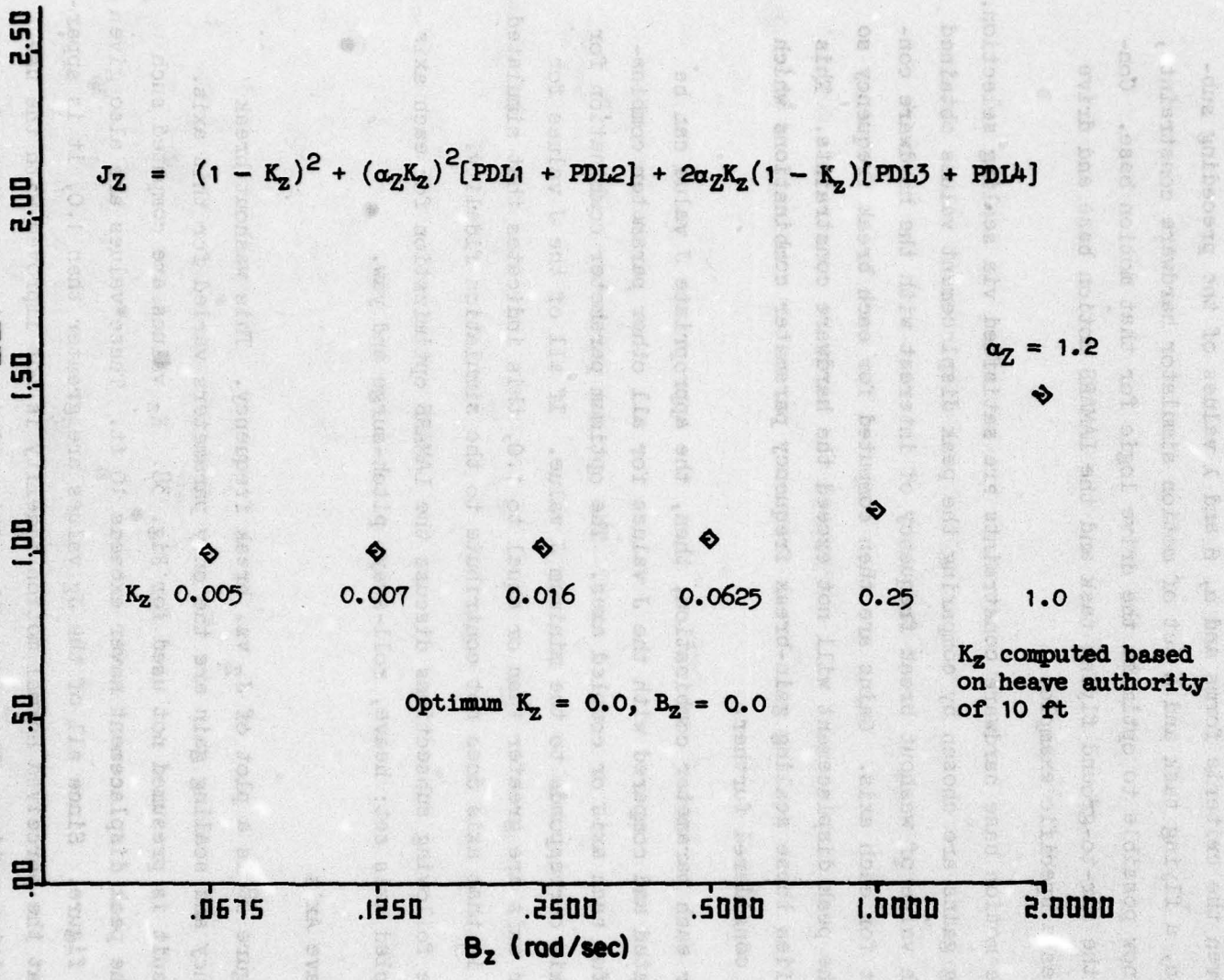

Figure 38. LAMARS Optimization — J_Z vs. B_z

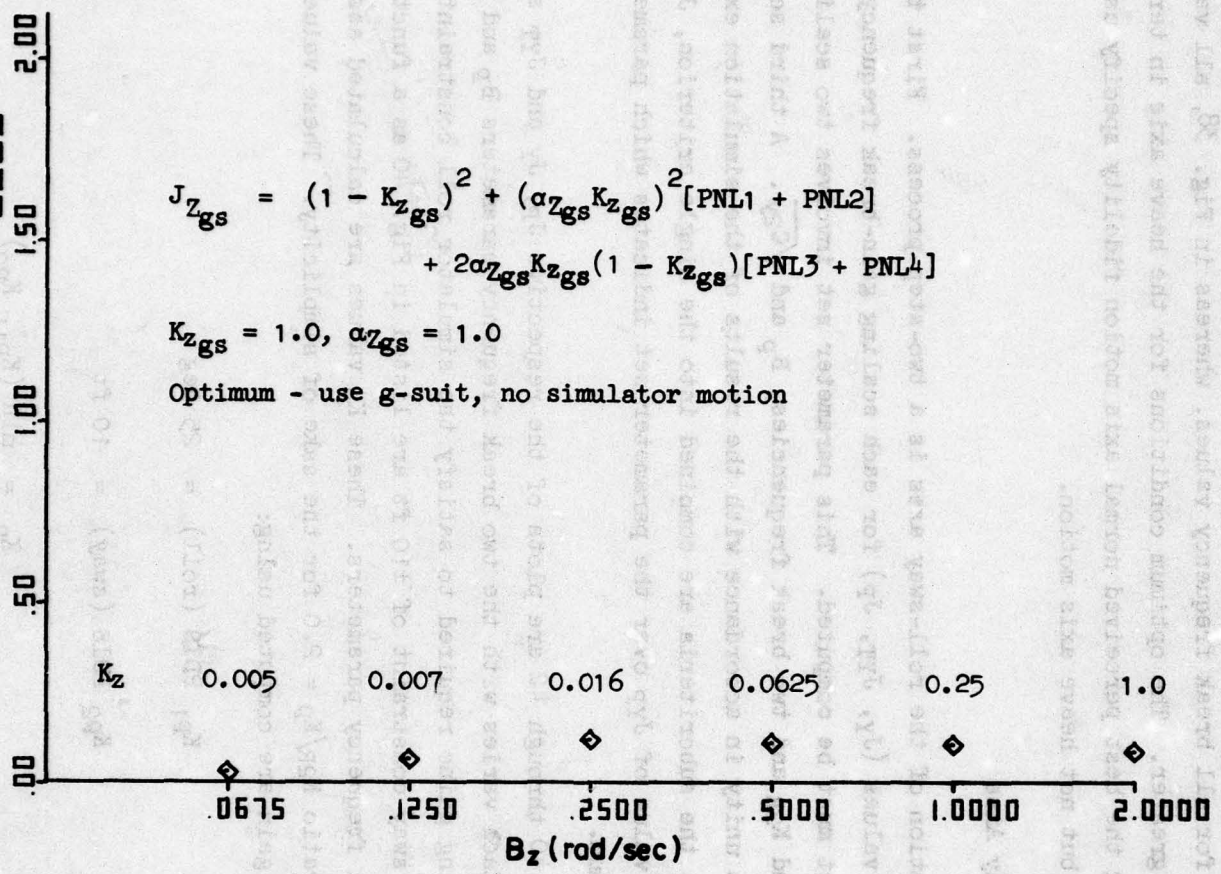

Figure 39. LAMARS Optimization — $J_{Z_{gs}}$ vs. B_z

are as indicated. The same K_z values apply for each break frequency as in Fig. 38. From this plot it is obvious that, although the heave motion does not contribute positively to perceived normal axis motion fidelity, the g-suit itself contributes a great deal. This is indicated by the small $J_{Z_{gs}}$ values for all break frequency values, whereas in Fig. 38, all values were 1.0 or greater. The optimum conditions for the heave axis in terms of attaining the best perceived normal axis motion fidelity specify using the g-suit, but not heave axis motion.

2. Roll-Sway Axes

Optimization of the roll-sway axes is a two-step process. First the subcriteria values (J_Y, J_{YT}, J_P) for each scaling gain-break frequency parameter set must be computed. This parameter set involves two scaling gains, K_p and K_{2R} and two break frequencies, B_p and $\sqrt{C_{2y}}$. A third scaling gain, K_y, is unity in accordance with the results of the simulation experiments. Next the subcriteria are combined into the single criterion, J_{YP}. The minimum value of J_{YP} over the parameter set indicates which parameter set is optimum.

Figures 40 through 42 are plots of the respective J_P, J_Y and J_{YT} subcriteria. Each varies with the two break frequency parameters B_p and C_{2y}. The K_p scaling gains required to satisfy the simulator roll constraint of ±25 deg and sway constraint of ±10 ft are listed in Fig. 40 as a function of the break frequency parameters. These K_p values are calculated assuming a constant ratio $K_{2R}/K_p = 2.0$ for the sake of simplicity. These values of the scaling gain are computed using:

$$K_{p_1} \text{ PDIS (roll)} = 25 \text{ deg}$$

$$K_{p_2} \text{ PDIS (sway)} = 10 \text{ ft}$$

$$K_p = \min (K_{p_1}, K_{p_2})$$

where the PDIS data are from Table C-11 through C-13 wherein $K_{2R}/K_p = 2.0$.

The three criteria, J_P, J_Y and J_{YT} are combined to form J_{YP}, which is plotted versus B_p and C_{2y} in Fig. 43. Now the optimum drive logic parameters

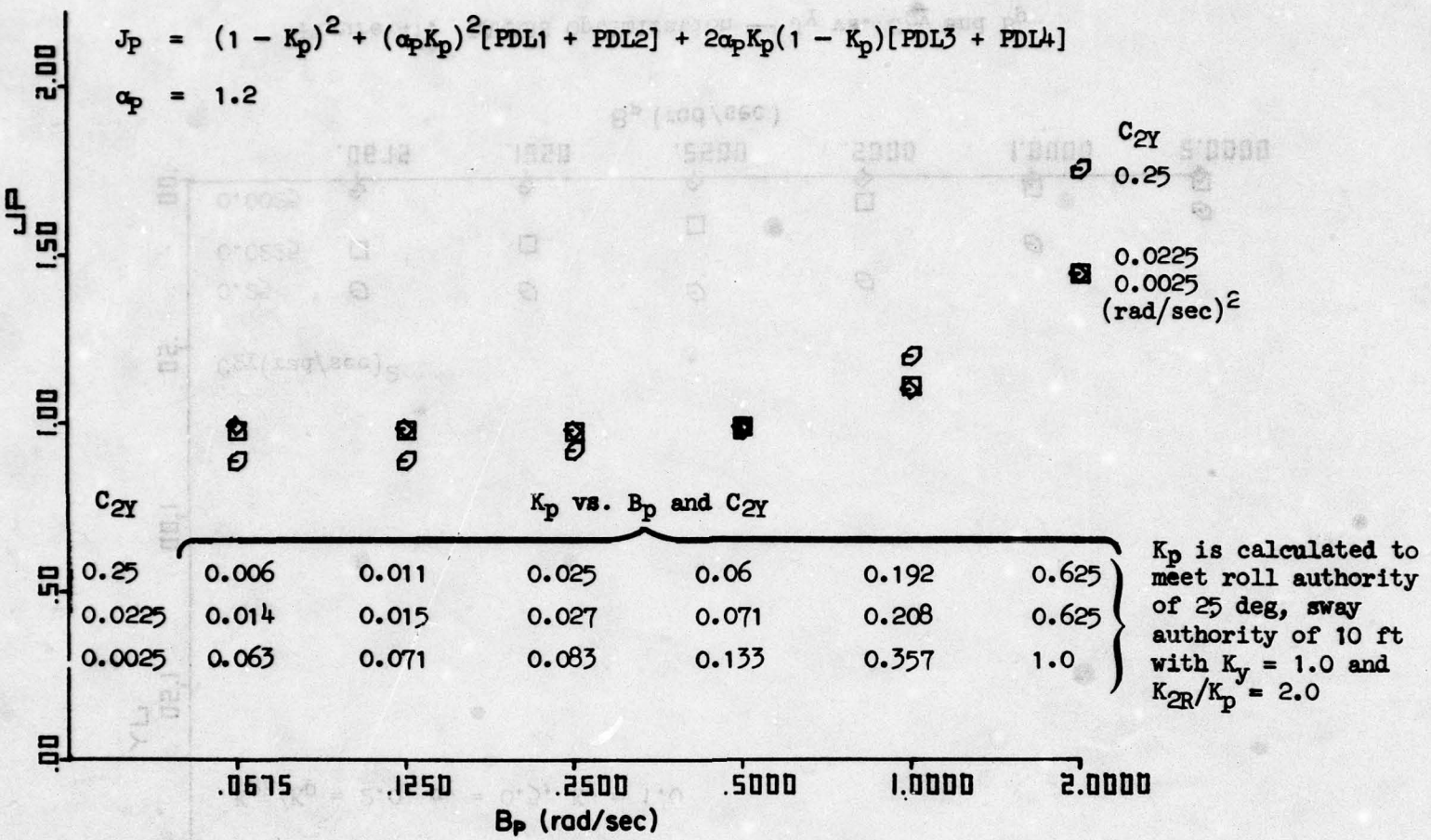

Figure 40. LAMARS Optimization — J_P vs. C_{2Y} and B_p

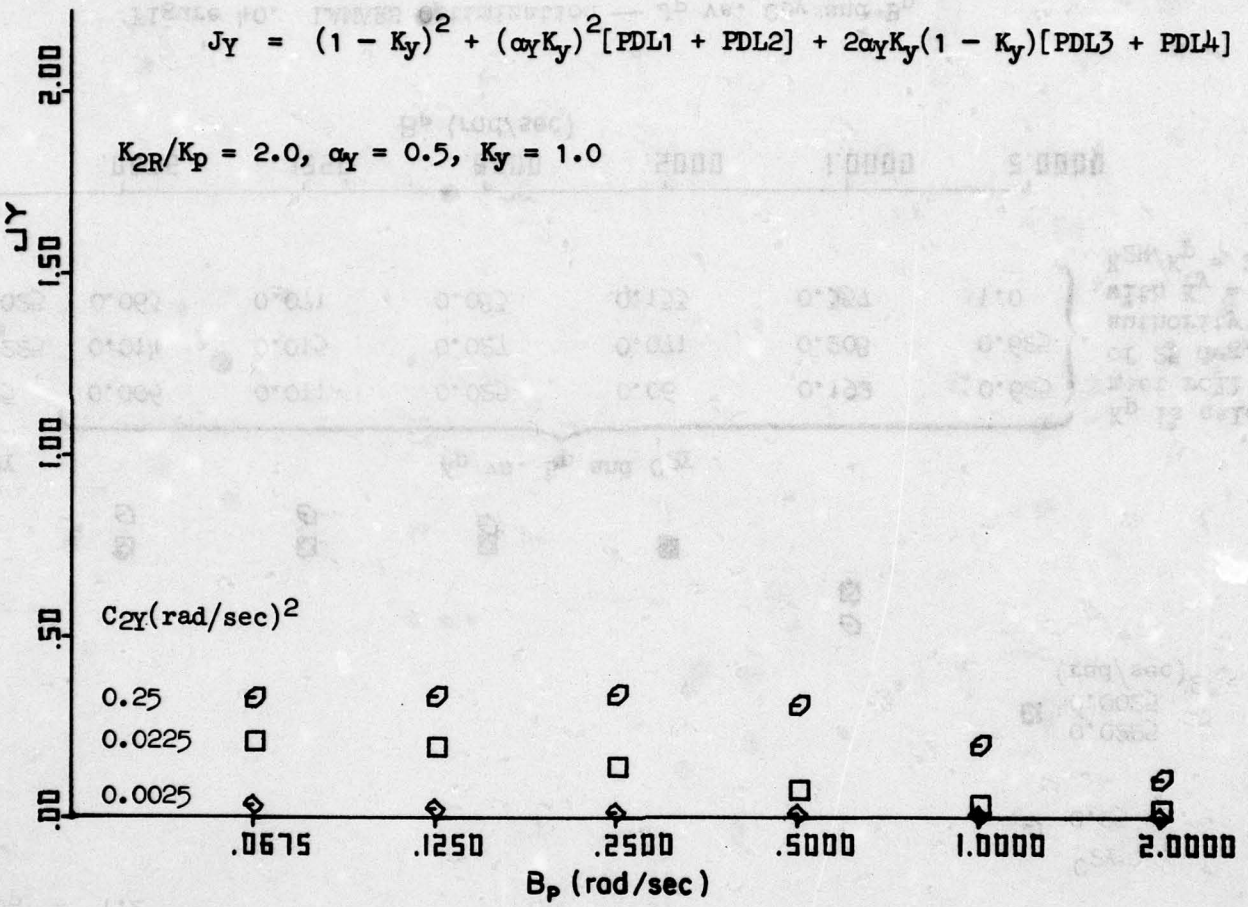

Figure 41. LAMARS Optimization — J_Y vs. C_{2Y} and B_p

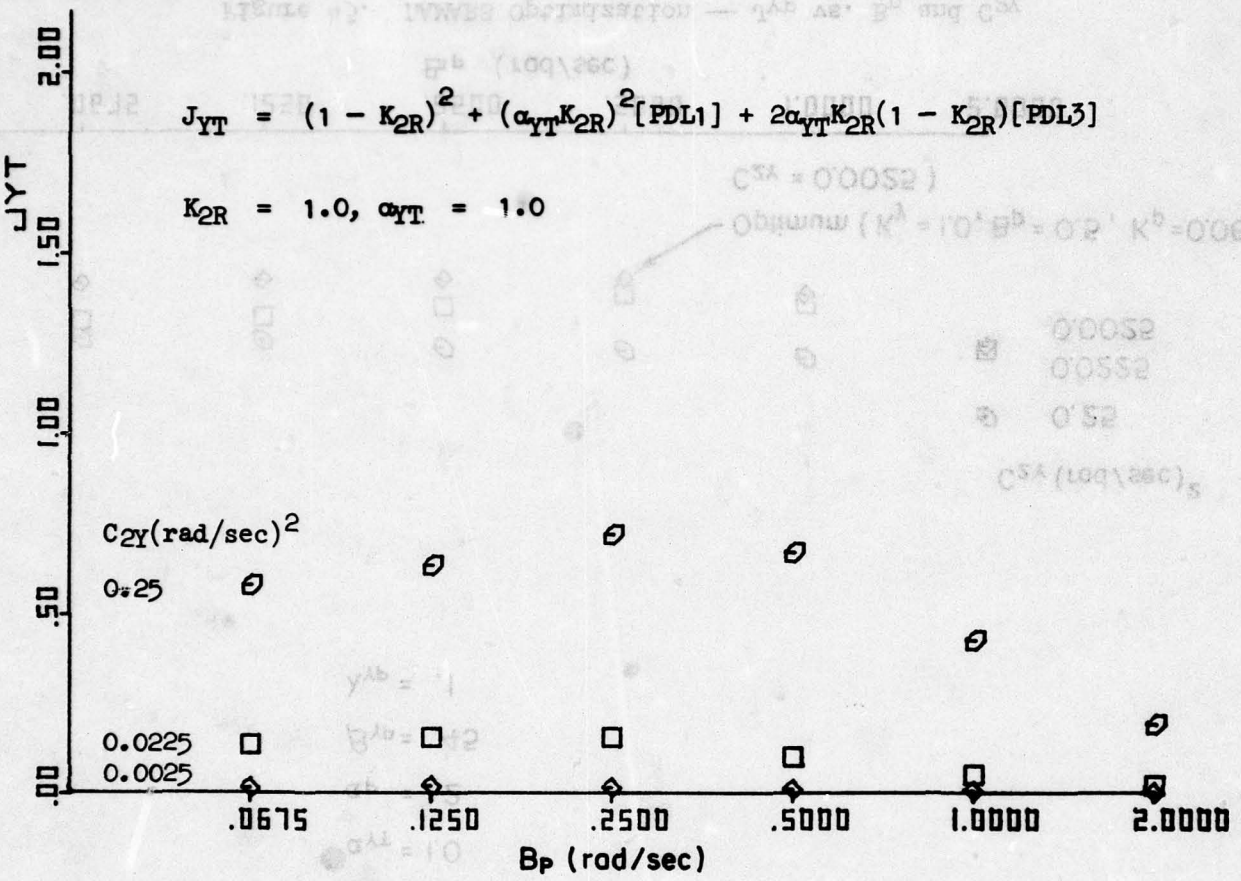

Figure 42. LAMARS Optimization — J_{YT} vs. C_{2Y} and B_p

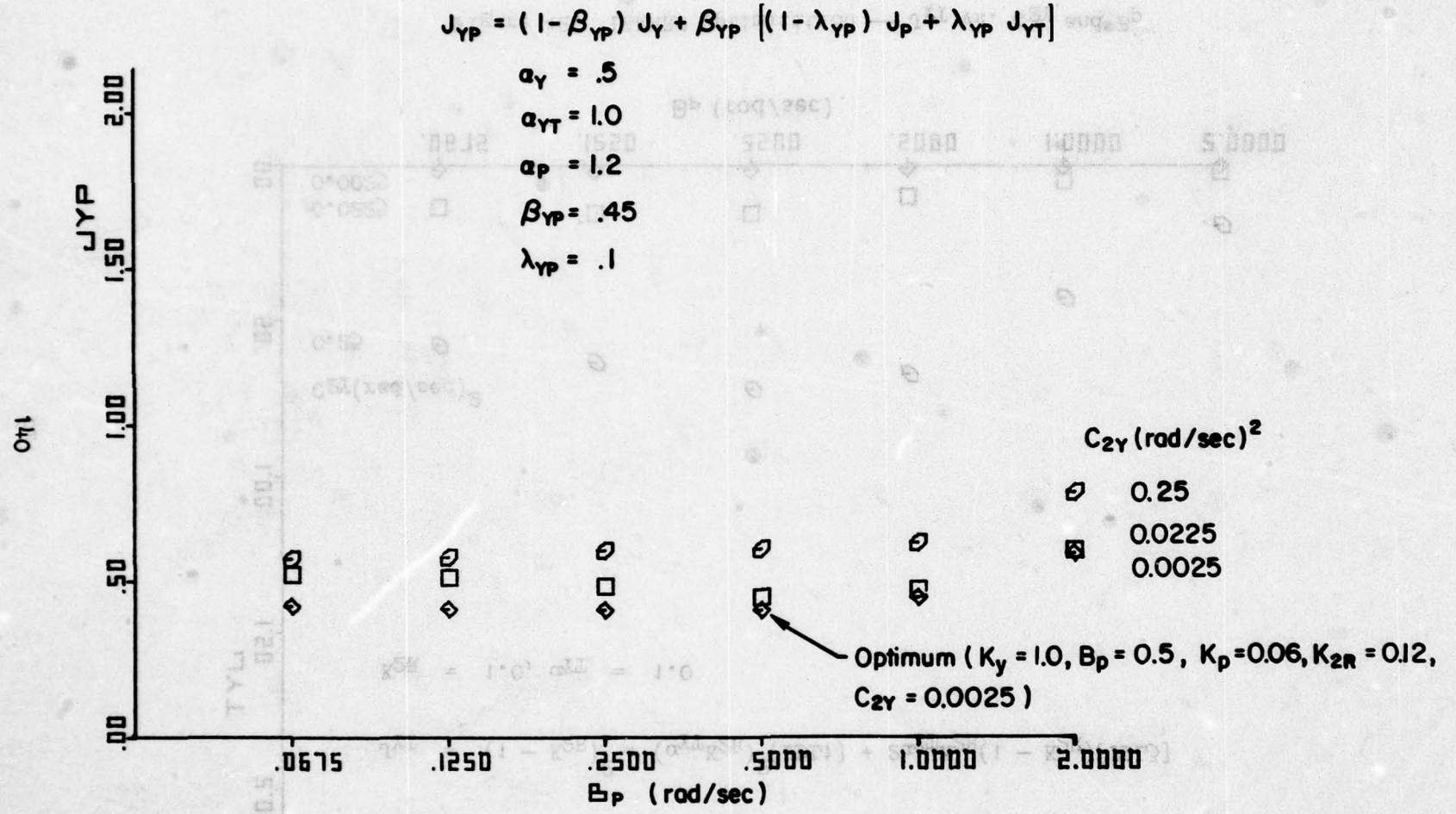

Figure 43. LAMARS Optimization — J_{YP} vs. B_p and C_{2Y}

parameters can be identified simply by choosing the set of parameters which results in the smallest value of J_{YP}. This point is identified on the plot as the point which corresponds to $K_y = 1.0$, $K_p = 0.06$, $K_{2R} = 0.12$, $C_{2y} = 0.0025$ and $B_p = 0.5$. These are then the optimum roll-sway drive logic parameters for the assumed form of the LAMARS drive logic and hardware constraints, and for the air-to-ground scenario.

This optimization does not include optimization with respect to the K_{2R}/K_p ratio. Simple expansion of the parametric study to include this effect, if desired, is possible.

3. Pitch-Surge Axes

Optimization of the pitch-surge axes in principle at least is similar to that for the roll-sway axes. However, the fact that there is no surge degree of freedom for the LAMARS motion simulator requires the K_x scaling gain to be zero and, in turn, makes the C_{2x} break frequency parameter superfluous. Consequently, optimization of the pitch-surge axis drive logic is considerably specialized by comparison with the roll-sway axis procedure for LAMARS. Two scaling gains, K_q and K_{2P}, and one break frequency, B_q are involved in optimization. Since only three parameters are involved, it is not necessary to form the ratio K_{2P}/K_q; K_{2P} effects can be included directly.

Figures 44 and 45 are the plots of J_Q and J_{XT}, respectively. Since $K_x = 0.0$, J_X is always unity. The values computed for K_q assume a derotated pitch authority of 4.76 deg. This authority is computed on the assumption that the heave axis would use its full authority*. Since the optimum J_Z

---

*Calculation of the approximate pitch and yaw authorities remaining after derotation (required to accommodate LAMARS simulator cab translation) is made as follows:

$$\Delta(\text{angular motion}) = 25 - \sin^{-1} \frac{(\text{max translation})}{(\text{beam length})} \text{ deg}$$

$$= 25 - \sin^{-1} 10/26 = 2.38 \text{ deg}$$

The available authority is obtained by applying a factor of 2.0 to the 2.38 deg in order to account for the correlation between heaving and pitching motions, and between swaying and yawing motions. The factor 2.0 is an educated guess as to an appropriate value, and may require revision in the future. The resulting estimate of available authority available for reproducing angular motions is 4.76 deg.

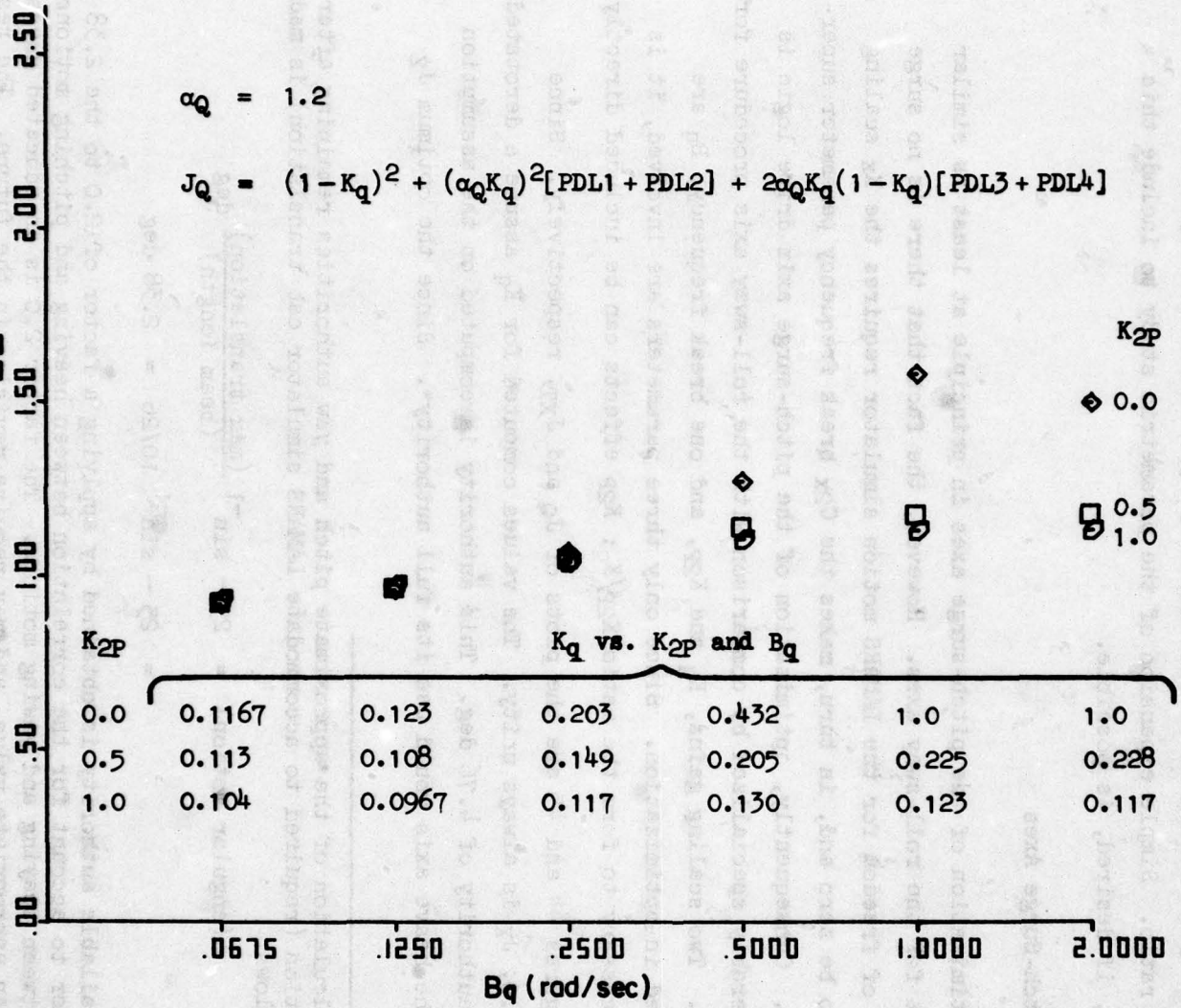

K_q vs. K_{2P} and B_q

K_{2P}						
0.0	0.1167	0.123	0.203	0.432	1.0	1.0
0.5	0.113	0.108	0.149	0.205	0.225	0.228
1.0	0.104	0.0967	0.117	0.130	0.123	0.117

K_q is calculated to meet pitch derotated authority of 4.76 deg for K_x = 0.0

Figure 44. LAMARS Optimization — J_Q vs. K_{2P} and B_q

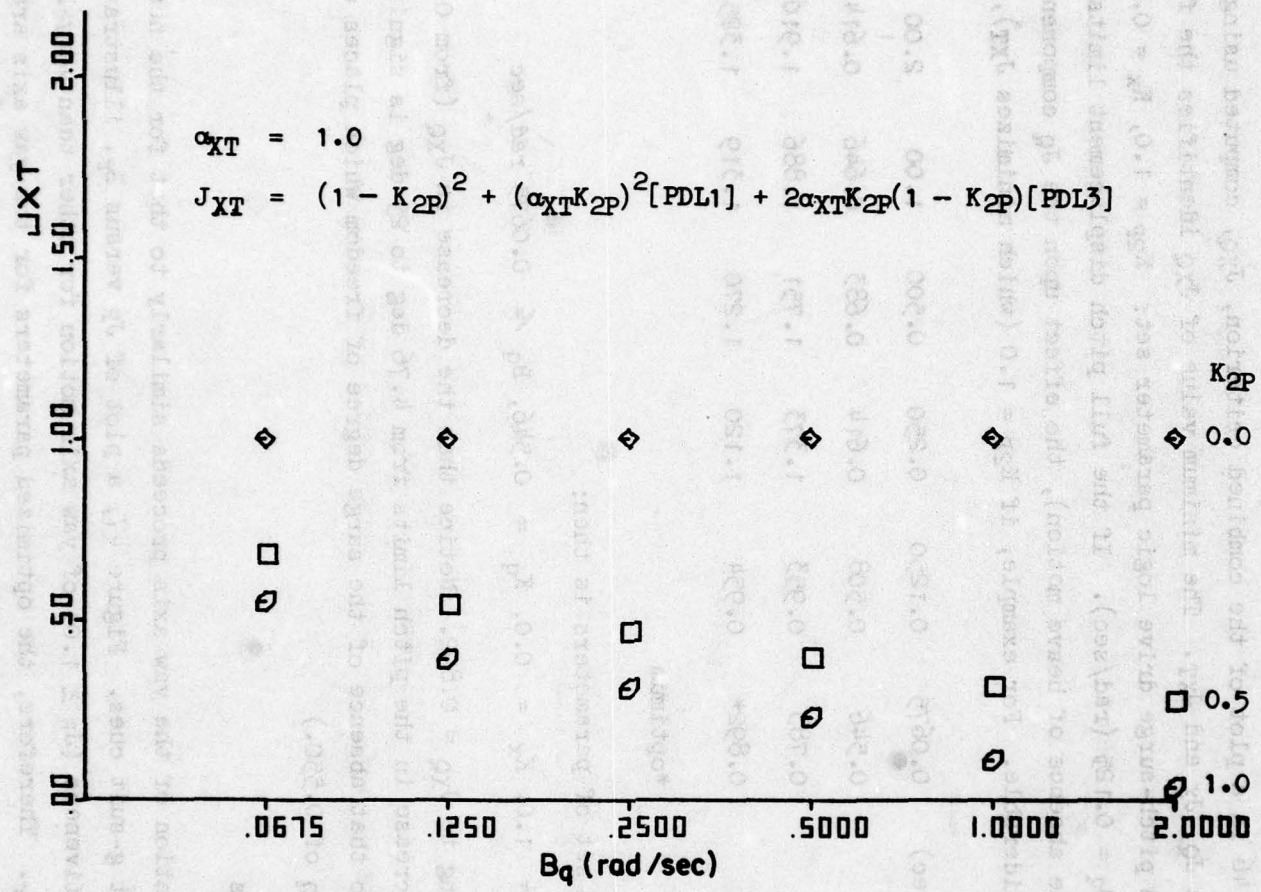

Figure 45. LAMARS Optimization — J_{XT} vs. K_{2P} and B_q

indicated that the heave axis should be stationary, a full 25 deg of pitch authority is actually available. Thus, the values for K_p shown in Fig. 44 could be multiplied by a factor of approximately 5 when the heave axis is stationary.

Figure 46 is a plot of the combined criterion, J_{XQ}, computed using the subcriteria J_Q, J_X and J_{XT}. The minimum value of J_{XQ} identifies the following optimum pitch-surge drive logic parameter set: $K_{2P} = 1.0$, $K_x = 0.0$, $K_q = 0.1$, $B_q = 0.125$ (rad/sec). If the full pitch displacement limits are used (in the absence of heave motion), the effect upon the J_Q component of J_{XQ} is considerable. For example, if $K_{2P} = 1.0$ (which minimizes J_{XT}), then

B_q (rad/sec)	0.0675	0.1250	0.250	0.500	1.00	2.00
K_q	0.546	0.508	0.614	0.683	0.646	0.614
J_Q	0.783	0.953	1.373	1.751	1.886	1.910
J_{XQ}	0.892*	0.954	1.120	1.270	1.319	1.325

*optimum

The optimum set of parameters is then:

$$K_{2P} = 1.0,\ K_x = 0.0,\ K_q = 0.546,\ B_q = 0.0675 \text{ rad/sec}$$

corresponding to $J_{XQ} = 0.892$. Notice that the decrease in J_{XQ} (from 0.950) with the increase in the pitch limits from 4.76 deg to 25 deg is significant. (Notice also that absence of the surge degree of freedom which places a lower bound on J_{XQ} of 0.550.)

4. Yaw Axis

Optimization of the yaw axis proceeds similarly to that for the heave axis without g-suit cues. Figure 47, a plot of J_R versus B_r, illustrates the ineffectiveness ($J_R \geq 1.0$) of yaw axis motion for other than very low values of B_r. Therefore, the optimized parameters for the yaw axis are that pair for which the computed value of J_R is least.

Two comments are in order. First, the optimum parameters for the yaw axis drive logic may be affected by the presence of dutch roll motions

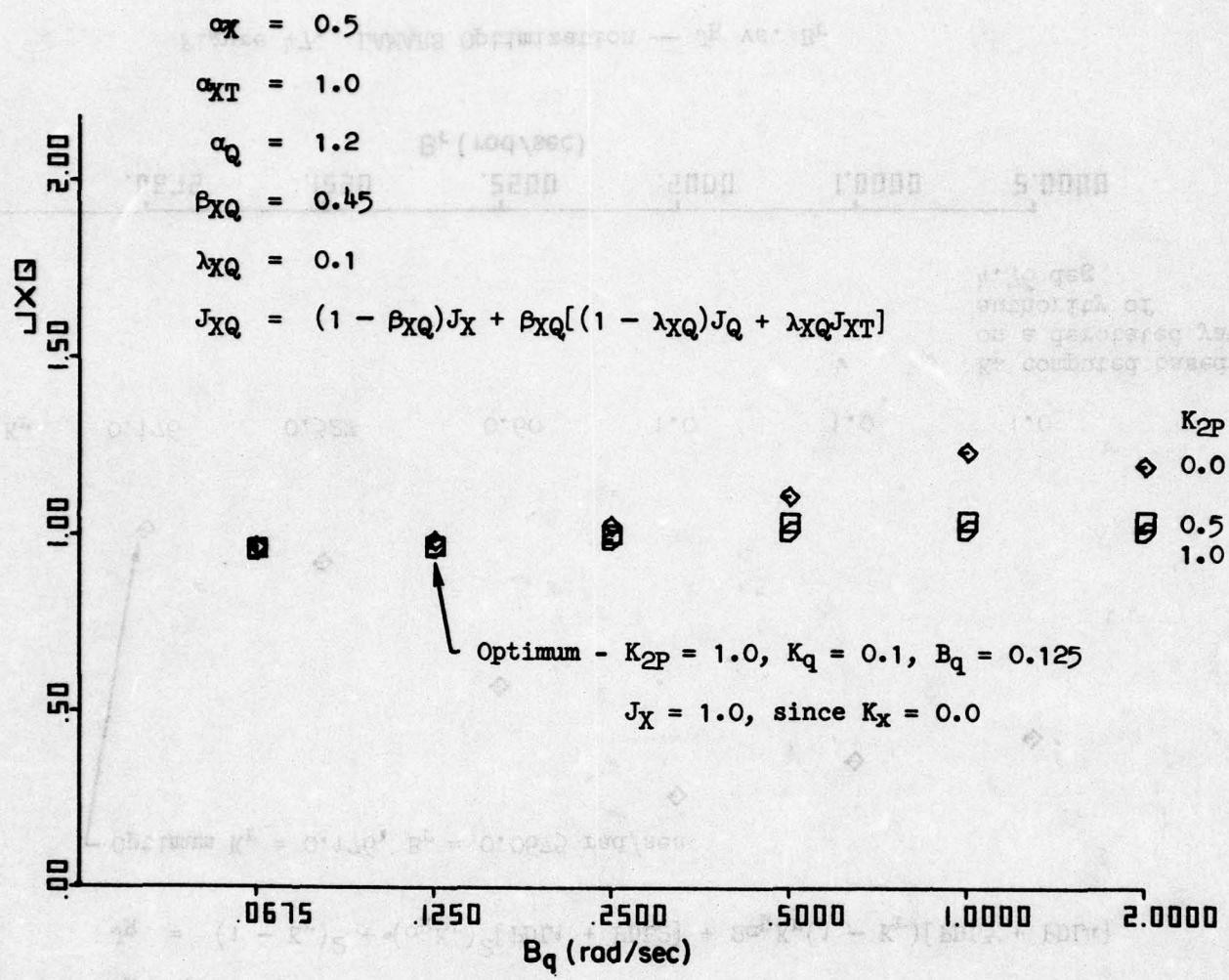

Figure 46. LAMARS Optimization — J_{XQ} vs. B_q

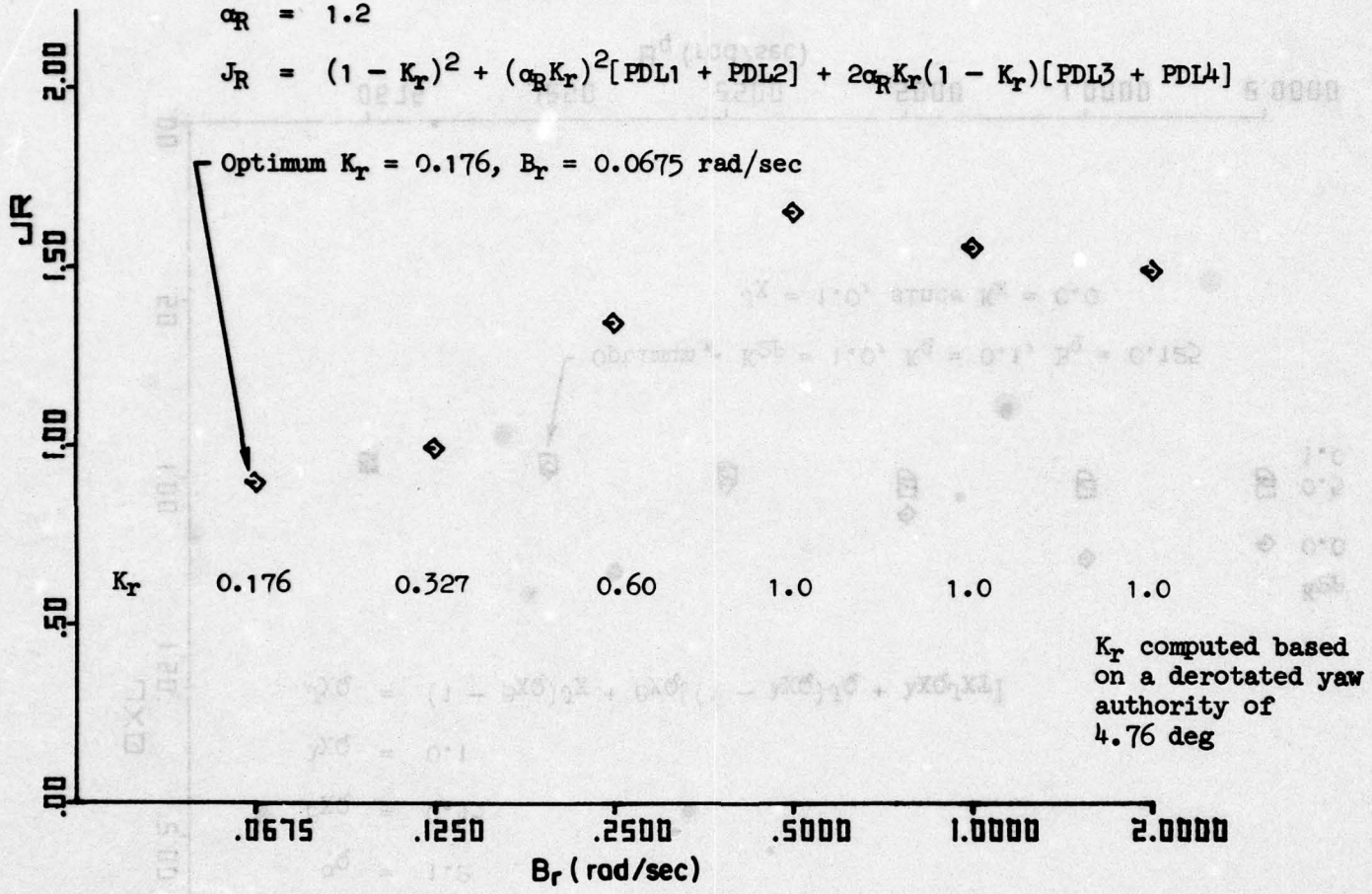

Figure 47. LAMARS Optimization — J_R vs. B_r

which are not represented in the simple math model used to generate the air-to-ground scenario data used here. This point may be gotten around by using data generated, say, in a manned simulation of the task or in-flight. Second, Fig. 47 implies that even lower values of B_q may produce lesser values of J_R than does the lowest value of B_r used in calculating J_R here. As B_r ultimately approaches zero it can be shown that K_r for this air-to-ground scenario approaches 25/360 = 0.0694 and J_R therefore approaches 0.866. Consequently, further reductions in the yaw axis washout break frequency, B_r from 0.0675 rad/sec will result in only slight reduction in J_R from 0.900 while the reduction in K_r is approximately by a factor of 2.5. Therefore, B_r = 0.0675 rad/sec is regarded as optimum.

Table 28 presents a summary of the optimum drive logic parameters as determined by identifying those parameter combinations for which the criterion value for each axis or set of axes was a minimum.

D. NONLINEAR WASHOUT INVESTIGATION

Once the linear drive logic parameters were optimized, a limited investigation of two nonlinear drive logic schemes was undertaken. These are the Parrish adaptive gain scheme, described in Section III and Refs. 7-9, and the subliminal scheme described in Section III, Appendix B and Refs. 10 and 11. Performance is compared (in terms of the motion fidelity criterion) for one set of parameters for the Parrish configuration, two sets of parameters for the subliminal scheme, and the optimized linear scheme. The parameters for each washout are summarized in Table 29. Note that parameters are chosen for both the Parrish and the subliminal washouts to make full use of the available authority limits of the LAMARS motion base. Tables of the motion fidelity measure data are included in Appendix C, Table C-18. It is interesting to observe the large increases in K_p or K_{2R} which are afforded by the subliminal schemes, compared to the linear scheme.

Several other sets of parameters for both the Parrish scheme and the subliminal scheme were investigated, but for brevity only the three cases producing the smallest criterion values are presented here.

Figure 40 presents a plot of J_P, J_Y and J_{YT} for each of the washout schemes. These subcriteria are the constituents of J_{YP}, and it is

TABLE 28. OPTIMUM LAMARS DRIVE LOGIC PARAMETERS

Pitch-Surge Axes		
K_q	0.1 }	*
K_{2P}	1.0 }	
ω_q (= 1.4 B_q)	0.175	rad/sec
ω_{3P} (= B_q)	0.125	rad/sec
ω_{4P} (= B_q)	0.125	rad/sec
ζ_{3P}	0.7	
Roll-Sway Axes		
K_p	0.06	
K_{2R}	0.1	
K_y	1.0	
ω_p (= 1.4 B_p)	0.7	rad/sec
ω_{1R}	0.0	rad/sec
ω_{2R}	0.0	rad/sec
ω_{3R} (= B_p)	0.5	rad/sec
ω_{4R} (= B_p)	0.5	rad/sec
$C_{1y}/(2\sqrt{C_{2y}})$	0.7	
C_{2y}	0.0025	$(\text{rad/sec})^2$
ζ_{3R}	0.7	
Yaw-Heave Axes		
K_r	0.176	
$K_z \cdot K_{2z}$	0.0	
ω_r (= B_r)	0.0675	rad/sec
C_{1Z}	0.0	rad/sec
C_{2Z}	0.0	$(\text{rad/sec})^2$
C_{3Z} (= B_z)	0.0	rad/sec
C_{4Z} (= B_z^2)	0.0	$(\text{rad/sec})^2$
C_{5Z} (= B_z)	0.0	rad/sec

*Gains computed based on a derotated pitch authority of 4.76 deg. If the heave axis is not used, as indicated, then the pitch authority is the full 25 deg, and the pitch gain, K_q, can be increased by a factor of approximately 5.

TABLE 29. SUMMARY OF PARAMETERS USED IN THE NONLINEAR WASHOUT INVESTIGATION

	LINEAR	PARRISH	SUBLIMINAL 1	SUBLIMINAL 2
K_p	0.06	(Adaptive)	0.12	0.05
K_{2R}	0.1	0.1	0.2	0.5
K_y	1.0	1.0	1.0	1.0
ω_p	0.7	0.7	0.7	0.7
ω_{1R}	0.0	0.0	0.0	0.0
ω_{2R}	0.0	0.0	0.0	0.0
ω_{3R}	0.5	0.5	0.5	0.5
ω_{4R}	0.5	0.5	0.5	0.5
C_{2y}	0.0025	0.0025	0.0025	0.0025
$K_{p_{min}}$		0.06		
C_φ		1.0*		
C_K		0.1*		
$C_{2y'}$			0.25	0.25

* These parameters were chosen from the investigation reported in Ref. 11.

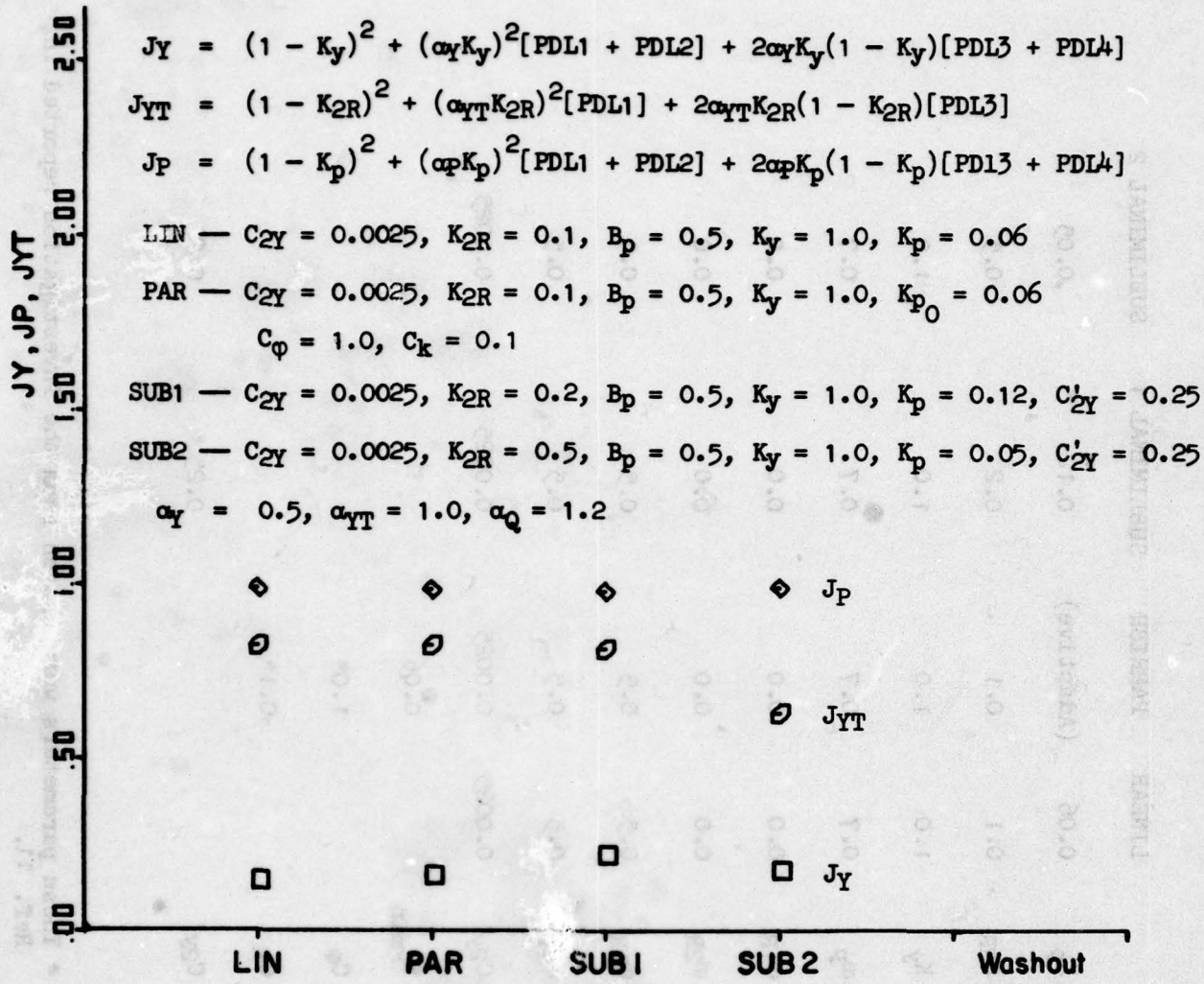

Figure 48. Washout Comparison — J_Y, J_{YT}, and J_P

interesting to compare the various J values among the washouts. Figure 49 is the plot of J_{YP} for each washout. There is no significant difference among the schemes on the basis of the motion fidelity criterion value alone, although the linear washout has a slightly smaller J_{YP} value than any of the nonlinear schemes. Within this limited context (which does not include subjective pilot evaluation), it would appear that the linear washouts used in the LAMARS roll-away drive logic cannot be improved upon by either of the two nonlinear configurations examined.

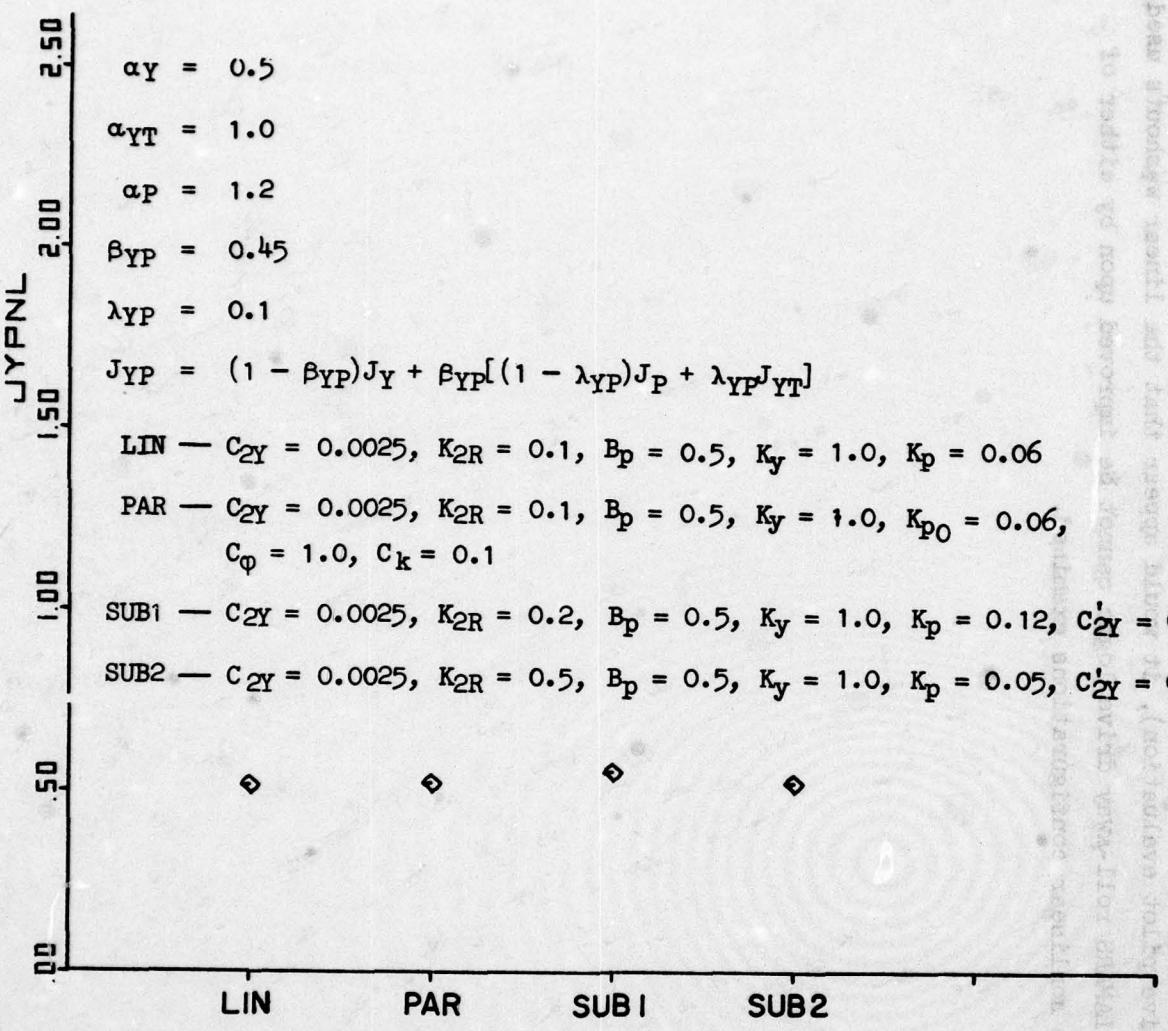

$\alpha_Y = 0.5$

$\alpha_{YT} = 1.0$

$\alpha_P = 1.2$

$\beta_{YP} = 0.45$

$\lambda_{YP} = 0.1$

$J_{YP} = (1 - \beta_{YP})J_Y + \beta_{YP}[(1 - \lambda_{YP})J_P + \lambda_{YP}J_{YT}]$

LIN — $C_{2Y} = 0.0025$, $K_{2R} = 0.1$, $B_p = 0.5$, $K_y = 1.0$, $K_p = 0.06$

PAR — $C_{2Y} = 0.0025$, $K_{2R} = 0.1$, $B_p = 0.5$, $K_y = 1.0$, $K_{p_0} = 0.06$, $C_\varphi = 1.0$, $C_k = 0.1$

SUB1 — $C_{2Y} = 0.0025$, $K_{2R} = 0.2$, $B_p = 0.5$, $K_y = 1.0$, $K_p = 0.12$, $C'_{2Y} = 0.25$

SUB2 — $C_{2Y} = 0.0025$, $K_{2R} = 0.5$, $B_p = 0.5$, $K_y = 1.0$, $K_p = 0.05$, $C'_{2Y} = 0.25$

Figure 49. Washout Comparison — J_{YP}

SECTION VII

RESULTS AND CONCLUSIONS

The results of this research can be summarized as follows:

1. A method for abstracting mission scenarios from strip chart data or verbal descriptions was developed and utilized. This method, implemented in FORTRAN, uses approximate time histories for $\dot{p}$, $\dot{q}$ and $\ddot{V}_T$ and linearized kinematic equations to compute body axis angular velocity and specific force time histories which approximate actual flight values for a particular scenario. The latter quantities provide realistic and relatively accurate inputs for evaluating and optimizing motion base drive logic.

2. A new nonlinear washout technique (the subliminal washout scheme) was developed. This scheme exploits the indifference threshold which is generally acknowledged to be present in the specific force sensory paths. In effect, the nonlinear washout scheme operates to increase the washout rate when the input specific force is subthreshold and the cab is in an off-center position. This is in order to drive the cab to its center position at faster rate than it would be for a comparable linear scheme. For one input, a roll-in to a constant 4 g turn, a 70 percent reduction in the peak lateral travel of the cab was demonstrated for the subliminal scheme relative to a comparable linear scheme.

3. Criteria for discerning fidelity of motion reproduction were developed. These criteria are composed of various mean-square error measures which reflect differences between simulated and actual in-flight motion. The criteria can be used to answer three questions which arise for every moving base simulation program:

- Is moving base simulation appropriate for the flying tasks to be investigated?
- How can motion base drive logic parameters be optimized for the flying tasks to be investigated?
- Will this set of motion drive logic parameters result in motion within simulator capabilities for the flying tasks to be investigated?

The impact of the three sets of variables which quantify the given elements of the above questions can be investigated individually or simultaneously via these motion fidelity measures and criteria: flying task variables, motion base hardware displacement, velocity and acceleration constraints, and parameters of the motion base drive logic.

Obviously, with such a large number of variables, it was necessary to limit the scope of the parametric study of this research investigation to those combinations required to demonstrate formalized, orderly methods for identifying answers to the three questions posed above.

4. The utility of the criteria and measures was demonstrated in an application to optimize the LAMARS drive logic with respect to its hardware constraints and drive logic parameters. An air-to-ground flying task was used. The optimized parameters were identified for the yaw, roll-sway and pitch-surge axes. Furthermore, the criterion value for the heave axis indicated that motion in that axis does not add to motion fidelity. The heave axis criterion did indicate the effectiveness of the g-suit for presenting normal specific force cues is significant. In addition, a comparison of the roll-sway criterion values for the optimized linear drive logic and two nonlinear schemes showed that in this case, no particular benefit was derived from using the nonlinear techniques.

It is interesting to compare the current LAMARS drive logic parameters for the F-17 configuration (Ref. 1) with the optimized drive logic parameters based upon the motion fidelity criteria. Such a comparison is made in Table 30. The major difference between the two parameter sets is in the heave axis — the fidelity criterion for that axis indicated that motion did not improve the simulation fidelity. Also, the parameters for the pitch-surge axis set are somewhat smaller than the current LAMARS values. This is due to the very low (4.76 deg) pitch authority which is assumed to remain after satisfying cab derotation requirements. As was pointed out in an earlier section, the pitch authority in the absence of heave axis motion is the full 25 deg. Thus, the optimized values correspond to this full authority since heave axis motion is not used for optimized drive logic.

In conclusion, the main goal of the research reported herein was to establish an orderly, relatively simple method for optimizing the presentation of motion cues in moving base simulations. This is accomplished via choice of the drive logic parameters for a given simulator and flying task. The method developed here is based upon use of motion fidelity criteria. It has been applied to optimize the LAMARS motion base drive logic parameters for an air-to-ground scenario. The software supporting the optimization process is documented in a separate volume. The methods and procedures of this report can be applied for any given motion base and any desired scenario. Preliminary results with this optimization procedure indicate that further applications and research in this area are warranted. Suggestions for directions which future research should take are found in the next and final section.

TABLE 30. CURRENT LAMARS DRIVE LOGIC PARAMETERS AND OPTIMIZED PARAMETERS

	Current LAMARS (F-17)	Optimized Linear LAMARS	
K_q	0.5	0.55 (0.1)*	
K_{2P}	1.0	1.0	
ω_q	0.5	0.0945 (0.175)*	rad/sec
ω_{3P}	0.2	0.0675 (0.125)*	rad/sec
ω_{4P}	0.2	0.0675 (0.125)*	rad/sec
ζ_{3P}	0.7	0.7	
ω_{6P}	0.0	0.0	rad/sec
K_p	0.05	0.06	
K_{2R}	0.2	0.1	
K_y	1.0	1.0	
ω_p	1.57	0.7	rad/sec
ω_{6R}	0.0	0.0	rad/sec
ω_{1R}	0.266	0.0	rad/sec
ω_{2R}	0.65	0.0	rad/sec
ω_{3R}	0.65	0.5	rad/sec
ω_{4R}	1.0	0.5	rad/sec
$C_{1y}/(2\sqrt{C_{2y}})$	0.7	0.7	
C_{2y}	0.0025†	0.0025	$(\text{rad/sec})^2$
ζ_{3R}	0.7	0.7	
K_r	0.5	0.176	
$K_z \cdot K_{2z}$	0.15	0.0	
ω_r	1.0	0.0675	rad/sec
ω_{6y}	0.0	0.0	rad/sec
C_{1Z}	0.05	0.0	rad/sec
C_{2Z}	0.0	0.0	$(\text{rad/sec})^2$
C_{3Z}	1.4	0.0	rad/sec
C_{4Z}	1.0	0.0	$(\text{rad/sec})^2$
C_{5Z}	0.3	0.0	rad/sec

*Optimized values if pitch limits are reduced to accommodate derotation requirements.

†Certain test data indicate that the installed value for LAMARS may be approximately 0.0225 $(\text{rad/sec})^2$.

SECTION VIII

SUGGESTIONS FOR FURTHER RESEARCH

The procedure developed for generating scenario data and optimizing motion simulator drive logic is a research tool at this stage. Figure 50 provides an overview of this tool, outlining the major steps of the procedure. Steps in blocks with light outlines are manual engineering procedures, while steps in blocks with heavy outlines are implemented in software. Further development of this tool should convert it to a form suitable for routine use as an engineering simulator experiment design aid. Three general areas deserve further attention:

1. Additional applications of the optimization procedure should be undertaken to shed light on its strengths and weaknesses and suggest areas which might be changed and improved. The greatest benefit would be derived if this tool was used in a variety of different simulation environments (different motion bases, different scenarios and different drive logic schemes).

2. Motion fidelity criteria should be sharpened. At present the four motion fidelity criteria (one for each of roll-sway, pitch-surge, yaw and heave motion axes) are each functions of several parameters (α, β, λ). Values for these parameters have been inferred from a rather small amount of experimental evidence. Additional critical experiments are recommended to strengthen the data base upon which the α, β and λ parameter values are based, and perhaps to provide revised values for those parameters.

3. Further applications of this tool would benefit from increased automation of the optimization procedure. This automation would result in less cumbersome "trial and error" choice of drive logic parameters, for example, if the motion fidelity criteria optimizations were performed via a computerized search.

With these three areas targeted, the following immediate research plan is suggested:

Task 1. Extend Capabilities of Software

1.1 Convert existing software from its present research configuration to an engineering simulator experiment design configuration.

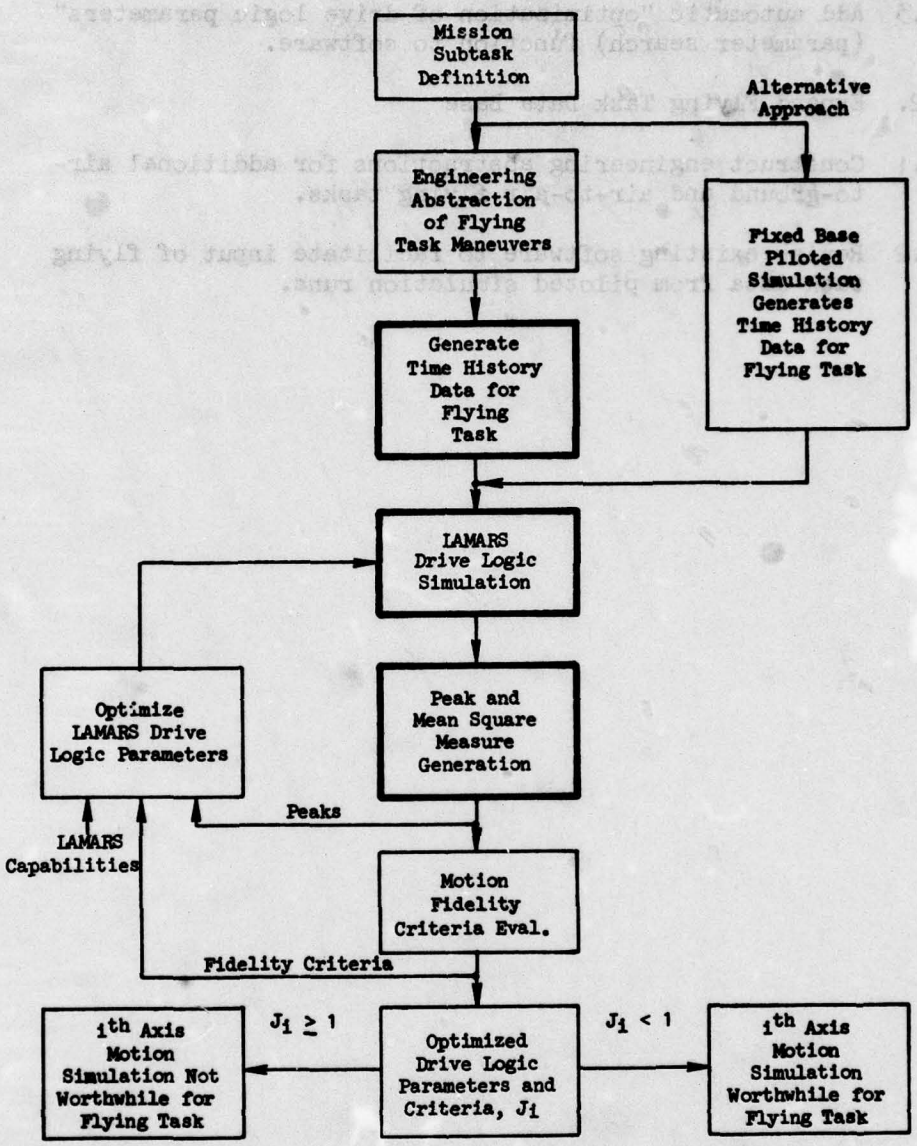

Figure 50. Flow of Optimization Procedure

1.2 Add "motion fidelity criteria evaluation" function to existing software.

1.3 Add automatic "optimization of drive logic parameters" (parameter search) function to software.

Task 2. Expand Flying Task Data Base

2.1 Construct engineering abstractions for additional air-to-ground and air-to-air flying tasks.

2.2 Revise existing software to facilitate input of flying task data from piloted simulation runs.

REFERENCES

1. Sinacori, J. B., "A Practical Approach to Motion Simulation," AIAA Visual and Motion Simulation Conf., Palo Alto, Calif., 10-12 Sept. 1973.

2. Riedel, S. A., Software User's Guide for Engineering Simulation Validation Optimum Presentation of Motion Cues, Systems Technology, Inc., TR-1110-2, 15 Sept. 1978.

3. Sinacori, J. B., R. L. Stapleford, W. F. Jewell, and J. M. Lehman, Researcher's Guide to the NASA Ames Flight Simulator for Advanced Aircraft (FSAA), Systems Technology, Inc., TR-1074-1, May 1977.

4. Schmidt, S. F., and B. Conrad, Motion Drive Signals for Piloted Flight Simulation, NASA CR-1601, May 1970.

5. Sinacori, J. B., A Brief Survey of Motion Simulators' Drive Logic with Emphasis on the Roll Axis, Systems Technology, Inc., WP-1094-2, May 1977.

6. Ashworth, B. R., and R. V. Parrish, "A Visual Motion Simulator for General Aviation Compensated Within the Nonlinear Adaptive Washout for Actuator Lag," AIAA Paper 76-022, Apr. 1976.

7. Parrish, R. V., and D. J. Martin, Jr., "Empirical Comparison of a Linear and a Nonlinear Washout for Motion Simulators," AIAA Paper 75-106, Jan. 1975.

8. Parrish, R. V., and D. J. Martin, Jr., Comparison of a Linear and a Nonlinear Washout for Motion Simulators Utilizing Objective and Subjective Data from CTOL Transport Landing Approaches, NASA TN D-8157, June 1976.

9. Parrish, R. V., J. E. Dieudonne, R. L. Bowles, and D. J. Martin, Jr., "Coordinated Adaptive Washout for Motion Simulators," J. Aircraft, Vol. 12, No. 1, Jan. 1975, pp. 44-50.

10. Riedel, S. A., and L. G. Hofmann, Preliminary Investigation of a New Nonlinear Washout System, Systems Technology, Inc., WP-1110-1, Dec. 1977.

11. Riedel, S. A., and L. G. Hofmann, "Investigation of Nonlinear Motion Simulator Washout Schemes," presented at the 14th Annual Conf. on Manual Control, USC, 25-27 Apr. 1978.

12. Borah, J. D., Human Dynamic Orientation Model Applied to Motion Simulation, MIT, M.S. Thesis, May 1976.

13. Borah, J. D., Sensory Mechanism Modeling Study; Draft of Final Technical Report, AFSC Contract F33615-76-C-0039, Applied Sciences Lab., Waltham, Mass., June 15, 1977.

14. Ormsby, C. C., Model of Human Dynamic Orientation, MIT, Ph.D. Thesis, Jan. 1974.

15. Young, L. R., "Current Status of Vestibular System Models," Automatica, Vol. 5, 1969, pp. 369-383.

16. Stapleford, R. L., R. A. Peters, and F. R. Alex, Experiments and a Model for Pilot Dynamics with Visual and Motion Inputs, NASA CR-1325, May 1969.

17. Young, L. R., "Role of the Vestibular System in Posture and Movement," in V. B. Mountcastle, ed., Medical Psychology. 13th ed. St. Louis, C. V. Mosby and Co., 1974. Vol. I, pp. 704-721.

18. Young, L. R., and J. L. Meiry, "A Revised Dynamic Otolith Model," Aerospace Med., Vol. 39, No. 6, June 1968, pp. 606-608.

19. Chambers, A., and H. C. Vykukel, The Effects of Bed Rest on Crew Performance During Simulated Shuttle Re-Entry, NASA TN D-7503, Oct. 1974.

20. Roark, Marvin, and Andrew Junker, "The Effects of Closed Loop Tracking on a Subjective Tilt Threshold in the Roll Axis," presented at the 14th Annual Conference on Manual Control, Apr. 1978.

APPENDIX A

KINEMATIC EQUATIONS FOR SCENARIO GENERATION

The overall description of the method used to generate scenarios for this research was presented in a previous section. The purpose of this Appendix is to present approximated kinematic equations, derived from the exact equations of motion. These are used to compute the drive logic inputs corresponding to various flying tasks. The summary of assumptions needed to arrive at the kinematic equations from the equations of motion is given below:

- For a given small angle ϵ, $\sin \epsilon = \epsilon$, $\tan \epsilon = \epsilon$, $\cos \epsilon = 1$
- ξ_o and θ are small angles
- a_y and β are identically zero
- $\dot{\alpha}$ is small

where θ is pitch attitude, α is angle of attack and ξ_o is the thrust inclination angle.

The ten basic kinematic equations are given below. The additions or deletions to this list, which are scenario-dependent, are discussed in the succeeding paragraphs.

$$\left.\begin{aligned} \dot{p} &\triangleq \frac{d}{dt}p \\ \dot{q} &\triangleq \frac{d}{dt}q \\ \ddot{V}_T &\triangleq \frac{d}{dt}\dot{V}_T \end{aligned}\right\}$$

inputs resulting from an engineering abstraction of the flying task

$$\dot{V}_T = \frac{d}{dt}V_T \qquad \text{(longitudinal kinematic acceleration)}$$

$$\dot{\varphi} \doteq p \qquad \text{(bank angle rate/roll rate)}$$

$$\dot{\theta} \doteq q \cos \varphi - r \sin \varphi \qquad \text{(pitch attitude rate)}$$

$$\dot{\psi} \doteq r \cos\varphi + q \sin\varphi \qquad \text{(heading rate)}$$

$$r = \frac{g}{V_T} \sin\varphi \qquad \text{(yaw rate; from requiring } a_y \equiv 0\text{)}$$

$$a_x \doteq \dot{V}_T + g\theta \qquad \text{(longitudinal acceleration)}$$

$$a_z \doteq -V_T q - g \cos\varphi \qquad \text{(normal acceleration)}$$

The first seven equations are integrated, at each time interval, resulting in ten variables. Except as indicated below, all initial conditions are zero.

For Scenarios 1 and 2 (the first two HQDT scenarios) $\dot{q}$ is not an input. Instead, $\dot{q}$ is computed from an equation which, if satisfied, assures that the airplane is in constant altitude flight.

Maintenance of constant altitude while in a coordinated turn requires the vertical component of lift to equal the weight. Let load factor, N_z, be defined by:

$$N_z \triangleq -(1 + a_z/g)$$

Then

$$mg(1 + N_z)\cos\varphi = mg = W$$

Solving for $(1 + N_z)$ and differentiating both sides of the resulting equation gives

$$\dot{N}_z = p \sin\varphi/\cos^2\varphi$$

where p is in rad/sec units. Normal acceleration, load factor, and pitch rate are related in the following equation wherein $\dot{w} = \alpha\dot{V}_T + \dot{\alpha}V_T$ has been assumed to be zero.

$$a_z = -g(1 + N_z) \doteq -V_T q - g\cos\varphi$$

Solving for q in terms of N_Z, and differentiating (assuming V_T is constant) results in:

$$\dot{q} = \frac{g}{V_T}\left(\dot{N}_Z + p \sin \varphi\right)$$

Substitution for $\dot{N}_Z$ results in:

$$\dot{q} = p \frac{g \sin \varphi}{V_T}\left(1 + \frac{1}{\cos^2 \varphi}\right)$$

In addition, the following initial condition is imposed:

$$V_T(0) = 560 \text{ ft/sec}$$

For Scenario 3 (the HQDT4 scenario), $\dot{p}$ and $\dot{q}$ are not always input as discrete values. During certain intervals the roll and pitch rates required to achieve a given load factor onset rate while maintaining constant altitude flight, must be computed on the basis of the appropriate constraint equations. The following equations are used to compute inputs to the kinematic equations during these intervals.

If the previous equation for $\dot{N}_Z$ is solved for p and then differentiated assuming $\dot{N}_Z$ is constant the result is:

$$\dot{p} = -p N_Z \cos \varphi\left(\frac{1 + \sin^2 \varphi}{\sin^2 \varphi}\right)$$

If the assumption that V_T is constant is relaxed in obtaining the $\dot{q}$ equation, the result is:

$$\dot{q} = (g/V_T)[\dot{N}_Z + p \sin \varphi - (\dot{V}_T/V_T)(1 + N_Z - \cos \varphi)] \quad \text{rad/sec}$$

where

$$\dot{N}_Z = p \sin \varphi/\cos^2 \varphi$$

$$N_Z = 1/\cos \varphi - 1$$

As was true for the other, HQDT scenarios, the following initial condition is imposed:

$$V_T(0) = 560 \text{ ft/sec}$$

Scenario 4, the air-to-ground task, imposes the following initial conditions:

$$V_T(0) = 420 \text{ ft/sec}$$
$$\dot{V}_T(0) = -5 \text{ ft/sec}^2$$

In order to simulate the air-to-air tasks (Scenarios 5-8), it was necessary to remove the assumption that $\dot{\alpha}$, the angle of attack rate of change, is small. A $\Delta\dot{\alpha}$ equation was added, and several equations were changed to include the effect of α. In addition, it was necessary to make one new assumption. This assumption and the resulting changes in the kinematic equations which are affected, are given below:

$$\alpha = \alpha_o + \Delta\alpha$$

where α_o is the trim angle of attack for straight, level, upright, constant speed flight.

The kinematic terms

$$-pw/V_T \doteq -p(\Delta\alpha + \alpha_o)$$

$$wq - V_T \sin(\alpha_o + \Delta\alpha)\Delta\dot{\alpha} \doteq V_T(\alpha_o + \Delta\alpha)(q - \Delta\dot{\alpha})$$

$$\dot{w} \doteq \Delta\dot{\alpha}V_T + V_T(\alpha_o + \Delta\alpha)$$

are restored to the a_y/V_T, a_x and a_z equations, respectively.

$$r = (g/V_T)\sin\varphi + p(\Delta\alpha + \alpha_o)$$

$$a_x = \dot{V}_T + g\theta + V_T(\alpha_o + \Delta\alpha)(q - \Delta\dot{\alpha})$$

$$a_z = -V_T q - g\cos\varphi + \Delta\dot{\alpha}V + \dot{V}_T(\alpha_o + \Delta\alpha)$$

The normal acceleration is alternatively given by

$$a_z \doteq -g + Z_w V_T \Delta\alpha[V_T/V_T(0)]$$

where Z_w represents the primary aerodynamic characteristic of the aircraft via

$$Z_w = -\frac{\rho S V_T(0)}{2m}(C_{L_\alpha} + C_D)$$

If a_z is eliminated from the two expressions for a_z above, and the resulting expression is solved for $\Delta\dot{\alpha}$, the result is

$$\Delta\dot{\alpha} = q - \frac{g(1 - \cos\varphi)}{V_T} - \frac{(-Z_w)\Delta\alpha V_T}{V_T(0)} - \frac{\dot{V}_T(\alpha_o + \Delta\alpha)}{V_T}$$

where $\dot{V}_T(\alpha_o + \Delta\alpha)/V_T$ is usually negligible with respect to the other terms of the equation.

Also, the following initial conditions or constants apply:

$$\alpha_o = 4 \text{ deg}$$
$$\theta(0) = 4 \text{ deg}$$
$$V_T(0) = 800 \text{ ft/sec}$$
$$-Z_w = 1$$

Thus, for each scenario there exists a set of ten (or eleven, for the air-to-air tasks) state and algebraic equations, and the assumption that $a_y = 0$. The drive logic inputs are generated from these. For the angular inputs, this is a trivial matter:

$$p_A = p$$
$$q_A = q$$
$$r_A = r$$

The specific force inputs are complicated by the fact that the pilot's location in the aircraft is significantly displaced from the aircraft c.g. In order to transform the a_x, a_y and a_z quantities to $\dot{u}_{po}$, $\dot{v}_{po}$, $\dot{w}_{po}$ specific forces as sensed by the pilot, it is necessary to use the following equations.

$$\dot{u}_{po} = a_x + \ell_z\dot{q} + \ell_z rp - \ell_z q^2 - \ell_x r^2$$

$$\dot{v}_{po} = -\ell_z\dot{p} + \ell_x\dot{r} + \ell_z rq + \ell_x pq$$

$$\dot{w}_{po} = a_z - \ell_x\dot{q} - \ell_z p^2 - \ell_z q^2 + \ell_x pr$$

In each case, the following numbers were used for the "location" constants (typical for the A-10 aircraft):

$$\ell_x = 17.67 \text{ ft}$$

$$\ell_z = -3.1 \text{ ft}$$

For details on the implementation of these kinematic equations as computer software, refer to the Software User's Guide (Ref. 2).

APPENDIX B

SUBLIMINAL WASHOUT SCHEME INVESTIGATION

This appendix presents the nonlinear washout scheme designed in the course of the LAMARS optimization research. Figure B-1 depicts an application of this subliminal washout scheme to a first-order roll axis washout. This concept is the result of an attempt to utilize so-called "indifference" thresholds which pilots exhibit under normal workload. These thresholds may be operative for both angular velocity and specific force perception. The hypothesis is that pilots do not perceive angular velocities and specific forces which have magnitudes below the respective indifference thresholds. It was hoped that exploitation of this particular phenomenon would yield a design which reduced simulator travel requirements.

The overall design goal is to drive the simulator cab towards its zero position more rapidly than would the underlying linear washout whenever

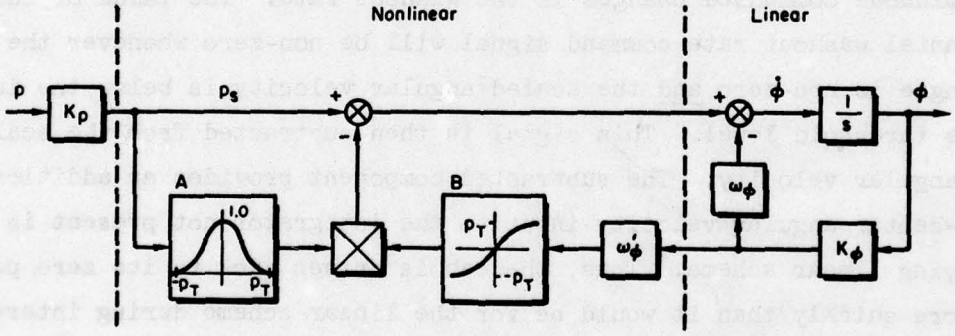

p = Input Angular Velocity

p_S = Scaled Angular Velocity

p_T = Indifference Threshold Level

$\dot{\phi}$ = Commanded Cab Roll Rate

ϕ = Commanded Cab Roll Angle

Figure B-1. Subliminal Washout Filter, First-Order Case

the motion stimulus is below the indifference threshold level. This is accomplished by using the two nonlinear functions in boxes A and B of Fig. B-1. The input to the function in A is the scaled angular velocity. This function produces a weighting factor which serves as a variable feedback gain in the washout circuit. If the input magnitude is larger than the indifference threshold, p_T, the weighting factor is zero. If the input is less than p_T, the weighting factor is a fraction less than 1.0, which is a sinusoid-like function of the input (for the form of the weighting function used here).

The input to B, a soft saturation nonlinear function, is cab roll angle φ. If φ is large, the value of the function output is equal to the indifference threshold, $\pm p_T$. If φ is small, the value of the function output is proportional to φ.

The outputs from boxes A and B are then multiplied to arrive at an incremental washout rate command signal. The particular choice of functions assures that this signal's magnitude never exceeds the indifference threshold level. Also, the smoothness of those functions tends to prevent discontinuous commanded changes in the washout rate. The value of this incremental washout rate command signal will be non-zero whenever the cab roll angle is non-zero and the scaled angular velocity is below the indifference threshold level. This signal is then subtracted from the scaled input angular velocity. The subtracted component provides an additional toward-center angular velocity input to the integrator not present in the underlying linear scheme. Thus, the cab is driven back to its zero position more quickly than it would be for the linear scheme during intervals of subthreshold angular velocity inputs.

The assumed form of the indifference threshold is shown in Fig. B-2a. The soft saturation function of box B, Fig. B-1, is complementary to the indifference threshold function and is shown in Fig. B-2b. The nonlinear function in box A (which generates the weighting factor) approximates the partial derivative of the soft saturation function with respect to its argument. This function is shown in Fig. B-2c. The specific choice of

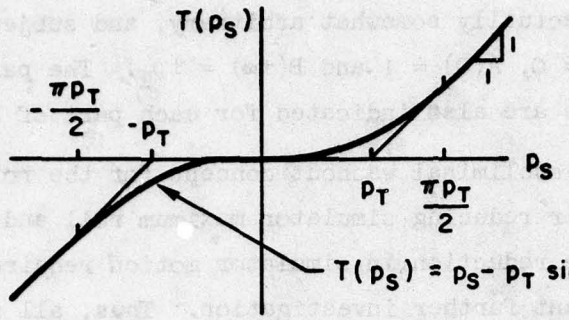

a) Presumed Form of Indifference Threshold

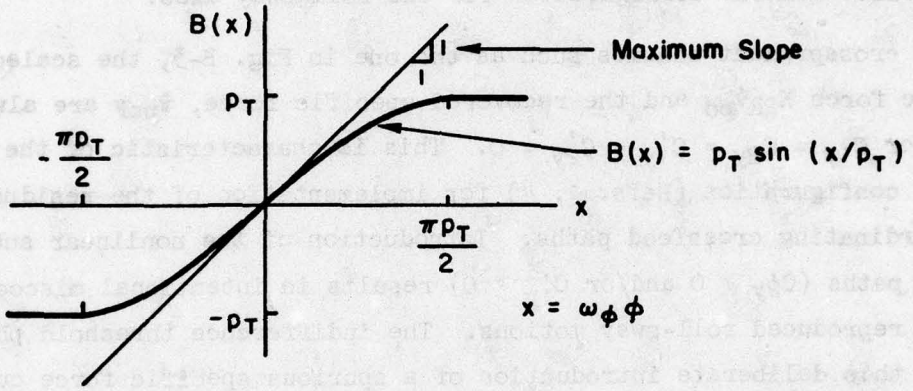

b) Complementary Function For Indifference Threshold

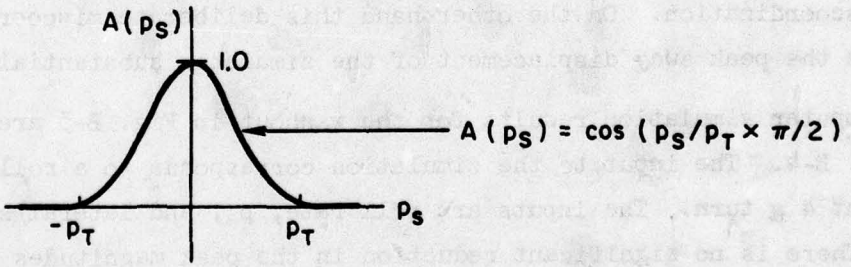

c) Approximate "Partial Derivative" of Complementary Function

Figure B-2. Summary of Nonlinear Functions

the indifference function is actually somewhat arbitrary, and subject only to the constraints that $T(0) = 0$, $A(0) = 1$ and $B(\pm\infty) = \pm p_T$. The particular analytical functions used here are also indicated for each part of Fig. B-2.

Preliminary tests of this subliminal washout concept for the roll axis showed it to be ineffective for reducing simulator maximum roll and sway displacements. There was some reduction in simulator motion requirements, but not really enough to warrant further investigation. Thus, all subsequent study centered around schemes which included the subliminal functions in the specific force paths only. Figure B-3 shows an application of the subliminal washout concept within the lateral specific force channel of a crossproduct washout configuration for the roll-sway axes.

For crossproduct schemes such as the one in Fig. B-3, the scaled input specific force $K_{2R}\dot{v}_{po}$ and the recovered specific force, $\dot{v}_{poF}$ are always equal for $C_{1y} = C_{2y} = C'_{1y} = C'_{2y} = 0$. This is characteristic of the crossproduct configuration (Refs. 1, 4) for implementation of the residual tilt and coordinating crossfeed paths. Introduction of the nonlinear subliminal washout paths ($C'_{2y} > 0$ and/or $C'_{1y} > 0$) results in intentional miscoordination of reproduced roll-sway motions. The indifference threshold phenomenon permits this deliberate introduction of a spurious specific force cue due to miscoordination. As long as the degree of miscoordination does not cause a spurious lateral specific force cue which exceeds the specific force indifference threshold level, the pilot, under normal workload, should not detect the miscoordination. On the other hand this deliberate miscoordination reduces the peak sway displacement of the simulator substantially.

Computer simulation results for the washout in Fig. B-3 are presented in Fig. B-4. The input to the simulation corresponds to a roll-in to a constant 4 g turn. The inputs are roll rate, p_A, and lateral specific force, $\dot{v}_{po}$. There is no significant reduction in the peak magnitudes of the sway acceleration, $\ddot{y}$, or the sway velocity, $\dot{y}$. But these results clearly show a substantial reduction in the maximum sway displacement, y. The subliminal washout scheme accounts for a 70 percent reduction in y compared to the linear case (maximum required y equals 13 ft for linear washout, 4 ft for subliminal washout).

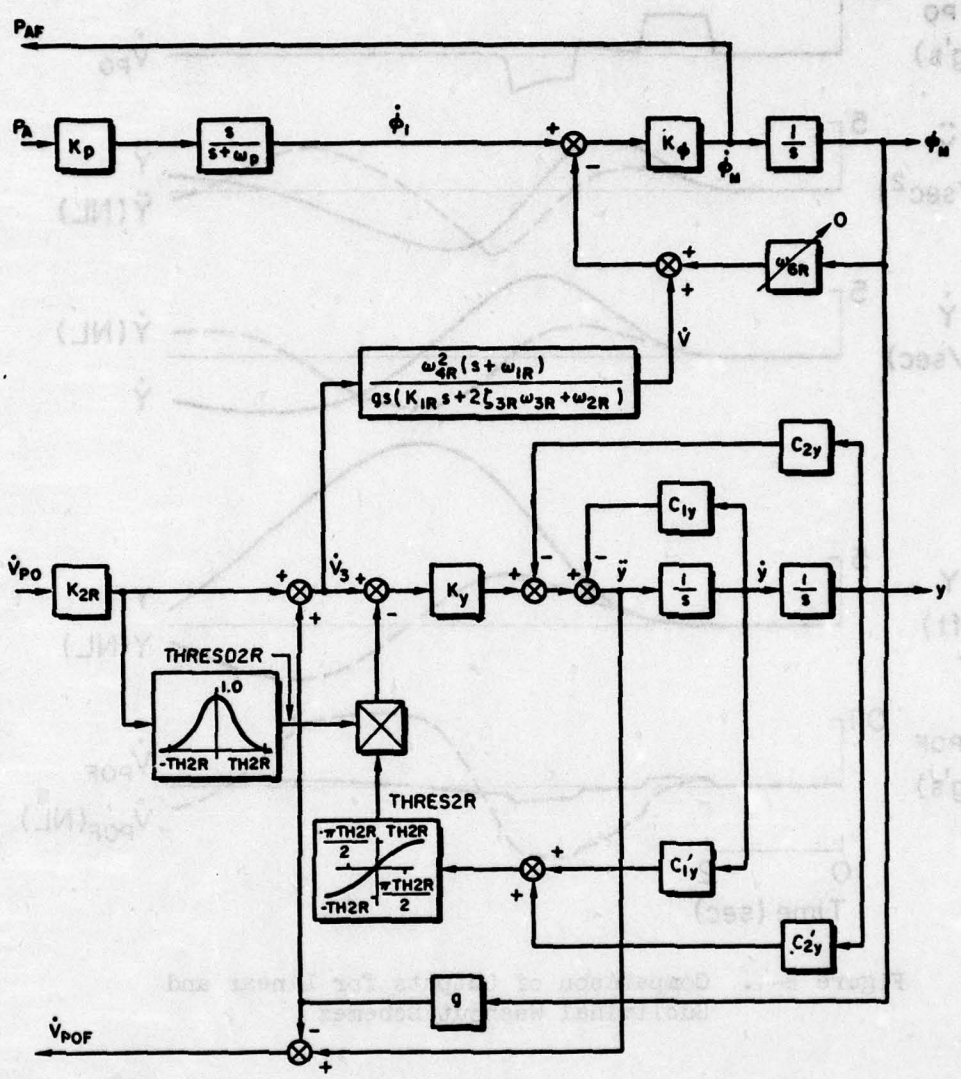

Figure B-3. Subliminal Scheme Applied to Specific Force Path of LAMARS Roll-Sway Axes

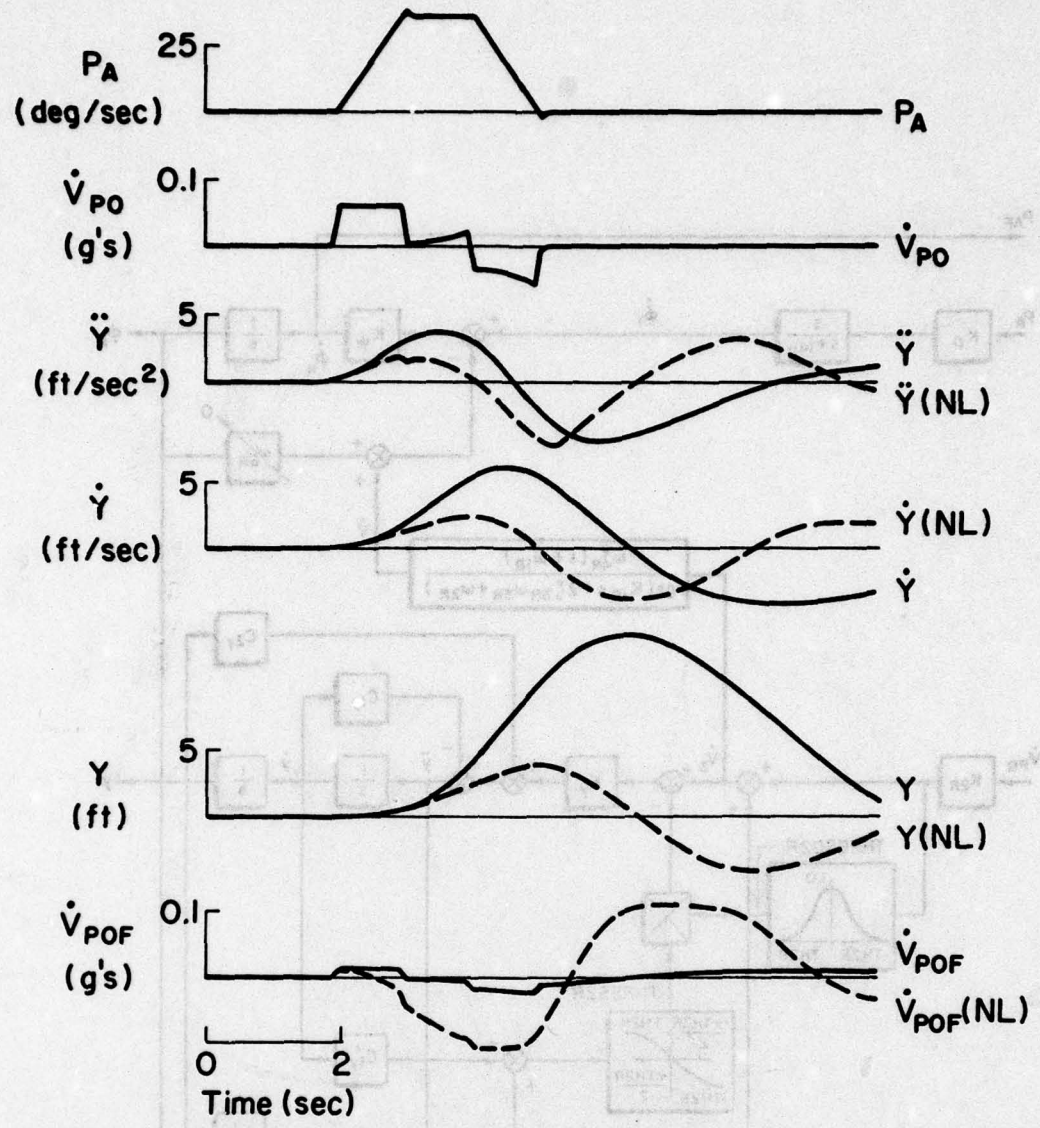

Figure B-4. Comparison of Outputs for Linear and Subliminal Washout Schemes

In order to accomplish this substantial reduction in lateral translation, however, a substantial increase in recovered specific force, $\dot{v}_{poF}$, which is spurious is observed. This is due to the miscoordination deliberately introduced to increase the washout rate. Notice that this component of miscoordination is constrained to be approximately within the assumed indifference threshold level of 0.1 g. Under normal workload, the pilot should not be able to detect this level of miscoordination.

The computer simulation of the subliminal washout has been exercised for a variety of inputs. Significant reductions in translational requirements have been observed. On the basis of these results, the following conclusions are drawn:

1. The subliminal washout concepts, as implemented in the translational axes of the crossproduct scheme, are effective in reducing the maximum displacement requirements of the motion base.

2. The subliminal washout scheme is most effective for sub-indifference threshold specific force inputs. The washout effectively reduces the underlying linear scheme when inputs exceed this threshold by a very large amount.

3. The use of the subliminal washout scheme results in an increase in recovered specific force which is spurious. This spurious motion is due to additional miscoordination. The nonlinear implementation insures that this miscoordination component is never greater than the assumed indifference threshold level. Thus, under normal workload the pilot should be unable to detect this false cue.

APPENDIX C

TABLES OF MEASURES

This appendix presents the raw measures data generated by the measures software. The following Tables are included:

Table C-1: Pitch and Surge axis measures versus scenario

Table C-2: Roll and Sway axis measures versus scenario

Table C-3: Yaw and Heave axis measures versus scenario

Table C-4: Pitch and Surge axis measures versus break frequency, $K_{2p} = 0.0$

Table C-5: Pitch and Surge axis measures versus break frequency, $K_{2p} = 0.5$

Table C-6: Pitch and Surge axis measures versus break frequency, $K_{2p} = 1.0$

Table C-7: Roll and Sway axis measures versus break frequency, $K_{2R} = 0.0$, $C_{2y} = 0.0025$ and $K_p = 0.5$

Table C-8: Roll and Sway axis measures versus break frequency, $K_{2R} = 0.0$, $C_{2y} = 0.0225$ and $K_p = 0.5$

Table C-9: Roll and Sway axis measures versus break frequency, $K_{2R} = 0.0$, $C_{2y} = 0.25$ and $K_p = 0.5$

Table C-10: Roll and Sway axis measures versus break frequency, $K_{2R} = 0.5$, $C_{2y} = 0.0225$ and $K_p = 0.5$

Table C-11: Roll and Sway axis measures versus break frequency, $K_{2R} = 1.0$, $C_{2y} = 0.0025$ and $K_p = 0.5$

Table C-12: Roll and Sway axis measures versus break frequency, $K_{2R} = 1.0$, $C_{2y} = 0.0225$ and $K_p = 0.5$

Table C-13: Roll and Sway axis measures versus break frequency, $K_{2R} = 1.0$, $C_{2y} = 0.25$ and $K_p = 0.5$

Table C-14: Yaw and Heave axis measures versus break frequency

Table C-15: Revised measures, Pitch-Surge axes versus break frequency and K_{2p}

Table C-16: Revised measures, Roll-Sway axes versus break frequency and C_{2y}

Table C-17: Revised measures, Yaw and Heave axes versus break frequency

Table C-18: Revised measures, Roll-Sway axes versus washout configuration

TABLE C-1. PITCH AND SURGE MEASURES VERSUS SCENARIO

	1	2	3	4	5	6	7	8
PDLA	0.75E+02	0.68E+02	0.14E+03	0.26E+02	0.26E+02	0.31E+03	0.42E+02	0.70E+02
PDL1	0.62639	0.69404	0.96005	1.08905	0.91431	0.38442	0.18338	0.35533
PDL2	0.03152	0.02884	0.07142	0.05983	-0.07251	-0.12939	-0.02069	-0.04326
PDL3	0.75160	0.72728	0.97375	0.94394	0.91827	0.35970	0.41830	0.29831
PDL4	0.01937	0.01697	0.03537	-0.01619	-0.09861	-0.11135	-0.02692	0.03979
PDLS	2.17330	3.99232	0.47547	1.87816	1.33772	59.49042	3.96663	11.13155
PSENA	0.28E+02	0.26E+02	0.19E+02	0.92E+01	0.35E+01	0.20E+03	0.19E+02	0.59E+02
PSEN1	0.70044	0.49247	1.10686	1.04947	0.71742	0.17017	0.17841	0.26482
PSEN2	0.03407	0.02190	0.08566	-0.02999	0.03997	-0.05393	0.01669	-0.01967
PSEN3	0.74986	0.46449	1.02832	0.82517	0.62734	0.14103	0.40500	0.21558
PSEN4	0.01939	0.01509	0.03842	-0.09485	-0.23225	-0.06569	0.02438	0.05784
PSENS	1.38857	3.59124	0.27638	1.28337	0.85097	49.25410	1.60659	10.38558
PNLA	0.15E+02	0.13E+02	0.66E+01	0.32E+01	0.83E+00	0.18E+03	0.12E+02	0.45E+02
PNL1	0.81950	0.74655	0.99783	0.83605	0.81143	0.11708	0.36988	0.29627
PNL2	0.01256	0.01271	0.00302	-0.04638	-0.06634	-0.00377	0.10862	0.02058
PNL3	0.89725	0.78820	0.99880	0.88522	0.89440	0.13425	0.59638	0.36651
PNL4	0.00762	0.00766	0.00151	-0.07366	-0.05702	-0.04359	0.08899	0.07073
PNLS	0.08484	0.53403	0.00040	0.13301	0.01454	40.79810	0.31808	4.98215
GS1	0.00000	0.00000	0.00000	0.00000	0.00000	0.00000	0.00000	0.00000
GS2	0.00000	0.00000	0.00000	0.00000	0.00000	0.00000	0.00000	0.00000
GSS	0.00000	0.00000	0.00000	0.00000	0.00000	0.00000	0.00000	0.00000
PACC	0.00000	0.00000	0.00000	0.00000	0.00000	0.00000	0.00000	0.00000
PVEL	0.77E+01	0.79E+01	0.32E+01	0.10E+02	0.67E+01	0.11E+03	0.15E+02	0.22E+02
PDIS	17.99040	17.65545	14.30437	34.02669	41.84064	86.60170	22.90169	25.21867

a) Pitch Axis Measures vs. Scenarios

	1	2	3	4	5	6	7	8
PDLA	0.00044	0.00049	0.00304	0.01721	0.07357	0.64214	0.02893	0.08249
PDL1	0.72949	0.62285	0.37423	0.32217	0.42617	1.14220	1.07048	1.05091
PDL2	27.97088	14.72705	6.25722	0.31440	-0.01809	-0.11487	0.26158	-0.19794
PDL3	0.84603	0.75452	0.59972	0.30103	0.43858	1.00174	1.01873	1.01604
PDL4	4.23309	2.13022	1.89706	-0.07105	-0.04561	-0.10365	0.06017	-0.13039
PDLS	0.00851	0.00517	0.00802	0.02025	0.04577	0.14842	0.00504	0.00674
PSENA	0.00022	0.00023	0.00112	0.00525	0.02174	0.38365	0.01351	0.03357
PSEN1	0.75564	0.73141	0.36139	0.66433	0.73779	1.22880	1.06437	1.07506
PSEN2	28.41140	14.60515	5.95116	0.67220	-0.01640	-0.13519	0.24937	-0.30478
PSEN3	0.86104	0.81675	0.58409	0.56371	0.65744	1.06298	1.01575	1.02733
PSEN4	4.19120	1.55125	1.80800	-0.08536	-0.05411	-0.09795	0.06433	-0.19719
PSENS	0.00433	0.00267	0.00283	0.00725	0.01119	0.06274	0.00207	0.00369
PNLA	0.13E-07	0.16E-07	0.18E-05	0.50E-03	0.76E-02	0.30E+00	0.33E-02	0.18E-01
PNL1	0.98982	0.96470	0.76247	0.98460	0.92633	1.22936	1.01016	1.00033
PNL2	0.12E+05	0.41E+04	0.13E+02	0.14E+01	-0.74E-01	-0.13E+00	0.15E+00	-0.19E+00
PNL3	0.99481	0.98184	0.86988	0.96838	0.87962	1.08587	1.00505	1.00015
PNL4	73.21522	20.00813	1.77258	-0.10080	-0.05868	-0.09272	0.07185	-0.10343
PNLS	0.15E-03	0.65E-04	0.18E-04	0.83E-03	0.16E-02	0.33E-01	0.33E-04	0.37E-03
GS1	0.00000	0.00000	0.00000	0.00000	0.00000	0.00000	0.00000	0.00000
GS2	0.00000	0.00000	0.00000	0.00000	0.00000	0.00000	0.00000	0.00000
GSS	0.00000	0.00000	0.00000	0.00000	0.00000	0.00000	0.00000	0.00000
PACC	0.00000	0.00000	0.00000	0.00000	0.00000	0.00000	0.00000	0.00000
PVEL	0.00000	0.00000	0.00000	0.00000	0.00000	0.00000	0.00000	0.00000
PDIS	0.00000	0.00000	0.00000	0.00000	0.00000	0.00000	0.00000	0.00000

b) Surge Axis Measures vs. Scenarios

TABLE C-2. ROLL AND SWAY MEASURES VERSUS SCENARIO

	1	2	3	4	5	6	7	8
PDLA	0.17E+03	0.44E+03	0.78E+02	0.16E+03	0.65E+02	0.49E+04	0.73E+03	0.20E+03
PDL1	1.38120	1.42730	1.25512	1.31958	1.41428	1.32469	1.39301	1.03192
PDL2	-0.02564	0.01391	0.03747	0.22213	0.02631	-0.30410	0.11461	0.63262
PDL3	1.06949	1.13320	0.96080	0.98028	1.04476	0.97984	1.00646	0.78101
PDL4	0.03563	0.03391	0.10162	0.17313	0.09063	-0.12203	0.14208	0.33483
PDLS	0.06199	0.11664	0.03271	0.09679	0.02759	3.73685	0.38277	0.22039
PSENA	0.12E+03	0.32E+03	0.56E+02	0.14E+03	0.53E+02	0.38E+04	0.61E+03	0.16E+03
PSEN1	1.50638	1.49302	1.31497	1.33852	1.44843	1.20769	1.37130	1.02612
PSEN2	-0.01938	0.03665	0.05242	0.24990	0.03628	-0.26908	0.09437	0.75415
PSEN3	1.08929	1.14727	0.93887	0.96518	1.03784	0.90262	0.99503	0.72697
PSEN4	0.05724	0.05351	0.13570	0.19767	0.10771	-0.10614	0.13567	0.40287
PSENS	0.05679	0.10299	0.03057	0.08972	0.02566	3.31999	0.31328	0.20456
PNLA	0.87E+02	0.27E+03	0.42E+02	0.11E+03	0.35E+02	0.37E+04	0.55E+03	0.13E+03
PNL1	0.99951	1.00302	0.99742	0.99770	0.99939	1.06521	1.01440	0.96801
PNL2	0.00161	0.00029	0.00388	0.00878	0.00174	-0.20411	0.00267	0.04672
PNL3	0.99973	1.00149	0.99853	0.99832	0.99966	0.95896	1.00470	0.98307
PNL4	0.00083	0.00016	0.00210	0.00485	0.00090	-0.09478	0.00334	0.02354
PNLS	0.17E-05	0.14E-04	0.31E-05	0.40E-04	0.50E-06	0.12E+01	0.14E-02	0.48E-03
GS1	0.00000	0.00000	0.00000	0.00000	0.00000	0.00000	0.00000	0.00000
GS2	0.00000	0.00000	0.00000	0.00000	0.00000	0.00000	0.00000	0.00000
GSS	0.00000	0.00000	0.00000	0.00000	0.00000	0.00000	0.00000	0.00000
PACC	0.00000	0.00000	0.00000	0.00000	0.00000	0.00000	0.00000	0.00000
PVEL	0.11E+02	0.12E+02	0.13E+02	0.25E+02	0.10E+02	0.16E+03	0.33E+02	0.31E+02
PDIS	0.13E+02	0.25E+02	0.12E+02	0.31E+02	0.12E+02	0.11E+03	0.21E+02	0.30E+02

a) Roll Axis Measures vs. Scenarios

	1	2	3	4	5	6	7	8
PDLA	0.00027	0.00098	0.00027	0.00086	0.00021	0.21070	0.00241	0.00251
PDL1	0.00623	0.00947	0.00471	0.00750	0.00725	0.00122	0.00655	0.00414
PDL2	0.04376	0.05186	0.01986	0.02386	0.02664	-0.00034	0.01716	0.00901
PDL3	0.03755	0.06113	0.02539	0.04468	0.04324	0.00669	0.05267	0.02167
PDL4	-0.01691	0.05226	-0.01924	0.00734	-0.02448	-0.00848	-0.04058	0.00157
PDLS	0.11E-04	0.33E-04	0.11E-04	0.32E-04	0.85E-05	0.85E-02	0.96E-04	0.97E-04
PSENA	0.00011	0.00050	0.00011	0.00044	0.00011	0.04460	0.00126	0.00100
PSEN1	0.01017	0.01337	0.00724	0.01011	0.01004	0.00243	0.00774	0.00630
PSEN2	0.07037	0.06933	0.03493	0.03465	0.03950	-0.00058	0.01702	0.01605
PSEN3	0.06609	0.09010	0.04190	0.06247	0.06255	0.01693	0.06419	0.03645
PSEN4	-0.02569	0.07355	-0.02216	0.02013	-0.02797	-0.02370	-0.02866	0.01462
PSENS	0.45E-05	0.15E-04	0.45E-05	0.15E-04	0.41E-05	0.18E-02	0.48E-04	0.37E-04
PNLA	0.11E-07	0.11E-05	0.44E-07	0.28E-05	0.14E-07	0.30E-01	0.93E-05	0.45E-04
PNL1	0.92986	0.93376	0.92958	0.93129	0.92980	0.36245	0.93277	0.92194
PNL2	-0.00361	0.01182	-0.00086	0.00836	-0.00796	-0.01272	-0.00672	0.00253
PNL3	0.96429	0.96631	0.96414	0.96503	0.96426	0.57275	0.96580	0.96018
PNL4	-0.00191	0.00609	-0.00047	0.00431	-0.00417	-0.01229	-0.00350	0.00132
PNLS	0.63E-12	0.33E-10	0.24E-11	0.11E-09	0.90E-12	0.28E-03	0.54E-09	0.27E-08
GS1	0.00000	0.00000	0.00000	0.00000	0.00000	0.00000	0.00000	0.00000
GS2	0.00000	0.00000	0.00000	0.00000	0.00000	0.00000	0.00000	0.00000
GSS	0.00000	0.00000	0.00000	0.00000	0.00000	0.00000	0.00000	0.00000
PACC	0.11E+02	0.21E+02	0.12E+02	0.26E+02	0.11E+02	0.42E+03	0.26E+02	0.36E+02
PVEL	0.11E+02	0.26E+02	0.13E+02	0.34E+02	0.11E+02	0.12E+03	0.31E+02	0.25E+02
PDIS	29.63115	71.74157	27.69105	70.45265	26.21994	59.35406	37.14861	52.06571

b) Sway Axis Measures vs. Scenarios

TABLE C-3. YAW AND HEAVE MEASURES VERSUS SCENARIO

	1	2	3	4	5	6	7	8
PDLA	0.60E+01	0.61E+01	0.80E+01	0.53E+01	0.57E+01	0.44E+03	0.15E+02	0.15E+02
PDL1	0.79145	0.78756	0.91998	0.95179	0.91998	0.25066	0.47009	0.67853
PDL2	0.00000	0.00000	0.00000	0.00000	0.00000	0.00000	0.00000	0.00000
PDL3	0.87577	0.83831	0.95271	0.95178	0.92563	0.25663	0.56520	0.69159
PDL4	0.00000	0.00000	0.00000	0.00000	0.00000	0.00000	0.00000	0.00000
PDLS	0.05936	0.16875	0.02919	0.06390	0.09727	81.98996	1.23166	1.10752
PSENA	0.19E+01	0.42E+01	0.10E+01	0.16E+01	0.11E+01	0.40E+03	0.12E+02	0.76E+01
PSEN1	0.85264	0.80533	0.92171	0.87670	0.67222	0.24966	0.46983	0.46171
PSEN2	0.00000	0.00000	0.00000	0.00000	0.00000	0.00000	0.00000	0.00000
PSEN3	0.88767	0.84598	0.92257	0.87832	0.67258	0.25636	0.57746	0.46106
PSEN4	0.00000	0.00000	0.00000	0.00000	0.00000	0.00000	0.00000	0.00000
PSENS	0.03645	0.11785	0.01954	0.04893	0.08829	74.19031	0.96381	1.02355
PNLA	0.39E-01	0.44E+00	0.16E-01	0.77E-01	0.38E-01	0.37E+03	0.52E+01	0.41E+01
PNL1	0.98990	0.98341	0.98422	0.97030	0.92177	0.26059	0.83033	0.64527
PNL2	0.00000	0.00000	0.00000	0.00000	0.00000	0.00000	0.00000	0.00000
PNL3	0.99490	0.99154	0.99200	0.98478	0.95847	0.29229	0.90660	0.77358
PNL4	0.00000	0.00000	0.00000	0.00000	0.00000	0.00000	0.00000	0.00000
PNLS	0.98E-06	0.37E-04	0.86E-06	0.14E-04	0.46E-04	0.62E+02	0.22E-01	0.10E+00
GS1	0.00000	0.00000	0.00000	0.00000	0.00000	0.00000	0.00000	0.00000
GS2	0.00000	0.00000	0.00000	0.00000	0.00000	0.00000	0.00000	0.00000
GSS	0.00000	0.00000	0.00000	0.00000	0.00000	0.00000	0.00000	0.00000
PACC	0.00000	0.00000	0.00000	0.00000	0.00000	0.00000	0.00000	0.00000
PVEL	1.02345	1.84346	1.14587	2.10096	2.51962	76.72181	5.47180	9.86203
PDIS	3.18341	3.15170	3.24885	4.12562	4.50007	47.79432	6.09939	8.49522

a) Yaw Axis Measures vs. Scenarios

	1	2	3	4	5	6	7	8
PDLA	4.39132	3.93376	9.01536	1.10385	2.22176	10.95854	1.95161	4.76030
PDL1	1.13511	1.27072	1.01426	1.08413	1.00985	1.12655	0.67929	1.57623
PDL2	0.00000	0.00000	0.00000	0.00000	0.00000	0.00000	0.00000	0.00000
PDL3	1.05480	1.09117	1.00682	1.02876	0.99876	1.01628	0.82061	1.13016
PDL4	0.00000	0.00000	0.00000	0.00000	0.00000	0.00000	0.00000	0.00000
PDLS	0.00252	0.00782	0.00013	0.00066	0.00062	0.02317	0.00167	0.03384
PSENA	2.22446	1.84669	3.20140	0.48922	0.68658	5.44358	0.62359	3.18802
PSEN1	1.18063	1.39273	1.01839	1.13910	1.07205	1.23213	0.75093	1.60677
PSEN2	0.00000	0.00000	0.00000	0.00000	0.00000	0.00000	0.00000	0.00000
PSEN3	1.07596	1.13698	1.00875	1.05238	1.02336	1.07342	0.86290	1.16094
PSEN4	0.00000	0.00000	0.00000	0.00000	0.00000	0.00000	0.00000	0.00000
PSENS	0.00144	0.00493	0.00006	0.00038	0.00039	0.01045	0.00035	0.02044
PNLA	4.52700	4.17595	9.02534	1.15541	2.19557	11.50537	1.30719	5.59484
PNL1	0.08683	0.17472	0.02389	0.07023	0.04445	0.11701	0.08469	0.36638
PNL2	0.00000	0.00000	0.00000	0.00000	0.00000	0.00000	0.00000	0.00000
PNL3	0.20341	0.17851	0.14407	0.13427	0.14448	0.17943	0.42278	0.24648
PNL4	0.00000	0.00000	0.00000	0.00000	0.00000	0.00000	0.00000	0.00000
PNLS	0.06681	0.06848	0.14919	0.02038	0.03697	0.19322	0.00994	0.09554
GS1	1.06651	1.19282	1.00386	1.03471	1.00466	1.06264	0.87321	1.36615
GS2	1.02978	1.08399	1.00185	1.01363	1.00077	1.02096	0.93339	1.13817
GSS	0.71E-03	0.23E-02	0.34E-04	0.19E-03	0.15E-03	0.54E-02	0.19E-03	0.01130
PACC	0.23E+02	0.38E+02	0.88E+01	0.38E+02	0.23E+02	0.15E+03	0.37E+02	96.41149
PVEL	0.29E+02	0.45E+02	0.10E+02	0.37E+02	0.26E+02	0.10E+03	0.31E+02	0.10E+03
PDIS	0.54E+02	0.54E+02	0.25E+02	0.62E+02	0.45E+02	0.13E+03	0.36E+02	99.66941

b) Heave Axis Measures vs. Scenarios

TABLE C-4

PITCH AND SURGE MEASURES VERSUS BREAK FREQUENCY
K_{2P} = 0.0

	.0675	.125	.25	.5	1.0	2.0
PDLA	25.60710	25.60710	25.60710	25.60710	25.60710	25.60710
PDL1	0.58238	0.80460	1.16504	1.20203	1.09463	1.03307
PDL2	0.00000	0.00000	0.00000	0.00000	0.00000	0.00000
PDL3	0.49643	0.64237	0.93280	1.05512	1.03705	1.01463
PDL4	0.00000	0.00000	0.00000	0.00000	0.00000	0.00000
PDLS	3.77401	3.32806	1.91691	0.58764	0.13143	0.02441
PSENA	9.18581	9.18581	9.18581	9.18581	9.18581	9.18581
PSEN1	0.15987	0.49218	1.16178	1.35200	1.19229	1.07247
PSEN2	0.00000	0.00000	0.00000	0.00000	0.00000	0.00000
PSEN3	0.09075	0.29474	0.78554	1.07126	1.07042	1.03138
PSEN4	0.00000	0.00000	0.00000	0.00000	0.00000	0.00000
PSENS	2.24677	2.07303	1.35653	0.48104	0.11815	0.02230
PNLA	3.19468	3.19468	3.19468	3.19468	3.19468	3.19468
PNL1	0.29299	0.46650	0.78778	1.00181	1.00512	1.00107
PNL2	0.00000	0.00000	0.00000	0.00000	0.00000	0.00000
PNL3	0.47081	0.55040	0.81790	0.99801	1.00234	1.00053
PNL4	0.00000	0.00000	0.00000	0.00000	0.00000	0.00000
PNLS	0.28E+00	0.29E+00	0.12E+00	0.46E-02	0.34E-03	0.10E-04
GS1	0.00000	0.00000	0.00000	0.00000	0.00000	0.00000
GS2	0.00000	0.00000	0.00000	0.00000	0.00000	0.00000
GSS	0.00000	0.00000	0.00000	0.00000	0.00000	0.00000
PACC	0.00000	0.00000	0.00000	0.00000	0.00000	0.00000
PVEL	11.17123	10.86064	9.98160	6.59412	4.31896	2.18626
PDIS	40.78298	38.81647	23.41467	11.02253	4.25406	1.94151

a) Pitch Axis Measures vs. Break Frequencies (rad/sec)

	.0675	.125	.25	.5	1.0	2.0
PDLA	0.01721	0.01721	0.01721	0.01721	0.01721	0.01721
PDL1	0.00000	0.00000	0.00000	0.00000	0.00000	0.00000
PDL2	1.84815	1.11629	0.42077	0.06658	0.00652	0.00052
PDL3	0.00000	0.00000	0.00000	0.00000	0.00000	0.00000
PDL4	0.02261	0.00913	-0.08146	-0.06634	-0.02554	-0.00663
PDLS	0.32E-01	0.19E-01	0.72E-02	0.11E-02	0.11E-03	0.90E-05
PSENA	0.00525	0.00525	0.00525	0.00525	0.00525	0.00525
PSEN1	0.00000	0.00000	0.00000	0.00000	0.00000	0.00000
PSEN2	2.71456	2.00411	0.86713	0.14935	0.01491	0.00114
PSEN3	0.00000	0.00000	0.00000	0.00000	0.00000	0.00000
PSEN4	0.27864	0.13130	-0.09114	-0.12497	-0.05415	-0.01431
PSENS	0.14E-01	0.11E-01	0.46E-02	0.78E-03	0.78E-04	0.60E-05
PNLA	0.00050	0.00050	0.00050	0.00050	0.00050	0.00050
PNL1	0.00000	0.00000	0.00000	0.00000	0.00000	0.00000
PNL2	0.50E+01	0.26E+01	0.43E+00	0.82E-02	0.15E-04	0.11E-07
PNL3	0.00000	0.00000	0.00000	0.00000	0.00000	0.00000
PNL4	0.64E+00	0.36E+00	0.27E-02	-0.23E-01	-0.18E-02	-0.45E-04
PNLS	0.25E-02	0.13E-02	0.21E-03	0.41E-05	0.74E-08	0.56E-11
GS1	0.00000	0.00000	0.00000	0.00000	0.00000	0.00000
GS2	0.00000	0.00000	0.00000	0.00000	0.00000	0.00000
GSS	0.00000	0.00000	0.00000	0.00000	0.00000	0.00000
PACC	0.00000	0.00000	0.00000	0.00000	0.00000	0.00000
PVEL	0.00000	0.00000	0.00000	0.00000	0.00000	0.00000
PDIS	0.00000	0.00000	0.00000	0.00000	0.00000	0.00000

b) Surge Axis Measures vs Break Frequencies (rad/sec)

TABLE C-5

PITCH AND SURGE MEASURES VERSUS SCENARIO
$K_{2P} = 0.5$

	.0675	.125	.25	.5	1.0	2.0
PDLA	25.60710	25.60710	25.60710	25.60710	25.60710	25.60710
PDL1	0.58238	0.80460	1.16504	1.20203	1.09463	1.03307
PDL2	0.02788	0.03552	0.05757	0.16119	0.28006	0.33848
PDL3	0.49643	0.64237	0.93280	1.05512	1.03705	1.01463
PDL4	0.00623	0.00024	-0.00954	0.02321	0.07816	0.10190
PDLS	3.87278	3.55240	2.40768	1.32235	0.92362	0.88666
PSENA	9.18581	9.18581	9.18581	9.18581	9.18581	9.18581
PSEN1	0.15987	0.49218	1.16178	1.35200	1.19229	1.07247
PSEN2	0.00036	0.00220	0.03911	0.25779	0.53792	0.68060
PSEN3	0.09075	0.29474	0.78554	1.07126	1.07042	1.03138
PSEN4	-0.00823	-0.02505	-0.05377	0.00393	0.12426	0.17725
PSENS	2.28539	2.19314	1.69329	1.05496	0.78275	0.77118
PNLA	3.19468	3.19468	3.19468	3.19468	3.19468	3.19468
PNL1	0.29299	0.46650	0.78778	1.00181	1.00512	1.00107
PNL2	-0.00649	-0.01420	-0.00737	0.06551	0.18484	0.25358
PNL3	0.47081	0.55040	0.81790	0.99801	1.00234	1.00053
PNL4	-0.00958	-0.02711	-0.05951	-0.01521	0.05584	0.07938
PNLS	0.29074	0.32403	0.21055	0.08123	0.05877	0.07573
GS1	0.00000	0.00000	0.00000	0.00000	0.00000	0.00000
GS2	0.00000	0.00000	0.00000	0.00000	0.00000	0.00000
GSS	0.00000	0.00000	0.00000	0.00000	0.00000	0.00000
PACC	0.00000	0.00000	0.00000	0.00000	0.00000	0.00000
PVEL	11.34271	11.30964	11.46019	9.68026	7.91454	9.02811
PDIS	42.11644	44.01939	31.98684	23.17263	21.10955	20.85443

a) Pitch Axis Measures vs. Break Frequencies (rad/sec)

	.0675	.125	.25	.5	1.0	2.0
PDLA	0.01721	0.01721	0.01721	0.01721	0.01721	0.01721
PDL1	0.54471	0.38330	0.30462	0.22573	0.10453	0.03229
PDL2	8.43034	5.12656	1.90130	0.31086	0.02417	0.00101
PDL3	0.57889	0.38000	0.27126	0.17188	0.07261	0.02288
PDL4	0.04523	0.01827	-0.16291	-0.13268	-0.05109	-0.01326
PDLS	0.03755	0.02458	0.01286	0.00627	0.00467	0.00436
PSENA	0.00525	0.00525	0.00525	0.00525	0.00525	0.00525
PSEN1	0.74129	0.67474	0.66411	0.53426	0.24390	0.07021
PSEN2	12.73880	9.30336	4.02552	0.72150	0.05737	0.00205
PSEN3	0.72690	0.61555	0.53706	0.36979	0.14863	0.04002
PSEN4	0.55729	0.26261	-0.18229	-0.24995	-0.10829	-0.02863
PSENS	0.01565	0.01211	0.00654	0.00265	0.00160	0.00138
PNLA	0.00050	0.00050	0.00050	0.00050	0.00050	0.00050
PNL1	0.99281	0.98927	0.98764	0.94572	0.76359	0.53764
PNL2	27.16108	16.63425	4.88605	0.36250	-0.13047	-0.06035
PNL3	0.99594	0.99357	0.99176	0.96264	0.84420	0.71094
PNL4	1.21951	0.50589	-0.15706	-0.23020	-0.13887	-0.04731
PNLS	0.31E-02	0.20E-02	0.65E-03	0.11E-03	0.28E-04	0.19E-04
GS1	0.00000	0.00000	0.00000	0.00000	0.00000	0.00000
GS2	0.00000	0.00000	0.00000	0.00000	0.00000	0.00000
GSS	0.00000	0.00000	0.00000	0.00000	0.00000	0.00000
PACC	0.00000	0.00000	0.00000	0.00000	0.00000	0.00000
PVEL	0.00000	0.00000	0.00000	0.00000	0.00000	0.00000
PDIS	0.00000	0.00000	0.00000	0.00000	0.00000	0.00000

b) Surge Axis Measures vs. Break Frequencies (rad/sec)

TABLE C-6

PITCH AND SURGE MEASURES VERSUS SCENARIO
K_{2P} = 1.0

	.0675	.125	.25	.5	1.0	2.0
PDLA	25.60710	25.60710	25.60710	25.60710	25.60710	25.60710
PDL1	0.58238	0.80460	1.16504	1.20203	1.09463	1.03307
PDL2	0.05846	0.07709	0.13621	0.40432	0.74707	0.93538
PDL3	0.49643	0.64237	0.93280	1.05512	1.03705	1.01463
PDL4	0.01246	0.00048	-0.01909	0.04643	0.15632	0.20379
PDLS	3.98881	3.81546	3.03328	2.58161	2.91259	3.40321
PSENA	9.18581	9.18581	9.18581	9.18581	9.18581	9.18581
PSEN1	0.15987	0.49218	1.16178	1.35200	1.19229	1.07247
PSEN2	0.00145	0.00882	0.11164	0.69043	1.51697	1.98977
PSEN3	0.09075	0.29474	0.78554	1.07126	1.07042	1.03138
PSEN4	-0.01646	-0.05010	-0.10754	0.00787	0.24852	0.35450
PSENS	2.32570	2.32341	2.10681	2.03044	2.46040	2.96353
PNLA	3.19468	3.19468	3.19468	3.19468	3.19468	3.19468
PNL1	0.29299	0.46650	0.78778	1.00181	1.00512	1.00107
PNL2	-0.01259	-0.02613	0.01055	0.37498	1.21500	1.89129
PNL3	0.47081	0.55040	0.81790	0.99801	1.00234	1.00053
PNL4	-0.01937	-0.05560	-0.13136	-0.05927	0.16582	0.31532
PNLS	0.30150	0.36002	0.33963	0.39879	0.70585	1.00685
GS1	0.00000	0.00000	0.00000	0.00000	0.00000	0.00000
GS2	0.00000	0.00000	0.00000	0.00000	0.00000	0.00000
GSS	0.00000	0.00000	0.00000	0.00000	0.00000	0.00000
PACC	0.00000	0.00000	0.00000	0.00000	0.00000	0.00000
PVEL	11.51418	11.75864	12.93877	14.15045	14.27637	17.88819
PDIS	45.58288	49.22908	40.69039	36.51659	39.03415	40.81094

a) Pitch Axis Measures vs. Break Frequencies (rad/sec)

	.0675	.125	.25	.5	1.0	2.0
PDLA	0.01721	0.01721	0.01721	0.01721	0.01721	0.01721
PDL1	0.54471	0.38330	0.30462	0.22573	0.10453	0.03229
PDL2	0.24E+01	0.14E+01	0.53E+00	0.89E-01	0.56E-02	-0.19E-04
PDL3	0.57889	0.38000	0.27126	0.17188	0.07261	0.02288
PDL4	0.02261	0.00913	-0.08146	-0.06634	-0.02554	-0.00663
PDLS	0.04662	0.03532	0.02504	0.01899	0.01748	0.01721
PSENA	0.00525	0.00525	0.00525	0.00525	0.00525	0.00525
PSEN1	0.74129	0.67474	0.66411	0.53426	0.24390	0.07021
PSEN2	3.65484	2.64757	1.14563	0.21140	0.01377	-0.00011
PSEN3	0.72690	0.61555	0.53706	0.36979	0.14863	0.04002
PSEN4	0.27864	0.13130	-0.09114	-0.12497	-0.05415	-0.01431
PSENS	0.01779	0.01486	0.01008	0.00660	0.00562	0.00535
PNLA	0.00050	0.00050	0.00050	0.00050	0.00050	0.00050
PNL1	0.98246	0.98219	0.99727	0.99779	0.71798	0.25056
PNL2	9.14106	6.77975	3.08539	0.87414	0.09893	-0.00116
PNL3	0.98405	0.97474	0.96753	0.85732	0.47550	0.13738
PNL4	0.59223	0.17472	-0.13692	-0.24333	-0.15984	-0.05162
PNLS	0.00400	0.00325	0.00172	0.00083	0.00060	0.00054
GS1	0.00000	0.00000	0.00000	0.00000	0.00000	0.00000
GS2	0.00000	0.00000	0.00000	0.00000	0.00000	0.00000
GSS	0.00000	0.00000	0.00000	0.00000	0.00000	0.00000
PACC	0.00000	0.00000	0.00000	0.00000	0.00000	0.00000
PVEL	0.00000	0.00000	0.00000	0.00000	0.00000	0.00000
PDIS	0.00000	0.00000	0.00000	0.00000	0.00000	0.00000

b) Surge Axis Measures vs. Break Frequencies (rad/sec)

AD-A071 394 SYSTEMS TECHNOLOGY INC HAWTHORNE CALIF F/G 14/2
MANNED ENGINEERING FLIGHT SIMULATION VALIDATION. PART I. SIMULA--ETC(U)
FEB 79 L G HOFMANN, S A RIEDEL F33615-77-C-2065
UNCLASSIFIED STI-TR-1110-1 AFFDL-TR-78-192-PT-1 NL

3 OF 3
AD A071394

END
DATE FILMED
8-79
DDC

TABLE C-7

ROLL AND SWAY MEASURES VERSUS BREAK FREQUENCY
K_{2R} = 0.0, C_{2Y} = .0025 and K_p = 0.5

	.0675	.125	.25	.5	1.0	2.0
PDLA	0.16E+03	0.16E+03	0.16E+03	0.16E+03	0.16E+03	0.16E+03
PDL1	0.06404	0.20797	0.55343	0.94366	1.21167	1.26063
PDL2	0.00000	0.00000	0.00000	0.00000	0.00000	0.00000
PDL3	0.03543	0.11937	0.35261	0.66463	0.93627	1.08140
PDL4	0.00000	0.00000	0.00000	0.00000	0.00000	0.00000
PDLS	40.89412	39.90810	34.92462	25.29759	13.96307	4.02845
PSENA	0.14E+03	0.14E+03	0.14E+03	0.14E+03	0.14E+03	0.14E+03
PSEN1	0.04375	0.14694	0.44244	0.88056	1.22006	1.29518
PSEN2	0.00000	0.00000	0.00000	0.00000	0.00000	0.00000
PSEN3	0.02246	0.08052	0.27222	0.59837	0.91663	1.09239
PSEN4	0.00000	0.00000	0.00000	0.00000	0.00000	0.00000
PSENS	34.08286	33.64171	30.64212	23.33425	13.19895	3.76732
PNLA	0.11E+03	0.11E+03	0.11E+03	0.11E+03	0.11E+03	0.11E+03
PNL1	0.04425	0.14389	0.43573	0.83028	1.07373	1.13259
PNL2	0.00000	0.00000	0.00000	0.00000	0.00000	0.00000
PNL3	0.13203	0.19718	0.37823	0.66028	0.90999	1.04815
PNL4	0.00000	0.00000	0.00000	0.00000	0.00000	0.00000
PNLS	21.89133	21.03117	19.03984	14.30231	7.12027	1.01812
GS1	0.00000	0.00000	0.00000	0.00000	0.00000	0.00000
GS2	0.00000	0.00000	0.00000	0.00000	0.00000	0.00000
GSS	0.00000	0.00000	0.00000	0.00000	0.00000	0.00000
PACC	0.00000	0.00000	0.00000	0.00000	0.00000	0.00000
PVEL	55.80147	56.66270	48.01708	42.05910	32.62257	15.77460
PDIS	85.77427	87.79826	83.26992	52.10756	22.10156	10.66587

a) Roll Axis Measures vs. Break Frequencies (rad/sec)

	.0675	.125	.25	.5	1.0	2.0
PDLA	0.00085	0.00085	0.00085	0.00085	0.00085	0.00085
PDL1	0.00000	0.00000	0.00000	0.00000	0.00000	0.00000
PDL2	12.53404	8.28724	2.93902	0.46169	0.04881	0.00412
PDL3	0.00000	0.00000	0.00000	0.00000	0.00000	0.00000
PDL4	-0.96844	-0.73905	-0.28230	-0.06037	-0.00681	0.00612
PDLS	0.11E-01	0.71E-02	0.25E-02	0.39E-03	0.42E-04	0.35E-05
PSENA	0.00044	0.00044	0.00044	0.00044	0.00044	0.00044
PSEN1	0.00000	0.00000	0.00000	0.00000	0.00000	0.00000
PSEN2	11.64152	8.78923	3.49040	0.60979	0.06606	0.00532
PSEN3	0.00000	0.00000	0.00000	0.00000	0.00000	0.00000
PSEN4	-1.21305	-0.98930	-0.44138	-0.10207	0.00317	0.01496
PSENS	0.51E-02	0.38E-02	0.15E-02	0.27E-03	0.29E-04	0.23E-05
PNLA	0.28E-05	0.28E-05	0.28E-05	0.28E-05	0.28E-05	0.28E-05
PNL1	0.00000	0.00000	0.00000	0.00000	0.00000	0.00000
PNL2	0.38E+02	0.33E+02	0.25E+01	0.53E-01	0.11E-03	0.94E-07
PNL3	0.00000	0.00000	0.00000	0.00000	0.00000	0.00000
PNL4	-0.21E+01	-0.21E+01	-0.14E+00	-0.30E-02	0.17E-03	0.31E-04
PNLS	0.11E-03	0.91E-04	0.69E-05	0.15E-06	0.32E-09	0.26E-12
GS1	0.00000	0.00000	0.00000	0.00000	0.00000	0.00000
GS2	0.00000	0.00000	0.00000	0.00000	0.00000	0.00000
GSS	0.00000	0.00000	0.00000	0.00000	0.00000	0.00000
PACC	53.82566	47.30611	48.32876	27.41887	11.68266	6.28094
PVEL	0.17E+03	0.18E+03	0.97E+02	0.55E+02	0.22E+02	0.72E+01
PDIS	0.18E+04	0.92E+03	0.39E+03	0.15E+03	0.43E+02	0.11E+02

b) Sway Axis Measures vs. Break Frequencies (rad/sec)

TABLE C-8

ROLL AND SWAY MEASURES VERSUS SCENARIO
K_{2R} = 0.5, C_{2Y} = .0025, and K_p = 0.5

	.0675	.125	.25	.5	1.0	2.0
PDLA	0.16E+03	0.16E+03	0.16E+03	0.16E+03	0.16E+03	0.16E+03
PDL1	0.06404	0.20797	0.55343	0.94366	1.21167	1.26063
PDL2	0.00000	0.00000	0.00000	0.00000	0.00000	0.00000
PDL3	0.03543	0.11937	0.35261	0.66463	0.93627	1.08140
PDL4	0.00000	0.00000	0.00000	0.00000	0.00000	0.00000
PDLS	40.89412	39.90810	34.92462	25.29759	13.96307	4.02845
PSENA	0.14E+03	0.14E+03	0.14E+03	0.14E+03	0.14E+03	0.14E+03
PSEN1	0.04375	0.14694	0.44244	0.88056	1.22006	1.29518
PSEN2	0.00000	0.00000	0.00000	0.00000	0.00000	0.00000
PSEN3	0.02246	0.08052	0.27222	0.59837	0.91663	1.09239
PSEN4	0.00000	0.00000	0.00000	0.00000	0.00000	0.00000
PSENS	34.08286	33.64171	30.64212	23.33425	13.19895	3.76732
PNLA	0.11E+03	0.11E+03	0.11E+03	0.11E+03	0.11E+03	0.11E+03
PNL1	0.04425	0.14389	0.43573	0.83028	1.07373	1.13259
PNL2	0.00000	0.00000	0.00000	0.00000	0.00000	0.00000
PNL3	0.13203	0.19718	0.37823	0.66028	0.90999	1.04815
PNL4	0.00000	0.00000	0.00000	0.00000	0.00000	0.00000
PNLS	21.89133	21.03117	19.05984	14.30231	7.12027	1.01812
GS1	0.00000	0.00000	0.00000	0.00000	0.00000	0.00000
GS2	0.00000	0.00000	0.00000	0.00000	0.00000	0.00000
GSS	0.00000	0.00000	0.00000	0.00000	0.00000	0.00000
PACC	0.00000	0.00000	0.00000	0.00000	0.00000	0.00000
PVEL	55.80147	56.66270	48.01708	42.05910	32.62257	15.77460
PDIS	85.77427	87.79826	83.26992	52.10756	22.10156	10.66587

a) Roll Axis Measures vs. Break Frequencies (rad/sec)

	.0675	.125	.25	.5	1.0	2.0
PDLA	0.00085	0.00085	0.00085	0.00085	0.00085	0.00085
PDL1	0.00000	0.00000	0.00000	0.00000	0.00000	0.00000
PDL2	78.33399	62.59290	24.50791	4.07210	0.43979	0.03723
PDL3	0.00000	0.00000	0.00000	0.00000	0.00000	0.00000
PDL4	-2.24497	-1.50476	-0.37052	-0.03195	0.01814	0.02822
PDLS	0.67E-01	0.53E-01	0.21E-01	0.35E-02	0.38E-03	0.32E-04
PSENA	0.00044	0.00044	0.00044	0.00044	0.00044	0.00044
PSEN1	0.00000	0.00000	0.00000	0.00000	0.00000	0.00000
PSEN2	83.83268	69.90791	29.67314	5.47468	0.60242	0.04851
PSEN3	0.00000	0.00000	0.00000	0.00000	0.00000	0.00000
PSEN4	-3.01640	-2.19215	-0.73313	-0.09376	0.06814	0.05917
PSENS	0.37E-01	0.31E-01	0.13E-01	0.24E-02	0.26E-03	0.21E-04
PNLA	0.28E-05	0.28E-05	0.28E-05	0.28E-05	0.28E-05	0.28E-05
PNL1	0.00000	0.00000	0.00000	0.00000	0.00000	0.00000
PNL2	0.47E+04	0.36E+04	0.90E+03	0.38E+02	0.69E-01	0.55E-04
PNL3	0.00000	0.00000	0.00000	0.00000	0.00000	0.00000
PNL4	-19.74601	-11.75227	-0.06778	0.04731	0.01714	0.00106
PNLS	0.13E-01	0.10E-01	0.25E-02	0.11E-03	0.19E-06	0.15E-09
GS1	0.00000	0.00000	0.00000	0.00000	0.00000	0.00000
GS2	0.00000	0.00000	0.00000	0.00000	0.00000	0.00000
GSS	0.00000	0.00000	0.00000	0.00000	0.00000	0.00000
PACC	52.76090	56.02879	43.55520	21.44993	12.65569	6.79812
PVEL	0.16E+03	0.13E+03	0.11E+03	0.60E+02	0.21E+02	0.68E+01
PDIS	0.73E+03	0.68E+03	0.36E+03	0.13E+03	0.40E+02	0.11E+02

b) Sway Axis Measures vs. Break Frequencies (rad/sec)

TABLE C-9

ROLL AND SWAY MEASURES VERSUS SCENARIO
K_{2R} = 1.0, C_{2Y} = .0025, and K_p = 0.5

	.0675	.125	.25	.5	1.0	2.0
PDLA	0.16E+03	0.16E+03	0.16E+03	0.16E+03	0.16E+03	0.16E+03
PDL1	0.06404	0.20797	0.55343	0.94366	1.21167	1.26063
PDL2	0.00000	0.00000	0.00000	0.00000	0.00000	0.00000
PDL3	0.03543	0.11937	0.35261	0.66463	0.93627	1.08140
PDL4	0.00000	0.00000	0.00000	0.00000	0.00000	0.00000
PDLS	40.89412	39.90810	34.92462	25.29759	13.96307	4.02845
PSENA	0.14E+03	0.14E+03	0.14E+03	0.14E+03	0.14E+03	0.14E+03
PSEN1	0.04375	0.14694	0.44244	0.88056	1.22006	1.29518
PSEN2	0.00000	0.00000	0.00000	0.00000	0.00000	0.00000
PSEN3	0.02246	0.08052	0.27222	0.59837	0.91663	1.09239
PSEN4	0.00000	0.00000	0.00000	0.00000	0.00000	0.00000
PSENS	34.08286	33.64171	30.64212	23.33425	13.19895	3.76732
PNLA	0.11E+03	0.11E+03	0.11E+03	0.11E+03	0.11E+03	0.11E+03
PNL1	0.04425	0.14389	0.43573	0.83028	1.07373	1.13259
PNL2	0.00000	0.00000	0.00000	0.00000	0.00000	0.00000
PNL3	0.13203	0.19718	0.37823	0.66028	0.90999	1.04815
PNL4	0.00000	0.00000	0.00000	0.00000	0.00000	0.00000
PNLS	21.89133	21.03117	19.05984	14.30231	7.12027	1.01812
GS1	0.00000	0.00000	0.00000	0.00000	0.00000	0.00000
GS2	0.00000	0.00000	0.00000	0.00000	0.00000	0.00000
GSS	0.00000	0.00000	0.00000	0.00000	0.00000	0.00000
PACC	0.00000	0.00000	0.00000	0.00000	0.00000	0.00000
PVEL	55.80147	56.66270	48.01708	42.05910	32.62257	15.77460
PDIS	85.77427	87.79826	83.26992	52.10756	22.10156	10.66587

a) Roll Axis Measures vs. Break Frequencies (rad/sec)

	.0675	.125	.25	.5	1.0	2.0
PDLA	0.00085	0.00085	0.00085	0.00085	0.00085	0.00085
PDL1	0.00000	0.00000	0.00000	0.00000	0.00000	0.00000
PDL2	0.13E+03	0.11E+03	0.62E+02	0.19E+02	0.30E+01	0.30E+00
PDL3	0.00000	0.00000	0.00000	0.00000	0.00000	0.00000
PDL4	-2.29020	-1.18560	-0.09902	0.14211	0.09097	0.10069
PDLS	0.10960	0.09541	0.05300	0.01653	0.00256	0.00025
PSENA	0.00044	0.00044	0.00044	0.00044	0.00044	0.00044
PSEN1	0.00000	0.00000	0.00000	0.00000	0.00000	0.00000
PSEN2	0.16E+03	0.14E+03	0.84E+02	0.28E+02	0.42E+01	0.39E+00
PSEN3	0.00000	0.00000	0.00000	0.00000	0.00000	0.00000
PSEN4	-3.45136	-2.04522	-0.36981	0.36459	0.34690	0.20934
PSENS	0.06809	0.06083	0.03683	0.01232	0.00185	0.00017
PNLA	0.28E-05	0.28E-05	0.28E-05	0.28E-05	0.28E-05	0.28E-05
PNL1	0.00000	0.00000	0.00000	0.00000	0.00000	0.00000
PNL2	0.14E+05	0.12E+05	0.59E+04	0.10E+04	0.88E+01	0.10E-01
PNL3	0.00000	0.00000	0.00000	0.00000	0.00000	0.00000
PNL4	-12.83748	-1.73929	5.01623	6.57397	0.26171	0.01518
PNLS	0.38E-01	0.32E-01	0.16E-01	0.29E-02	0.25E-04	0.28E-07
GS1	0.00000	0.00000	0.00000	0.00000	0.00000	0.00000
GS2	0.00000	0.00000	0.00000	0.00000	0.00000	0.00000
GSS	0.00000	0.00000	0.00000	0.00000	0.00000	0.00000
PACC	26.57902	23.12729	21.70629	19.97275	12.70632	6.24403
PVEL	56.81534	60.44103	49.64578	25.94772	12.70869	4.65805
PDIS	0.16E+03	0.14E+03	0.12E+03	0.70E+02	0.24E+02	0.69E+01

b) Sway Axis Measures vs. Break Frequencies (rad/sec)

TABLE C-10

ROLL AND SWAY MEASURES VERSUS SCENARIO
K_{2R} = 0.5, C_{2Y} = .0225, and K_p = 0.5

	.0675	.125	.25	.5	1.0	2.0
PDLA	0.16E+03	0.16E+03	0.16E+03	0.16E+03	0.16E+03	0.16E+03
PDL1	0.06404	0.20797	0.55343	0.94366	1.21167	1.26063
PDL2	0.00038	0.00207	0.00860	0.01730	0.01024	-0.04193
PDL3	0.03543	0.11937	0.35261	0.66463	0.93627	1.08140
PDL4	0.00064	0.00250	0.00942	0.02325	0.03523	0.00700
PDLS	40.85743	39.78760	34.50283	24.09550	11.48383	1.72578
PSENA	0.14E+03	0.14E+03	0.14E+03	0.14E+03	0.14E+03	0.14E+03
PSEN1	0.04375	0.14694	0.44244	0.88056	1.22006	1.29518
PSEN2	0.00028	0.00158	0.00749	0.01753	0.01141	-0.04732
PSEN3	0.02246	0.08052	0.27222	0.59837	0.91663	1.09239
PSEN4	0.00058	0.00229	0.00919	0.02502	0.04007	0.00791
PSENS	34.05270	33.53963	30.27024	22.22493	10.85342	1.61305
PNLA	0.11E+03	0.11E+03	0.11E+03	0.11E+03	0.11E+03	0.11E+03
PNL1	0.04425	0.14389	0.43573	0.83028	1.07373	1.13259
PNL2	0.00036	0.00193	0.00847	0.01608	0.00942	-0.04423
PNL3	0.13203	0.19718	0.37823	0.66028	0.90999	1.04815
PNL4	0.00066	0.00247	0.00928	0.02330	0.03542	-0.00741
PNLS	21.86415	20.94668	18.77669	13.44626	5.39690	0.19314
GS1	0.00000	0.00000	0.00000	0.00000	0.00000	0.00000
GS2	0.00000	0.00000	0.00000	0.00000	0.00000	0.00000
GSS	0.00000	0.00000	0.00000	0.00000	0.00000	0.00000
PACC	0.00000	0.00000	0.00000	0.00000	0.00000	0.00000
PVEL	55.78326	56.56514	47.50300	41.55858	29.52164	10.22700
PDIS	85.76524	87.63050	83.00689	49.94592	18.74533	9.31515

a) Roll Axis Measures vs. Break Frequencies (rad/sec)

	.0675	.125	.25	.5	1.0	2.0
PDLA	0.00085	0.00085	0.00085	0.00085	0.00085	0.00085
PDL1	0.13388	0.15424	0.15556	0.09845	0.04766	0.01888
PDL2	0.31E+03	0.25E+03	0.10E+03	0.17E+02	0.20E+01	0.19E+00
PDL3	0.07317	0.08893	0.12110	0.13250	0.12665	0.10854
PDL4	-4.48994	-3.00953	-0.74104	-0.06390	0.03628	0.05644
PDLS	0.06930	0.05573	0.02222	0.00394	0.00058	0.00019
PSENA	0.00044	0.00044	0.00044	0.00044	0.00044	0.00044
PSEN1	0.16723	0.19347	0.20283	0.13402	0.06113	0.02154
PSEN2	0.34E+03	0.28E+03	0.12E+03	0.23E+02	0.28E+01	0.25E+00
PSEN3	0.09116	0.11134	0.15772	0.18366	0.16938	0.12879
PSEN4	-6.03280	-4.38430	-1.46627	-0.18753	0.13628	0.11834
PSENS	0.03824	0.03208	0.01388	0.00270	0.00035	0.00009
PNLA	0.28E-05	0.28E-05	0.28E-05	0.28E-05	0.28E-05	0.28E-05
PNL1	0.71289	0.73721	0.77065	0.76175	0.71571	0.67643
PNL2	0.20E+05	0.16E+05	0.42E+04	0.24E+03	0.13E+01	0.12E+00
PNL3	0.84135	0.85539	0.87444	0.87092	0.84537	0.82225
PNL4	-45.74344	-29.58179	-2.27563	-0.23843	0.06402	0.06728
PNLS	0.14E-01	0.11E-01	0.29E-02	0.17E-03	0.81E-06	0.13E-07
GS1	0.00000	0.00000	0.00000	0.00000	0.00000	0.00000
GS2	0.00000	0.00000	0.00000	0.00000	0.00000	0.00000
GSS	0.00000	0.00000	0.00000	0.00000	0.00000	0.00000
PACC	50.02423	53.44072	42.96724	21.40831	12.77244	8.12718
PVEL	0.16E+03	0.13E+03	0.11E+03	0.61E+02	0.23E+02	0.80E+01
PDIS	0.73E+03	0.69E+03	0.36E+03	0.13E+03	0.44E+02	0.13E+02

b) Sway Axis Measures vs. Break Frequencies (rad/sec)

TABLE C-11

ROLL AND SWAY MEASURES VERSUS SCENARIO
$K_{2R} = 0.0$, $C_{2Y} = 0.5$, and $K_p = 0.5$

	.0675	.125	.25	.5	1.0	2.0
PDLA	0.16E+03	0.16E+03	0.16E+03	0.16E+03	0.16E+03	0.16E+03
PDL1	0.06404	0.20797	0.55343	0.94366	1.21167	1.26063
PDL2	0.00077	0.00416	0.01742	0.03621	0.03016	-0.04607
PDL3	0.03543	0.11937	0.35261	0.66463	0.93627	1.08140
PDL4	0.00127	0.00499	0.01885	0.04650	0.07045	0.01399
PDLS	40.82082	39.66796	34.09004	22.95970	9.40313	0.97914
PSENA	0.14E+03	0.14E+03	0.14E+03	0.14E+03	0.14E+03	0.14E+03
PSEN1	0.04375	0.14694	0.44244	0.88056	1.22006	1.29518
PSEN2	0.00057	0.00317	0.01518	0.03677	0.03372	-0.05190
PSEN3	0.02246	0.08052	0.27222	0.59837	0.91663	1.09239
PSEN4	0.00117	0.00457	0.01839	0.05004	0.08014	0.01581
PSENS	34.02260	33.43813	29.90532	21.17370	8.87997	0.91714
PNLA	0.11E+03	0.11E+03	0.11E+03	0.11E+03	0.11E+03	0.11E+03
PNL1	0.04425	0.14389	0.43573	0.83028	1.07373	1.13259
PNL2	0.00072	0.00389	0.01712	0.03307	0.02789	-0.07058
PNL3	0.13203	0.19718	0.37823	0.66028	0.90999	1.04815
PNL4	0.00133	0.00495	0.01855	0.04618	0.06958	-0.01901
PNLS	21.83703	20.86272	18.49943	12.63848	3.99825	0.10469
GS1	0.00000	0.00000	0.00000	0.00000	0.00000	0.00000
GS2	0.00000	0.00000	0.00000	0.00000	0.00000	0.00000
GSS	0.00000	0.00000	0.00000	0.00000	0.00000	0.00000
PACC	0.00000	0.00000	0.00000	0.00000	0.00000	0.00000
PVEL	55.76504	56.46758	46.98891	41.05805	26.72289	8.58769
PDIS	85.75620	87.46274	82.74385	47.78429	18.30605	9.33734

a) Roll Axis Measures vs. Break Frequencies (rad/sec)

	.0675	.125	.25	.5	1.0	2.0
PDLA	0.00085	0.00085	0.00085	0.00085	0.00085	0.00085
PDL1	0.01630	0.01819	0.01745	0.01078	0.00522	0.00208
PDL2	12.60749	8.51663	3.15231	0.52832	0.06196	0.00641
PDL3	0.00956	0.01481	0.02934	0.03886	0.04014	0.03564
PDL4	-0.96844	-0.73905	-0.28230	-0.06037	-0.00681	0.00612
PDLS	0.01328	0.00939	0.00400	0.00135	0.00085	0.00079
PSENA	0.00044	0.00044	0.00044	0.00044	0.00044	0.00044
PSEN1	0.01942	0.02208	0.02238	0.01456	0.00666	0.00236
PSEN2	11.70503	9.02788	3.73847	0.69734	0.08480	0.00857
PSEN3	0.01091	0.01737	0.03712	0.05339	0.05367	0.04233
PSEN4	-1.21305	-0.98930	-0.44138	-0.10207	0.00317	0.01496
PSENS	0.00662	0.00525	0.00244	0.00079	0.00043	0.00039
PNLA	0.28E-05	0.28E-05	0.28E-05	0.28E-05	0.28E-05	0.28E-05
PNL1	0.01955	0.02490	0.03930	0.04222	0.02530	0.01345
PNL2	0.12E+03	0.11E+03	0.10E+02	0.67E+00	0.10E+00	0.22E-01
PNL3	0.09081	0.11454	0.17182	0.18659	0.14820	0.11185
PNL4	-7.91721	-6.58732	-1.39134	0.11111	0.13706	0.05968
PNLS	0.37E-03	0.35E-03	0.38E-04	0.31E-05	0.16E-05	0.19E-05
GS1	0.00000	0.00000	0.00000	0.00000	0.00000	0.00000
GS2	0.00000	0.00000	0.00000	0.00000	0.00000	0.00000
GSS	0.00000	0.00000	0.00000	0.00000	0.00000	0.00000
PACC	51.23702	45.25141	48.24283	28.31316	14.79704	10.28296
PVEL	0.17E+03	0.18E+03	0.10E+03	0.38E+02	0.25E+02	0.10E+02
PDIS	0.18E+04	0.94E+03	0.40E+03	0.17E+03	0.52E+02	0.16E+02

b) Sway Axis Measures vs. Break Frequencies (rad/sec)

TABLE C-12

ROLL AND SWAY MEASURES VERSUS SCENARIO
K_{2R} = 0.5, C_{2Y} = 0.5, and K_p = 0.5

	.0675	.125	.25	.5	1.0	2.0
PDLA	0.16E+03	0.16E+03	0.16E+03	0.16E+03	0.16E+03	0.16E+03
PDL1	0.06404	0.20797	0.55343	0.94366	1.21167	1.26063
PDL2	0.00077	0.00416	0.01742	0.03621	0.03016	-0.04607
PDL3	0.03543	0.11937	0.35261	0.66463	0.93627	1.08140
PDL4	0.00127	0.00499	0.01885	0.04650	0.07045	0.01399
PDLS	40.82082	39.66796	34.09004	22.95970	9.40313	0.97914
PSENA	0.14E+03	0.14E+03	0.14E+03	0.14E+03	0.14E+03	0.14E+03
PSEN1	0.04375	0.14694	0.44244	0.88056	1.22006	1.29518
PSEN2	0.00057	0.00317	0.01518	0.03677	0.03372	-0.05190
PSEN3	0.02246	0.08052	0.27222	0.59837	0.91663	1.09239
PSEN4	0.00117	0.00457	0.01839	0.05004	0.08014	0.01581
PSENS	34.02260	33.43813	29.90532	21.17370	8.87997	0.91714
PNLA	0.11E+03	0.11E+03	0.11E+03	0.11E+03	0.11E+03	0.11E+03
PNL1	0.04425	0.14389	0.43573	0.83028	1.07373	1.13259
PNL2	0.00072	0.00389	0.01712	0.03307	0.02789	-0.07058
PNL3	0.13203	0.19718	0.37823	0.66028	0.90999	1.04815
PNL4	0.00133	0.00495	0.01855	0.04618	0.06958	-0.01901
PNLS	21.83703	20.86272	18.49943	12.63848	3.99825	0.10469
GS1	0.00000	0.00000	0.00000	0.00000	0.00000	0.00000
GS2	0.00000	0.00000	0.00000	0.00000	0.00000	0.00000
GSS	0.00000	0.00000	0.00000	0.00000	0.00000	0.00000
PACC	0.00000	0.00000	0.00000	0.00000	0.00000	0.00000
PVEL	55.76504	56.46758	46.98891	41.05805	26.72289	8.58769
PDIS	85.75620	87.46274	82.74385	47.78429	18.30605	9.33734

a) Roll Axis Measures vs. Break Frequencies (rad/sec)

	.0675	.125	.25	.5	1.0	2.0
PDLA	0.00085	0.00085	0.00085	0.00085	0.00085	0.00085
PDL1	0.13388	0.15424	0.15556	0.09845	0.04766	0.01888
PDL2	78.87490	64.35049	26.29375	4.66591	0.55924	0.05810
PDL3	0.07317	0.08893	0.12110	0.13250	0.12665	0.10854
PDL4	-2.24497	-1.50476	-0.37052	-0.03195	0.01814	0.02822
PDLS	0.07208	0.05839	0.02388	0.00475	0.00113	0.00069
PSENA	0.00044	0.00044	0.00044	0.00044	0.00044	0.00044
PSEN1	0.16723	0.19347	0.20283	0.13402	0.06113	0.02154
PSEN2	84.27433	71.75887	31.80060	6.27024	0.77469	0.07833
PSEN3	0.09116	0.11134	0.15772	0.18366	0.16938	0.12879
PSEN4	-3.01640	-2.19215	-0.73313	-0.09376	0.06814	0.05917
PSENS	0.03998	0.03377	0.01496	0.00316	0.00060	0.00032
PNLA	0.28E-05	0.28E-05	0.28E-05	0.28E-05	0.28E-05	0.28E-05
PNL1	0.22018	0.27235	0.34915	0.29266	0.17065	0.09692
PNL2	0.54E+04	0.43E+04	0.12E+04	0.92E+02	0.13E+01	0.14E+00
PNL3	0.37808	0.43235	0.50626	0.49243	0.39319	0.30342
PNL4	-25.58068	-17.39147	-2.15347	0.04884	0.26198	0.15039
PNLS	0.15E-01	0.12E-01	0.34E-02	0.26E-03	0.33E-05	0.91E-06
GS1	0.00000	0.00000	0.00000	0.00000	0.00000	0.00000
GS2	0.00000	0.00000	0.00000	0.00000	0.00000	0.00000
GSS	0.00000	0.00000	0.00000	0.00000	0.00000	0.00000
PACC	48.85858	53.79541	43.62885	23.17445	14.18067	10.37257
PVEL	0.16E+03	0.13E+03	0.11E+03	0.62E+02	0.25E+02	0.98E+01
PDIS	0.73E+03	0.69E+03	0.37E+03	0.14E+03	0.48E+02	0.16E+02

b) Sway Axis Measures vs. Break Frequencies (rad/sec)

TABLE C-13

ROLL AND SWAY MEASURES VERSUS SCENARIO
K_{2R} = 1.0, C_{2Y} = 0.5, and K_p = 0.5

	.0675	.125	.25	.5	1.0	2.0
PDLA	0.16E+03	0.16E+03	0.16E+03	0.16E+03	0.16E+03	0.16E+03
PDL1	0.06404	0.20797	0.55343	0.94366	1.21167	1.26063
PDL2	0.00077	0.00416	0.01742	0.03621	0.03016	-0.04607
PDL3	0.03543	0.11937	0.35261	0.66463	0.93627	1.08140
PDL4	0.00127	0.00499	0.01885	0.04650	0.07045	0.01399
PDLS	40.82082	39.66796	34.09004	22.95970	9.40313	0.97914
PSENA	0.14E+03	0.14E+03	0.14E+03	0.14E+03	0.14E+03	0.14E+03
PSEN1	0.04375	0.14694	0.44244	0.88056	1.22006	1.29518
PSEN2	0.00057	0.00317	0.01518	0.03677	0.03372	-0.05190
PSEN3	0.02246	0.08052	0.27222	0.59837	0.91663	1.09239
PSEN4	0.00117	0.00457	0.01839	0.05004	0.08014	0.01581
PSENS	34.02260	33.43813	29.90532	21.17370	8.87997	0.91714
PNLA	0.11E+03	0.11E+03	0.11E+03	0.11E+03	0.11E+03	0.11E+03
PNL1	0.04425	0.14389	0.43573	0.83028	1.07373	1.13259
PNL2	0.00072	0.00389	0.01712	0.03307	0.02789	-0.07058
PNL3	0.13203	0.19718	0.37823	0.66028	0.90999	1.04815
PNL4	0.00133	0.00495	0.01855	0.04618	0.06958	-0.01901
PNLS	21.83703	20.86272	18.49943	12.63848	3.99825	0.10469
GS1	0.00000	0.00000	0.00000	0.00000	0.00000	0.00000
GS2	0.00000	0.00000	0.00000	0.00000	0.00000	0.00000
GSS	0.00000	0.00000	0.00000	0.00000	0.00000	0.00000
PACC	0.00000	0.00000	0.00000	0.00000	0.00000	0.00000
PVEL	55.76504	56.46758	46.98891	41.05805	26.72289	8.58769
PDIS	85.75620	87.46274	82.74385	47.78429	18.30605	9.33734

a) Roll Axis Measures vs. Break Frequencies (rad/sec)

	.0675	.125	.25	.5	1.0	2.0
PDLA	0.00085	0.00085	0.00085	0.00085	0.00085	0.00085
PDL1	0.58151	0.63654	0.72090	0.67231	0.42521	0.18765
PDL2	0.13E+03	0.11E+03	0.65E+02	0.21E+02	0.36E+01	0.43E+00
PDL3	0.37263	0.39351	0.41913	0.41995	0.38547	0.32607
PDL4	-2.29020	-1.18560	-0.09902	0.14211	0.09097	0.10069
PDLS	0.11265	0.09868	0.05612	0.01856	0.00345	0.00065
PSENA	0.00044	0.00044	0.00044	0.00044	0.00044	0.00044
PSEN1	0.77512	0.85079	0.98157	0.92471	0.53516	0.20753
PSEN2	0.15E+03	0.14E+03	0.87E+02	0.31E+02	0.51E+01	0.59E+00
PSEN3	0.50260	0.53212	0.57781	0.58743	0.49624	0.36670
PSEN4	-3.45136	-2.04522	-0.36981	0.36459	0.34690	0.20934
PSENS	0.07012	0.06305	0.03898	0.01355	0.00218	0.00028
PNLA	0.28E-05	0.28E-05	0.28E-05	0.28E-05	0.28E-05	0.28E-05
PNL1	1.08436	1.14903	1.04723	0.78052	0.54066	0.40748
PNL2	0.14E+05	0.12E+05	0.64E+04	0.12E+04	0.19E+02	0.26E+00
PNL3	0.84317	0.85745	0.86095	0.84389	0.71683	0.62937
PNL4	-14.90417	-3.91391	3.52785	4.37840	0.14775	0.16286
PNLS	0.39E-01	0.34E-01	0.18E-01	0.34E-02	0.54E-04	0.22E-06
GS1	0.00000	0.00000	0.00000	0.00000	0.00000	0.00000
GS2	0.00000	0.00000	0.00000	0.00000	0.00000	0.00000
GSS	0.00000	0.00000	0.00000	0.00000	0.00000	0.00000
PACC	24.49761	21.74777	21.37760	19.47116	15.87156	9.51661
PVEL	54.30840	58.02134	48.68298	27.54009	14.45196	6.83523
PDIS	0.16E+03	0.14E+03	0.12E+03	0.75E+02	0.28E+02	0.10E+02

b) Sway Axis Measures vs. Break Frequencies (rad/sec)

TABLE C-14

YAW AND HEAVE AXIS MEASURES VERSUS BREAK FREQUENCY

	.0675	.125	.25	.5	1.0	2.0
PDLA	5.29930	5.29930	5.29930	5.29930	5.29930	5.29930
PDL1	0.65466	0.93944	1.18190	1.14679	1.07502	1.03102
PDL2	0.00000	0.00000	0.00000	0.00000	0.00000	0.00000
PDL3	0.54160	0.74246	0.98077	1.03396	1.02612	1.01335
PDL4	0.00000	0.00000	0.00000	0.00000	0.00000	0.00000
PDLS	0.75709	0.60215	0.29193	0.10448	0.03017	0.00572
PSENA	1.63021	1.63021	1.63021	1.63021	1.63021	1.63021
PSEN1	0.21707	0.59527	1.15282	1.26259	1.17356	1.08087
PSEN2	0.00000	0.00000	0.00000	0.00000	0.00000	0.00000
PSEN3	0.13114	0.38600	0.82608	1.02317	1.05268	1.03382
PSEN4	0.00000	0.00000	0.00000	0.00000	0.00000	0.00000
PSENS	0.38913	0.33553	0.20405	0.08813	0.02779	0.00539
PNLA	0.07667	0.07667	0.07667	0.07667	0.07667	0.07667
PNL1	0.50633	0.66803	0.88223	0.97459	1.00178	1.00108
PNL2	0.00000	0.00000	0.00000	0.00000	0.00000	0.00000
PNL3	0.70278	0.79854	0.93250	0.98675	1.00086	1.00054
PNL4	0.00000	0.00000	0.00000	0.00000	0.00000	0.00000
PNLS	0.19E-02	0.14E-02	0.33E-03	0.21E-04	0.13E-05	0.26E-07
GS1	0.00000	0.00000	0.00000	0.00000	0.00000	0.00000
GS2	0.00000	0.00000	0.00000	0.00000	0.00000	0.00000
GSS	0.00000	0.00000	0.00000	0.00000	0.00000	0.00000
PACC	0.00000	0.00000	0.00000	0.00000	0.00000	0.00000
PVEL	3.87879	4.36360	3.66914	2.31082	1.44214	0.72981
PDIS	26.99819	14.55148	7.73515	3.92446	1.84893	0.69747

a) Yaw Axis Measures vs. Break Frequencies (rad/sec)

	.0675	.125	.25	.5	1.0	2.0
PDLA	1.10385	1.10385	1.10385	1.10385	1.10385	1.10385
PDL1	0.83764	1.21807	1.55947	1.18993	1.06558	1.01853
PDL2	0.00000	0.00000	0.00000	0.00000	0.00000	0.00000
PDL3	0.63075	0.85105	1.12942	1.05578	1.02024	1.00642
PDL4	0.00000	0.00000	0.00000	0.00000	0.00000	0.00000
PDLS	0.01431	0.01281	0.00747	0.00195	0.00062	0.00014
PSENA	0.48922	0.48922	0.48922	0.48922	0.48922	0.48922
PSEN1	0.65404	1.19463	1.83484	1.32172	1.10502	1.02095
PSEN2	0.00000	0.00000	0.00000	0.00000	0.00000	0.00000
PSEN3	0.42263	0.72214	1.18275	1.10095	1.03699	1.00848
PSEN4	0.00000	0.00000	0.00000	0.00000	0.00000	0.00000
PSENS	0.89E-02	0.83E-02	0.52E-02	0.13E-02	0.34E-03	0.44E-04
PNLA	1.15541	1.15541	1.15541	1.15541	1.15541	1.15541
PNL1	0.02100	0.04448	0.08403	0.07643	0.07223	0.05933
PNL2	0.00000	0.00000	0.00000	0.00000	0.00000	0.00000
PNL3	0.16689	0.11625	0.08720	0.13090	0.13625	0.14512
PNL4	0.00000	0.00000	0.00000	0.00000	0.00000	0.00000
PNLS	0.02217	0.02412	0.02404	0.02097	0.02022	0.01978
GS1	1.01189	1.11171	1.15905	1.05259	1.03069	1.00686
GS2	0.98101	1.03165	1.06070	1.01700	1.01165	1.00278
GSS	0.13E-02	0.13E-02	0.98E-03	0.48E-03	0.19E-03	0.34E-04
PACC	0.96E+02	0.10E+03	0.87E+02	0.56E+02	0.32E+02	0.26E+02
PVEL	0.28E+03	0.23E+03	0.19E+03	0.58E+02	0.30E+02	0.10E+02
PDIS	0.20E+04	0.14E+04	0.61E+03	0.16E+03	0.40E+02	0.94E+01

b) Heave Axis Measures vs. Break Frequencies (rad/sec)

TABLE C-15. . REVISED MEASURES, PITCH-SURGE AXES VERSUS BREAK FREQUENCY AND K_{2P}

BF	.0675	.125	.25	.5	1.0	2.0	
PDL1	0.58238	0.80460	1.16504	1.20203	1.09463	1.03307	
PDL2	0.00000	0.00000	0.00000	0.00000	0.00000	0.00000	
PDL3	0.49643	0.64237	0.93280	1.05512	1.03705	1.01463	J_Q measures,
PDL4	0.00000	0.00000	0.00000	0.00000	0.00000	0.00000	$K_{2P} = 0.0$
PVEL	11.17123	10.86064	9.98160	6.59412	4.31896	2.18626	
PDIS	40.78298	38.81647	23.41467	11.02253	4.25406	1.94151	
MDL1	0.00000	0.00000	0.00000	0.00000	0.00000	0.00000	
MDL2	0.00000	0.00000	0.00000	0.00000	0.00000	0.00000	
MDL3	0.00000	0.00000	0.00000	0.00000	0.00000	0.00000	J_X measures,
MDL4	0.00000	0.00000	0.00000	0.00000	0.00000	0.00000	$K_{2P} = 0.0$
PACC	0.00000	0.00000	0.00000	0.00000	0.00000	0.00000	
PVEL	0.00000	0.00000	0.00000	0.00000	0.00000	0.00000	
PDIS	0.00000	0.00000	0.00000	0.00000	0.00000	0.00000	
PDL1	0.00000	0.00000	0.00000	0.00000	0.00000	0.00000	J_{XT} measures,
PDL3	0.00000	0.00000	0.00000	0.00000	0.00000	0.00000	$K_{2P} = 0.0$
PDL1	0.58238	0.80460	1.16504	1.20203	1.09463	1.03307	
PDL2	0.02788	0.03552	0.05757	0.16119	0.28006	0.33848	
PDL3	0.49643	0.64237	0.93280	1.05512	1.03705	1.01463	J_Q measures,
PDL4	0.00623	0.00024	-0.00954	0.02321	0.07816	0.10190	$K_{2P} = 0.5$
PVEL	11.34271	11.30964	11.46019	9.68026	7.91454	9.02811	
PDIS	42.11644	44.01939	31.98684	23.17263	21.10955	20.85443	
PDL1	0.00000	0.00000	0.00000	0.00000	0.00000	0.00000	
PDL2	0.00000	0.00000	0.00000	0.00000	0.00000	0.00000	
PDL3	0.00000	0.00000	0.00000	0.00000	0.00000	0.00000	J_X measures,
PDL4	0.00000	0.00000	0.00000	0.00000	0.00000	0.00000	$K_{2P} = 0.5$
PACC	0.00000	0.00000	0.00000	0.00000	0.00000	0.00000	
PVEL	0.00000	0.00000	0.00000	0.00000	0.00000	0.00000	
PDIS	0.00000	0.00000	0.00000	0.00000	0.00000	0.00000	
PDL1	0.54471	0.38330	0.30462	0.22573	0.10453	0.03229	J_{XT} measures,
PDL3	0.57889	0.38000	0.27126	0.17188	0.07261	0.02288	$K_{2P} = 0.5$
PDL1	0.58238	0.80460	1.16504	1.20203	1.09463	1.03307	
PDL2	0.05846	0.07709	0.13621	0.40432	0.74707	0.93538	
PDL3	0.49643	0.64237	0.93280	1.05512	1.03705	1.01463	J_Q measures,
PDL4	0.01246	0.00048	-0.01909	0.04643	0.15632	0.20379	$K_{2P} = 1.0$
PVEL	11.51418	11.75864	12.93877	14.15045	14.27637	17.88819	
PDIS	45.58288	49.22908	40.69039	36.51659	39.03415	40.81094	
PDL1	0.00000	0.00000	0.00000	0.00000	0.00000	0.00000	
PDL2	0.00000	0.00000	0.00000	0.00000	0.00000	0.00000	
PDL3	0.00000	0.00000	0.00000	0.00000	0.00000	0.00000	J_X measures,
PDL4	0.00000	0.00000	0.00000	0.00000	0.00000	0.00000	$K_{2P} = 1.0$
PACC	0.00000	0.00000	0.00000	0.00000	0.00000	0.00000	
PVEL	0.00000	0.00000	0.00000	0.00000	0.00000	0.00000	
PDIS	0.00000	0.00000	0.00000	0.00000	0.00000	0.00000	
PDL1	0.54471	0.38330	0.30462	0.22573	0.10453	0.03229	J_{XT} measures,
PDL3	0.57889	0.38000	0.27126	0.17188	0.07261	0.02288	$K_{2P} = 1.0$

TABLE C-16. REVISED MEASURES, ROLL-SWAY AXES VERSUS BREAK BREAK FREQUENCY AND C_{2Y}

BF	.0675	.125	.25	.5	1.0	2.0	
PDL1	0.06404	0.20797	0.55343	0.94366	1.21167	1.26063	J_P measures,
PDL2	0.00077	0.00416	0.01742	0.03621	0.03016	-0.04607	
PDL3	0.03543	0.11937	0.35261	0.66463	0.93627	1.08140	K_{2R} = 1.0,
PDL4	0.00127	0.00499	0.01885	0.04650	0.07045	0.01399	
PVEL	55.76504	56.46758	46.98891	41.05805	26.72289	8.58769	C_{2Y} = .0025
PDIS	85.75620	87.46274	82.74385	47.78429	18.30605	9.33734	
PDL1	0.00017	0.00022	0.00036	0.00061	0.00104	0.00138	
PDL2	0.13064	0.10071	0.06550	0.03001	0.01231	0.00425	J_Y measures,
PDL3	0.96949	0.98749	0.97636	0.93235	0.76758	0.44862	
PDL4	-0.91526	-0.92514	-0.94044	-0.91701	-0.76099	-0.44598	K_{2R} = 1.0
PACC	31.23702	45.25141	48.24283	28.31316	14.79704	10.28296	
PVEL	0.17E+03	0.18E+03	0.10E+03	0.58E+02	0.25E+02	0.10E+02	C_{2Y} = .0025
PDIS	0.19E+04	0.94E+03	0.40E+03	0.17E+03	0.52E+02	0.16E+02	
PDL1	0.01630	0.01819	0.01745	0.01078	0.00522	0.00208	J_{YT} measures,
PDL3	0.00956	0.01481	0.02934	0.03886	0.04014	0.03564	K_{2R} = 1.0
							C_{2Y} = .0025
PDL1	0.06404	0.20797	0.55343	0.94366	1.21167	1.26063	
PDL2	0.00077	0.00416	0.01742	0.03621	0.03016	-0.04607	J_P measures,
PDL3	0.03543	0.11937	0.35261	0.66463	0.93627	1.08140	
PDL4	0.00127	0.00499	0.01885	0.04650	0.07045	0.01399	K_{2R} = 1.0,
PVEL	55.76504	56.46758	46.98891	41.05805	26.72289	8.58769	
PDIS	85.75620	87.46274	82.74385	47.78429	18.30605	9.33734	C_{2Y} = .0225
PDL1	0.00139	0.00182	0.00323	0.00559	0.00947	0.01252	
PDL2	0.81730	0.76097	0.54631	0.26503	0.11113	0.03852	J_Y measures,
PDL3	0.99017	0.98840	0.97797	0.93499	0.77185	0.45397	
PDL4	-0.45101	-0.49975	-0.65545	-0.78325	-0.70723	-0.42770	K_{2R} = 1.0,
PACC	48.85858	53.79541	43.62885	23.17445	14.18067	10.37257	
PVEL	0.16E+03	0.13E+03	0.11E+03	0.62E+02	0.25E+02	0.98E+01	C_{2Y} = .0225
PDIS	0.73E+03	0.69E+03	0.37E+03	0.14E+03	0.48E+02	0.16E+02	
PDL1	0.13388	0.15424	0.15556	0.09845	0.04766	0.01888	J_{YT} measures,
PDL3	0.07317	0.08893	0.12110	0.13250	0.12665	0.10854	K_{2R} = 1.0,
							C_{2Y} = .0225
PDL1	0.06404	0.20797	0.55343	0.94366	1.21167	1.26063	
PDL2	0.00077	0.00416	0.01742	0.03621	0.03016	-0.04607	
PDL3	0.03543	0.11937	0.35261	0.66463	0.93627	1.08140	J_P measures,
PDL4	0.00127	0.00499	0.01885	0.04650	0.07045	0.01399	
PVEL	55.76504	56.46758	46.98891	41.05805	26.72289	8.58769	K_{2R} = 1.0,
PDIS	85.75620	87.46274	82.74385	47.78429	18.30605	9.33734	
PDL1	0.00603	0.00753	0.01498	0.03819	0.08450	0.12441	C_{2Y} = .25
PDL2	1.30986	1.32757	1.34221	1.20246	0.70853	0.28572	
PDL3	0.99337	0.99241	0.98613	0.95597	0.81586	0.51537	J_Y measures,
PDL4	0.09124	0.09040	0.05361	-0.09672	-0.31008	-0.27295	
PACC	24.49761	21.74777	21.37760	19.47116	15.87156	9.51661	K_{2R} = 1.0,
PVEL	54.30840	58.02134	48.68298	27.54009	14.45196	6.83523	
PDIS	0.16E+03	0.14E+03	0.12E+03	0.75E+02	0.28E+02	0.10E+02	C_{2Y} = .25
PDL1	0.58151	0.63654	0.72090	0.67231✓	0.42521	0.18765	J_{YT} measures,
PDL3	0.37263	0.39351	0.41913	0.41995✓	0.38547	0.32607	K_{2R} = 1.0,
							C_{2Y} = .25

TABLE C-17. REVISED MEASURES, YAW AND HEAVE AXES VERSUS BREAK FREQUENCY

BF	.0675	.125	.25	.5	1.0	2.0	
PDL1	0.65466	0.93944	1.18190	1.14679	1.07502	1.03102	
PDL3	0.54160	0.74246	0.98077	1.03396	1.02612	1.01335	J_R measures
PVEL	3.87879	4.36360	3.66914	2.31082	1.44214	0.72981	
PDIS	26.99819	14.55148	7.93515	3.92446	1.84893	0.69747	
PDL1	0.83764	1.21807	1.55947	1.18993	1.06558	1.01853	
PDL3	0.63075	0.85105	1.12942	1.05578	1.02024	1.00642	
PACC	0.96E+02	0.10E+03	0.87E+02	0.56E+02	0.32E+02	0.26E+02	J_Z measures
PVEL	0.28E+03	0.23E+03	0.19E+03	0.58E+02	0.30E+02	0.10E+02	
PDIS	0.20E+04	0.14E+04	0.61E+03	0.16E+03	0.40E+02	0.94E+01	
PDL1	0.02100	0.04448	0.08403	0.07643	0.07223	0.05933	$J_{Z_{gs}}$ measures
PDL3	0.16689	0.11625	0.08720	0.13090	0.13625	0.14512	
PDL1	1.01189	1.11171	1.15905	1.05259	1.03069	1.00686	$J_{Z_{ngs}}$ measures
PDL3	0.98101	1.03165	1.06070	1.01700	1.01165	1.00278	

TABLE C-18. REVISED MEASURES, ROLL-SWAY AXES VERSUS WASHOUT CONFIGURATION

Washout	LIN	PAR1	SUB1	SUB2	
PDL1	0.94366	0.94366	0.94366	0.94366	
PDL2	0.02973	0.02973	0.02973	0.24546	
PDL3	0.66463	0.66463	0.66463	0.66463	J_P measures
PDL4	0.03875	0.03875	0.03875	0.23249	
PVEL	41.22489	41.22489	41.22489	37.05385	
PDIS	48.50484	48.50484	48.50484	32.50349	
PDL1	0.57632	0.57632	0.35551	0.47515	
PDL2	-0.00394	-0.00394	0.02727	0.21557	
PDL3	0.93013	0.93013	0.94677	0.73261	J_Y measures
PDL4	-0.23146	-0.23146	-0.11319	-0.00663	
PACC	28.09876	28.09876	21.42446	47.22521	
PVEL	57.85407	57.85408	27.83716	50.11210	
PDIS	0.16E+03	0.16E+03	80.36674	0.12E+03	
PDL1	0.01078	0.01078	0.57715	0.66065	J_{YT} measures
PDL3	0.03886	0.03886	0.43479	0.40566	

APPENDIX D

COMPARISON METHOD FOR PHASE CHARACTERISTICS OF DIFFERENT DRIVE LOGIC CIRCUITS

Parametric study of drive logic response characteristics can be extremely complex if many parameters are involved. It is also difficult to compare the characteristics of drive logic for different simulators which may not only have different parameter definitions, but may also have different drive logic forms. Both of these circumstances motivate development of simple metrics which can serve to quantify basic dynamic performance of drive logic circuits independently of their complexity or form. The metrics proposed here focus upon the effective phase lead introduced by washout circuits at high frequencies, and the effective phase lag introduced by residual tilt circuits at low frequencies. The matter of drive logic scaling gain constitutes another key characteristic in itself. Its significance is obvious, and it will not be considered further here.

The method for calculating effective leading and lagging phase characteristics is based upon Pade approximants for exponential functions. A table of these approximants is given below.

Use of these approximations is illustrated with some simple examples.

EXAMPLE #1

Compare the drive logic for the roll axes of two simulators.

Simulator #1*

Roll washout transfer function is:

$$\frac{s}{s + \omega_p} \quad \frac{s}{s + \omega_p}$$

*The Vought Corp. LAMBS simulator roll axis drive logic has this form.

TABLE D-1. APPROXIMATIONS FOR DRIVE LOGIC TRANSFER FUNCTION FACTORS

For $|s| < 1/\tau$ or $1/\nu$ (i.e., at low frequencies)

$$\frac{1}{1 + \tau s} \doteq e^{-\tau s}$$

$$\frac{1}{1 + \eta s + \nu^2 s^2} \doteq e^{-\eta s}$$

$$1 + \tau s \doteq e^{\tau s}$$

$$1 + \eta s + \nu^2 s^2 \doteq e^{\eta s}$$

For $|s| > \alpha$ or γ (i.e., at high frequencies)

$$\frac{s}{s + \alpha} = (1 + \alpha/s)^{-1} \doteq e^{-\alpha/s}$$

$$\frac{s^2}{s^2 + \beta s + \gamma^2} = (1 + \beta/s + \gamma^2/s^2)^{-1} \doteq e^{-\beta/s}$$

$$\frac{s + \alpha}{s} = 1 + \alpha/s \doteq e^{\alpha/s}$$

$$\frac{s^2 + \beta s + \gamma^2}{s^2} = 1 + \beta/s + \gamma^2/s^2 \doteq e^{\beta/s}$$

The effective lead at high frequencies is obtained from

$$\frac{s}{s + \omega_\varphi} \frac{s}{s + \omega_p} \doteq e^{-\omega_\varphi/s} e^{-\omega_p/s} = e^{-(\omega_\varphi + \omega_p)/s}$$

using the fifth entry in Table D-1. The effective lead frequency parameter is $(\omega_\varphi + \omega_p)$ rad/sec.

Simulator #2*

Roll washout transfer function is:

$$\frac{s^3}{(s + 0.65)[s^2 + 2(0.707)0.65s + (0.65)^2]}$$

$$\doteq e^{-0.65/s} e^{-2(0.707)0.65/s} = e^{-1.57/s}$$

The effective lead frequency parameter is 1.57 rad/sec.

INTERPRETATION

In order that the roll washout for Simulator #1 introduce less phase (lead) distortion than Simulator #2 it is necessary that $(\omega_\varphi + \omega_p) < 1.57$ rad/sec. In order that their phase distortions be comparable, $(\omega_\varphi + \omega_p) = 1.57$ rad/sec. Furthermore, notice that alternative selections for the ω_φ and ω_p parameters of Simulator #1 satisfying

$$\omega_\varphi + \omega_p = 1.57 \text{ rad/sec}$$

are possible. Still further, all alternatives satisfying the above equation are equivalent in terms of the phase distortion metric used here.

The usefulness of this approach for reducing the number of parameters which must be varied in a parametric study is illustrated by the last point above. By way of further illustration, consider equivalent break frequency combinations for the first and second order transfer function factors for Simulator #2. Any combination of break frequencies satisfying

$$\omega_{fo} + 2(0.707)\omega_{so} = 1.57$$

*The Air Force LAMARS simulator roll axis drive logic for the F-17 is reported to have this transfer function (Ref. 1).

will have equivalent phase distortion metrics. Further, if the factor $(s + 0.3)(s + 0.1)/(s + 0.2)^2$ is included in the transfer function for Simulator #2, the phase distortion metric will be unchanged.

EXAMPLE #2

Evaluate the high and low frequency phase distortion in lateral specific force reproduction for the nominal configuration of the Vought Corp. LAMBS drive logic with and without addition of a lateral residual tilt feature.

NOMINAL LAMBS

Lateral specific force transfer function is:

$$0.20 \frac{s^2}{s^2 + 2(0.707)2.0\, s + (2.0)^2} \quad \frac{s^2}{s^2 + 0.45s + 0.1}$$

RESIDUAL TILT ADDITION

Residual tilt transfer function is:

$$0.50 \frac{1}{1 + 2.0\, s}$$

Phase lead distortion at high frequencies without residual tilt is obtained from the first transfer function. The effective lead frequency parameter is:

$$2(0.707)2.0 + 0.45 = 3.28 \text{ rad/sec}$$

The phase lag distortion at low frequencies is asymptotic to -360 deg in the absence of residual tilt. However, the amplitude ratio at low frequencies is very small (proportional to frequency to the fourth power).

Phase distortion with residual tilt is obtained by adding the two transfer functions and factoring the resulting numerator polynomials.

$$0.2 \frac{(s + 1.413)[s^2 + 2(0.713)0.32s + (0.32)^2][s^2 + 2(-0.031)1.89s + (1.89)^2]}{(s + 0.5)[s^2 + 2(0.707)2.0s + (2.0)^2][s^2 + 0.45s + 0.1]}$$

Phase lead distortion at high frequencies with residual tilt results in the effective lead frequency parameter:

$$-1.413 - 2(0.713)0.32 - 2(-0.031)1.89 + 0.5 + 2(0.707)2.0 + 0.45$$

$$= 2.03 \text{ rad/sec}$$

Phase lag distortion at low frequencies with residual tilt results in the effective delay parameter:

$$-\frac{1}{1.413} - \frac{2(0.713)}{0.32} - \frac{2(-0.031)}{1.89} + \frac{1}{0.5} + \frac{2(0.707)}{2.0} + \frac{0.45}{0.1}$$

$$= 2.08 \text{ sec}$$

The effective phase lag is asymptotic to 0 degrees.

INTERPRETATION

Addition of residual tilt reduces leading phase distortion at high frequencies significantly.

Addition of residual tilt reduces lagging phase distortion at low frequencies dramatically.

As a general rule, small values of the effective lead frequency parameter, and of the effective delay parameter are desirable from the point of view of minimizing phase distortion in simulated motion cues. Values between 1.0 and 2.0 rad/sec for effective lead frequency and between 0.5 and 1.0 sec for effective delay are to be considered "good". Certain cautions must be presented along with this information, however.

- "Good" values of the effective lead frequency or effective delay parameters obtained by means of extreme motion scaling in the drive logic are counter-productive.
- Given motion scaling and simulation tasks will place lower bounds on the effective lead frequency parameters based on the available simulator travels.

Spurious motion cue generation will result in bounds on the effective lead frequency and effective delay parameters. A lower bound on the effective delay parameters is set by the tolerable level of spurious pitch and roll rate cues. These cues result from the residual tilt feature. A lower bound on the effective lead frequency parameters in the pitch and roll axis drive logic and an upper bound on the lead frequency parameters in the longitudinal and lateral translational drive logic is set by the tolerable level of spurious longitudinal and lateral specific force cues. These cues are the result of imperfect simulator coordination.

*U.S.Government Printing Office: 1979 — 657-002/690